SANDIA REPORT
SAND2020-5466
Printed May 2020

Sandia National Laboratories

Alternative Fuel Vehicles in Tunnels

Chris B. LaFleur, Austin M. Glover, Austin R. Baird, Cyrus J. Jordan, Brian D. Ehrhart

Prepared by
Sandia National Laboratories
Albuquerque, New Mexico
87185 and Livermore,
California 94550

Issued by Sandia National Laboratories, operated for the United States Department of Energy by National Technology & Engineering Solutions of Sandia, LLC.

Available to DOE and DOE contractors from
U.S. Department of Energy
Office of Scientific and Technical Information
P.O. Box 62
Oak Ridge, TN 37831

Telephone: (865) 576-8401
Facsimile: (865) 576-5728
E-Mail: reports@osti.gov
Online ordering: http://www.osti.gov/scitech

Available to the public from
U.S. Department of Commerce
National Technical Information Service
5301 Shawnee Rd
Alexandria, VA 22312

Telephone: (800) 553-6847
Facsimile: (703) 605-6900
E-Mail: orders@ntis.gov
Online order: https://classic.ntis.gov/help/order-methods/

ABSTRACT

Many types of vehicles using fuels that differ from typical hydrocarbons such as gasoline and diesel are in use throughout the world. These include vehicles running on the combustion of natural gas and propane as well as electrical drive vehicles utilizing batteries or hydrogen as energy storage. These alternative fuels pose hazards that are different from traditional fuels and the safety of these vehicles are being questioned in areas such as tunnels and other enclosed spaces. Much scientific research and analysis has been conducted on tunnel and garage hazard scenarios; however, the data and conclusions might not seem to be immediately applicable to highway tunnel owners and authorities having jurisdiction over tunnels. This report provides a comprehensive, concise summary of the literature available characterizing the various hazards presented by all alternative fuel vehicles, including light-duty, medium- and heavy-duty, as well as buses. Research characterizing both worst-case and more plausible scenarios and risk-based analysis is also summarized. Gaps in the research are identified in order to guide future research efforts to provide a complete analysis of the hazards and recommendations for the use of alternative fuel vehicles in tunnels.

ACKNOWLEDGEMENTS

This work was initiated as a result of feedback from multiple stakeholders, including government, industry, authorities having jurisdiction, and the Hydrogen and Fuel Cell Technical Advisory Committee to the U.S. Department of Energy (DOE). Sandia National Laboratories led this effort, in coordination with the U.S. DOE Office of Energy Efficiency and Renewable Energy (EERE) Hydrogen and Fuel Cell Technologies Office (HFTO) and the U.S. Department of Transportation (DOT) Federal Highway Administration (FHWA). This report was reviewed and input was provided by Mark Smith of the U.S. DOE EERE Vehicle Technologies Office (VTO), William Bergeson of the U.S. DOT FHWA, and Laura Hill and Mark Richards of HFTO. In addition to the reviewers listed previously, the authors also acknowledge those who reviewed the Hydrogen Fuel Cell Vehicles in Tunnels white paper which forms the basis for the hydrogen section in this work: members of the workshop on hydrogen vehicles in tunnels and Alice Muna (Sandia). Financial support was provided by the U.S. DOE HFTO.

CONTENTS

LIST OF FIGURES

LIST OF TABLES

This page left blank

EXECUTIVE SUMMARY

Vehicles of all sizes use internal combustion engines powered by hydrocarbons such as gasoline, diesel, ethanol, and various blends. As alternative fuel vehicles and the infrastructure to support them become more widely available, safety concerns become a more important topic because these fuels are different from the typical safety hazards that have been accepted since the widespread adoption of the automobile. Road tunnels and other enclosures have additional concerns due to limited access and egress, ventilation system capacity, and emergency response limitations. Therefore, tunnel owners, authorities, and other stakeholders have raised concerns about alternative fuel vehicles traveling through tunnels, particularly in urban and high commuter areas. Natural gas and propane are used to replace traditional fuels as cleaner or more efficient alternative fuel in combustion engines. Alternative fuel vehicles also include those powered by electricity using lithium-ion batteries or hydrogen fuel cells. The intent of this document is to help illustrate the level of risk for all types of fuel, provide a full understanding of what codes & standards are applicable to these alternative fuel vehicles, and to review relevant research that has been conducted to date. Risks to life safety and infrastructure damage always exist, regardless if the fuel type is traditional or alternative. The goal for acceptance of alternative fuel vehicles may be to maintain the same level of risk that is generally accepted for traditional fuel vehicles.

For each fuel type, including traditional fuels such as gasoline and diesel, an overview with a summary of fuel properties and hazards, applicable codes and standards, and tunnel-specific research in the literature is provided. Additionally, information to compare the various classes of vehicles such as passenger, light-duty, heavy-duty, and cargo are reviewed where available. This information helps characterize the severity of the hazard for each classification of vehicle. The different codes and standards applicable come from organizations such as National Fire Protection Association, Society of Automotive Engineers, Underwriters Laboratories, and more. While these organizations provide various codes and standards, it is up to state and local jurisdiction to help adopt, regulate, and enforce them. The literature review provides information organized by experiments, modeling, and theoretical calculations/analyses performed regarding the specific fuel in tunnels. Some of the fuel types are not as well studied as others, specifically in tunnels. In these cases, research that is applicable to tunnels is reviewed. For example, battery electric vehicles real-world incidents from the last few years are presented because few full-scale experiments have been conducted. Research gaps identified are provided for each fuel type.

Battery

There are two distinct hazards from battery electric vehicles (BEVs): deflagration from the flammable vent gas and a unique fire hazard due to thermal runaway propagation between cells. Unlike flammable gases with well-known properties, characteristics of the vent gases from a battery cell failure are not as well defined. Variations in cell chemistry, capacity, thermal runaway propagation between cells, state of charge, form factor, and other variations affect hazards such as vent gas species, volume production, and production rates. These are further discussed in the associated hazards for BEVs. Due to these factors, the hazards associated with BEVs are not as well characterized as some of the other alternative fuel vehicles. Studies to understand the heat release rate compared with traditional fuel vehicles has been reviewed. Also, studies characterizing fire spread within a BEV and tactics to slow or stop thermal propagation based using water and other methods has been studied. Testing and analysis to understand the failure scenarios and modes pertaining to BEVs is limited but also included. This includes understanding thermal, mechanical,

and electrical failures. A variety of research gaps are discussed for BEVs in tunnels and lithium-ion batteries in general.

Natural Gas

Most of the studies surveyed involve compressed natural gas (CNG) in gaseous form, showing the need to further understand liquefied natural gas (LNG) hazards and the differences for this lower pressure, liquid fuel. Harmful and lethal distances due to fire or overpressure from a CNG release can exceed comparable distances for LNG due to the higher storage pressures of CNG. A variety of tunnel studies have been summarized that characterized CNG releases of vapor clouds that are considered equivalent to amounts of CNG in city bus and passenger car configurations. One study looks at different initiating events of a natural gas leak from a vehicle in a tunnel and how the flammable mass and overpressures change based on those events. Another study shows the difference in characteristics such as harmful distances from a vapor cloud explosion for CNG and LNG. This helps understand the fundamental differences for this fuel based on its state. As more research is conducted, the focus specifically for tunnels should include experimental studies of natural gas dispersion and overpressure in actual or scaled down tunnels as well as large scale natural gas flames heat transfer analysis.

Propane

There were relatively few studies evaluating the failure modes and consequences associated with liquefied propane gas (LPG) vehicles in tunnels. One study used a failure tree to inform the experimental setup. The experimental data was then used and compared with a CFD model for validation. This model can be further used to understand the gaseous dispersion characteristics of propane vehicles failing in tunnels and other confined spaces. Additionally, an experiment was also conducted to understand smoke dispersion in a tunnel using a propane fire to understand the effect of ventilation and tunnel slope. Modeling was done to help understand the dispersion and evaporation of an LPG spill. Future work should investigate thermal consequences of failures, which have not been reported for many of the studies included in this literature survey. This includes the heat release rate, temperature, and structural damage resulting from different failure modes.

Hydrogen

There are a number of studies evaluating the failure modes and consequences associated with hydrogen fuel cell electric vehicles (FCEVs) in tunnels. Multiple studies have identified possible release events that could occur. Other studies have begun to quantify probabilities and likelihoods for these various events. Modeling on the consequences of releases has also been performed; multiple studies have investigated hydrogen accumulation followed by ignition, resulting in an overpressure. One study looked at the thermal effects on tunnel components of a jet fire rather than an overpressure. Multiple experimental studies have also investigated overpressures resulting from delayed hydrogen ignition, though some have investigated thermal effects of jet fires as well. Some research gaps identified for FCEVs in tunnels are the need for an increased focused on thermal effects of jet fires on tunnel structures. Similarly, while some studies have investigated the extent of overpressures in tunnels, more information is needed on what type of critical tunnel infrastructure might be affected by such hazards. More information is needed on how likely hydrogen is to ignite in different release configurations which will greatly inform risk analyses. Most current studies have focused on light-duty vehicles, and so more modeling and experiments on larger fuel-capacity vehicles would be important to consider. Some of these gaps as well as others will be addressed in the current HyTunnel-CS project.

ACRONYMS AND DEFINITIONS

Abbreviation	Definition
AEGL	acute exposure guideline levels
AHJ	authority having jurisdiction
AIT	auto-ignition temperature
ASHRAE	American Society of Heating, Refrigerating and Air-Conditioning Engineers
BEV	battery electric vehicle
BLEVE	boiling liquid expanding vapor explosion
CANA	Central Artery North Area
CFAST	Consolidated Model of Fire and Smoke Transport
CFD	computational fluid dynamics
CNG	compressed natural gas
DDT	deflagration-to-detonation transition
DEC	diethyl carbonate
DMC	dimethyl carbonate
DOE	Department of Energy
DOT	Department of Transportation
EC	ethylene carbonate
EMC	ethyl methyl carbonate
FCEV	fuel cell electric vehicle
FDS	Fire Dynamics Simulator
FHWA	Federal Highway Administration
FL	flammability limit
FLACS	FLame ACceleration Simulator
FMEA	failure mode and effect analysis
FMVSS	Federal Motor Vehicle Safety Standards
GGE	gasoline-gallon-equivalent
GVWR	gross vehicle weight rating
HF	hydrogen fluoride
HGV	heavy goods vehicle
HRR	heat release rate
ICE	internal combustion engine
IDLF	immediate danger to life or health
ISO	International Organization for Standardization

Abbreviation	Definition
LCO	lithium cobalt oxide
LEL	lower explosive limit
LFL	lower flammability limit
LFP	lithium iron phosphate
LMO	lithium manganese oxide
LNG	liquefied natural gas
LPG	liquefied petroleum gas
NCA	nickel cobalt aluminum
NCHRP	National Cooperative Highway Research Program Guidelines
NFPA	National Fire Protection Association
NGV	natural gas vehicle
NHTSA	National Highway Traffic Safety Administration
NIST	National Institute of Standards and Technology
NMC	nickel manganese cobalt
MIE	minimum ignition energy
MPC	methyl propyl carbonate
PC	propylene carbonate
PHEV	plug-in hybrid electric vehicles
PIARC	Permanent International Association of Road Congresses
PRA	probabilistic risk assessment
PRD	pressure relief device
PTC	positive temperature coefficient
QRA	quantitative risk analysis
RVP	Reid vapor pressure
RWS	Rijkswaterstaat, a time-temperature curve used in safety standards
SAE	Society of Automotive Engineers
SUV	sport utility vehicle
THC	total hydrocarbons
THR	total heat released
TPRD	thermally activated pressure relief device
UEL	upper explosive limit
UFL	upper flammability limit

1. INTRODUCTION

The purpose of this report is to present tunnel owners and other stakeholders with a summary of the current body of scientific information about the use of alternative fuel vehicles in tunnels. This will allow tunnel regulators to determine requirements for alternative fuel vehicle transit through tunnels on a national level. This objective is accomplished through performing a comprehensive literature review of publicly available tunnel research experiments and modeling focused on the hazards associated with alternative fuel vehicles. Gaps in the existing research are identified and suggestions to address these gaps are presented. This includes a review of the scenarios and failure modes and the range of consequences associated with the failures. This work expands upon a previously published hydrogen-specific white paper [1] by including other alternative fuels.

The scope of this report is to summarize hazard research in tunnels for road vehicles powered by traditional fuels, battery electric systems, compressed natural gas, liquefied natural gas, propane, and hydrogen. The volume of fuel in each vehicle is an important consideration, so the class of vehicle is noted where applicable to help further understand the potential consequences of light-duty, medium-duty, or heavy-duty vehicle incidents.

Note that some of the research presented in this document assess theoretical scenarios that are implausible in the real world, such as large stoichiometric mixtures. These situations are included in this paper to recognize the scientific principle, but also point out the improbability of encountering these conditions outside a laboratory. However, consequence is only part of the overall risk. The likelihood of these scenarios is extremely low or virtually impossible, which significantly lowers the risk of the theoretical hazards.

1.1. Definitions for Hazard Metrics

The following section defines the various hazard metrics discussed in the literature:

- Flammability Limits

Flammability limits are important for fire and explosion analysis because it defines the volume fraction and conditions range of fuel required to create a flammable environment. Codes, standards, and practices have specific requirements regarding the flammable gas concentration permitted in any given environment. The lower flammability limit (LFL) is the lowest fuel concentration that will allow flame or flash propagation from an ignition source within the mixture. The upper flammability limit (UFL) is the highest fuel concentration that will allow flame or flash propagation from an ignition source within the mixture. Outside of these limits, no flame can occur [2]. Standard units of flammability limits are in volume percent (%) or volume fraction.

- Explosion

Explosion is a general term for the elevated release of energy that generates high temperatures. This causes expansion of a gas volume and leads to an overpressure [3]. A broad class of pre-mixed flames can cause this overpressure. To further define an explosion, the speed of the flame front determines whether it is a deflagration (subsonic speeds) or detonation (supersonic speeds).

- Explosion Limits

Explosion limits refer to the range of pressure and temperature for which an explosive reaction can occur for a fixed composition mixture. The explosion limit is given as a minimum autoignition temperature (AIT) which is a strong function of the fuel type, pressure, and overall fuel concentration [4]. The explosion limits are within the same concentration range as the flammability limits. Standard units of explosion limits are in volume percent (%) or volume fraction.

- Auto-Ignition Temperature

The auto-ignition temperature (AIT) is the lowest recorded temperature in which ignition occurs spontaneously or in the absence of piloted ignition source in a material. This applies to solids, liquids and gases. If the rate at which heat evolves in a gas or vapor is greater than the rate of heat loss to the surrounding area, ignition can result [2] [5]. Standard units for the auto-ignition temperature is degrees Celsius (°C) or degrees Fahrenheit (°F).

- Detonation/Deflagration

Deflagration is defined as a flame front which propagates through a gas at subsonic speeds. Typically, obstructions such as piping and conduit as well as confinement cause a flame front to accelerate to speeds greater than the speed of sound (343 m/s in ambient air). This causes the deflagration-to-detonation transition (DDT). A detonation is defined as a flame front which propagates through a gas at supersonic speeds. A deflagration will have flame speeds that vary from less than 1 m/s up to 3 m/s whereas detonation flame speeds are anywhere from 1.5 to 2.8 km/s [6].

- Detonation Limits

Detonation limits is the range at which a detonation can self-sustain. These limits typically have a narrower range within the flammability/explosion limits. This is due to the stronger dependence on confinement, mixture composition, and initial temperature and pressure compared with the flammability/explosion limits [4]. Standard units for detonation limits are in volume percent (%) or volume fraction.

- Laminar Flame Speed

The critical parameter controlling the rate of pressurization is the burning speed. The burning speed is correlated to a fundamental flame propagation rate into the unburned premixed gas. This flame speed generally increases with increasing temperature and decreases with increasing pressure [7]. The laminar flame speed is dependent on the chemical kinetics along with the thermal and mass diffusion [8]. Standard units for the laminar flame speed are meter-per-second (m/s) or feet-per-minute (ft/min).

- Overpressure

Overpressure defines the pressure wave that a flammable mixture generates during combustion. This pressure wave is caused by the energy released from initial deflagration/detonation. The maximum theoretical overpressure (P_{max}) is the pressure that is generated when the gas is combusted in a perfectly adiabatic process in a closed chamber. This is a value generated theoretically or at optimal conditions in a laboratory. P_{max} depends on the composition of gas produced as well as the concentration and other factors such as confinement [9]. Standard units for overpressure can be kilopascals (kPa), pounds-per-square-inch (psi), or bar.

- Equivalence Ratio

The ratio of actual molar fuel/air ratio to the stoichiometric molar fuel/air ratio is the equivalence ratio. If this ratio is below 1, this is a lean mixture with excess air after combustion. If the ratio is above 1, the mixture is fuel rich leading to incomplete consumption of the fuel. Combustion with an equivalence ratio equal to 1 leads to complete consumption of oxygen and fuel during a reaction.

- Stoichiometric Ratio

The stoichiometric ratio is the mixture of fuel and air in which there is exactly enough air to completely burn all of the fuel. Combustion in stoichiometric conditions (when the mixture is at the stoichiometric ratio) leads to complete consumption of both oxygen and fuel.

- Adiabatic Flame Temperature

Adiabatic flame temperature is the maximum temperature that can result from combustion of reactants. Heat transfer away from the reaction, incomplete combustion, and other dissociations will result in a lower temperature. The maximum adiabatic flame temperature occurs when a mixture is stoichiometric [10]. Standard units for flame temperature are Kelvin (K), degrees Celsius (°C), or degrees Fahrenheit (°F).

- Flash Point

The flash point is the lowest temperature at which a liquid solvent can form a mixture above the surface or within a container that is flammable or ignitable. Lower flash point temperatures indicate that it is easier for the mixture to ignite. There are two types of tests to measure the flash point: closed cup and open cup. These methods test flash point in an open pool type configuration and a closed container configuration [2]. Standard units for the flash point temperature degrees are degrees Celsius (°C) or degrees Fahrenheit (°F).

- Heat of Combustion

Heat of combustion is the amount of heat released when a substance is burned. The heat of combustion can be further defined as the higher and lower heating values. The lower heating value of a fuel is defined by combustion of a fuel at 25°C and returning the resulting mixture of combustion products down to 150°C. This assumes the latent heat of vaporization of water in the reaction products is not recovered. The higher heating value is similar, but the products have returned to a temperature of 25°C, which considers the latent heat of vaporization of water in the combustion products [11]. Standard units for the heat of combustion are Megajoule per Kilogram (MJ/kg), British Thermal Units per-pound-mass (Btu/lb_m), or kilojoule-per-mole (kJ/mol).

- Heat Release Rate

Heat release rate (HRR) is the rate of energy released from a fire. This rate is typically defined by a plotted curve, with time on the horizontal axis and energy released on the vertical axis [12]. The heat release rate curve is used to characterize fires by understanding the peak heat release rate as well as the duration of the fire. Standard units for the heat release rate are kilowatt (kW) or British Thermal Unit per hour (Btu/hr).

- Heat Flux

In addition to the HRR, the heat release rate flux or heat flux is the total energy flow over time per unit of surface area. Standard units for the heat flux are kilowatt per square meter (kW/m^2) or British Thermal Unit per square foot ($Btu/hr\text{-}ft^2$).

- Total Heat Release

The total area under the heat release rate curve defines the total heat released (THR) [12]. Total heat released is used to characterize the size of a fire. Standard units for the total heat released are megajoule (MJ) or British Thermal Unit (Btu).

1.2. Tenability Criteria

To better understand the consequence and take-away values from the literature review, the following tables illustrate the effects of overpressure, heat flux, and temperature hazards. The severity of injuries and damage with the increase in these metrics is shown in Table 1 through Table 3. Table 1 lists the human injury criteria due to overpressure from National Fire Protection Association (NFPA) 921: Guide for Fire and Explosion Investigations [13].

Table 1: Human Injury Criteria from Overpressure (from [13])

Overpressure			Effects or Injuries
psi	kPa	bar	
0.60	4.14	0.04	Threshold for injury from flying glass
1.00-2.00	6.90-13.80	0.070-0.140	Threshold for skin laceration from flying glass
2.40-2.80	16.50-19.30	0.170-0.19	Threshold for eardrum rupture/10% probability of eardrum rupture
2.00-3.00	13.80-20.70	0.140-0.21	Threshold for serious wounds from flying glass
3.00	20.70	0.21	Overpressure will hurl a person to the ground
3.40	23.4	0.23	1% eardrum rupture
4.00-5.00	27.60-34.500	0.28-0.35	Serious wounds from flying glass near 50% probability
5.80	40.00	0.40	Threshold for body-wall penetration from flying glass (bare skin)
6.30	43.40	0.43	50% probability of eardrum rupture
7.00-8.00	48.30-55.20	0.48-0.55	Serious wounds from flying glass near 100% probability
10.00	68.95	0.69	Threshold for lung hemorrhage
14.50	99.97	1.00	Fatality threshold for direct blast effects
16.00	110.30	1.10	50% eardrum rupture
17.50	120.70	1.21	10% probability of fatality from direct blast effects
20.50	141.30	1.41	50% probability of fatality from direct blast effects
25.50	175.80	1.76	90% probability of fatality from direct blast effects
27.00	186.20	1.86	1% mortality: A high incidence of severe lung injuries
29	199.9	2.00	99% probability of fatality from direct blast effects

Table 2 illustrates the levels and exposure durations at which blistering (second-degree burn) injuries occur due to heat flux exposure from NFPA 921: Guide for Fire and Explosion Investigations [13]. Both the heat flux and exposure time help in understanding consequences.

Table 2: Effects from Heat Flux (from [13])

Radiant Heat Flux		Effects or Injuries
kW/m^2	$Btu/hr\text{-}ft^2$	
2.5	793	Common thermal radiation exposure while firefighting. This energy level may cause burn injuries with prolonged exposure.
		Human skin experiences pain with a 33-second exposure and blisters in 79 seconds with second-degree burn injury.
5	1,586	Human skin experiences pain with a 13-second exposure and blisters in 29 seconds with second-degree burn injury.
10	3,172	Human skin experiences pain with a 5-second exposure and blisters in 10 seconds with second-degree burn injury.
15	4,758	Human skin experiences pain with a 3-second exposure and blisters in 6 seconds with second-degree burn injury.
20	6,344	Human skin experiences pain with a 2-second exposure and blisters in 4 seconds with second-degree burn injury.
80	25,377	Heat flux for protective clothing Thermal Protective Performance (TPP) Test.
100	31,720	Steel structure collapse (>30 min exposure) (from [14])

Table 3 illustrates various effects and injuries from temperature exposure from National Institute of Standards and Technology (NIST) [12]. Both the heat flux and exposure time help in understanding consequences.

Table 3: Human Injury Criteria from Temperature (from [12])

Temperature		Effects or Injuries
Celsius (°C)	Fahrenheit (°F)	
37.0	98.6	Average normal human oral/body temperature
38	101	Typical body core temperature for a working fire fighter
43	109	Human body core temperature that may cause death
44	111	Human skin temperature when pain is felt
48	118	Human skin temperature causing a first-degree burn injury
54	130	Hot water causes a scald burn injury with 30 second exposure
55	121	Human skin temperature with blistering and second degree burn injury
62	140	Temperature when burned human tissue becomes numb
72	162	Human skin temperature at which tissue is instantly destroyed
100	212	Temperature when water boils and produces steam
250	482	Temperature when charring of natural cotton begins
>300	>572	Modern synthetic protective clothing fabrics begin to char
≥400	≥752	Temperature of gases at the beginning of room flashover
≈1000	≈1832	Temperature inside a room undergoing flashover

1.3. Vehicle Classifications

Vehicle classifications are defined by the vehicle's gross vehicle weight rating (GVWR) which is the maximum operating weight of the vehicle. The GVWR includes all vehicle fluids, passengers, and the cargo capability but does not include trailers. Definitions from various administrations such as the U.S. Department of Transportation Federal Highway Administration (FHWA) and U.S. Environmental Protection Agency (EPA) are included along with examples and applications of each vehicle class.

Table 4: Vehicle Weight Classifications (from [15])

Vehicle Class	Examples/ Applications	DOT FHWA	EPA
Light-Duty Vehicle	Sedans, SUVs, Pickups, Utility Van	Class 1: <6,000 lbs.	Heavy-Duty Engine Light Light-Duty Truck: <6,000 lbs.
			Light-Duty Vehicle: <8,500 lbs.
			Light-Duty Trucks: <8,500 lbs.
		Class 2: 6,001 – 10,000 lbs.	Light-Duty Truck 3 and 4 and Heavy Engines Heavy Light-Duty Truck: 6,001 – 8,500 lbs.
			Medium-Duty Vehicle: 8,501 – 10,000 lbs.
Medium-Duty Vehicle	Delivery Truck, Bucket Truck, School Bus	Class 3: 10,001 – 14,000 lbs.	Heavy-Duty Vehicle Heavy-Duty Engine: >8,500 lbs.
			Heavy-Duty Vehicle 3: 10,001 – 14,000 lbs.
		Class 4: 14,001 – 16,000 lbs.	Heavy-Duty Vehicle 4: 14,001 – 16,000 lbs.
		Class 5: 16,001 – 19,500 lbs.	Heavy-Duty Vehicle 5: 16,001 – 19,500 lbs.
		Class 6: 19,501 – 26,000 lbs.	Heavy-Duty Vehicle 6: 19,501 – 26,000 lbs.
Heavy-Duty Vehicle	City Bus, Refuse, Moving Truck, Truck, Fuel Vehicle, Heavy Semi Tractor	Class 7: 26,001 – 33,000 lbs.	Medium Heavy-Duty Engine: 19,501 – 33,000 lbs.
			Heavy-Duty Vehicle 7: 26,001 – 33,000 lbs.
		Class 8: >33,000 lbs.	Heavy Heavy-Duty Engine Urban Bus: >33,000 lbs.
			Heavy-Duty Vehicle 8a: 33,001 – 60,000 lbs.
			Heavy-Duty Vehicle 8b: >60,000 lbs.

From Table 4, there are three distinct vehicle classes: light-duty, medium-duty, and heavy-duty vehicle. These classes are broken down into sub-classes for each specific administration.

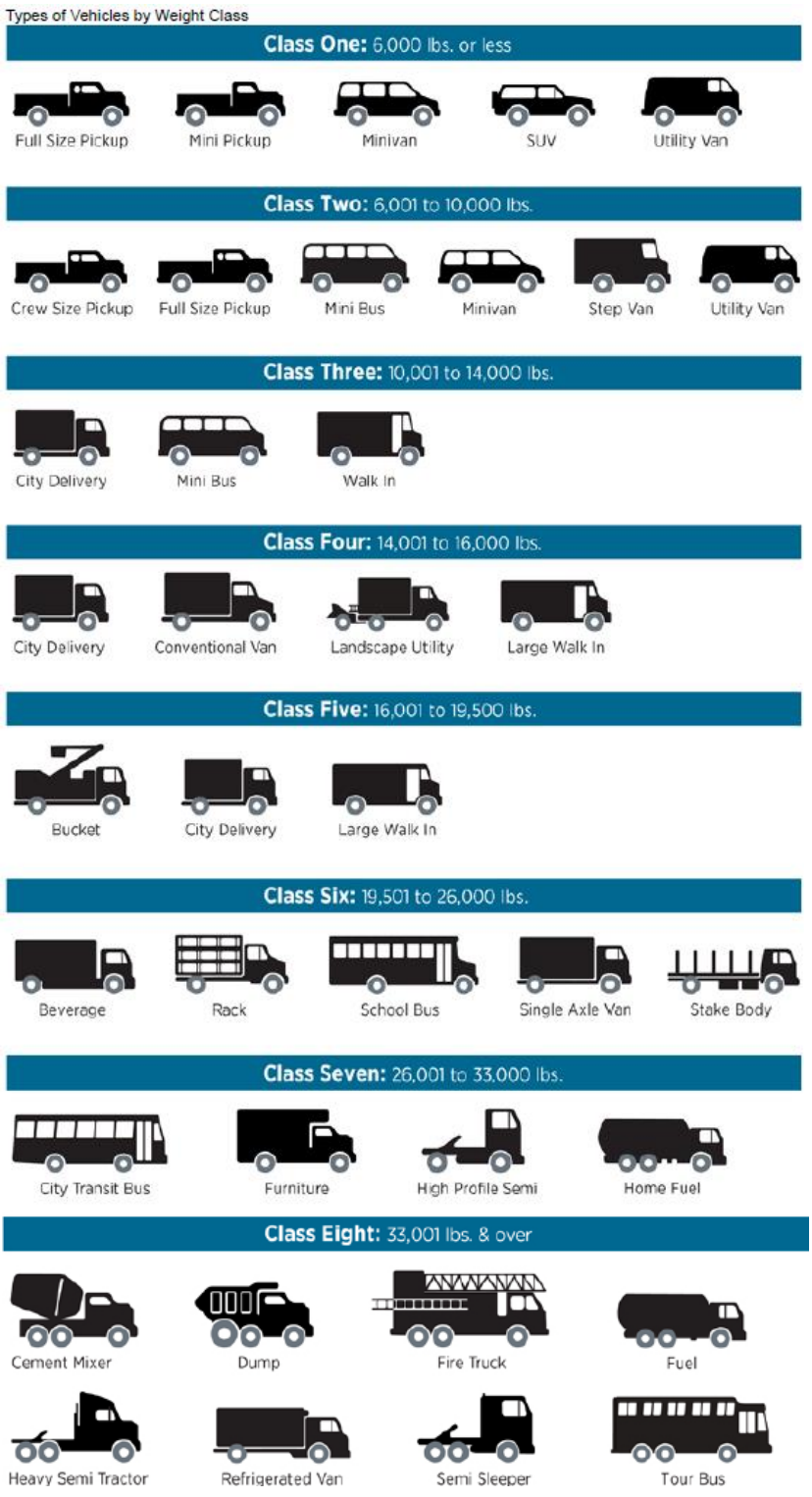

Figure 1: Vehicle Types by Weight Classification (from [16])

Figure 1 above gives further examples of various vehicles and what FHWA weight classification they fall under.

1.4. Report Organization

This report is organized into separate chapters based on the specific fuel type. Each of the chapters has a section that provides an overview of the fuel type, along with the general properties such as density, flammability limits, etc. Additionally, applicable regulations, codes, and standards are listed for reference. The literature review is broken down into three main section: experiments, modeling, and analysis. The experiment section reviews what work has been done that uses testing and measurement techniques to simulate fuel properties and characteristics such as dispersion, flammability limits, and overpressure in intermediate to full scale tunnels or confined areas. The modeling section shows computations done using various CFD software and other programs to simulate the characteristics and effects of fuels dispersion, fires, overpressure, and more in a tunnel. The analysis section describes work that studies hazard and risk of these fuels in tunnels. This work is done using engineering calculations and physics equations with experimental data and fuel properties as inputs to compare and further understand the effect of these fuels in tunnels. Each section has a research gap sections that goes into detail on what work has been completed and what work would be useful to help understand the overall hazard and consequence of these fuels in tunnels.

2. TUNNEL RESEARCH HIGHLIGHTS FOR TRADITIONAL FUELS

2.1. Overview of Traditional Fuels

Internal combustion engines (ICE) are the most commonly used powertrains in passenger, light-duty, heavy-duty and cargo vehicles. The main fuels are gasoline, diesel, and ethanol. Different ethanol-gasoline blends such as E15 (containing 15% ethanol by volume) or E85 Flex Fuel (containing 51% to 85% ethanol by volume) [17] are commonly found at gas stations. Usage of ethanol has increased in the U.S. from 1.7 billion gallons in 2001 to about 14.4 billion in 2016 [18]. In 2018, the U.S. consumed approximately 143 billion gallons of gasoline [19]. Diesel fuel is more common in larger commercial grade vehicles such as medium-duty, heavy-duty, and cargo, but is also becoming more common at the passenger and light-duty markets. In 2014, 78% of medium-duty and heavy-duty trucks sold were diesel powered, while only 1.5% of passenger and light-duty sold were diesel powered [20].

2.2. Properties of Traditional Fuels

Various properties of these traditional fuels help understand and compare with the properties of alternative fuels. Characteristics such as the liquid density and higher/lower heating values can be used to define the fuel loading. The gas density can be used to understand the flammability limits. The adiabatic flame temperature can be used to estimate the theoretical pressure rise from a confined explosion. The laminar flame speed or burning velocity determines how quickly the unburned mixture is consumed in a flame front. This value is affected by obstructions, temperature, fuel concentration and, other factors which can cause turbulent flame speeds leading to the deflagration-to-detonation transition.

Table 5: Properties of Traditional Fuels

Property	Gasoline	Diesel	Ethanol
Chemical Formula	C_4-C_{12} [21]	C_8-C_{25} [21]	C_2H_5OH [22]
Molecular Weight	95-120 g/mol [23]	204 g/mol [23]	46.07 g/mol [24]
Gas Density (25 °C, 1 atm)	1.227 kg/m^3 [22]	1.46 kg/m^3 [23]	1.214 kg/m^3 [22]
Liquid Density	0.742 g/m^3 [22]	0.87-0.95 g/m^3 [25]	0.79 g/m^3 [22]
Boiling Point	25-215 °C [22]	282-338 °C [25]	78.2 °C [24]
Flash Point	-45 °C [21]	55 °C [21]	13 °C [24]
Auto-Ignition Temperature	258 °C [23]	316 °C [25]	420 °C [22]
Flame Speed- Stoichiometric (φ=1)	0.33 m/s [22]	0.40 m/s [26]	0.41 m/s [22]
Adiabatic Flame Temperature	2289 K [23]	2327 K [23]	2234 K [22]
Flammability Limits (vol % in air)	1.2-7.1% [27]	0.6-6.5% [25]	3.5-15% [27]

Each fuel has variation and uncertainty in the properties, as different sources report slightly different values for each metric. This is because the chemical formulas and content in the fuel changes based on regional regulations, seasonal additives, refinery additives and detergents, water content, and other factors [28] [29]. One familiar example is winter gasoline blends verse summer gasoline blends. The winter blend must have a higher Reid vapor pressure (RVP) than summer blends to account for lower temperatures during the engine startup and to run smoother in colder conditions. The RVP varies from 9.0 psi down to 7.8 psi for summer months. Since ethanol has a lower vapor pressure, there is a 1.0 psi allowance for gasoline containing 9% to 10% ethanol [30]. Additionally, blends such as E85 have a range of 51% to 85% ethanol by volume [17] contributing further to the uncertainty or variations in the combustion properties. Since gasoline and ethanol have distinct properties, these factors should be considered when performing risk evaluations.

2.3. Associated Hazards of Traditional Fuels

Among traditional fuels, gasoline has the lowest flash point. It also has a higher vapor pressure, which typically causes the vapor mixture inside of a vehicles fuel tank to stay above the UFL [31]. Since the vapor pressure of ethanol is lower, in mixtures such as E85, this vapor pressure must be considered when both designing and adding this fuel to tanks. Based on the ASTM standard classification, the vapor pressure of E85 mixtures vary between 5.5 to 15.0 psi [17] which might cause the vapor mixture to fall within the flammable range. Since traditional fuel tanks have a high fuel concentration and use break-away and structurally weak plastic components, it is necessary to prevent high pressures from building up due to vapor pressure. While internal fire or deflagration hazard in a fuel tank might be possible, a fire hazard due to a leak is more of a concern. This is due to the volatility of gasoline and the hot surfaces of an ICE vehicle, such as the exhaust system. The associated HRR for gasoline peaks within seconds. Studies that have characterized pool fires for gasoline and ethanol have shown that as the amount of ethanol in a gasoline-ethanol blend increases, the heat flux and temperature of the pool fire decreases. A mixture with a higher ethanol content burns slower and has a lower flame height [32]. Diesel is much less volatile than gasoline and ethanol with a corresponding higher flash point. At normal ambient temperatures, diesel cannot be ignited without a very strong ignition source. Therefore, a diesel spill may not present as great a risk as a gasoline spill on the ground due to the lower chance of ignition from a higher vapor pressure. Yet leakage into the engine compartment after an impact or failure could still lead to a fire. This due to the hot surfaces such as the exhaust system or turbocharger assembly that has a large surface area. Also, diesel and gasoline have comparable auto-ignition temperatures [31].

With the fire and explosion hazards known, characterizing these hazards in tunnels can be addressed from reviewing and analyzing various incidents. There have been numerous major reported fire events in tunnels, in which many are caused by vehicle accidents and fires [33].

Table 6: Major ICE Road Tunnel Fire Incidents (from [34])

Year	Tunnel Information	Country	Comments
2007	Los Angeles Road Tunnel Interstate 5 167 m long Built in 1975	USA	Multiple big-rig trucks and passenger vehicles involved. Fire caused concrete spalling. 3 fatalities and 10 injuries [33].
2007	Melbourne Burnley Road Tunnel 3,400 m Built between 1996 and 2000	Australia	Vehicle collision due to shutdown lane and merging. The impact led to a reported fireball and one car bursting into flames. 3 fatalities [35].
2001	Gleinalm Road Tunnel 8.3 km Completed in 1978	Austria	Head on crash that led to a fire in the middle of the tunnel. 5 fatalities and 4 injuries [36].
2001	Gotthard Motorway Tunnel Opened in 1980	Switzerland	Head on crash that led to a fire in the tunnel. 11 fatalities and 19 injuries [33].
1999	Tauern Road Tunnel 6 km First bore completed in 1975. A second, parallel tube was officially opened in 2011	Austria	Vehicle crash that led to a fire in the tunnel. 12 fatalities and 49 injuries [37].

Table 6 shows more recent fire incidents in tunnels due to ICE vehicle collisions. The main cause of vehicular fires in road tunnels are engine fires, short circuits, ignition of flammable/combustible materials, collisions, and other defects. Collisions are mostly due to driver error. These major tunnel fires can result in a HRR above 20 MW. Fire temperatures can exceed 1000 °C and lead to quicker developing and spreading fires [34].

2.4. Pertinent Regulations and Safety Standards

Traditional fuel vehicles have robust safety standards and regulations with regard the vehicle itself and the roadway structures on which they operate for all ICE vehicles types.

2.4.1. National Fire Protection Association Standard 502

NFPA 502, *Standard for Road Tunnels, Bridges, and Other Limited Access Highways*, provides fire protection and life safety requirements as well as design criteria for authorities having jurisdiction (AHJs) to use in ensuring tunnel safety. Section 7.3.2 states that a tunnel shall be capable of withstanding the temperature exposure represented by the Rijkwaterstaat (RWS) time-temperature curve or other recognized standard time-temperature curve that is acceptable to the AHJ, as shown by an engineering analysis. The assumption is that every part of the tunnel should withstand these temperature exposures, irrespective of the fire location, ventilation rate, or ventilation type [38].

2.4.2. ASHRAE HVAC Applications Ch. 16: Enclosed Vehicular Facilities (2019)

American Society of Heating, Refrigerant, and Air-conditioning Engineers (ASHRAE) 2019 HVAC Applications Chapter 16: *Enclosed Vehicular Facilities* provides guidance on vehicular facilities that store vehicles and through which vehicles travel. These vehicles can be driven by an internal combustion engine or electric motors. Ventilation requirements including mechanical systems and natural ventilation, climate and temperature control, contaminant level control, and emergency smoke control. Additionally, ventilation concepts including normal operations and emergency operations are covered in this chapter [39].

2.4.3. NCHRP Guidelines for Emergency Ventilation Smoke Control in Roadway Tunnels (2017)

National Cooperative Highway Research Program (NCHRP) Guidelines for Emergency Ventilation Smoke Control in Roadway Tunnels Chapter 2: *Road Tunnel Fires* provides guidance on fire design parameters for tunnels. This includes consideration of the geometric parameters of the tunnel, fire protection features, and response times that leads to decision making using NFPA 502. Chapter 2 provides a framework on how to understand and determine fire and hazardous materials management in tunnels [40].

2.4.4. NCHRP Synthesis 415: Design Fires in Road Tunnels (2011)

National Cooperative Highway Research Program Synthesis 415*: Design Fires in Road Tunnels* provides review on current practices and knowledge for road tunnel fire designs. Additionally, a survey was completed by numerous transportation agencies and tunnel owners to understand their experiences and what practices they use for ventilation, fire protection, and detection [41].

2.5. Research Summary of Traditional Fuels in Tunnels

This section documents the results of the evaluations regarding ICE vehicle failure in a tunnel.

2.5.1. Experiments

A large variety of tests in tunnels have been conducted in response to the various incidents listed in Table 6. The tests in Table 7 are used to understand both the characteristics of a tunnel fire (such as temperature and HRR) and how different ventilation techniques affect these characteristics. Whether the fire is oxygen rich or oxygen lean will affect these characteristics, and these will drive the fire time and total damage done.

Table 7: List of Significant Full-Scale Tunnel Fire Tests (from [42])

Name	Type	Year	Country	Fire Source	Area	HRR	Ventilation
Ofenneg	Rail	1965	Switzerland	Gasoline Pool	24 m²	15-25 MW	natural, longitudinal, semi-transversal
Zwenberg	Rail	1976	Austria	Gasoline Pool	24 m²	15-25 MW	natural, longitudinal, semi-transversal
Rapperfijord	Mining Gallery	1990-1992	Norway	Train wagons, cars, HGV, calibrated fires	30-40 m²	15-100 MW	natural, transversal
Memorial	Road	1993-1995	USA	Diesel Oil Pool	60 m²	10-100 MW	natural, transversal
Colli Berici	Road	1999	Italy	Petrol/diesel oil pools, car mockup	60 m²	2-5 MW	natural
Rosa	Road	2002	Italy	Calibrated fires, cars, van	60 m²	2-20 MW	natural, longitudinal
Runehamar	Road	2003	Norway	Pellets, plastic, tires, HGV mockup	32.5 m²	70-200 MW	longitudinal

2.5.1.1. The Rijkswaterstaat (RWS) and Other Time-Temperature Curves

While tunnel design requirements are not specified for metrics such as overpressure, standard fire curves are used to design for road tunnel safety. This process typically involves selecting an expected type and size of fire and determining the distribution of temperature exposure to the construction materials. For example, the International Organization for Standardization (ISO) 834 curve represents a fully developed fire in a compartment, based on materials found in standard buildings. The ISO curve is what the World Road Association (PIARC) and the International Tunneling Association recommend for defining tunnel design criteria for personal vehicles and vans [43].

Because the ISO 834 curve does not represent all materials, especially chemicals which escalate fire growth, a hydrocarbon curve was developed in the 1970s for use in the petrochemical and off-shore

industries and began to be applied to tunnels [44]. The hydrocarbon curve (HC curve) exhibits a faster fire development and consequently is associated with faster temperature increase than the standard ISO 834 curve. The modified hydrocarbon curve (Mod. HC curve) exhibits an even faster fire development and is more conservative than the ISO 834 or the standard HC curve. The Mod. HC Curve is used for stricter regulations and has a much more severe temperature gradient over the first few minutes [45].

The RWS curve was developed during extensive testing conducted by the Dutch Ministry of Transport in cooperation with the Netherlands Organization for Applied Scientific Research (TNO) in the late 1970s. The RWS curve simulates an accident involving a gasoline tanker loaded with 45,000 liters (45 m^3) of gasoline with a fire load of approximately 300 MW released over two hours. The ISO 834, hydrocarbon, and RWS fire curves are illustrated in Figure 2. Also included in Figure 2 are the ASTM E119, *Standard Test Method for Fire Test of Building Construction and Materials*, and the UL 1709, *Standard for Rapid Rise Fire Tests of Protection Materials for Structural Steel,* time-temperature fire curves for comparison [46] [47].

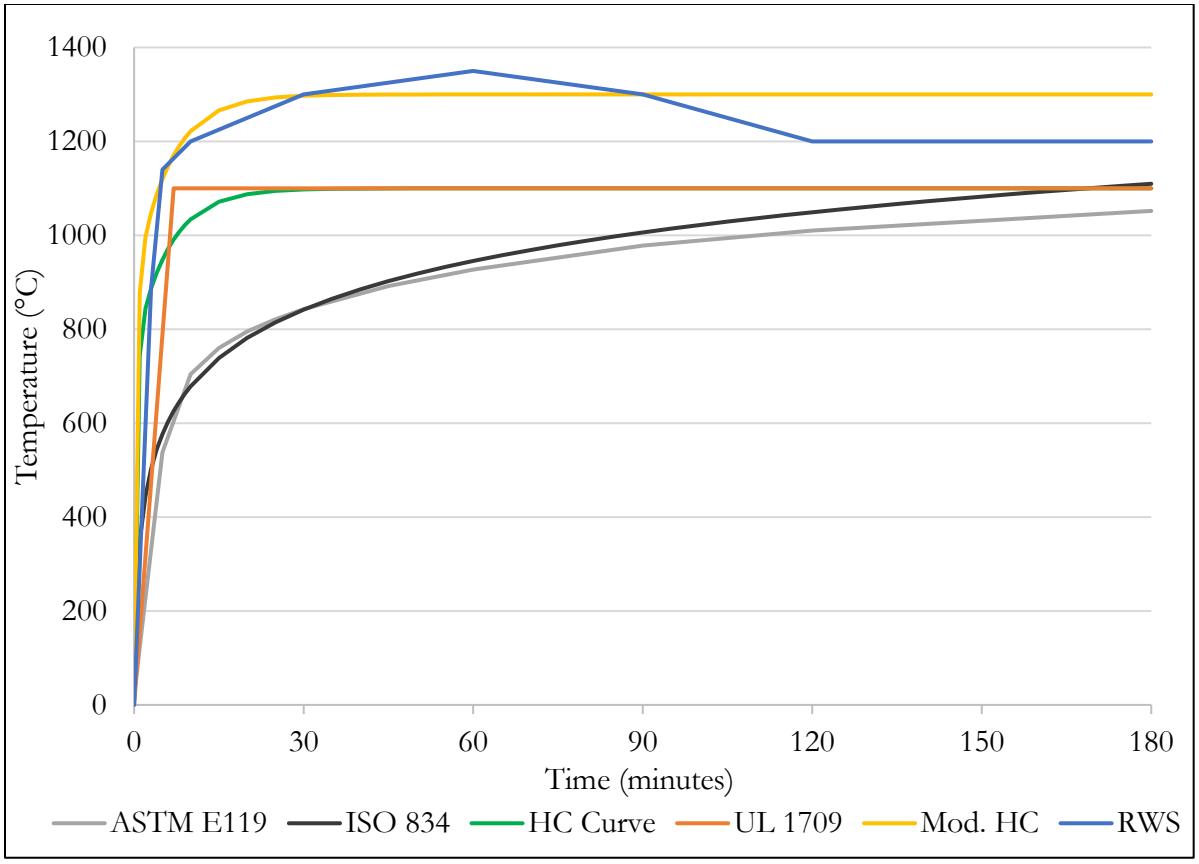

Figure 2: Standard time-temperature fire design curves at tunnel structure interfaces

2.5.1.2. The Runehamar Full Scale Tests

In September 2003, a European research program on tunnel safety conducted comprehensive large-scale fire tests in the abandoned Runehamar road tunnel in Norway [44] [48] [49]. These fire tests were intended to analyze fires from the cargo of heavy goods vehicle (HGV) trailers, which might

contain a large fuel source for fire. The fuel load of HGV and traditional vehicles contain hydrocarbons and hydrocarbon-based materials (e.g., tires, plastics, etc.) which form very sooty fires where radiation is the over-riding method of heat transfer to the surrounding materials.

The Runehamar tunnel is approximately 1,600 m long, 6 m high, and 9 m wide. The center of the fire was located 172 m from one entrance. Two mobile fan units were added to simulate ventilation, providing a velocity of about 3 m/s (centerline) in the tunnel. Because of the exposure to high temperatures, the tunnel was protected using PROMATECT–T fire protection boards over 75 m that were supported with a light steel structure. Fire sprinklers were not installed in the tunnel. Two small ignition sources, consisting of fiberboard cubes soaked with heptane, were placed within the lowest wood pallets. A total of four tests were performed with a fire in a semi-trailer set-up. In the trailer, four different commodities were tested, shown in Table 8. All tests produced time-temperature developments in line with the RWS curve, as stated in NFPA 502.

Table 8: Commodities used as fuel in the HGV tests (from [49])

Test #	Description of the fire load	Target	Peak HRR (MW)
0	200 L diesel pool fire with a 2.27 m diameter	-	6
1	360 wood pallets (1,200 x 800 x 150 mm) 20 wood pallets (1,200 x 1000 x 150 mm) 74 polyethylene (PE) plastic pallets (12,200 x 800 x 150 mm)	32 wood pallets and 6 PE pallets	200
2	216 wood pallets 240 polyurethane (PUR) mattresses (1,200 x 800 x 150 mm)	20 wood pallets and 20 PUR mattresses	160
3	Furniture and fixtures (tightly packed plastic and wood cabinet doors, household items) 10 large rubber tires (800 kg)	Upholstered sofa and arm rest	135
4	600 corrugated paper cartons with interiors (600 mm x 400 mm x 500 mm) 15% of total mass of unexpanded polystyrene (PS) cups (18,000 cups) and 40 wood pallets	4 wood pallets and 40 cartons with PS cups (1,800 cups)	65

Test 0 used a 200 L diesel pool fire with a 2.27 m diameter. Four other tests included various commodities such as wood pallets, mattresses, furniture, and more. Comparing the diesel pool fire with the other commodities shows that diesel might not have a large peak HRR, but it does quickly reach a peak and plateaus. While the intent of the diesel pool fire was for a baseline for calibration and checking instruments, it does show how large commodities are more of a hazard in terms of the peak HRR compared to the diesel pool fire. This also shows that since the HRR of diesel peaks quicker than the commodities, a diesel fire might lead to ignition of other fuel loads in a tunnel during a leak or spillage.

Test 1 with wood pallets and plastic pallets had the highest HRR, with a peak of 200 MW. The HRR is the most important variable in characterizing the flammability of products and their consequent fire hazard because it captures the driving force for the fire (i.e., power). Most other variables (temperature, smoke, toxic gases) are correlated to HRR which can also be linked to the severity of the fire [50]. Figure 3 illustrates the HRRs for the four large-scale tests. Figure 4 illustrates gas temperatures in the first test, which had the highest temperatures out of the four tests, compared

with four different standard fire curves. The maximum gas temperatures beneath the ceiling were approximately 1350°C.

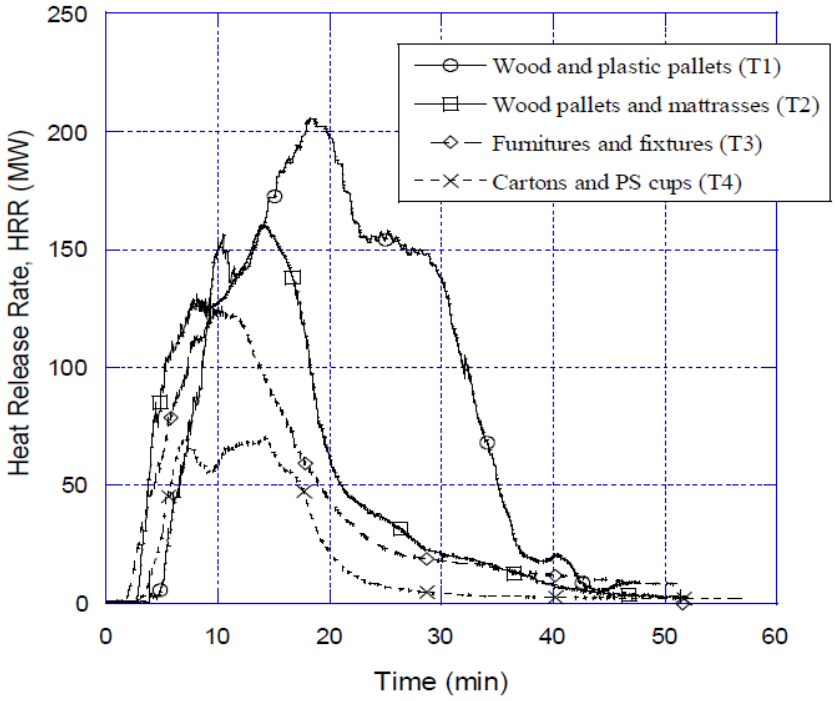

Figure 3: Heat release rates from the four large-scale fire tests (from [49])

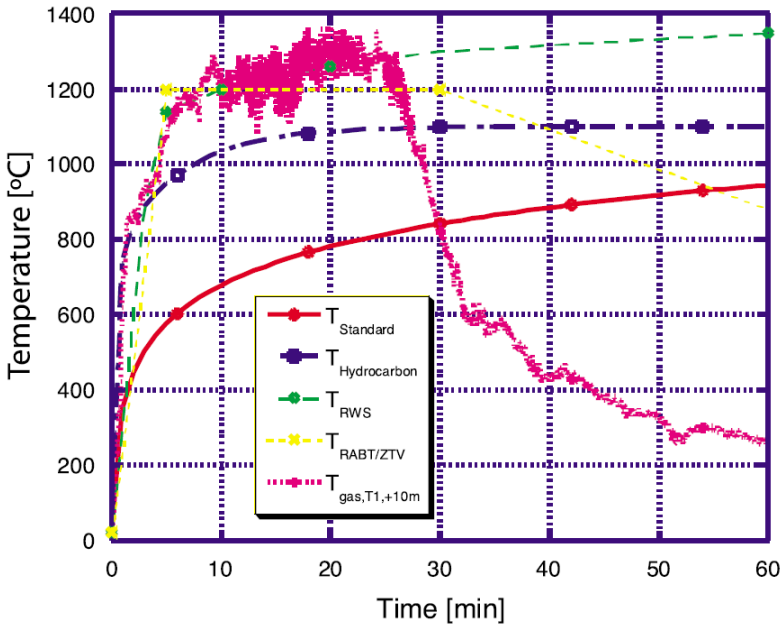

Figure 4: Test 1 temperature compared with standard fire curves (from [49])

Figure 4 shows the gas temperature from the wood and plastic pallets test shown in Figure 3 (labeled $T_{gas,T1}$) along with the HC ($T_{Hydrocarbon}$), RWS (T_{RWS}), RABT ZTV ($T_{RABT/ZTV}$) and ISO 834 ($T_{Standard}$) fire curves. The results from the Runehamar tunnel tests show that non-hazardous, solid commodities can give a fast increase in temperatures to significantly higher temperatures than had

been measured in connection with solid material in tunnel fire tests previously [44]. The temperatures measured in the post-flame gases downstream of the fire were high and the measurements indicate that the flaming zone could expand up to a length of 70-100 m. The high surface temperatures affected the entire tunnel ceiling downstream of the fire causing considerable spalling of the unprotected tunnel ceiling after the first test, which resulted in considerable rock debris completely covering the road. The long flames and high temperatures could also cause the fire to spread to other vehicles.

2.5.1.3. Large Scale Fire Tests in the Second Benelux Tunnel

Testing was conducted in 2000-2001 in the Second Benelux Tunnel in the Netherlands [51]. A total of fourteen full-scale tests were conducted. The intent of these tests was to determine conditions for escaping motorists along with how well ventilation, detection, and suppression systems operate. A multitude of measurements were collected such as temperature, radiant heat, smoke velocity, smoke density, and HRRs. The first four tests were pan fires using a mixture of 60% *n*-heptane and 40% toluene by mass. The next six tests consisted of cars and covered truck loads, with the loads consisting of 800 kg of wooden pallets and four tires. Ventilation through the tunnel varied stepwise from 0 m/s to 6 m/s. The final set of tests determined the effect of a deluge sprinkler system and examined the effect of delayed activation, effectiveness of the sprinkler system, and if the sprinkler system would prevent fire spread to other vehicles.

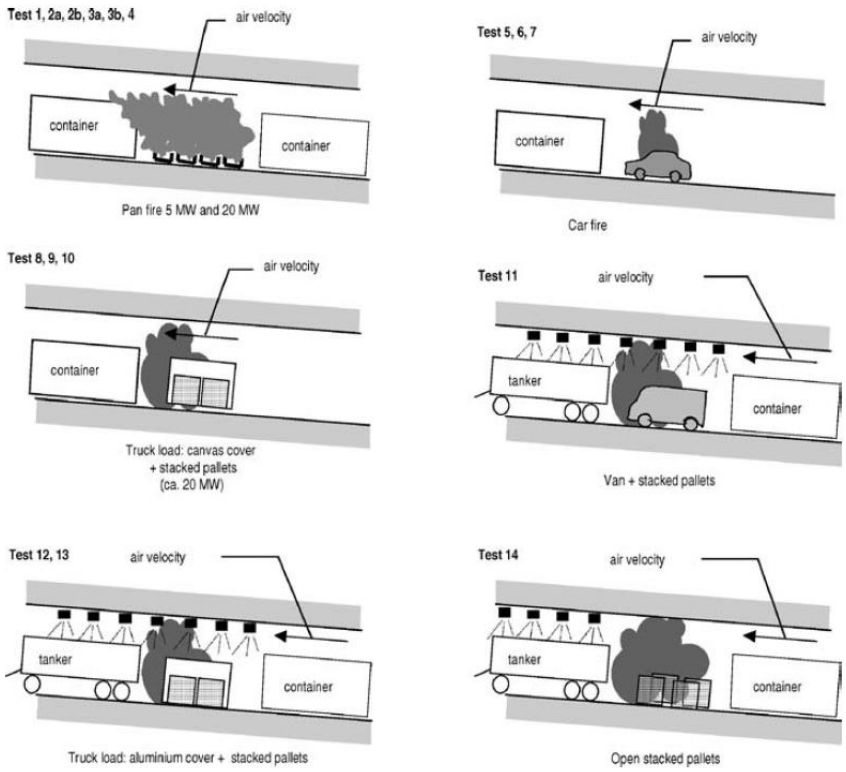

Figure 5: Test Overview for Second Benelux Tunnel (from [51])

Figure 5 shows the test configurations in the Second Benelux Tunnel. The report does not specify if any fuel was in the vehicles during the testing. Since the intent was to compare ventilation and obstructions of ventilation, the total commodity fuel load stayed nominally the same between tests.

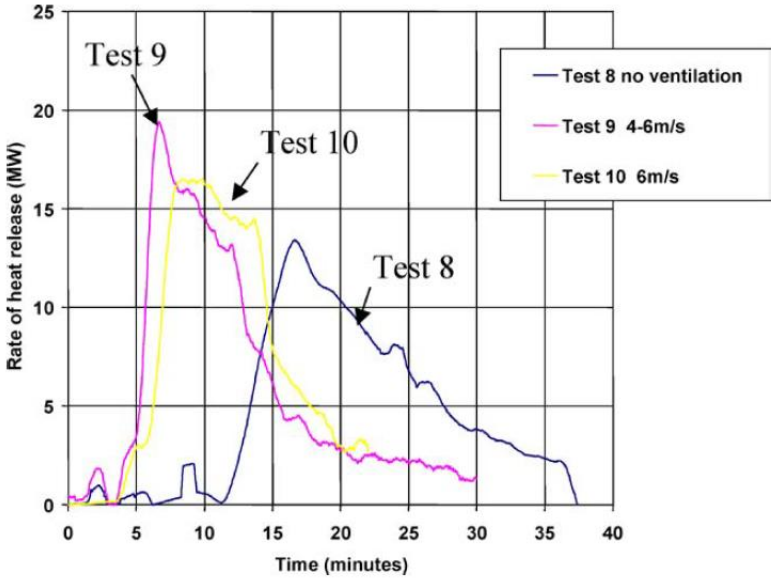

Figure 6: Fire development for small truck fires (from [51])

Figure 6 shows the effect of ventilation on the HRR of a small truck fire. As the ventilation increases, the peak HRR increases, but the total time from ignition to extinction decreases. This type of testing helps provide data for determining emergency ventilation controls.

2.5.2. Modeling

Different models for tunnel fires have been created using both computational fluid dynamic (CFD) programs and using other tools such as the zoning modeling tool Consolidated Model of Fire and Smoke Transport (CFAST), an open-source software package National Institute of Standards and Technology (NIST). CFAST is a zoning model that is used to evaluate the evolving distribution of smoke, fire, gases, and gas temperatures [52].

2.5.2.1. Simulation of Tunnel Fires Using a Zone Model

Modeling by Chow et al. [53] used CFAST to understand how zoning the tunnel into multiple sections compares with other similar CFD studies and experimental data. Various modeling has been conducted to understand the effect of smoke movement and temperature effects [53]. Different zoning methods were used with CFAST 2.0. Five different fire simulations were used for each zoned model: wood fire, passenger train fire, subway coach fire, truck fire, and a school bus fire. Smoke layer and temperature predictions were created with the different zoned sections: single compartment along with multiple compartment configurations designated as 2-room and 3-room. Figure 7 below gives a visual for each of these configurations as well as the spatial relationship between them.

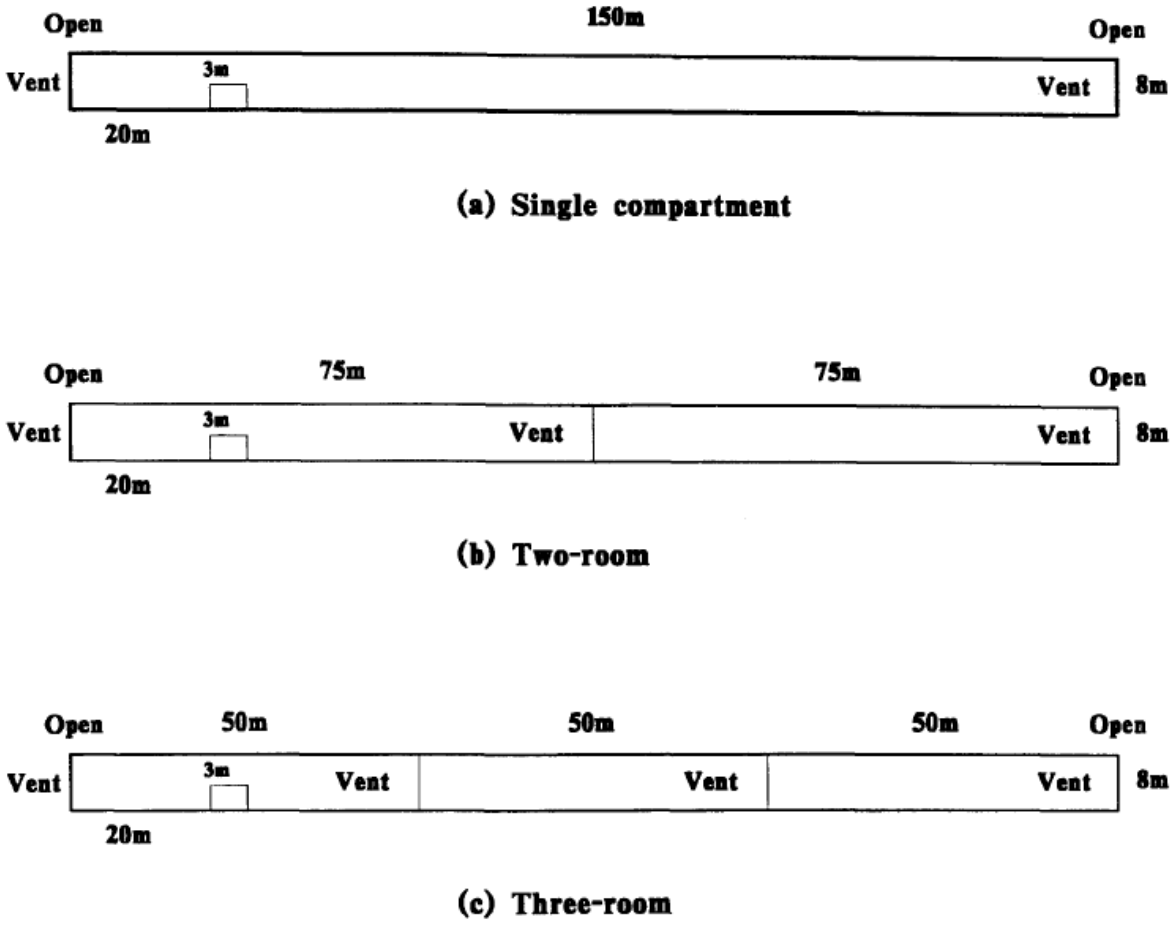

Figure 7: Compartment Configurations (from [53])

Figure 8 and Figure 9 below show the smoke temperature and layer height for the various zoned configurations for the truck fire. The colored and numbered circles are to help identify the smoke temperature and layer heights based on which configuration was used (single compartment, two-room, or three-room). The averages for the two and three-room configurations are very close to the single compartment configuration for both the truck and bus fire characteristics.

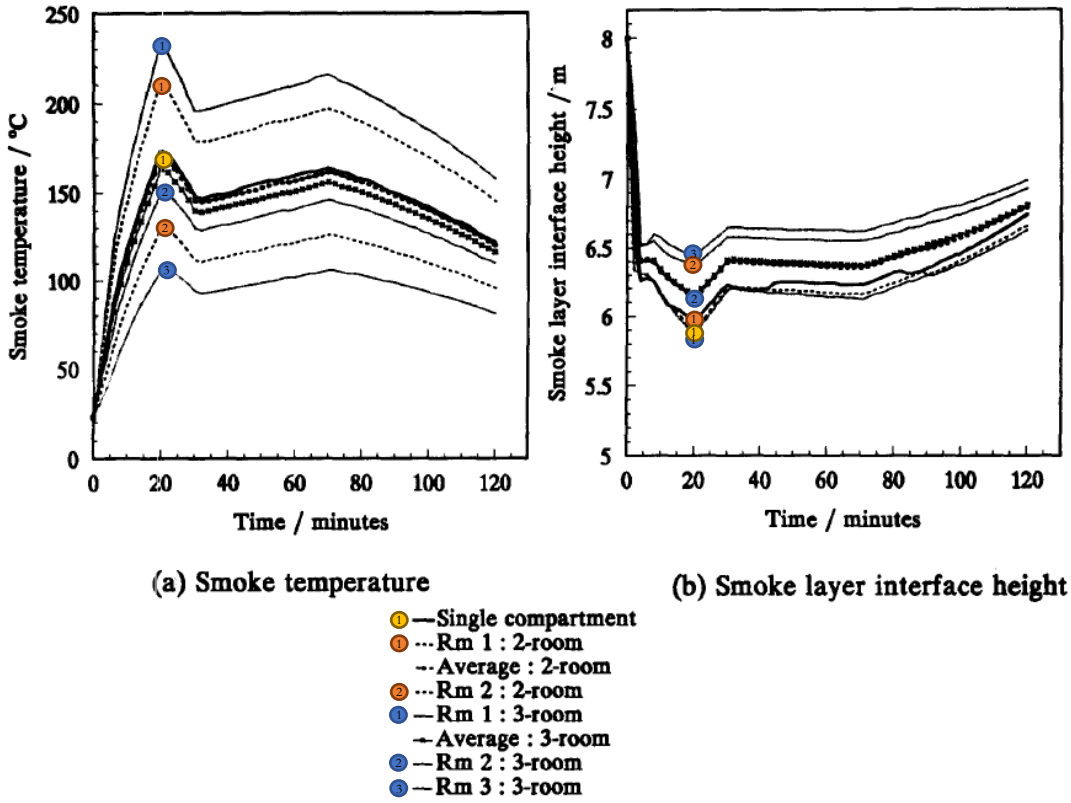

Figure 8: Smoke Characteristics Prediction of a Truck Fire (from [53])

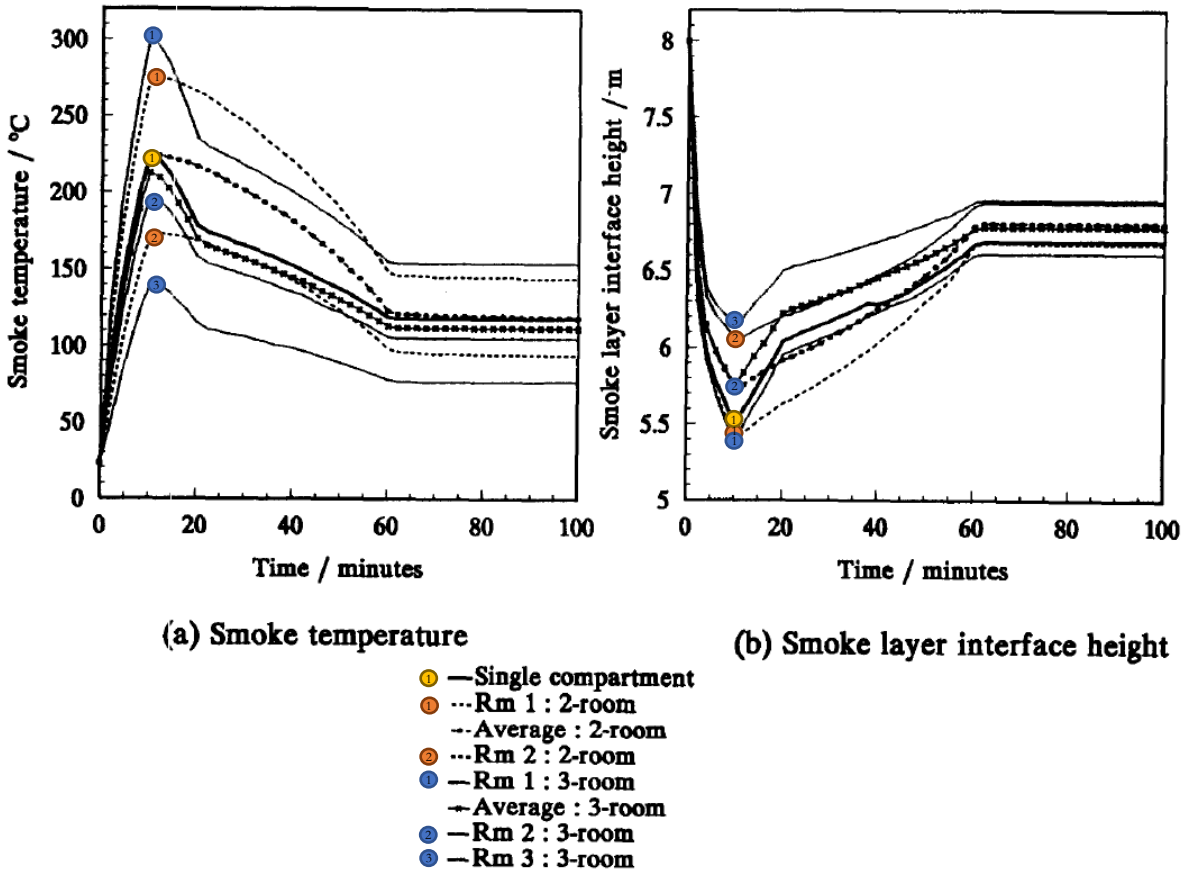

Figure 9: Smoke Characteristics Prediction of a School Bus Fire (from [53])

The CFAST models were validated with a tunnel fire experiment in Norway and compared with other models. It was determined the CFAST model gives similar results to other known fire models such as Consolidated Compartment Fire Model (CCFM.VENTS) on predicting the smoke temperature and layer interface heights. The CFAST zone model is a good baseline prior to using a more computationally heavy CFD program. By using a zoning technique as described by Chow et al. [53], the fire environment can be predicted. This can be used to design tunnel ventilation systems and suppression systems and where to add heat and smoke detecting devices based on the smoke temperature and spreading characteristics.

2.5.3. Analysis

Different studies have analyzed the various parameters of tunnels and how they affect the fire and smoke characteristics. A study by Haghighat et al. [54] goes over the effect of ventilation and tunnel cross-sectional area on fluid properties down-stream of a fire using CFD data. A study by Shafee et al. [55] determines how tunnel inclination, blockage, and ventilation effects the HRR of a fire.

2.5.3.1. Determination of critical parameters in the analysis of road tunnel fires

The intent of this study was to use CFD model data to determine fluid characteristics downstream from a fire in a tunnel. The selected characteristics to study in this analysis were the average temperature, the average density, the average viscosity, and the average velocity. How different

parameters interact with these response variables is determined [54]. The HRR was selected based on NFPA 502 recommended peak HRR for a bus or van. The HRR varied between 10 MW and up to 30 MW. It was determined the overall physical fire size, regardless of the HRR and fire intensity, did not influence the response variables downstream of the fire. The tunnel dimensions do affect the average temperature and density up to 220 m downstream and are insignificant at 400 m downstream. The inlet velocity does influence the average temperature and the average density drastically at 20 m and 400 m downstream of the fire source. The average velocity downstream of a fire is dependent on both the inlet velocity and the HRR.

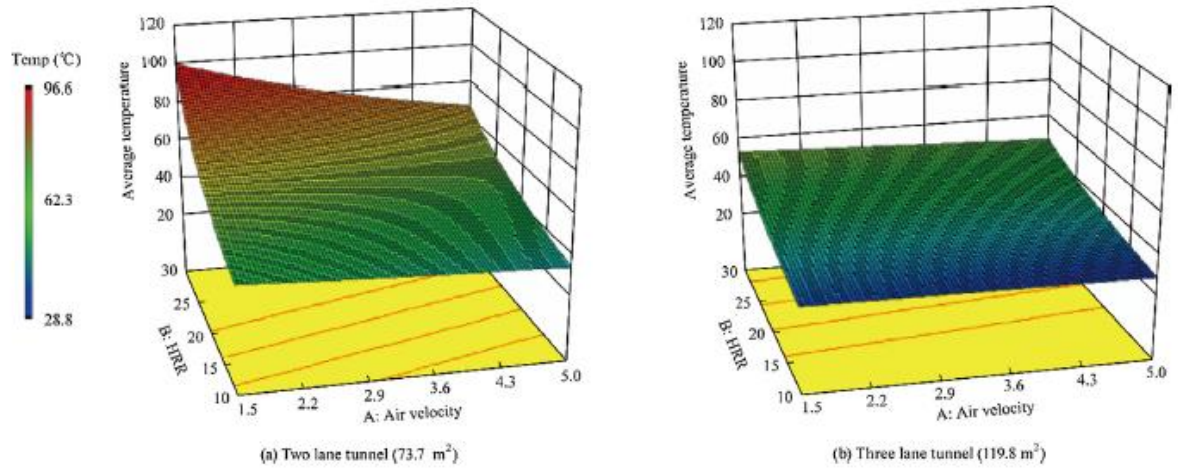

Figure 10: Tunnel Dimension Effect on Average Temperature (from [54])

This study by Haghighat et al. [54] proves to be useful for understanding what parameters effect the overall characteristics downstream of a tunnel fire for different burning vehicles. This helps analyze tunnel design, ventilation sequences, and firefighting techniques.

2.5.3.2. An analysis of tunnel fire characteristics under the effects of blockage

Ethanol pools were used in a study by Shafee et al. to understand how blockage, slopes, and ventilation rates effect the overall HRR, burning rate, and smoke back-layering [55]. The downhill and uphill slopes effect the fire-induced buoyancy effects. This study helps understand the downhill inclination effect on critical ventilation velocity and compares the results of this inclination with a horizontal study. Using a small-scale or reduced-scale test, these different parameters could be changed for each test.

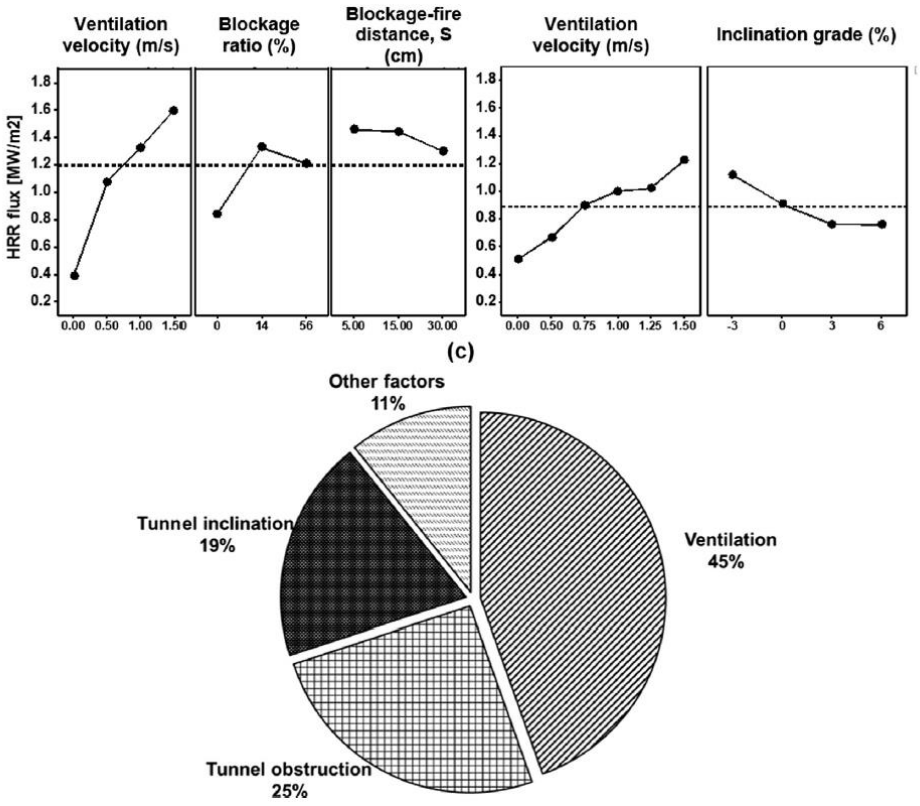

Figure 11: Mean Effect on HRR Flux (from [55])

The plot above is from Shafee et al. [55] and shows the overall effects of the inclination, blockage ratio, and ventilation velocity on the HRR. This study shows blockage and inclination do influence the overall HRR, but the ventilation velocity is a more important factor (45% overall mean effect) in controlling the overall HRR. The higher the mean effect, the more sensitive the HRR is to a smaller increase in that specific variable. The tunnel blockage effect accounted for 25% of the mean effect and the inclination accounted for 19%. The other factors that contribute to 11% mean effect include the blockage distance from the fire. The HRR flux decreases as that blockage distance increases from 5 cm to 30 cm. But there is less than a 0.2 MW/m^2 change with a 25 cm increase in the blockage distance. An increase in the ventilation velocity from 0.0 to 1.5 m/s multiples overall HRR flux by four from 0.4 MW/m^2 to 1.6 MW/m^2.

2.6. Traditional Fuels Research Gaps

Traditional fueled vehicles have been thoroughly studied for many years, with studies on the various time-temperature curves and how they are applied. Additionally, different studies have supported model development as well as understanding ventilation requirements. This section went through a variety of studies, but there are many more available for traditional fuels. As different fuel blends become available, such as ethanol and biodiesel, more work should be completed to further understand the consequence of these fuels. Additionally, as engine technology advances, combustion processes may require future work to help determine how higher temperatures and leaner mixtures might be a scenario that leads to a fire. This is discussed further in the research gaps below.

The following criteria were evaluated to determine where research gaps may exist regarding Traditional Fuel ICE powered vehicles in tunnels.

1. Scenario Identification
2. Failure Modes
3. Consequences
4. Validation

Scenarios that lead to failure modes have been determined as engine bay fires initiated by collisions or various vehicle defects (such as short circuits) as well as flammable or combustible materials igniting on the vehicle. A variety of incidents involving ICE vehicles in tunnels has led to a greater understanding of what the failure modes are. Collisions are mostly due to driver error while other initiating events are either due to collision or defects. Experiments such as those listed in Table 7 show the failure modes of various fuel spillages along with commodities that have been characterized in tunnels.

The consequence of these failures has led to major tunnel fires that can result in a HRR above 20 MW. Fire temperatures can exceed 1000 °C and lead to quicker developing and spreading fires [34]. Using real scenarios such as vehicle crashes or malfunctions has driven studies and experiments on tunnel fire characteristics of ICE vehicles. Some tunnel studies just involve fuels such as diesel and gasoline [49] [55] while other studies include other commodities or whole vehicles [51]. Typically, experiments are compared with the standard modeled time-temperature curves in order to validate the models. This comparison also helps understand how the model characteristics are different than that of the experiment. Preliminary findings from traditional fuel fires are shown in the study by Shafee et al. [55] in which a variety of parameters such as ventilation were increased to understand how the heat release rate changed (shown in Figure 11). Additionally, Lemaire and Kenyon [51] show that as the ventilation increases, the HRR also increases but the total time of the fire decreases.

Various sizes or classifications of vehicles have been involved in both real scenarios as well as testing to further understand how a passenger vehicle compares to a cargo-type vehicle regarding tunnel fires. The properties of gasoline, diesel, ethanol, and blends of these fuels are known and well regulated. For example, vapor pressure is closely regulated to ensure emissions and engine startup are controlled. This is important when designing fuel tanks systems to ensure a flammable mixture is not developed above the liquid fuel. Typically, the concentration above the liquid fuel exceeds UFL. Most of the failures and consequences from ICE vehicle fires in tunnels are well known through actual scenarios and further understood through testing and modeling. Yet the following research gaps have been identified:

- As ICE emission technology evolves, such as using technologies such as particulate filter regeneration, recirculating exhaust gases, and running vehicles with a leaner fuel mixture, further study of the effect on exhaust system component temperatures may be needed. Fuel spillage might accumulate directly under the vehicle and it is important to understand how higher exhaust temperatures might lead to potential ignition sources.
- Future technologies, such as compression-ignition gasoline engines or advanced forced air induction, might also lead to increased exhaust component temperature.
- As engine components advance, the ability to run hotter from leaner mixtures and higher pressures could lead to an increase in engine bay temperatures, which might increase potential ignition sources.

This page left blank

3. BATTERY ELECTRIC VEHICLES

3.1. Overview of Technology

Battery electric vehicles (BEVs) offer consumers an alternative transportation option to conventional internal combustion engines (ICE). In these vehicles, the internal combustion engine and powertrain system is replaced by an electrical powertrain. Plug-in hybrid electric vehicles (PHEVs) offer an electric motor powered by batteries with an onboard combustion engine that can charge the battery system when it gets depleted. The battery is charged through a cable connection when the vehicle is parked and not operating. Generally, BEVs offer many benefits such as high efficiency, no harmful tailpipe emissions, good performance, and low cost "refueling" (electricity through charging) [56].

BEVs utilize an electrochemical storage system in which energy is converted between electrical and chemical energy through a reversible process. This is done with a battery system consisting of lithium-ion or lithium secondary cells. The battery cells generally consist of a case, an anode and a cathode which are electrodes, a separator, and an electrolyte. Each of the different battery types consist of different materials for the casing, electrodes, and electrolyte, which result in varying performance and cost.

There are several different battery technologies in BEVs that offer a range of energy density, power density, cycle life, and calendar life. The lithium-ion or lithium secondary battery technology is regarded as the most promising because of its high energy density, high efficiency, and long lifespan. Unlike lithium or lithium primary cells that are disposable, lithium-ion or lithium secondary cells are rechargeable, making them suited for BEVs.

Table 9: Comparison of Lithium and Lithium-Ion Cells

Lithium (Primary)	Lithium-Ion (Secondary)
One-time use	Rechargeable
Smaller light weight applications	Custom, larger scale application
Metallic lithium as the Anode	Porous carbon as Anode

In addition to lithium-ion batteries, there are also lead acid, nickel metal hydride (Ni-MH), nickel cadmium (Ni-Cd), and sodium nickel chloride ($Na\text{-}NiCl_2$) battery technologies that have been used/considered for use in BEVs. However, there are limitations associated with each of these battery types that make them less desirable for future designs than the lithium-ion battery due to lower specific energy or specific power capabilities [56]. There are several different types of BEVs currently in operation, including buses, trucks, vans, and cars.

3.2. Properties of Lithium-ion Batteries

As discussed previously, lithium-ion batteries are considered the most promising battery technology due to the high energy density and light weight compared with other battery technologies mentioned above. This is further illustrated in Figure 12 below:

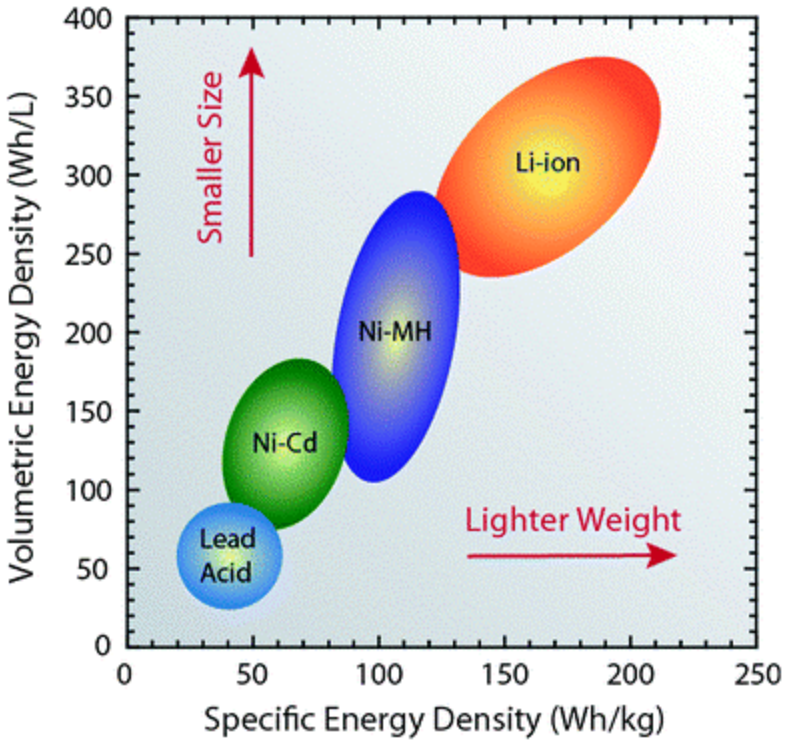

Figure 12: Battery Technology Energy Densities (from [57])

There are several different types of electrodes and electrolytes used in lithium-ion batteries. However, Figure 13 shows the general chemistry of the battery. As shown, during recharging operations, the positively charged lithium travels from the cathode to the anode through the electrolyte then combines with the charging electrons, which forms a lithium atom that gets deposited between carbon layers. This process is reversed during discharging activities [58].

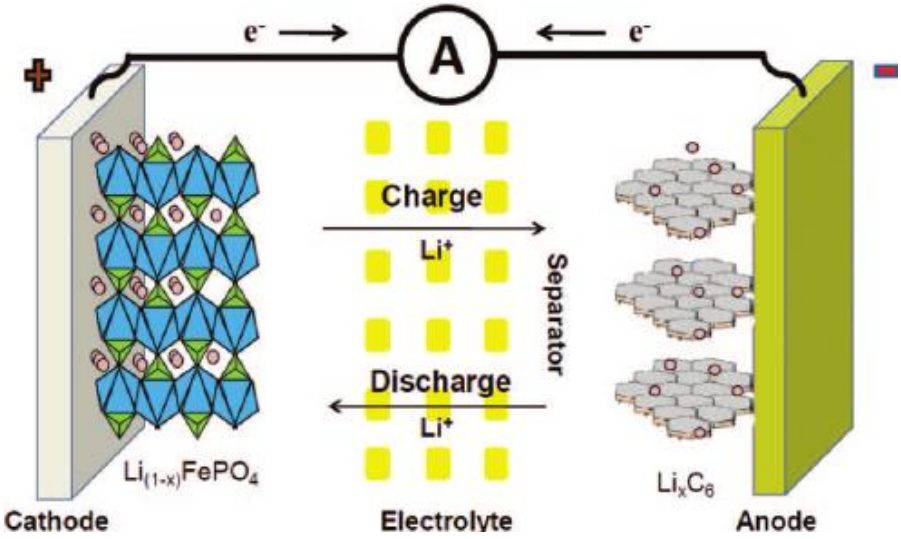

Figure 13: Lithium-ion Battery Chemistry (from [59])

Technology improvements for lithium-ion battery types are the most promising. A battery system is broken down into various sub-systems and sub-components as follows:

- Lithium-Ion (Lithium Secondary) Cell
    - Varies capacities, chemistries, form factors, manufacturers, etc.
- Module
    - Houses cells in various configurations
- System Casing/Housing
    - Houses complete battery system comprising of modules
- Battery Management System
    - Thermal management
    - Determines charging/discharging routines
    - Monitors system health
    - Controls State of Charge (SOC)

Different cathode chemistry varieties of the lithium-ion battery offer different battery characteristics: lithium cobalt oxide (LCO), nickel cobalt and aluminum (NCA), nickel manganese cobalt (NMC), lithium iron phosphate (LFP), lithium manganese oxide (LMO), lithium polymer and lithium ion phosphate offer different advantages and disadvantages in terms of power, energy density (Wh/kg), specific volume (m^3/kg), safety, and calendar and cycle life. Additionally, the various electrolytes such as ethylene carbonate (EC), dimethyl carbonate (DMC), ethyl methyl carbonate (EMC), diethyl carbonate (DEC), propylene carbonate (PC), and methyl propyl carbonate (MPC) offer different performance characteristics and have varying safety metrics. These are discussed in Section 3.3.2.

3.3. Associated Hazards

A catastrophic failure of the battery system can occur due to manufacturing defects, thermal abuse, electrical abuse, or mechanical damage.

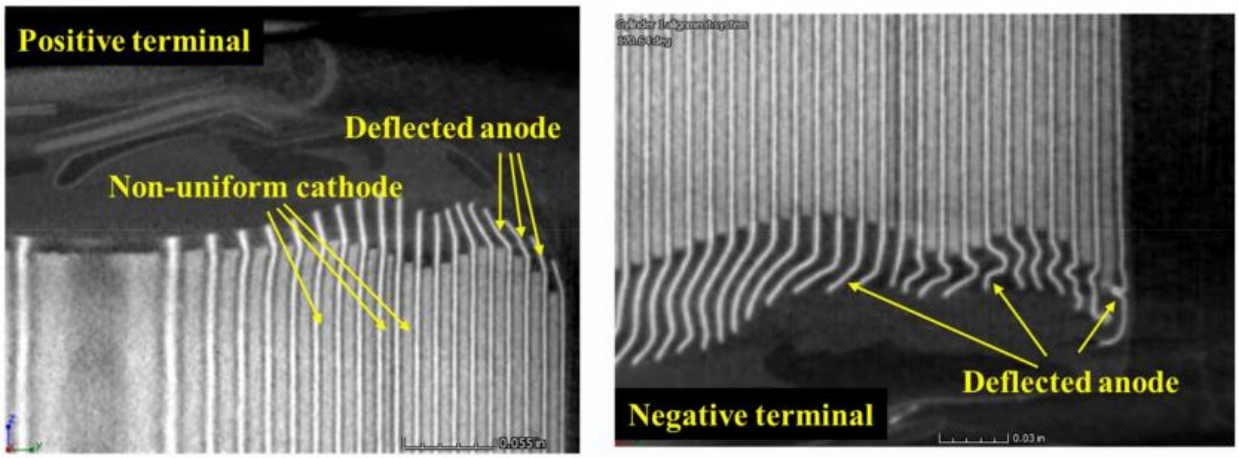

Figure 14: 18650 Cell Defect (from [60])

Figure 14 shows defects in an 18650 cell in both the cathode and the anode. An 18650 cell is a designation for a cylindrical cell that compares to a AA battery in terms of the form factor. Manufacturing defects could cause cells to have shorter overall life cycles, and when used in a

battery module, this could cause an imbalance of charge amongst cells and premature cell failure. Thermal abuse can be caused by failing or malfunctioning cooling or thermal management systems. Electrical abuse might occur if the battery management system incorrectly charges/discharges/cycles the cells. Mechanical damage could occur during an impact. Other mechanical abuse such as long-term vibrations might cause cells to have excess wear and create an internal or external short circuit.

Table 10 below gives an overview of the types of abuse testing that each standard provides guidance on by Ruiz et al. [61]. These are general practices and examples of standards that should be used to better understand the safety implications of these battery systems at various levels. The letter designations are the following: C-Cell level testing, M-Module level testing, P-Pack level testing and V-Vehicle level testing.

Table 10: Overview of Test Standards for Lithium-ion Battery Abuse (from [61])

	Test	SAE J2464 [62]			SAE J2929 [63]				UL 2580 [64]			FreedomCAR [65]		
Mechanical	Mechanical Shock	C	M	P	C	M	P	V	C	M	P	-	M	P
	Drop	-	-	P	-	-	P	-	C	-	P	-	-	P
	Penetration	C	M	P	-	-	-	-	-	-	-	C	M	P
	Immersion	-	M	P	-	-	P	-	-	M	P	-	M	P
	Crush/crash	C	M	P	-	-	P	V	C	M	P	C	M	P
	Rollover	-	M	P	-	-	P	-	-	-	P	-	M	P
	Vibration	-	-	-	C	M	P	-	C	M	P	C	M	P
Electrical	External Short Circuit	C	M	P	-	-	P	-	C	M	P	C	M	P
	Over Charge/Discharge	C	M	P	-	-	P	-	C	M	P	-	M	P
Environmental	Thermal Stability	C	-	-	-	-	-	-	C	-	-	C	M	P
	Thermal Shock/Cycling	C	M	P	C	M	P	-	C	M	P	C	M	P
	Overheat	-	M	P	-	-	P	-	-	-	-	-	-	-
	Fire	-	M	P	-	-	P	-	C	M	P	C	M	P
Chemical	Emissions	C	M	P	-	-	P	-	C	M	P	C	M	P
	Flammability	C	M	P	-	-	P	-	C	M	P	C	M	P

Certain failure modes within lithium-ion cells can lead to an exothermic reaction within the sealed cell. Examples of these failure modes include mechanical damage, manufacturing defect, overcharging/discharging, and/or over cycling. These reactions can lead the cell into thermal runaway. This is due to a series of exothermic reactions that increase the cell temperature, resulting in internal generation of gases. This builds pressure in the cell and can ultimately lead to rupture and a release of vent gas. Propagation of failure from the cell-to-cell chain reactions may occur due to

the thermal energy release from the failed cell. This can cause the entire module, pack, and system to go into thermal runaway. Studies such as the one conducted by Lopez et al. [66] in 2015 studied 18650 cells and prismatic cells in order to determine separation distances that would prevent cell-to-cell thermal runaway propagation. Based on various cell and tab configurations, it was recommended to maintain at least 2 mm of space in between cells to minimize the chance of thermal runaway propagation.

There are examples of safety devices to help prevent failures that lead to thermal runaway. One such example is the internal positive temperature coefficient (PTC) current limiting device used in the 18650 cells in a Tesla Roadster [67]. The only downside is that once the PTC activates, the state of charge can no longer be measured when disposing of this cell. A study by Balakrishnan et al. [68] in 2006 goes over other safety mechanisms associated with lithium-ion batteries. Safety vents relieve internal pressure build up in a cell that has failed. Built-in internal thermal fuses will melt when excess current flows through the cell, leaving the cell permanently disabled. Cell charge balancing can also be controlled by measuring and terminating charging/discharging to a specific cell in a module. This helps protect cells in a module from being overcharged/overdischarged. These are some examples of ways to help mitigate or slow thermal runaway between cells.

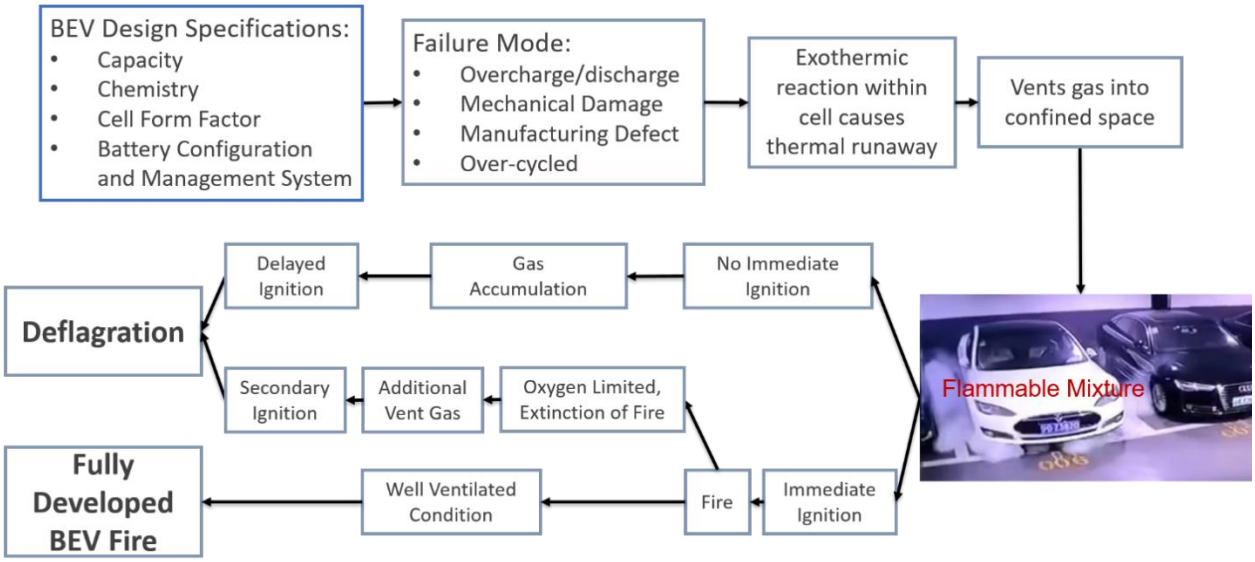

Figure 15: BEV Failure Event

Figure 15 shows how system design can lead to the generation of a flammable mixture and an eventual fire or deflagration from a BEV failure. In the event a failure occurs in a BEV and based on the confinement, the vent gas can accumulate. Based on factors such as gas species, gas concentration, release rates, and total vent gas volume, a flammable mixture can occur. With immediate ignition, a fire may occur that consumes surrounding oxygen and can lead to under-ventilated fire extinction. More vent gas can be produced from other cells that have failed. Based on confinement, this will determine if a fire scenario or deflagration/explosion scenario will exist. If the vehicle is in a well-ventilated area, with immediate ignition, a fully developed fire may occur. If vent gas can continue accumulating in a confined space, secondary ignition may cause a deflagration. There might be both a fire and deflagration that occurs or just one of them.

3.3.1. *Vent Gas Hazards*

It is already well known that battery systems such as lead-acid batteries can produce off-gas or vent gas such as hydrogen. What makes lithium-ion batteries unique is the large variation in not only the species of gases produced when venting, but also the variation in volume production and rate.

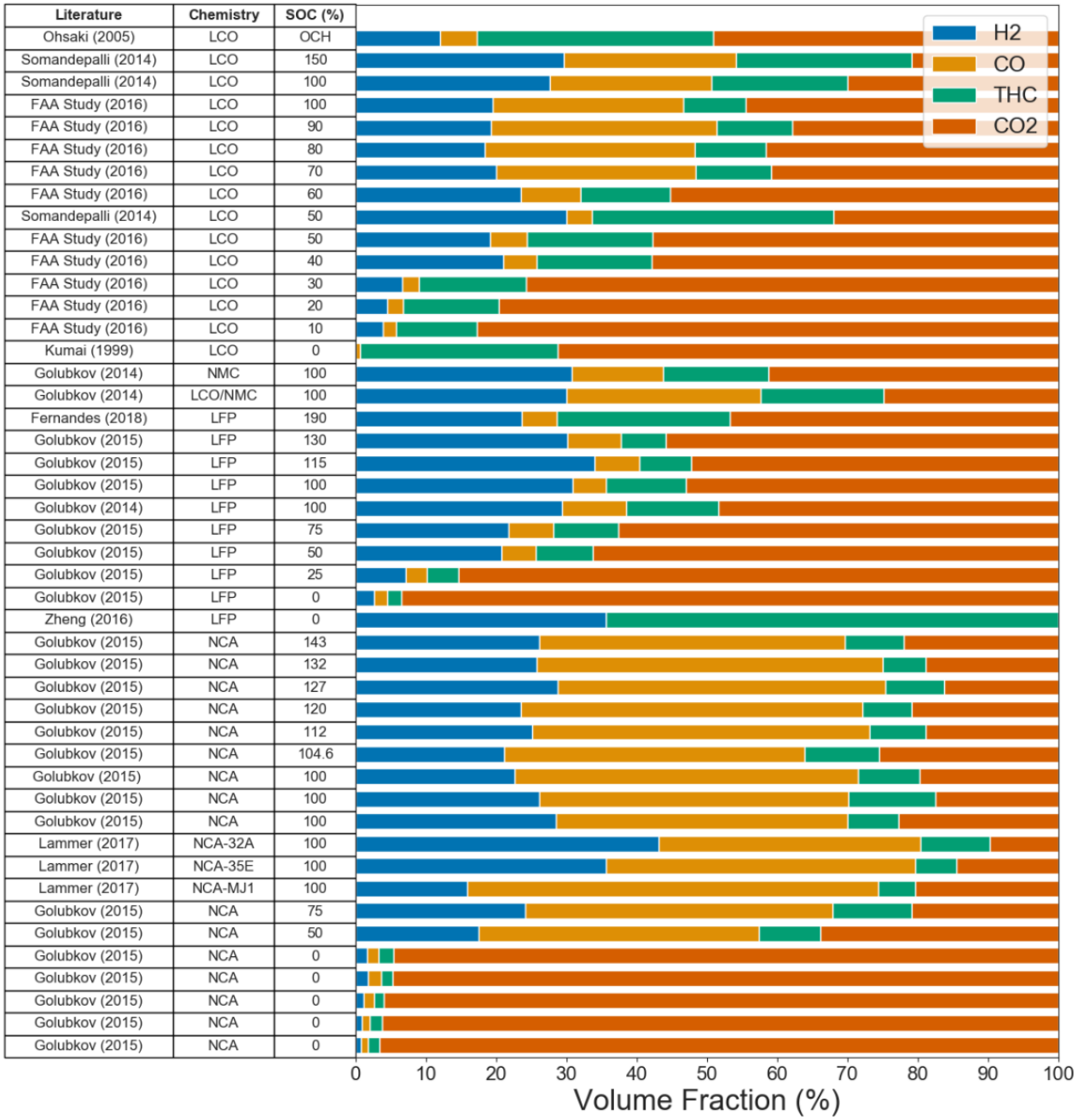

Literature	Chemistry	SOC (%)
Ohsaki (2005)	LCO	OCH
Somandepalli (2014)	LCO	150
Somandepalli (2014)	LCO	100
FAA Study (2016)	LCO	100
FAA Study (2016)	LCO	90
FAA Study (2016)	LCO	80
FAA Study (2016)	LCO	70
FAA Study (2016)	LCO	60
Somandepalli (2014)	LCO	50
FAA Study (2016)	LCO	50
FAA Study (2016)	LCO	40
FAA Study (2016)	LCO	30
FAA Study (2016)	LCO	20
FAA Study (2016)	LCO	10
Kumai (1999)	LCO	0
Golubkov (2014)	NMC	100
Golubkov (2014)	LCO/NMC	100
Fernandes (2018)	LFP	190
Golubkov (2015)	LFP	130
Golubkov (2015)	LFP	115
Golubkov (2015)	LFP	100
Golubkov (2014)	LFP	100
Golubkov (2015)	LFP	75
Golubkov (2015)	LFP	50
Golubkov (2015)	LFP	25
Golubkov (2015)	LFP	0
Zheng (2016)	LFP	0
Golubkov (2015)	NCA	143
Golubkov (2015)	NCA	132
Golubkov (2015)	NCA	127
Golubkov (2015)	NCA	120
Golubkov (2015)	NCA	112
Golubkov (2015)	NCA	104.6
Golubkov (2015)	NCA	100
Golubkov (2015)	NCA	100
Golubkov (2015)	NCA	100
Lammer (2017)	NCA-32A	100
Lammer (2017)	NCA-35E	100
Lammer (2017)	NCA-MJ1	100
Golubkov (2015)	NCA	75
Golubkov (2015)	NCA	50
Golubkov (2015)	NCA	0
Golubkov (2015)	NCA	0
Golubkov (2015)	NCA	0
Golubkov (2015)	NCA	0
Golubkov (2015)	NCA	0

Figure 16: Battery Vent Gas Species Compositions SOC (from [69])

Figure 16 by Baird et al. [69] shows the vent gas composition for various cell chemistries and states of charge (SOC). In some cases, the state of charge is greater than 100%, indicating that the battery has been overcharged (where current is applied and there is an increase in voltage over the nominal

capacity). This could simulate an instance where the battery management system failed and allowed the charging system to continue even after charging is complete. The vent gas released from these failed lithium-ion cells contain a flammable gas mixture that contains various species such as hydrogen (blue), carbon monoxide (orange) which is also toxic, various hydrocarbons such as methane and propane (green), and carbon dioxide (red) which is an asphyxiant. The species composition and vent gas volume production vary for other tests based on SOC, cathode chemistries, cell form factor, capacity, etc. In addition, Somandepalli et al. [70] reported an estimated vent gas production rate of 0.32 L/Wh from a 7.7 Wh cell. This is at the cell level, so further experiments would need to be studied to determine if this estimated vent gas production holds on a larger scale. Current BEVs have a capacity of 30 kWh to 100 kWh [71]. The rate at which the battery cells fail in a module is also important to understand. This will ultimately lead to the gas production rate which will vary based on the system parameters and the failure mode.

A deflagration hazard can exist due to lithium-ion cell failure. One example of this occurring was in a substation explosion in Surprise, AZ, where a lithium-ion battery energy storage system failed, releasing this flammable vent gas. The flammable vent gas ignited after a delay, and the resulting shock wave threw multiple firefighters back [72]. Explosion hazards are based on five parameters that must be present: oxidizer, ignition source, fuel, confinement, and dispersion of the gas. The confinement of the gas and the amount of gas produced by a BEV battery failure will determine the severity of the deflagration/explosion. These parameters will affect key deflagration metrics such as flame speed and maximum overpressure.

3.3.2. Fire Hazards

In addition to the deflagration/detonation hazard, BEVs present a unique fire hazard as well due to the potential for cascading failure. When a lithium-ion cell fails, flammable gases are usually ejected due to the liquid electrolyte reacting during the combustion process. These gases can remain unburned or might be ignited and burned as a jet flame. This jet flame from one cell in the battery system can heat other cells, converting the potential chemical energy rapidly into thermal energy. If there is enough oxygen present, fuel from the flammable gases along with heat provided by the failed cells (as well as the potentially flammable packaging) could lead to a fire hazard.

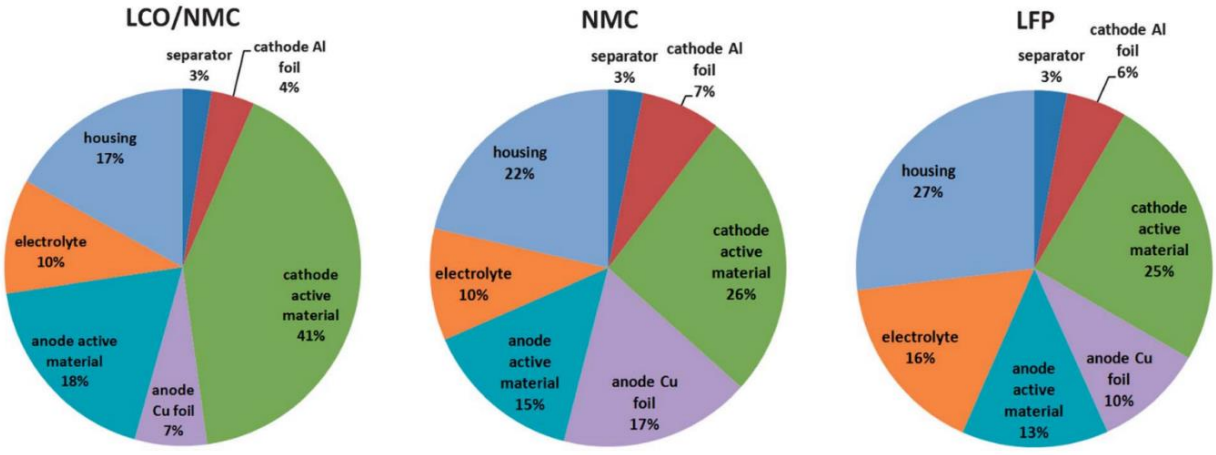

Figure 17: Cell Component Breakdown by % Mass (from [73])

Figure 17 gives the material breakdown of each part of the cell in a study by Golubkov et al. [73]. Below, in Table 11, further breakdowns are provided for comparison.

Table 11: Cell Deconstruction Breakdown by % Mass

Reference	Form Factor	Nominal Capacity (Ah)	Cathode Chemistry	Cathode (%)	Anode (%)	Electrolyte (%)	Separator (%)	Packaging (%)
Ribiere (2012) [74]	Pouch	2.9	LMO	44.0	35.0	11.0	2.0	6.0
Somandepalli (2014) [70]	Pouch	2.1	LCO	42.4	34.9	9.5	6.4	6.8
Golubkov (2014) [73]	18650	2.6	LCO/NMC	45.1	24.8	10.4	2.7	16.9
Golubkov (2014) [73]	18650	1.5	NMC	33.4	31.8	10.2	3.2	21.3
Golubkov (2014) [73]	18650	1.1	LFP	30.3	23.3	16.4	3.1	26.9

Not only is there the hazard of the flammable gases, but the various materials used to construct lithium-ion cells (such as nylon and polypropylene) can add to the fuel load. Table 11 shows the cell deconstruction by Ribiere et al. [74] in 2012, Somandepalli et al. [75] in 2014, and Golubkov et al. [73] in 2014. There are five major components: cathode, anode, electrolyte, separator, and the packaging.

The specific materials can be used to understand the heat of combustion and what the total heat release will be at the cell level. For example, Somandepalli et al. [75] report nylon and polypropylene as some of the various assumed compounds for the packaging. The actual heat of combustion various for those two compounds are from 27.1 kJ/g for nylon to 38.6 kJ/g for polypropylene from Quintiere et al. [6]. In addition to the various well-known materials used in the packaging of the lithium-ion cells, the electrolyte composition is also required to understand the complete fuel load. This component is not well known due to the mixtures not being published consistently from manufacturers. The study by Somandepalli et al. [75] provides a value of 19.31 kJ/g for the heat of combustion of the electrolyte. A study by Zhang et al. [76] has various electrolyte heat of combustion values, with 13.2 kJ/g for EC, 20.9 kJ/g for DEC, and 14.5 kJ/g for the DMC electrolyte. This shows the range that the heat of combustion for the electrolyte might fall under, which can be used to estimate the total fuel load.

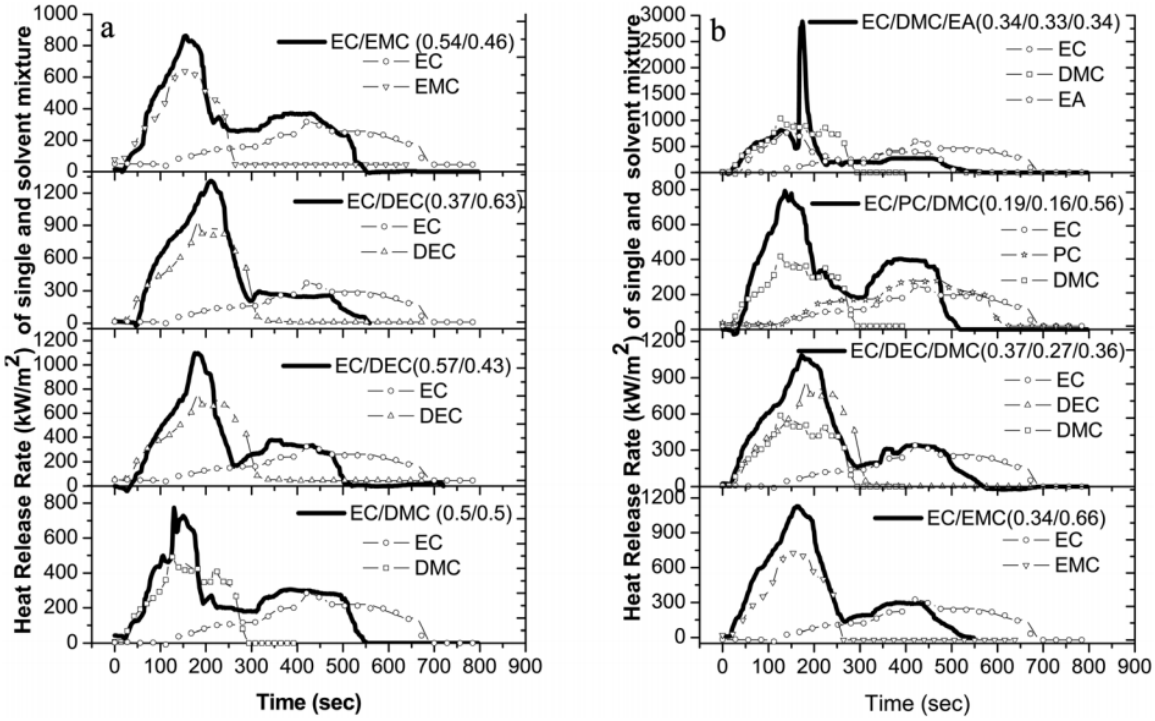

Figure 18: HRR Curves for various Electrolyte Compositions and Mixtures (from [77])

The HRRs of each electrolyte and various mixtures are all unique. A study by Eshetu et al. [77] shows how the HRR peaks and characteristics vary for each individual and mixture of electrolyte. The total heat released for the electrolyte mixture is based on the combustion conditions, mixture ratios, and electrolytes in the mixture and can vary from 12 to 24 kJ/g, which is much lower than some of the packaging materials.

A study by Larsson et al. [78] looked at toxic emissions from battery fires. Various tests of a variety of cells at a SOC from 0% up to 100% were conducted to measure the HRR and the hydrogen fluoride (HF) and phosphoryl fluoride production. The hydrogen fluoride production ranged anywhere from 15 to 198 mg/Wh. Larsson noted the immediately dangerous to life or health (IDLH) level for HF is 25 mg/m^3 (30 parts per million) and the lethal 10 minute HF toxicity value (Acute Exposure Guideline Levels 3) is 139 mg/m^3 (170 ppm). Table 12 below gives ranges based on the exposure time for the different AEGL levels from [79].

Table 12: Summary of AEGL Values (from [79])

Classification	10 min	30 min	1 h	4 h	8 h	End Point (Reference)
AEGL-1 (Nondisabling)	1.0 (0.8)	1.0 (0.8)	1.0 (0.8)	1.0 (0.8)	1.0 (0.8)	Threshold, pulmonary inflammation in humans (Lund et al. 1997, 1999)
AEGL-2 (Disabling)	95 (78)	34 (28)	24 (20)	12 (9.8)	12 (9.8)	NOAEL for lung effects in cannulated rats (Dalbey 1996; Dalbey et al. 1998a);[a] sensory irritation in dogs (Rosenholtz et al. 1963)[b]
AEGL-3 (Lethal)	170 (139)	62 (51)	44 (36)	22 (18)	22 (18)	Lethality threshold in cannulated rats (Dalbey 1996; Dalbey et al. 1998a);[c] lethality threshold in mice (Wohlslagel et al. 1976)[d]

[a]10-min AEGL-2 value.
[b]30-min and 1-, 4-, and 8-h AEGL-2 values.
[c]10-min AEGL-3 value.
[d]30-min and 1-, 4-, and 8-h AEGL-3 values.
Abbreviations: mg/m^3, milligrams per cubic meter; ppm, parts per million.

If the production rate of 198 mg/Wh is scaled for a 100 kWh BEV fire, the results could be as much as 20 kg of HF produced. Based on confinement and ventilation the IDLH or lethal threshold could be reached.

3.4. Pertinent Regulations and Safety Standards

BEVs have robust safety standards and practices regarding the battery system, the vehicle itself, and the roadway structures on which they operate in.

3.4.1. National Fire Protection Association Standard 502

NFPA 502, *Standard for Road Tunnels, Bridges, and Other Limited Access Highways*, provides fire protection and life safety requirements as well as design criteria for AHJs to use in ensuring tunnel safety. Section 7.3.2 states that a tunnel shall be capable of withstanding the temperature exposure represented by the RWS time-temperature curve or other recognized standard time-temperature curve that is acceptable to the AHJ, as shown by an engineering analysis. The assumption is that every part of the tunnel should withstand these temperature exposures, irrespective of the ventilation rate, type of ventilation, or location of fire [38].

3.4.2. ASHRAE HVAC Applications Ch. 16: Enclosed Vehicular Facilities (2019)

ASHRAE 2019 HVAC Applications Chapter 16: *Enclosed Vehicular Facilities* provides guidance on vehicular facilities that store and/or through which vehicles travel. These vehicles can be driven by an internal combustion engine or electric motors. Ventilation requirements including mechanical systems and natural ventilation, climate and temperature control, contaminant level control, and emergency smoke control. Additionally, ventilation concepts including normal operations and emergency operations are covered [39].

3.4.3. NCHRP Guidelines for Emergency Ventilation Smoke Control in Roadway Tunnels (2017)

NCHRP Guidelines for Emergency Ventilation Smoke Control in Roadway Tunnels Chapter 2: *Road Tunnel Fires* provides guidance on fire design parameters for tunnels. This includes consideration of the geometric parameters of the tunnel, fire protection features, and response times that leads to decision making using NFPA 502. This is chapter provides a framework on how to understand and determine fire and hazardous materials management in tunnels [40].

3.4.4. UL 2580 Standard for Safety Batteries for Use in Electric Vehicles

UL Standard 2580 *Batteries for Use in Electric Vehicles* covers requirements for electrical energy storage assemblies including battery packs, sub-assemblies, and modules that make up the main assembly for electric-powered vehicles. The electrical energy storage assemblies are tested to determine the ability to withstand abuse testing and conditions. The manufacturer's specified charging and discharging parameters are used to test the assemblies and modules at the specified temperatures [64].

3.4.5. SAE J2464 Electric and Hybrid Electric Vehicle Rechargeable Energy Storage System Safety and Abuse Testing

Society of Automotive Engineers (SAE) J2464 *Electric and Hybrid Electric Vehicle Rechargeable Energy Storage System Safety and Abuse Testing* gives guidance on abuse testing performed to characterize rechargeable energy storage systems and response to off-normal conditions and environmental impacts. The response information collected can be used to determine various hazards due to abuse conditions. This data can be used to create hazard mitigation efforts for specific energy storage designs [62].

3.4.6. SAE J2929 Electric and Hybrid Vehicle Propulsion Battery System Safety Standard - Lithium-based Rechargeable Cells

SAE J2929 *Electric and Hybrid Electric Vehicle Rechargeable Energy Storage System Safety and Abuse Testing* gives guidance on minimum safety criteria for the complete battery system, including cells, modules, packs and complete battery system. This includes understanding how physical support, enclosure, thermal management and electronic controls operate. This standard focuses on evaluating the battery system alone [63].

3.4.7. FreedomCAR Battery Test Manual for Power-Assist Hybrid Electric Vehicles

FreedomCAR *Battery Test Manual for Power-Assist Hybrid Electric Vehicles* gives guidance testing for cycle life behavior and performance for batteries in hybrid electric vehicle applications. These tests are applicable to the full battery system as well as using scaling to apply to cells and modules [65].

3.5. BEV Research Summary in Tunnels

This section documents the results of evaluations regarding BEV failure in a tunnel.

3.5.1. Experiments

A large variety of experiments for BEVs in tunnels have been conducted. Additionally, real world failures have also occurred. These different reported incidents and experiments conducted provide an understanding of both what might cause a failure and the characteristics of that failure.

3.5.1.1. Reported BEV Failures and Incidents

Various instances of failed BEVs have occurred due to crash damage, factory defects, and battery management issues while charging. One example of crash damage was during the 2011 Chevrolet Volt crash testing. After the test was completed, the vehicle caught fire over the weekend when no lab personnel were present. The Chevrolet Volt had been involved in a New Car Assessment Program (NCAP) pole test three week prior to the fire. This is an impact test with a solid pole for crash testing ratings. During the investigation, it was determined the battery was damaged but only over time did it catch fire [80]. Additionally, a Tesla Model 3 collided with a parked tow truck in Moscow, Russia. The BEV ignited after a short time, though the time is not specified. During the fully developed vehicle fire there were two distinct 'bursts' that occurred [81].

One instance of a BEV failure due to either a defect or battery management error occurred in Los Angeles in 2018. A Tesla Model S was driving slowly through traffic and began to vent gases and the vehicle ignited. The fire department responded and consulted Tesla via telephone to advice on how to safely contain the vehicle. Approximately 300 gallons of foam and water was used to extinguish the flames and the vehicle was transported to Tesla for inspection [82]. A more recent example is a Tesla Model S bursting into flames while parked in a Shanghai parking garage [83]. An image of this is shown in Figure 15. Another example comes from a BMW i8 hybrid that began venting inside of a Dutch showroom. The car was quickly driven outside where it was then immersed in a giant tank of water where it remained for 24 hours [84].

3.5.1.2. Fire Analysis of BEVs in a Road Tunnel

An experimental analysis was performed to evaluate the worst-case effects of a damaged electric vehicle battery in a road tunnel [85]. The batteries were evaluated without the chemical and electrical safety modules or the protective battery housing to eliminate influencing factors on the test. Because lithium-ion batteries are the most promising battery technology, these batteries were the focus of these experiments. The consequences of a large battery fire are large energy release, leakage, and gas venting. Table 13 shows the characteristics of the lithium-ion batteries used in this experimental analysis [85].

Table 13: Lithium-ion Battery Characteristics (from [85])

Characteristic	Description
Number of Cells	96 cells (8 modules)
Anode Active Material	Graphite
Cathode Active Material	NMC
Electrolyte	Lithium hexafluorophosphate ($LiPF_6$)
Energy (gross)	33.182 kWh
Energy (net)	27.2 kWh
Specific Energy (gross)	0.14 kWh/kg
Specific Energy (net)	0.12 kWh/kg
Thermal Runaway	From 210 °C typical. High charge promotes thermal runaway.

Four test scenarios were evaluated to induce a fire. Three scenarios focused on mechanical damage to the battery: wedge-shaped penetration with an explosively accelerated steel plate, blunt impact with an explosively accelerated steel plate, and central puncturing with an explosively formed projectile. The fourth scenario focused on thermal stress in which the battery module was exposed to a propane gas fire until the module caught fire. Illustrations and additional descriptions can be seen in Table 14. These experiments showed that the fire hazards of BEVs are similar to those of conventional vehicles. However, a different hazard is introduced in the release of potentially more severe chemical aerosols such as cobalt, lithium, and manganese which are toxic [85].

Table 14: Test Scenarios (from [85])

#	Scenario	Illustration
1	**Wedge-shaped penetration**: Detonation of explosive charges accelerated a steel plate in the direction of the battery module. As a result, the wedges on the underside penetrated evenly into the two cell rows of the battery module, where they remained and caused electrical short-circuits.	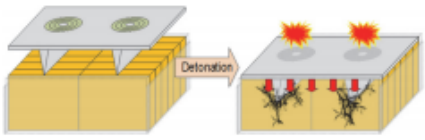
2	**Blunt impact**: Detonation of explosive charges accelerated a steel plate in the direction of the battery module. The module thus suffered a blunt impact over its entire surface so that all cells were structuraly damaged without penetration.	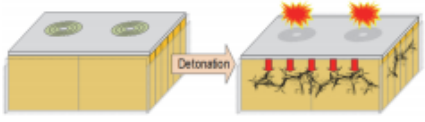
3	**Central puncturing**: Battery module was shot at centrally with an explosively formed projectile (EFP) from a distance of 10 cm. As a result, both cell rows were to be damaged with a continuous penetration of all 12 cells.	
4	**Thermal stress**: Battery module was evenly underfired with a propane gas fire until the module caught fire. The fire source was then removed and the thermal runaway of the battery observed.	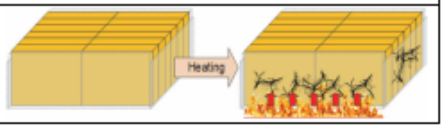

Figure 19 shows the layout of the test site where the experiment was conducted, indicating the battery location (labeled Test site), ventilated section (colored blue), closed bypass section (pink), and measuring site. The tunnel had a cross-sectional area of 56 m^2 at the test site and 43 m^2 at the measuring site. Due to the difference in a fire involving a BEV when compared to a conventional ICE vehicle, pollutants and aerosols were measured in addition to thermal parameters. The bypass to the main ventilation duct was closed during all tests to control air flow and prevent dilution [86].

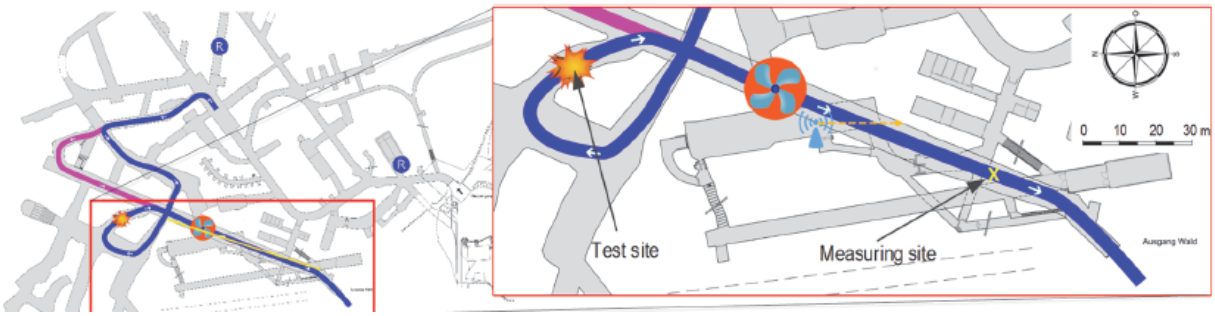

Figure 19: Test tunnel area layout (from [86])

Table 15 gives the release quantities for the four different tests listed above. Also listed is the total test duration. It was discussed that toxic aerosols such as cobalt, lithium, and manganese are released, which is unlike traditional ICE vehicle fires. One thing the authors noted was while hydrogen fluoride gas was expected to be detected, no large quantities were measured. An additional note was that the three mechanical damage tests caused each cell in the battery to go into thermal runaway almost simultaneously, while the thermal test caused a chain reaction of thermal runaway between cells.

Table 15: Release Quantities (from [85])

Parameter	Test 1 (wedge)	Test 2 (plate)	Test 3 (puncture)	Test 4 (fire)
PH_3 [g]	< 0.4	---	< 0.4	---
F^- as HF [g]	1.1	3.1	< 1	< 0.5
PO_4-P as H_3PO_4 [g]	< 1.5	< 1.5	11.3	< 1
Co [g]	457	567	190	364
Li [g]	107	124	42	92
Mn [g]	445	536	184	349
F^- Aerosol [g]	152	160	68	126
NO [g]	< 1	1.1	< 1	1.5
NO_2 [g]	< 1	< 1	< 1	< 1
CO [g]	76	181	97	141
CO_2 [g]	8500	6000	2000	7800
TVOC [g]	20	196	93	32
∑ Aromate [g]	1.6	8.6	3.2	3.1
Benzene [g]	1.1	3	1.6	1.7
Toluene [g]	0.2	1.1	0.5	0.4
Xylene [g]	0.1	0.6	0.3	0.2
Styrene [g]	0.1	3.0	0.5	0.6
Duration	***16 min***	***21 min***	***16 min***	***26 min***

3.5.1.3. Electric Vehicle Crash and Fire Damage

An experiment was performed to show the effect of both crash and fire damage using a Tata Indica GLX Electric Vehicle that uses a 26 kWh, 12 module NMC lithium-ion battery [87]. Overall, the goal was to better understand if a BEV battery system will ignite with heavy crash damage and how much water is required to extinguish a BEV fire after thermal runaway. The first test was a drop test from 20 meters that simulated a 70 km/h rear impact. After seven minutes, the vehicle had visible flames appear. After 2.5 hours of free burning, the temperatures around the battery containment ranged between 310°C to 540°C. This test showed that with severe mechanical damage, the battery can ignite. It is concluded that many factors such as the angle and energy of impact will affect the outcome, and this is good knowledge to have for emergency responders and even towing companies hauling wrecked or damaged EVs through tunnels.

The next test used a propane flame under the vehicle to attempt to ignite the battery pack externally. The windows were rolled down for this test. After ten minutes, ignition occurred, and two attempts had to be made to extinguish the fire. The first attempt used 100 L of water to extinguish the flames. After a short time period, re-ignition occurred that led to a fully developed car fire. It took an additional 550 L of water to fully extinguish the second fire, which was declared extinguished when temperatures were no longer increasing. The major observation with this second test was the actual battery pack did not go into thermal runaway. After investigating the battery pack, it was determined that while the external fire did not cause the battery pack to ignite, it did ignite other combustibles of the vehicle. The fire had characteristics comparable with a traditional ICE vehicle. This is unlike the mechanical damage that caused the cells to go into thermal runaway and ignite [87].

3.5.1.4. Comparison of the Fire Consequences of a BEV and ICE

Testing to compare ICE and BEV fires was performed in a 50 m long, 3.5 m high fire gallery by the National Institute of Industrial Environment and Risks [88]. There was a total of five different fire tests performed on the following:

1. Modular assembly of battery cells to represent a portion of an EV battery
2. The same battery assembly with firefighting operation
3. A full battery pack with late firefighting attempts
4. EV with a fully charged battery
5. An analogous diesel vehicle with a full fuel tank

A 6-kW burner was used for an ignition source for each test, and an exhaust system with a volumetric flow of 25,000 m^3/hr would collect the products for analyzing. The HRR, total heat released (THR), and heat of combustion (Δh_c) were captured for two different EV vehicles and ICE vehicles presented in Table 16 below:

Table 16: BEV vs. ICE Fire Characteristics (from [88])

	BEV Manufacturer 1	BEV Manufacturer 2	ICE Manufacturer 1	ICE Manufacturer 2
Nominal Voltage (V)	330	355	N/A	N/A
Capacity (Ah)	50	66.6	N/A	N/A
Energy (kWh)	16.5	23.5	N/A	N/A
Mass (kg)	1122	1501	1128	1404
Mass Loss (kg)	212	278.5	192	275
Max HRR (MW)	4.2	4.7	4.8	6.1
THR (MJ)	6314	8540	6890	10000
Δh_c (MJ/kg)	29.8	30.7	35.9	36.4
HF Production (g)	1540	1470	621	813

The total hydrogen fluoride production for the BEV was about double that of the ICE vehicle. This was due to the combustion of the lithium-ion batteries and is noted in other cell-level studies [78]. Additionally, the heat of combustion for the EV was less than the ICE vehicle. This could be due to the lithium-ion battery electrolyte having a lower Δh_c, which lowers the overall heat of combustion of the vehicle. The intent of this test was to use the data as an input for modeling toxic gas dispersion and the thermal effects in a confined space such as a tunnel or underground parking facility [88].

3.5.2. Modeling

Modeling for BEVs in tunnels has not been explicitly researched and developed. Currently, the majority of modeling for batteries takes place to understand cell failures and modeling battery management systems [89] [90]. Once a better understanding of how BEVs fail is developed, models to characterize these failures in tunnels can be developed.

3.5.3. Analysis

While no specific studies to analyze BEVs in tunnels have been conducted, one analysis goes over the various failures that might occur.

3.5.3.1. Safety Test Methods for EV Batteries

A study analyzing three different failure modes in BEVs was performed by Davidsson et al. [91] to help understand the safety that should be maintained through the whole life of the battery: assembly, usage, servicing, accidents, and recycling.

The first test was a short circuit test, which consisted of shorting out various batteries and measuring the current discharge. This short circuit could come from for example crash damage or chassis flex/deformation. One cell exploded, one ruptured and vented, and the last one was not physically affected. The fire test consisted of a battery pack with a 25-kW propane burner located underneath within a furniture calorimeter. The fire effluents were collected and analyzed to understand the toxicology. Hydrogen fluoride and carbon monoxide were both measured in parts per million by volume (PPMV) [91]. This helps understand required ventilation rates, and as more tests are performed, the total production of these chemicals can be determined as a function of the battery system capacity.

3.6. BEV Research Gaps

At a cell level, lithium-ion batteries are still being studied to understand how cells might fail and what the impact is. With battery technology constantly changing to improve performance metrics, the safety and consequences are also changing. This drives the need for further work which are included in the research gaps below. There are two distinct hazards: the flammable vent gas and unique hazards due to thermal runaway and propagation between cells. Studies conducted to understand the safety of BEVs in tunnels is limited and ranged from real world vehicle crash tests such as the Chevrolet Volt NCAP pole test to actual reported incidents on public roadways. Attention should be given to the size or class of the vehicle. As vehicular class increases so does the amount of stored energy. Currently, most BEVs are passenger vehicles. As the technology and energy density of lithium-ion cells improve, medium- and heavy-duty BEVs will be developed. Hybrid-ICE vehicles are becoming more common using larger battery packs in each scale of vehicle and should also be evaluated. In addition to the scale of a BEV increasing, the transportation of damaged BEVs should be considered. Reported incidents of damaged and failed BEVs reigniting shows that studying and understanding how to mitigate this is important [92].

The following criteria were evaluated to determine where research gaps may exist regarding BEVs in tunnels.

1. Scenario Identification
2. Failure Modes
3. Consequences
4. Validation

The scenarios that lead to a failure mode have been identified by real world examples. Section 3.5.1.1 goes over the various incidents that have been reported. These involve but may not be limited to impacts that cause mechanical damage and thermal issues such as internal cooling systems failure that leads to cell thermal runaway as well as internal shorts and/or incorrect charging/discharging rates and cycles that lead to a failure mode.

The failure modes can lead to an exothermic reaction in the cell(s) which leads to self-heating. This reaction can propagate failure throughout a module and release of flammable vent gas from multiple cells. For each of the failure modes, there are several variables that effect the magnitude of the consequence such as the following: battery vent gas volume production, type of cell, vent gas species, rate of failure propagation through cells and modules, whether there is a delayed ignition, tunnel geometry, etc. The failures described in Section 3.5.1.1 and as shown in Figure 15 show trends of delayed fire or ignition during a BEV incident. With the complexity of these vehicles, most research is at the bench-scale to study lithium-ion cell safety. More complete evaluations on failure modes needs to be completed as more data becomes available.

In contrast to the some of the other alternative fuels, there has not been significant research on BEV vehicles in tunnels or BEV fires/deflagrations in general. The measurements of the consequences include vent gas deflagration metrics, HRR, battery vent gas dispersion, and resulting structural damage. One experiment on has been performed to understand the consequence of mechanical impact and external fires on BEVs [91]. Yet most experiments conducted to understand mechanical, thermal, overcharging and cycling abuse tests have been performed at the cell level. These types of tests need to be scaled from bench-scale to intermediate- and large-scale tests. One large scale test [88] shows that BEVs are very similar in terms of the fire hazard compared with

ICEs when compared the HRR and THR. One of the differences found in this study is the hydrogen fluoride production is over double during a BEV fire compared to an ICE vehicle fire. Validation amongst various experiments to understand the vent gas composition has also been done (see Figure 16).

Additional testing needs to be performed to help understand how to characterize these failures and the consequences in tunnels. Examples would be understanding the HRR and THR of a BEV fire and how ventilation and confinement in a tunnel effects these metrics. The following research gaps were identified:

- Fully evaluate the deflagration metrics, such as the vent gas volume production, lower flammability limit, laminar flame speed, and adiabatic overpressure.
- Deflagration metrics are dependent on the fuel concentration as well as ambient conditions for well-known combustible gases. Battery vent gas is based on these parameters as well as effects of cell chemistry, state of charge, cell capacity, cell form factor, electrolyte chemistry and composition, cell to cell propagation, and failure mode.
- Fully evaluate the fire characteristics of both cells, cell arrays, and modules to understand the HRR characteristics, temperatures, time to ignition, and effect of different cell configurations in modules.
- Understand the effects on fire characteristics of cell chemistry, state of charge, cell capacity, cell form factor, electrolyte chemistry and composition, cell to cell propagation, and failure mode.
- Fully evaluate the failure initiating events that are risk significant in terms of BEV vehicles in tunnels such as mechanical damage or cell defects.
- Evaluate different BEV classes (light, medium, and heavy duty), including how the deflagration metrics and fire characteristics scale up, as well as how does propagation of failure between cells change.
- Assess how flame speed and overpressure from various vent gas compositions change in tunnels with different geometric parameters (such as length/diameter ratio) and the effect on structural components of tunnels.
- Validation of modeling efforts through direct comparison to experimental results, especially since the battery vent gas contains multiple species (hydrocarbons, carbon monoxide, hydrogen, carbon dioxide).
- Understand the amount of toxic chemicals release rate and total volume released during a battery fire to understand emergency ventilation.
- Assess required ventilation rates for battery off-gas without ignition (deflagration hazard) and fire effluent from combustion of battery system (toxicity hazard).

4. NATURAL GAS VEHICLES

4.1. Overview of Technology

The natural gas vehicle (NGV) is an alternative fuel vehicle that uses compressed natural gas (CNG) or liquefied natural gas (LNG). Natural gas is comprised primarily of methane (with concentrations ranging from about 85% to 96% by volume) and combustion of this fuel produces less emissions compared to other hydrocarbon fuels (e.g. gasoline or diesel). In the transportation sector, NGVs span the range of light- to heavy-duty vehicles. Natural gas (NG) can be used to run internal combustion engines (ICE) as a dedicated fuel or as a bi-fuel mixed with gasoline, diesel, etc. CNG can also be utilized to spin small gas turbines to power electric generators and therefore can support hybrid vehicles as well. In 2019 there were a reported 27.7 million NGVs on the road [93]. Also, as seen in Figure 20, over the years CNG has become a less expensive alternative compared with more popular fuels such as gasoline and diesel in dollars per gasoline-gallon-equivalent (GGE). With fast-fill stations for retail use and time-fill for commercial use, there are a variety of refueling options for the range of consumers [94]. Fast-fill stations use a series of storage tanks that store high pressure CNG that is then used to fast-fill a vehicle 20-gallon equivalent tank in less than five minutes, for example. A time-fill station fills directly from the compressor rather than using high pressure tanks and requires less fueling equipment at the expense of longer fill times.

According to the DOE Alternative Fuels Data Center [95] as of 2019 there are 945 CNG and 71 LNG fueling stations in the continental U.S. Stronger global demand for cleaner burning fuel drives rapid growth in CNG and LNG [96]. Due to the existing fleets of NGVs and the forecasted continued growth [97] we are reviewing the hazards associated with NGVs specifically in the context of accidents that might occur in tunnels.

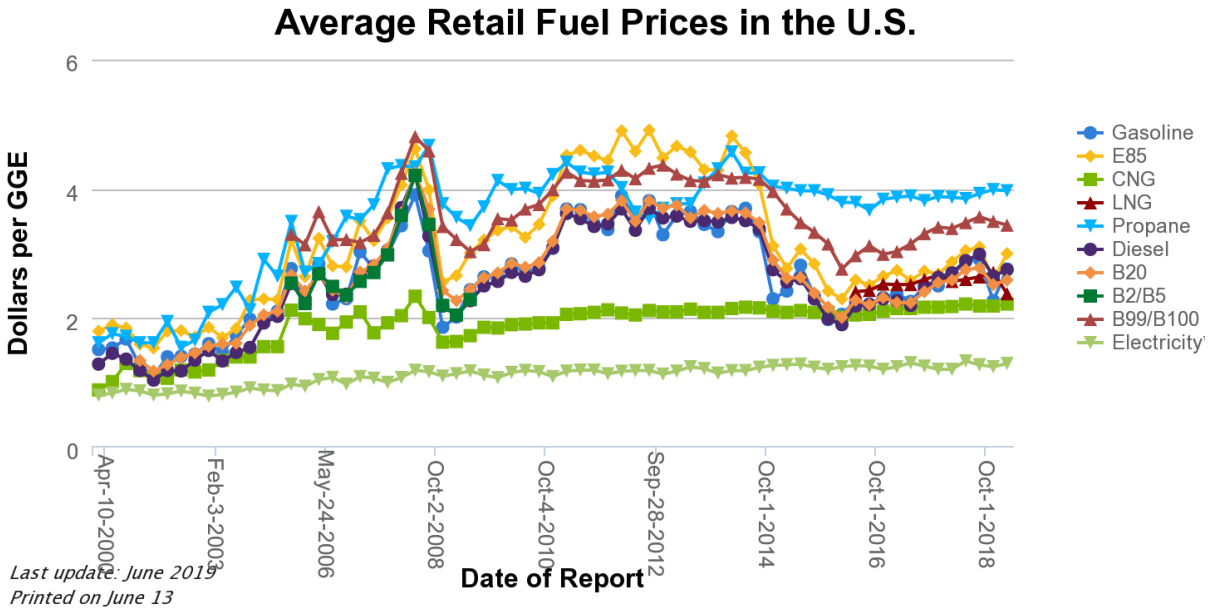

Figure 20: Cost of common fuel types over an 18-year span (from [98])

4.2. Properties of Methane and Natural Gas

To obtain the energy density required for onboard storage, CNG is stored as a pressurized gas while LNG is stored cryogenically (see Figure 21). NG under standard conditions is roughly half as dense as air and has a range of chemical properties shown in Table 17. Additionally, methane properties are listed since some experiments and models discussed below are for pure methane gas. The energy released upon ignition (heating value) of methane is higher than that of natural gas, which would result in a conservative risk estimate for fires from natural gas systems when using methane as a surrogate. Liquid methane has an expansion ratio of 621.3 which is the ratio of volume occupied by one unit of mass in liquid form to that in gas form. The energy density of NG (both CNG and LNG) per unit mass is approximately 43 MJ/kg. This is similar to that of gasoline which is 45 MJ/kg [99]. The energy density per unit volume for CNG (at 250 bar) is 9 MJ/L versus the 22.2 MJ/L for LNG at -162 °C compared with 34.6 MJ/L for conventional gasoline [100]. Figure 21 below shows the density contour for methane. Two points on the graph are highlighted – the density at CNG tank conditions (250 bar, atmospheric temperature), and LNG tank conditions (atmospheric pressure, -162 °C).

Table 17. Physical and Chemical Properties of Natural Gas & Methane (from [100])

Property	Methane	Natural Gas
Molecular weight	16.043 g/mol	19.5 g/mol
Gas Density	0.657 g/L, 25°C, 1 atm	0.7–0.9 g/L, 25°C, 1 atm
Relative Vapor Density	0.5536	0.5809–0.7468
Liquid Density	422.62 g/L, −162°C	470 g/L, −162°C
Melting Point	−182.5°C	−182.0°C
Boiling Point	−161.50°C	−162.0°C
Auto-ignition Temperature	580°C	723°C
Flammability Limits (vol % in air)	5–15%	4.3–15%

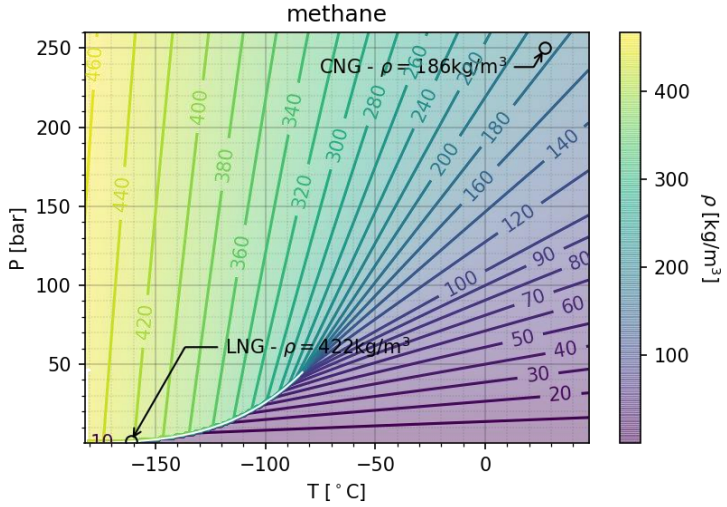

Figure 21. Density contours for methane (created using data from [101])

4.3. Associated Hazards

The primary safety hazards associated with natural gas is the same as most other fuels, namely flammability and uncontrolled combustion. There are additional hazards are associated with LNG due to the storage temperature and the potential for rapid expansion, which will be covered in more detail later. Naturally occurring NG is odorless and for safety reasons the gas is odorized prior to distribution. According to [102], the odorized gas is detectable at concentrations as low as 0.3% by volume in air. As shown above in Table 18, the lower flammability limit (LFL) is 5.3% (vol% in air). Thus, a leak is detectable by odor at concentrations roughly 15 times lower the concentration required for combustion. Flammability properties of methane along with other common fuel types are shown in Table 18. Note that these properties vary based on lab testing uncertainties along with regional and various seasonal additives.

Table 18: Flammability Properties of Hydrogen and Other Fuels

Property		Hydrogen	Methane	Propane	Gasoline Vapor
Flammability in Air (vol%) [27]	LFL	4.0%	5.0%	2.1%	1.2%
	UFL	75.0%	15.0%	9.5%	7.1%
Most easily ignited mixture in air (vol%)		29% [103]	8.5% [104]	5% [105]	2% [106]
Adiabatic Flame Temperature [107]		2483 K	2236 K	2250 K	2289 K
Buoyancy (ratio to air)		0.07	0.54	1.52	4
MIE [108] [109]		0.011-0.017 mJ	0.28-0.30 mJ	0.25-0.26 mJ	0.8 mJ
Autoignition Temperature [110]		500 °C	580 °C	455 °C	246 – 280 °C

Figure 22 and Figure 23 graphically represent the minimum ignition energy and flammability limits (FL) of methane compared to other fuel types. As shown methane has a similar minimum ignition energy to other hydrocarbons when the concentration lies within the FL.

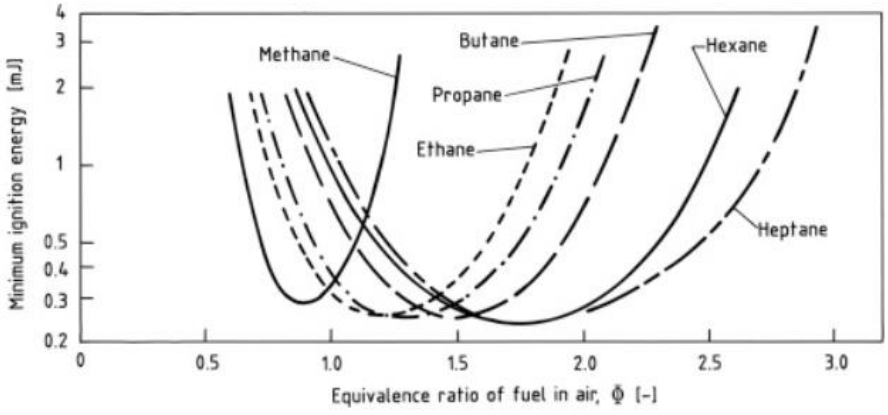

Figure 22: Minimum ignition energy for common fuels types (from [111])

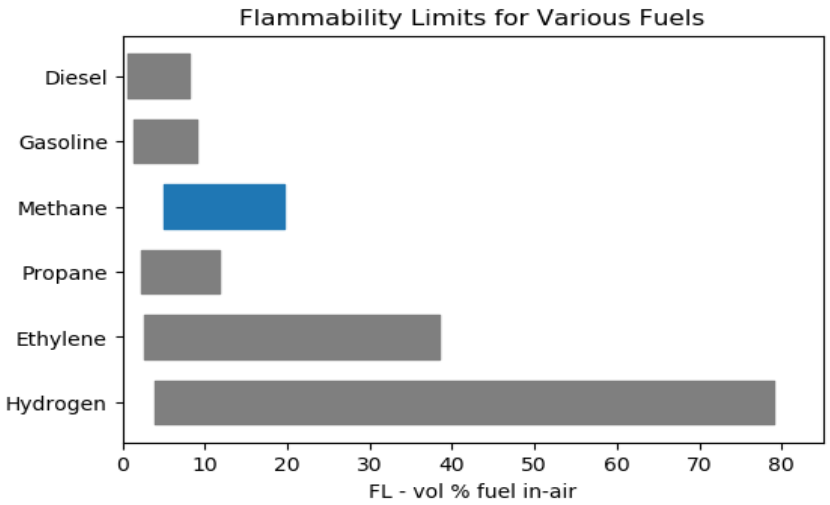

Figure 23: Flammability limits for common fuels types (from [111])

An important consideration in safety analyses is the fact that methane is less dense than air at standard conditions. This means that during an event that yields a leak or rupture of a NGV fuel container the flammable mass will in most cases dissipate upwards and away from the ground due to buoyancy. This improves safety for cases where potential ignition sources are located near the ground. Buoyant diffusion is also preferred unless there exists a restrictive surface above the release leading to an accumulation of gas at the surface. At this point, the flammable mass must be dissipated through proper ventilation and air flow, otherwise the hazard can linger for quite some time. This hazard is reviewed in detail in Section 4.5.

Note that due to the high storage pressures of CNG and the small flammable range, this lowers the chance of ignition. This was confirmed with modeling in a study by Zalosh et al. [112] that compared flammable gas dispersion of CNG and gasoline fuel leaks in a tunnel. Using the CFD code Fluent, the models showed that leaked CNG from vehicle storage containers dilute to levels outside of the FL shortly after release. Additionally, Zalosh concluded that CNG fueled vans are much less likely to ignite compared to those of gasoline when there is ventilation of 0.10 m/s or higher in a tunnel. This is based on the model results having a smaller flammable vapor cloud compared with the gasoline vapor clouds shown in the dispersion model results.

LNG releases, similar to CNG, can also produce flammable vapor clouds contained by restrictive structures. But in the case of an LNG vehicle release, the vapor cloud has the potential to be larger because of the typically larger amount of LNG stored onboard a vehicle [31]. In the event of a release at the bottom of an LNG container, the liquid will cool the surface below which could allow an LNG pool to form which will prolong the dissipation period. In addition, the density of recently vaporized LNG is higher, reducing buoyant dispersion. Initially the vapor is much heavier than air but as the gas temperature warms up and the density decreases, it will become lighter than air. Both factors also increase the chances of ignition by a source on the ground.

Many tests have been carried out looking into the conditions required to cause DDT with methane vapor clouds (see 4.5.1). Specific to LNG, liquefied fuels come with the risk of a boiling liquid expanding vapor explosion (BLEVE). BLEVE corresponds to a rapid heating of the super cooled liquid causing a rapid change in phase. As LNG vaporizes, its volume increases over 600 times. If the rate at which the gas is released is less than the rate of expansion, the vessel can over-pressurize and rupture. According to [31] this scenario has been witnessed under the extreme conditions of a

tanker with compromised insulation in contact with an external fire. For BLEVE to occur the superheat temperature limit must be reached by the liquid. In the case of LNG this is roughly -93 °C [31].

4.4. Pertinent Regulations and Safety Standards

NGVs have robust safety standards and regulations regarding the fuel storage system, the vehicle itself, and the roadway structures on which they operate.

4.4.1. National Fire Protection Association Standard 502

NFPA 502, *Standard for Road Tunnels, Bridges, and Other Limited Access Highways*, provides fire protection and life safety requirements as well as design criteria for authorities having jurisdiction (AHJs) to use in ensuring tunnel safety. Section 7.3.2 states that a tunnel shall be capable of withstanding the temperature exposure represented by the Rijkwaterstaat (RWS) time-temperature curve or other recognized standard time-temperature curve that is acceptable to the AHJ, as shown by an engineering analysis. The assumption is that every part of the tunnel should withstand these temperature exposures, irrespective of the fire location, ventilation rate or type [113]. With regards to NGVs in tunnels, appendix G.2.1 states that CNG fuel systems have a superior safety record than that of current conventional systems (i.e. gas and diesel).

4.4.2. ASHRAE HVAC Applications Ch. 16: Enclosed Vehicular Facilities (2019)

ASHRAE 2019 HVAC Applications Chapter 16: *Enclosed Vehicular Facilities* provides guidance on vehicular facilities that store and/or through which vehicles travel. These vehicles can be driven by an internal combustion engine or electric motors. Ventilation requirements including mechanical systems and natural ventilation, climate and temperature control, contaminant level control, and emergency smoke control. Additionally, ventilation concepts including normal operations and emergency operations are covered.

4.4.3. NCHRP Guidelines for Emergency Ventilation Smoke Control in Roadway Tunnels (2017)

NCHRP Guidelines for Emergency Ventilation Smoke Control in Roadway Tunnels Chapter 2: *Road Tunnel Fires* provides guidance on fire design parameters for tunnels. This includes consideration of the geometric parameters of the tunnel, fire protection features and response times that leads to decision making using NFPA 502. This is chapter provides a framework on how to understand and determine fire and hazardous materials management in tunnels [40].

4.4.4. National Fire Protection Association 52

NFPA 52, *Vehicular Natural Gas Fuel Systems Code*, provides design, installation, operation, and maintenance requirements for CNG and LNG fuel systems, storage containers, and dispensing systems [114].

4.4.5. National Fire Protection Association 55

NFPA 55, *Compressed Gases and Cryogenic Fluids Code*, provides storage, use, and handling requirements for both compressed and cryogenic liquid hydrogen in portable containers, cylinders, and tanks. Sections 10 and 11 deal with bulk hydrogen compressed gas systems and bulk liquefied hydrogen systems, respectively [115].

4.4.6. National Fire Protection Association 57

NFPA 57, *Liquefied Natural Gas (LNG) Vehicular Fuel Systems Code*, provides storage, use, and handling requirements for liquid natural gas fuel in storage containers [116].

4.4.7. National Fire Protection Association 59A

NFPA 59A, *Standard for the Production, Storage, and Handling of Liquefied Natural Gas (LNG)*, provides guidance for construction and operation equipment for production, storage, and handling of LNG [117].

4.4.8. SAE J1616: Recommended Practice for Compressed Natural Gas Vehicle Fuel

SAE J1616, *Recommended Practice for Compressed Natural Gas Vehicle Fuel*, provides recommended practices for fuel systems on vehicles that are powered by CNG [118].

4.4.9. SAE J2406: Recommended Practices for CNG Powered Medium and Heavy-Duty Trucks

SAE J2406, *Recommended Practices for CNG Powered Medium and Heavy-Duty Trucks*, provides recommended practices for construction, maintenance, and operation of CNG powered medium- and heavy-duty trucks [119].

4.5. NGV Research Summary in Tunnels

A significant amount of work exists evaluating the risks of NG ignition in various scenarios. The following section documents some of the most pertinent studies.

4.5.1. Experiments

Due to the high storage pressures of natural gas onboard NGVs, compromised fuel containers could produce large flammable masses. This flammable mass is unlikely to ignite without an external ignition source [112].

Multiple studies review the outcomes of ignited NG vapor clouds and high-pressure jets. An experiment determined that congestion had a strong influence on the maximum overpressure produced by the combustion of vapor clouds (see section 4.5.1.1) [120]. The occurrence of DDT, even in confined environments with obstructions was shown to be highly unlikely [121] [120] [122]. Specifically, Harris et al. [122] showed that even over the length of a 45 m pipe with repeated obstructions, DDT for NG did not occur. A strong correlation for heat transfer to a ceiling based on the flame height to ceiling distance was shown for large scale flames impinging on a ceiling (see Section 4.5.1.1) [120]. Royle et al. [123] studied the distribution of overpressure resulting from the ignition of NG contained in a congested region. An array of sensors was used to obtain the pressure as a function of distance from the ignition source for an uncontained but congested explosion. More details are provided in the sections below.

4.5.1.1. Vapor Cloud Explosions in a Long-Congested Region

A series of large-scale natural gas vapor clouds were ignited in a 3 m x 3 m x 18 m long region with variable congestion by Lowesmith et al. [120]. The aim of the study was to determine the risk of DDT when flame speed was accelerated by congestion. Flame speed and overpressure values were measured. Initial flame speed prior to entering the congestion was varied from 45 m/s to 156 m/s. Note the speed of sound for NG is approximately 446 m/s at standard conditions.

The experiment took place inside of a 26 m long enclosure. The enclosure contained two regions, a congested region of 18 m length and 3 m x 3 m cross section and a free region of 8.25 m length and 3 m x 2.8 m cross section (W x H). The entire enclosure was filled with a gas mixture of air and methane at 1.16 and 1.09 equivalence ratios. These mixtures were ignited in the free region at variable locations to obtain specific flame speeds prior to congestion. The congested region was formed from 12 racks (designated R1–R12), spaced 1.5 m apart, supporting alternately six or seven horizontal pipes, each 0.18 m diameter. This created a cross-sectional area blockage ratio of 0.36 to 0.42. Images of the enclosure are shown in Figure 24.

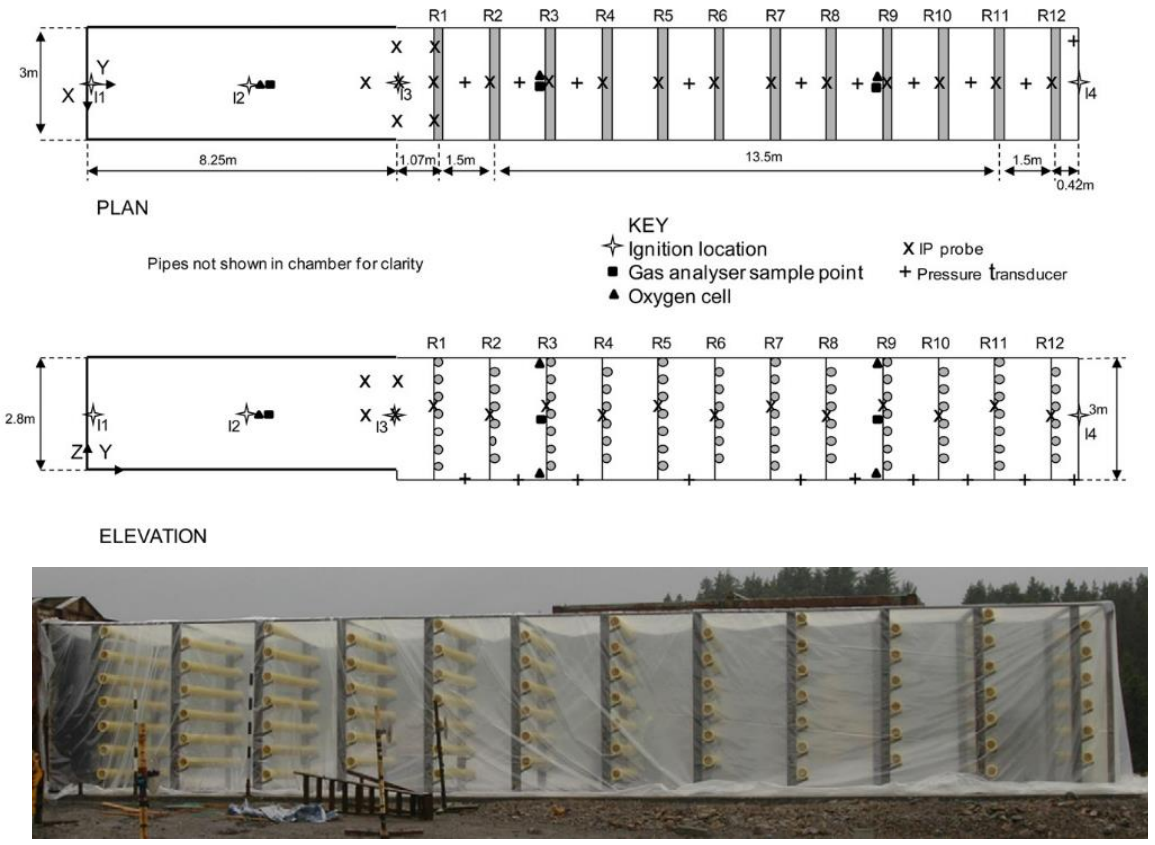

Figure 24: Schematic of Experimental Configuration (from [120])

The gas within the confinement flowed left to right and was recirculated until a desired uniform mixture was obtained. Note that within this study NG as well as NG-hydrogen mixes were evaluated. Lowesmith et al. carried out two tests pertaining to NG air mixtures. These correspond to test numbers VCE01 and VCE04. The test details are highlighted in Table 19:

Table 19: Test Results Summary for CH4 Vapor Cloud Combustions (from [120])

Test	Gas and ER[a]	Ignition details[b]	Initial speed ($m\,s^{-1}$)[c]	Flame speed in congestion	Overpressure in congestion (based on 0.1 ms rolling average data)
VCE01	CH4 (1.16)	I2, 17	~45	Flame accelerated for 4 m to ~130 $m\,s^{-1}$, steadied for 6 m then decelerated	Highest near beginning of congestion peaking at ~340 mbar after 3 m. Thereafter decreased
VCE02	81:19 (1.15)	I2, 17	~57	Flame accelerated to ~200 $m\,s^{-1}$, steadied, then decelerated	Increased over first half of congestion to up to 812 mbar then decreased. Became progressively more shocked up
VCE03	51:49 (1.12)	I2, 0	~70	Flame accelerated throughout congestion and reached over 600 $m\,s^{-1}$	Increased through congestion to over 5 bar and became more shocked up. Some shredded polythene
VCE04	CH4 (1.09)	I1, 10	~156	Flame accelerated quickly to about 300 $m\,s^{-1}$ then remained constant, decelerating near end	Increased over first part, peaking about halfway at about 2 bar then decreased

[a] Methane:hydrogen ratio by volume and equivalence ratio (in brackets) from analyser data (except for VCE04 which was based on manual record).
[b] Ignition location (see Fig. 2) and number of pipes in chamber.
[c] Flame speed entering congestion determined from video and/or IP data.
[d] Reduced congestion arrangement.

For VCE01, Lowesmith et al. report a maximum witnessed flame speed of ~130 m/s and max overpressure of 0.34 bar. For the high initial speed test VCE04, the flame speed accelerated to a maximum of 300 m/s with an over-pressure value reaching 2 bar. These results are graphically shown in Figure 25.

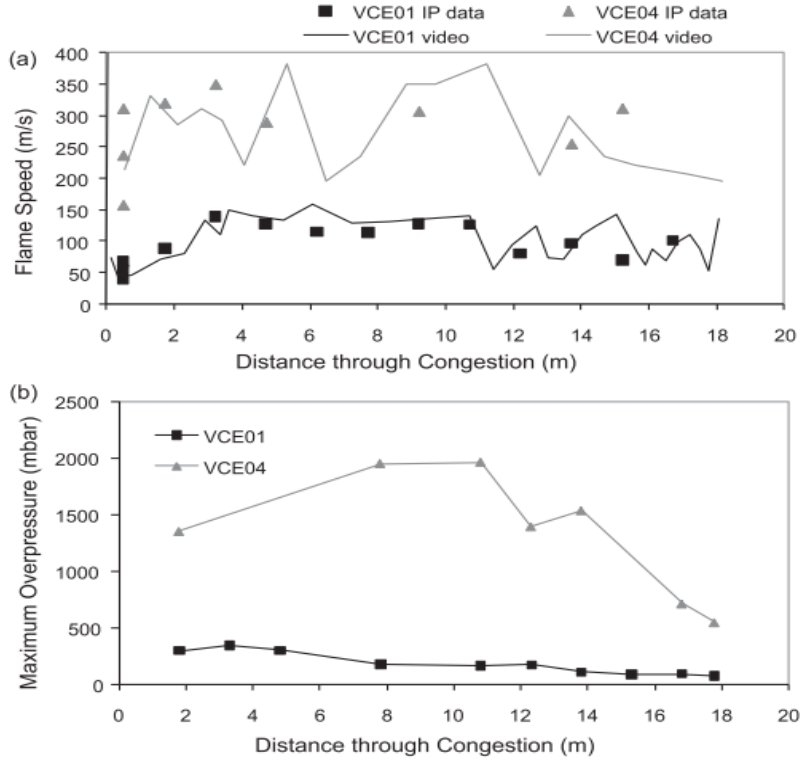

Figure 25: Spatial variation of flame speed and overpressure within the congestion region [120]

Lowesmith et al. explain that despite the high flame speeds and amount of obstructions, the transition to detonation did not occur. This aligns with the work of Harris and Wickens [122] who in a similar study only witnessed deflagration as the flame front accelerated along the length of a highly congested 45 m tube. For cases where methane-air combustions yield DDT severe test conditions are required. The experiments ran by Zipf et al. [124] demonstrated DDT under the conditions of a uniform pre-mixed gas, 0.5 cross-sectional area blockage ratios, high energy ignition sources, and significant geometric confinement. Under these conditions DDT occurred with maximum flame velocities of 812 m/s (Mach 1.82) and greater. These conditions are unlikely to develop from a NGV release in a tunnel due to non-uniform mixing, a lack of confinement/blockage, and no high-energy ignition sources. Thus, the chances of DDT occurring are unlikely.

4.5.1.2. Heat Transfer to Ceiling and Impinging Diffusion Flame

This experiment was designed to study heat transfer from impinging buoyant natural gas jet flames by Kokkala et al. [125]. Heat transfer was measured at the stagnation point of an impinged diffusion flame for various ceiling to flame height ratios. Flame powers ranging from 2.9 to 10.5 kW were studied. Figure 26 displays the experimental setup.

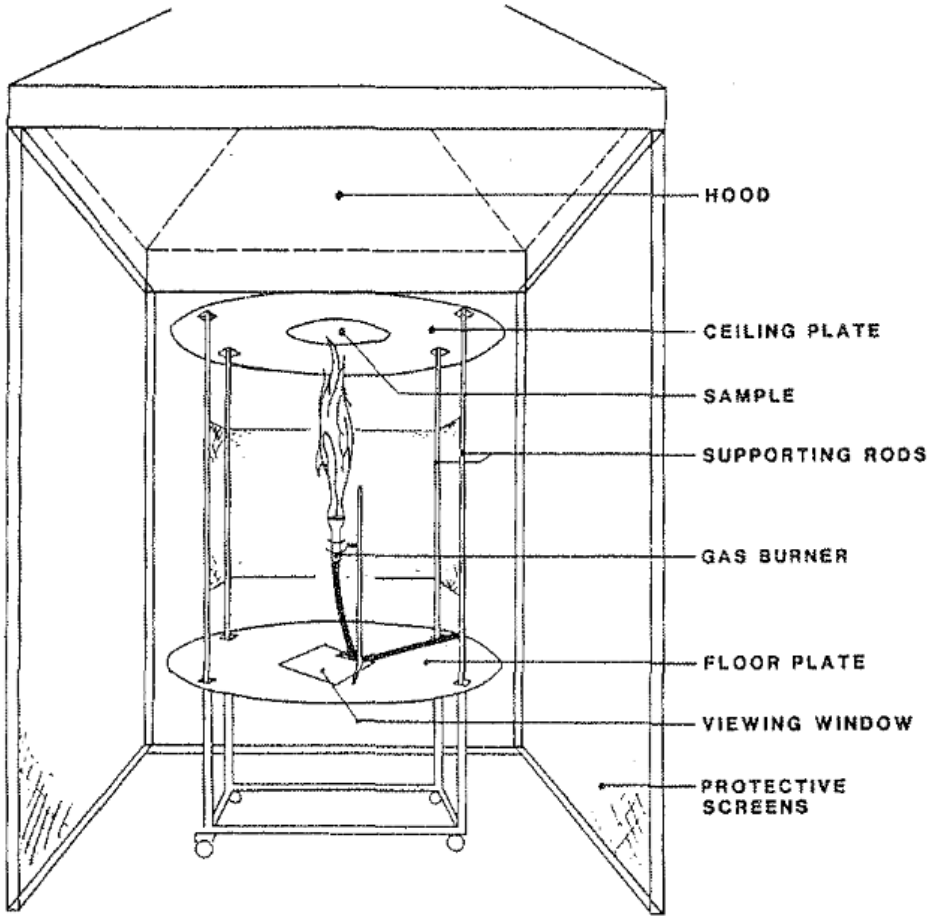

Figure 26: Experimental Configuration (from [125])

As shown, the artificial ceiling consists of a circular plate held in place by four support rods. The support rods also support the floor panel where the burner rests. To protect the experiment from the fluctuating conditions of the lab, the apparatus was surrounded by double screens on all sides. The fuel for the diffusion jet was reported to contain 96% volume of methane gas, which is a typical concentration for CNG.

The thermal readings taken off the ceiling plate consisted of thermocouples for surface temperature and both Gardon type and Schmidt-Boelter type heat flux gauges which provided material independent heat flux readings. The configuration of these sensors on the ceiling plate are shown in Figure 27.

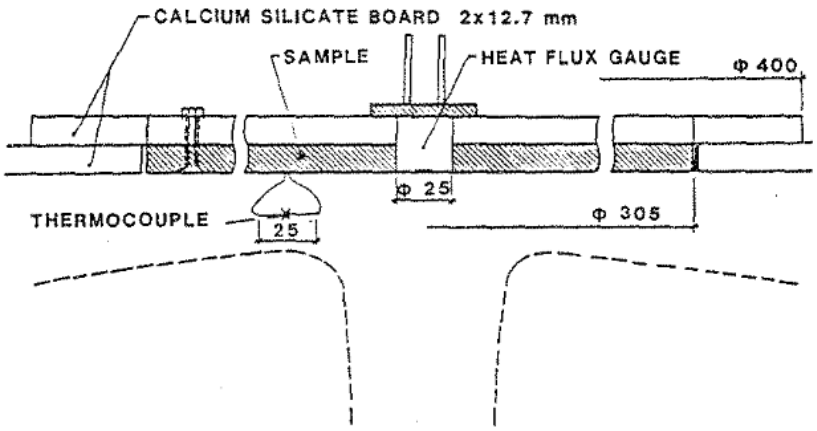

Figure 27: Configuration of thermal sensors on ceiling plate (from [125])

The heat flux gauge is located at the stagnation point of the impinged diffusion flame. This should represent the location of maximum heat flux. Results for the measured heat transfer rates are shown in Figure 28 as a function of the ratio of flame to ceiling height.

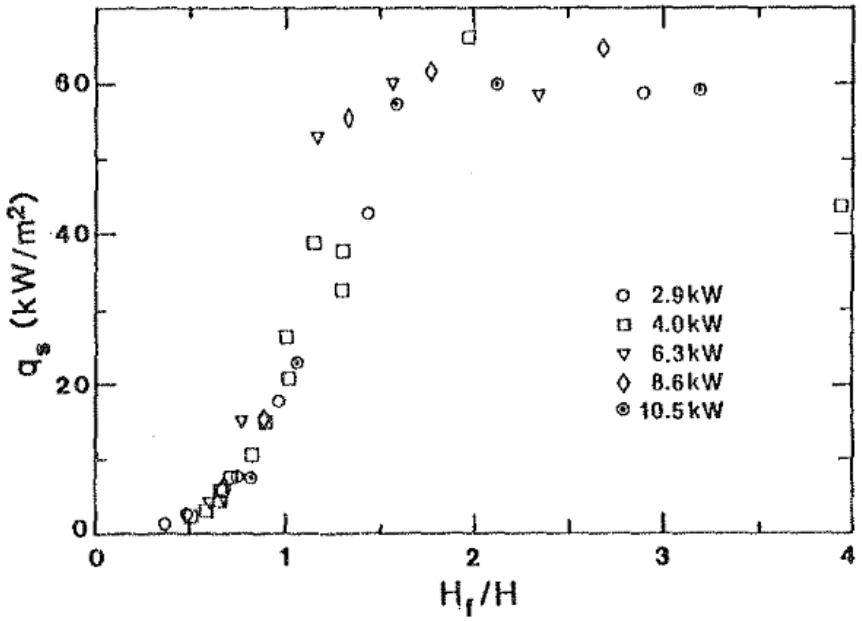

Figure 28: Total heat flux at stagnation point vs. flame height over ceiling height (from [125])

As shown, the rate of heat transfer is varying with the ratio of the flame height to ceiling height. The gradient of heat transfer begins to steepen at the point where H_f/H reaches unity and plateaus around $H_f/H > 1.5$. Regardless of the flame power, the maximum heat transfer rate was measured to be approximately 60 kW/m^2. In other words, for the worst-case scenario, the maximum expected heat flux is around 60 kW/m^2 for the type of leak sizes and studied. Thus, tunnels capable of withstanding a 60 kW/m^2 heat flux over the duration of a NGV fuel release should have a low risk of failure from an impinged jet flame.

4.5.1.3. Vapor Cloud Explosions from Ignition of Gaseous Mixtures in a Congested Region

A series of studies were carried out by Royle et al. [123] to measure the overpressure produced from methane and methane/hydrogen mixtures premixed with air when ignited within congested spaces. The experimental space was a 3 x 3 x 2 m region containing multiple layers of pipes. An image of the congested region is shown in Figure 29. A concrete wall sits adjacent to the one side of the congested region. The wall is positioned there to protect the control room and has been shown to not interfere with free field overpressure [123]. Additionally, the wall has embedded pressure sensors at different heights. For this series of experiments, the blockage ratio was reported as 4.40% the total volume. The outside of the grid was covered in a 23 μm thin plastic film which contained the gas prior to ignition. The plastic film was used only to contain the premixed gas mixtures prior to combustion and did not significantly restrict the outflow of gas or the pressure wave.

Figure 29: Congestion region or grid where gas was filled then ignited (from [123])

Methane gas was mixed with air to form a stoichiometric ratio of 1.1 which reportedly produces the highest overpressures. Other gases evaluated in this study were mixtures of methane, air, and hydrogen which are all included in some of the figures and tables below. For this section, only results pertaining to methane alone are discussed. Section 6.5.1.7 discusses the hydrogen portion of this experiment.

The ignition source was located at a height of 0.5 m off the ground and positioned at the center of the grid. For ignition a 2.25 J capacitor was discharged through a spark gap of 6 mm. It was noted that the spark exhibited lower energy than what was discharged from the capacitor. For the instrumentation, overpressure values were measured by an array of low- and high-pressure pressure sensors. The location of the pressure sensors can be seen in Figure 30. All pressure sensors were positioned 500 mm above the ground except for the far field pressure sensors, which were mounted at higher locations due to the topology of the testing pad.

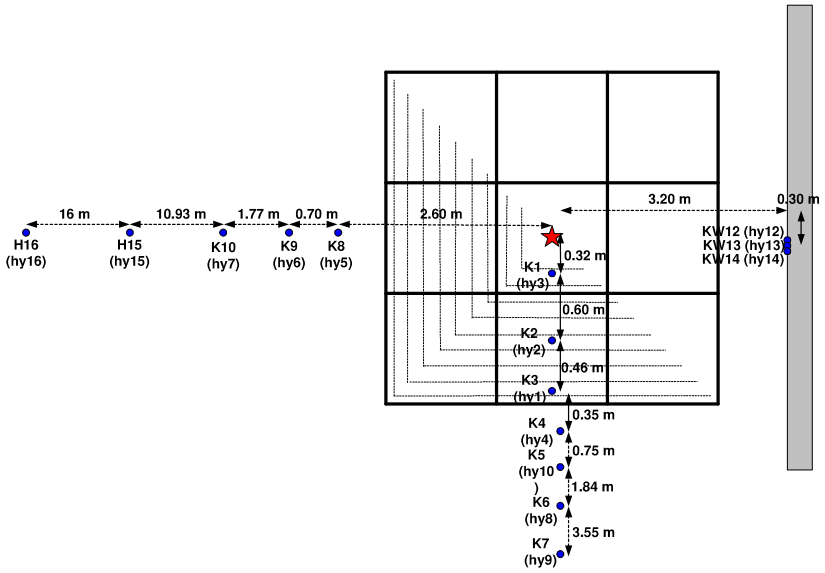

Figure 30: Pressure Sensors distributed in and around grid structure (from [123])

Pressures were measured across a wide span of locations including up the adjacent wall. Table 20 lists the initial conditions prior to ignition. The pure methane is labeled as NatHy_02. For the results of hydrogen/methane mixture experiments, we refer the reader to the paper [123].

Table 20: Initial Conditions of Experiment (from [123])

Measurement	Test Conditions: NatHy_02
Methane (vol. %)	100
Number of Layers	9
Free Volume	17.207
Gas mixture temperature (°C)	4.8
Relative Humidity (%)	85.1
Atmospheric Pressure (kPa)	97.71
Mean Oxygen Concentration (%)	18.71
Partial Oxygen Pressure (kPa)	0.1871
Partial Nitrogen Pressure (kPa)	0.7059
Partial Water Vapor Pressure (kPa)	0.0076
Partial Fuel Gas Pressure (kPa)	0.0994
Mass of Methane (kg)	1.160

It was noted that during experiment the humidity was uncontrolled but was assumed to have a minor effect on the resultant explosion overpressure values. Figure 31 displays an image of the explosion immediately after ignition.

Figure 31: Image of pure methane combustion right after ignition (from [123])

Figure 32 and Figure 33 show the measured overpressure values at various locations for all mixtures. Recall that NatHy_02 corresponds to the hydrogen-free methane gas. Pressures were reported in the near-field (within and just outside of the grid) and far-field regions.

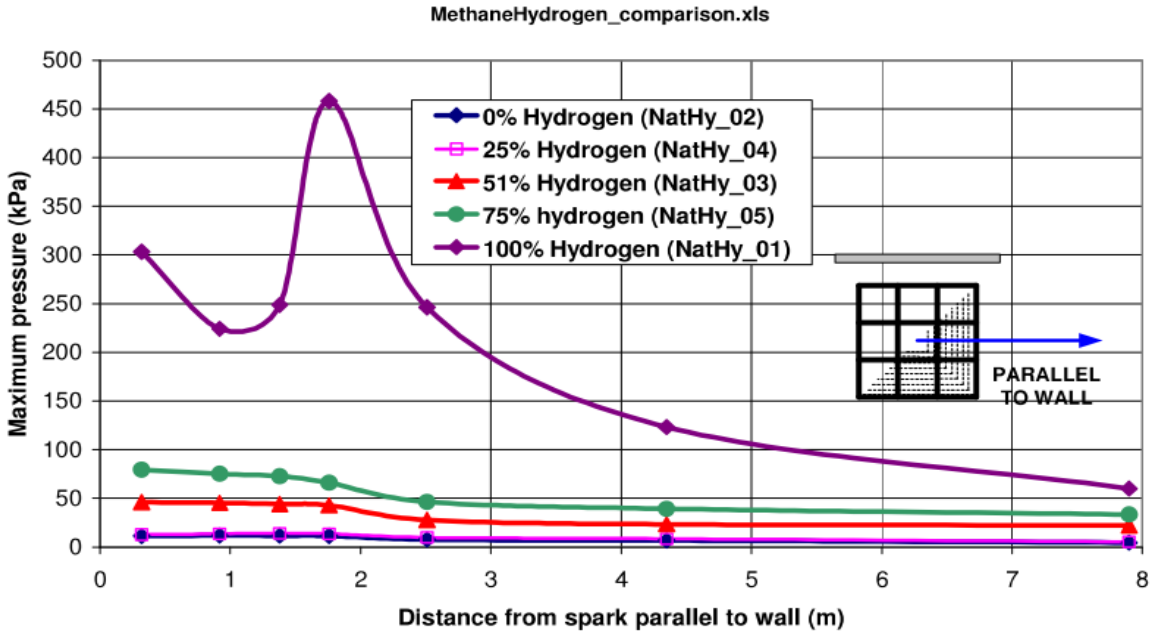

Figure 32: Overpressure vs. of distance parallel to the wall in the near field region (from [123])

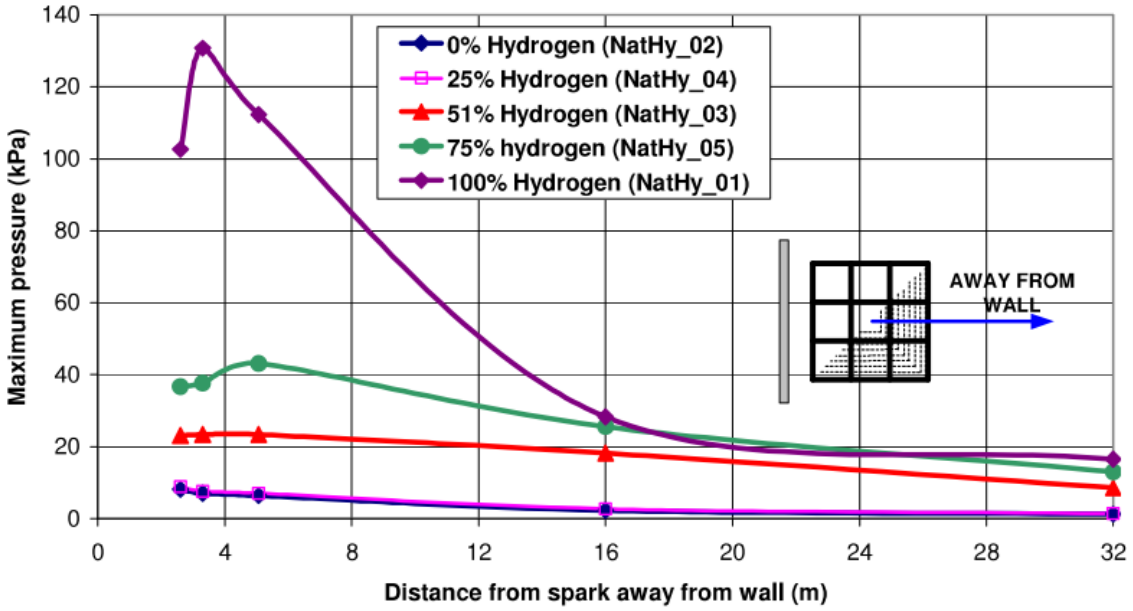

Figure 33: Overpressure vs. distance perpendicular to the wall in the far field region (from [123])

In the near field, overpressure values were 11 to 15 kPa. Inside of the rig, overpressure reached 11.8 kPa and 1.4 kPa just outside the rig. At 32 m away, the overpressure was 1.2 kPa. Referring to Table 1, 11.8 kPa is the threshold for skin laceration from flying glass. Anything below 4 kPa is below the threshold for injury from flying glass. Note that this experiment represented the ignition of a pre-mixed, near-stoichiometric 18 m^3 region with a high level of congestion—both the stoichiometric mixture size and level of congestion are probably unlikely to occur in a tunnel, especially simultaneously.

4.5.2. Modeling

A variety of literature exists on simulations evaluating the risk and consequences of CNG and LNG releases. In one paper specific to CNG vehicles in tunnels, the goal was to capture the likelihood and worst-case scenarios associated with failures of a NGV. The dispersion of CNG was simulated with Fluent to compute the effect ventilation had on mitigating flammable masses (see Section 4.5.2.1). Other simulations have been used to evaluate the release of CNG from a bus in a tunnel, the hazardous overpressures from the combustion of these releases, as well as the flame lengths for several failure scenarios (see Section 4.5.2.2). In Section 4.5.2.3, overpressures were calculated due to the combustion of NG vapor clouds in tunnels, along with a risk analysis study. We also summarize modeling that compared the risk associated with equivalent CNG and LNG vehicle failures in terms of harm and lethality distance (see Section 4.5.2.4). In this work, both the flammable and non-flammable effects on occupants within the tunnel were considered. Overall it has been shown that the associated risks of harm to people and the structure of the tunnel itself is low in most cases of failure. In absolute worst-case scenarios where full instantaneous fuel releases of commercial vehicles occur with no tunnel ventilation and perfect mixing, hazardous overpressures can develop. However, the likelihoods of the worse-case scenarios are implausible, and the hazard can be reduced with proper ventilation.

4.5.2.1. Dispersion of CNG Fuel Releases in Naturally Ventilated Tunnels

Three naturally ventilated tunnels were studied with respect to the transient dispersion of vapor or gas clouds produced during an accidental fuel release by Zalosh et al. [104]. The purpose of this study was to determine the effect ventilation speed had on flammable volume formation and dissipation. Gasoline and CNG releases were compared, sourced from CNG vans with equivalent fuel capacity/driving range to conventional gasoline. For CNG, 24 kg of gas stored at 20,684 kPa (3,000 psig) was released through a 6.35 mm (¼") pipe under choked flow conditions. For gasoline, a tank of 35 gallons was released in a liquid state through a 12.7 mm (½") pipe. The gasoline pooled and subsequently evaporated forming a vapor cloud. The specifics of the vaporization and flow models can be found in [112].

Zalosh measured the average velocity profile during "low traffic" conditions for several tunnels in Boston, including the Rutherford Avenue, Storrow Drive, and Prudential tunnels. The velocity profiles for each tunnel was measured using a hotwire probe on a telescopic pole at various heights (~1 - 5.5 m). During measurements, one lane was closed so readings could be taken from the center of the tunnel. The probe was also moved along the length of the tunnel to obtain the variation along the length. Table 21 provides the tunnel dimensions as well as the cross-sectionally averaged velocities for each tunnel.

Table 21: Tunnel dimensions and averaged velocities (from [112])

Tunnel	Tunnel Dimensions (L x W x H) [m]	Avg Velocity [m/s]
Rutherford Avenue	121.9 x 15.2 x 5.4	1.24
Storrow Drive	304.8 x 9.1 x 15	1.00
Prudential Tunnel	224.0 x 18.3 x 4.6-7.1	1.10
	Average	**1.11**

The CNG release rate was calculated as choked isentropic flow, as described in detail in [112]. Gasoline was assumed to be 53 % pentane, 22% hexane, and 25% benzene which results in a vapor pressure of 5.3 psia at 20 °C and a viscosity of 5.0×10^{-7} kg/m-s.

Fluent was utilized to simulate the dispersion of the two fuels when the van was located at the center of the tunnel. The dispersion models simulated the release occurring inside a computation domain of 100.0 × 8.25 × 4.27 m (L × W × H). The size and shape of the flammable cloud was defined by the lower flammability limit (LFL) for each fuel. The LFL is 5.0 % by volume in air for CNG while the LFL is 1.6 % by volume in air for gasoline vapor. The volume of the flammable region was measured from the release point (van location) to the end of the computational domain set for the model. Figure 34 displays the volume of flammable region obtained for each fuel as a function of ventilation speed.

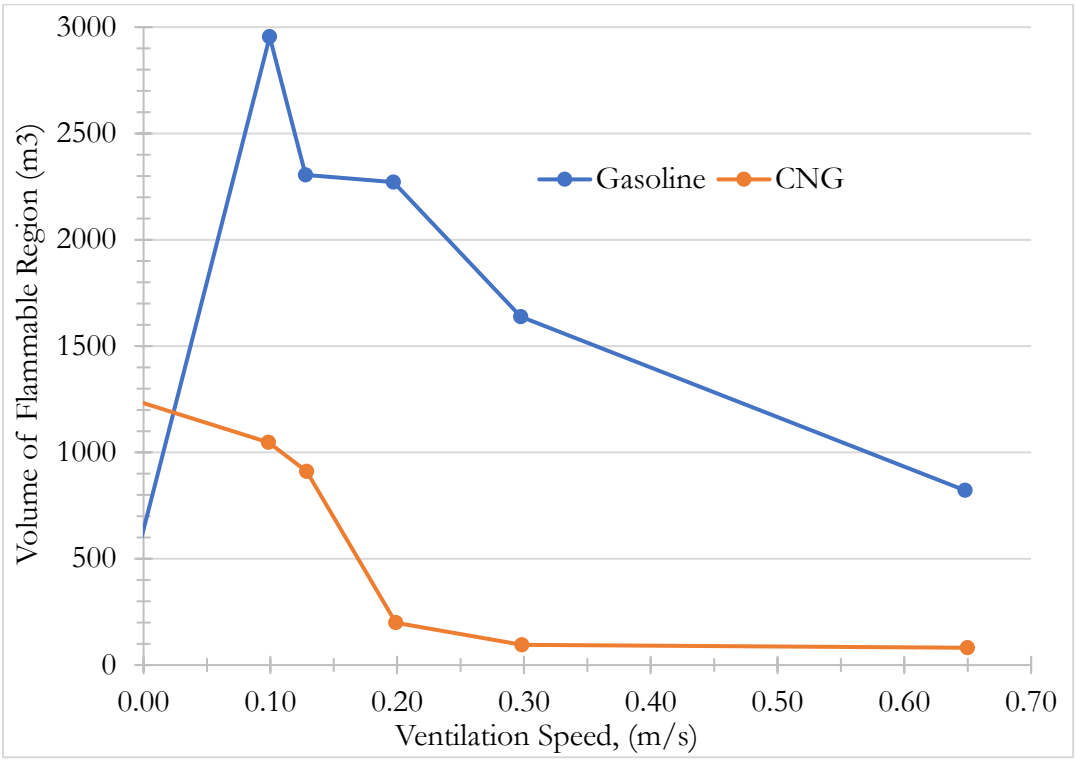

Figure 34: Volume of flammable region versus ventilation speed from simulation (from [112])

An equivalent CNG release produces a much smaller flammable volume when there is minimal ventilation (0.1 m/s). As the ventilation speed increases, so does the gasoline pool evaporation. This relation can be seen in Figure 35. Note that the CNG release rate is constant because the flow is choked regardless of the ventilation speed.

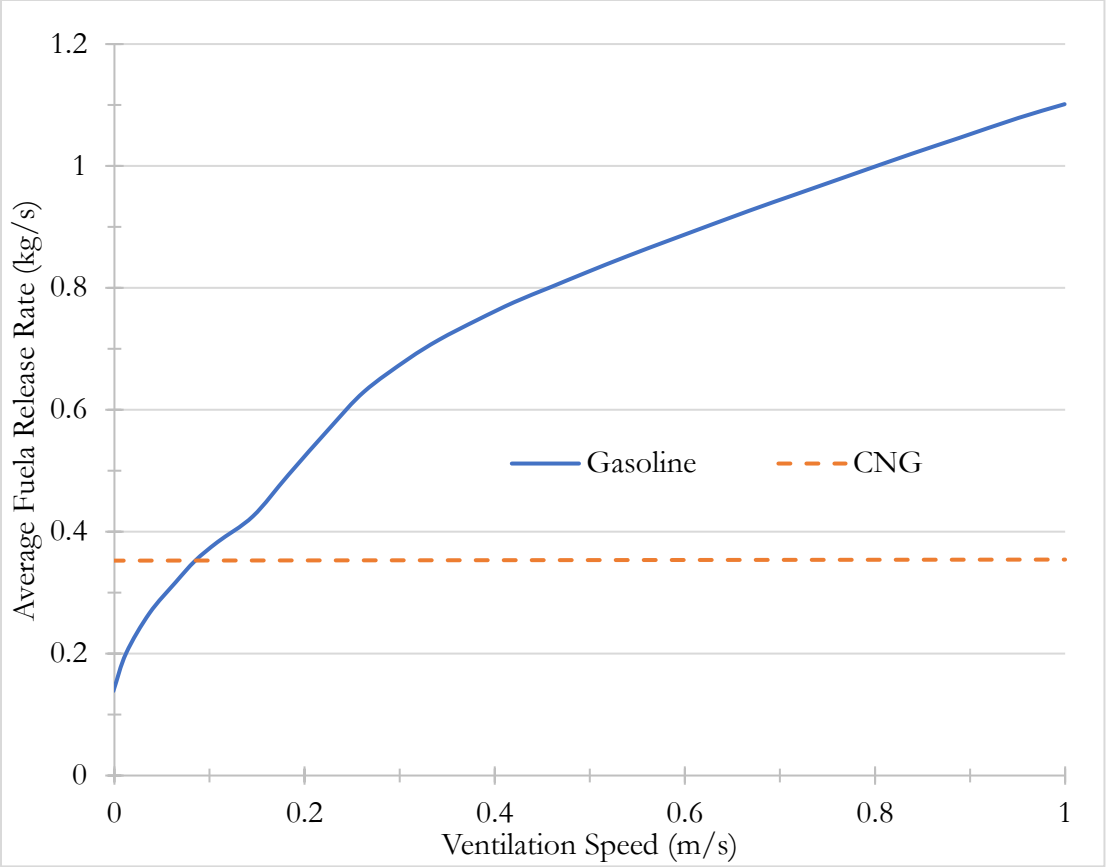

Figure 35: Gasoline Vapor and CNG Release Rates vs Ventilation Velocity (from [112])

The gasoline release rate, on the other hand, increases as the ventilation velocity increases due to increased evaporation. This increase in severity begins to reduce as ventilation speed increases beyond 0.2 m/s. The CNG release rate is independent of the ventilation velocity. Note these values are much lower than the measured average vapor release. Overall, with enough ventilation, CNG releases produce smaller flammable masses than that of gasoline when released in a naturally ventilated tunnel during low traffic ventilation velocity. Zalosh et al. [112] concludes that a CNG vehicle poses a smaller overall flammable region.

4.5.2.2. Gaseous release, dispersion, and combustion for automotive scenarios

Venetsanos et al. [126] CFD was used to study the effects of a compressed gas release from a commercial vehicle in urban areas. One urban area simulated was a tunnel with a single deck city bus located centrally along the length. Variable releases from both hydrogen and CNG fuel tanks were evaluated. The fuel storage systems modeled represented that of a typical European bus with fuel containers located along the roof, forward from the midpoint. The system consisted of 2 sets of 4

tanks connected as displayed in Table 34. The specific CFD solvers utilized were ADREA-HF for dispersion and REACFLOW for combustion.

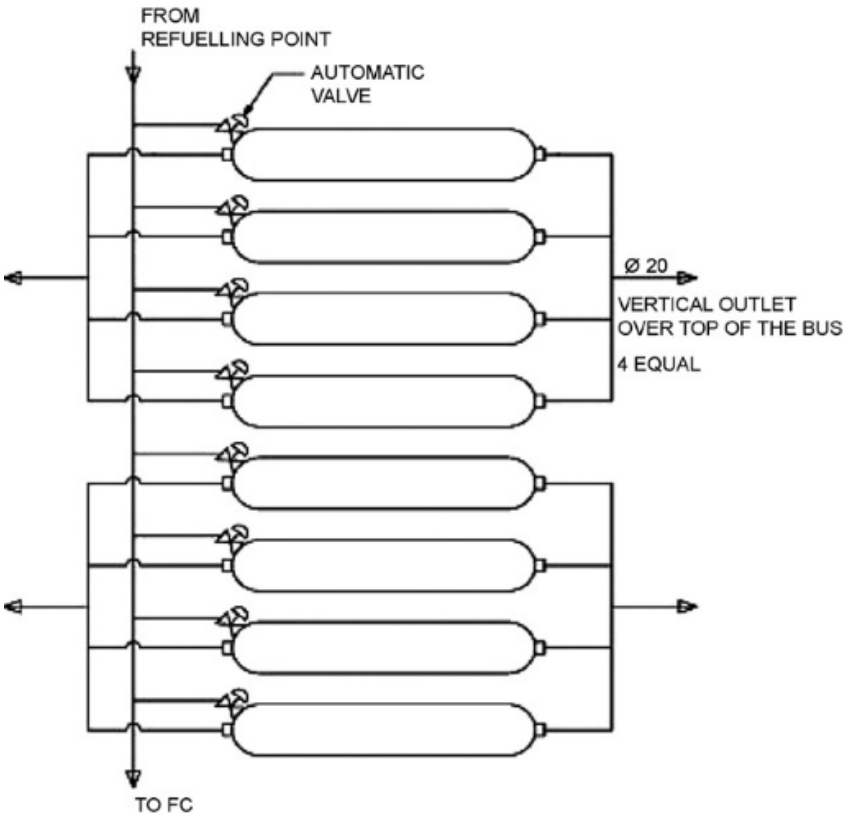

Figure 36: Fuel tanks configuration for both CNG and CH2 gas (from [126])

The tanks contained a total of 168 kg at 20 MPa of CNG. This is representative of a standard CNG bus. The main vent lines are controlled by thermally activated pressure relief devices (TPRD). As shown, each TPRD is attached to a manifold connected to 4 tanks (2 TPRDs per set of 8 tanks). Multiple release scenarios were evaluated by varying TPRD orifice size and tank evacuations. A summation of storage parameters is shown in Table 22. Note this study and the figures below have results for hydrogen systems as well.

Table 22: Storage Configurations (from [126])

Fuel	Pressure (MPa)	Fuel density at 15 °C (kg m^{-3})	Total storage volume (l)	Single cylinder volume (l)	Total fuel mass (in 8 cylinders) (kg)	Fuel mass in one cylinder (kg)
H_2	20	14.96	2672	334	40	5
H_2	35	24.02	1600	200	40	5
H_2	70	40.18	996	124.5	40	5
CH_4	20	168	1000	125	168	21

The computational domain was modeled as a tunnel of 212 m length with a cross-sectional area displayed in Figure 37. As mentioned, the bus was located along half the length of the tunnel in a centralized location. Besides the bus, the tunnel was assumed to be empty and the walls were modeled as smooth surfaces. Additionally, the air was assumed quiescent to represent a worst-case scenario.

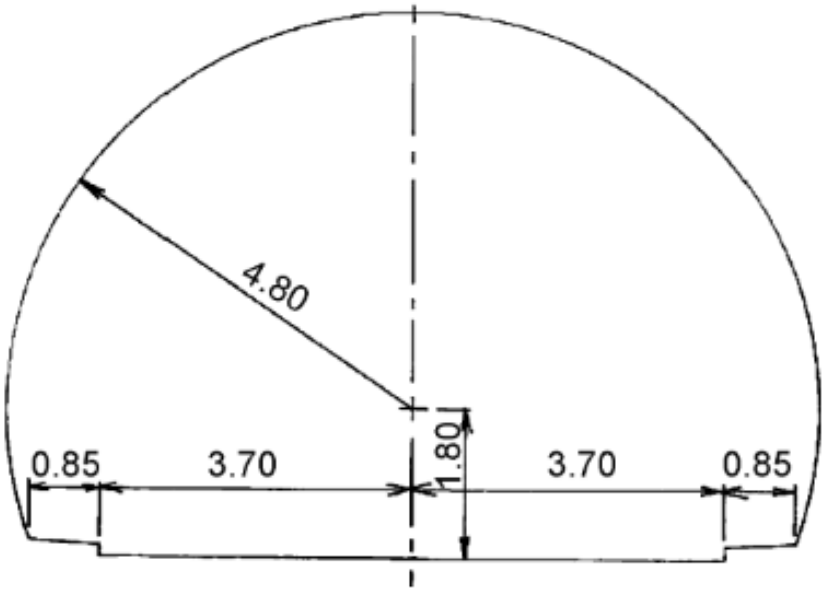

Figure 37: Tunnel Cross Section (from [126])

Two release cases were evaluated for CNG. Table 23 lists the descriptions of all cases, Case 1, and 3 were selected since Case 2 lies between them.

Table 23: Storage Configurations Details (from [126])

Case no.	Possible release	Description	Gas released (kg)
1	Vehicle out of service (automatic valves closed) and one random PRD fuse fails open OR Fire causes a single PRD to trigger[a]	Gas from one cylinder released through 1 PRD vent and 1 outlet	Hydrogen—5 Natural gas—21
2	Vehicle in service (automatic valves open) and one random PRD fuse fails open OR Fire causes a single PRD to trigger[a]	Gas from all cylinders released through 1 outlet	Hydrogen—40 Natural gas—168
3	Fire causes all PRDs to trigger simultaneously[a]	Gas from all cylinders released through all 4 outlets	Hydrogen—40 Natural gas—168

[a]It is assumed that the fire does not ignite the gas. Anecdotal reports by various research and testing organizations indicate that fires that cause temperature triggered PRD to open may not immediately ignite the vented gas. The fire that triggers the thermally activated PRD may not be in a position that causes the vented gas to ignite, since the exit from the vent may not be situated in the fire.

The results for Case 1, where only one cylinder was released through a single TPRD, are shown in Figure 38. The left frame shows the flammable mass and the right frame the total available energy. The available energy was computed by multiplying the released mass of fuel by the lower heat of combustion. The flammable mass was calculated from the amount of fuel/air mixture released which was within the FL. Figure 39 displays the results for Case 3, where all 8 cylinders released through all 4 TPRDs simultaneously. This case may be implausible.

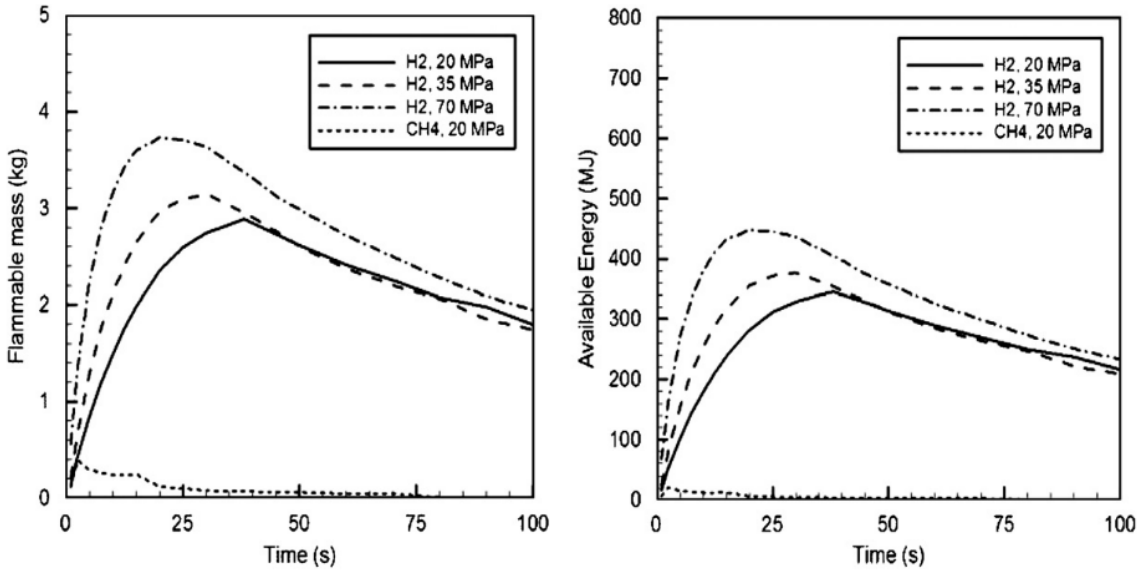

Figure 38: Flammable mass and available energy of released gas in Case 1 (from [126])

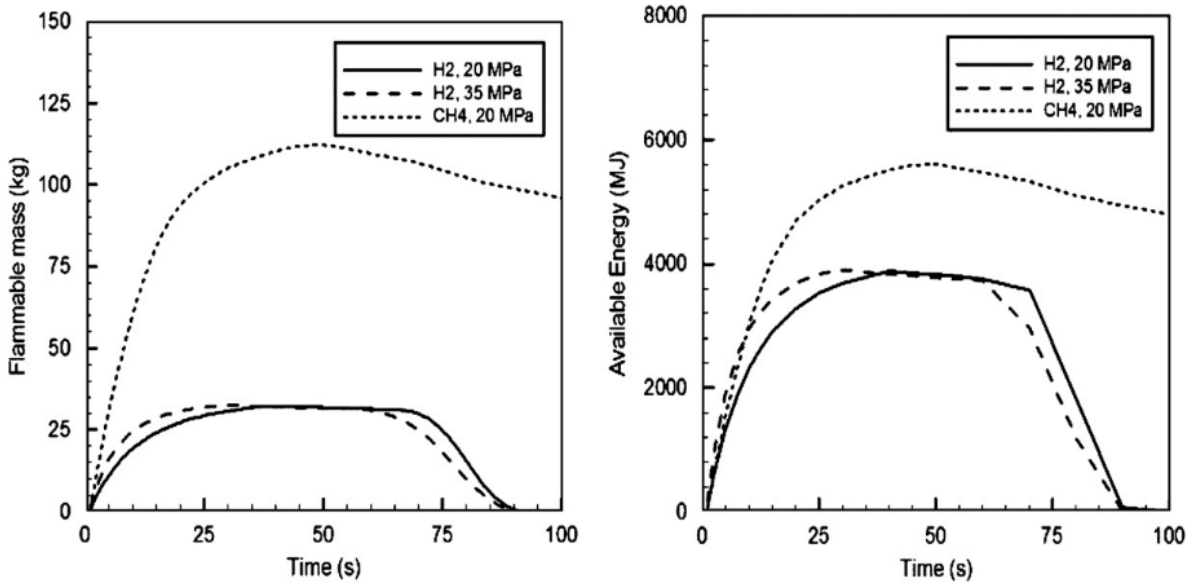

Figure 39: Flammable mass and available energy of released gases in Case 3 (from [126])

Note the change in scales between Figure 38 and Figure 39. For Case 1, both the flammable mass and available energy maintained lower values and dissipated rapidly in time. For Case 3, the flammable mass and available energy reached dangerous levels which persisted over the length of the simulation.

It was assumed the Case 1 overpressures would be negligible because the total flammable mass was less than 0.5 kg. For Case 3, the overpressure values are displayed in Figure 40. The overpressure was calculated assuming that the cloud was ignited after 40 seconds, corresponding to maximum flammable mass. The ignition point was assumed to be at the center of tunnel at the top of the bus.

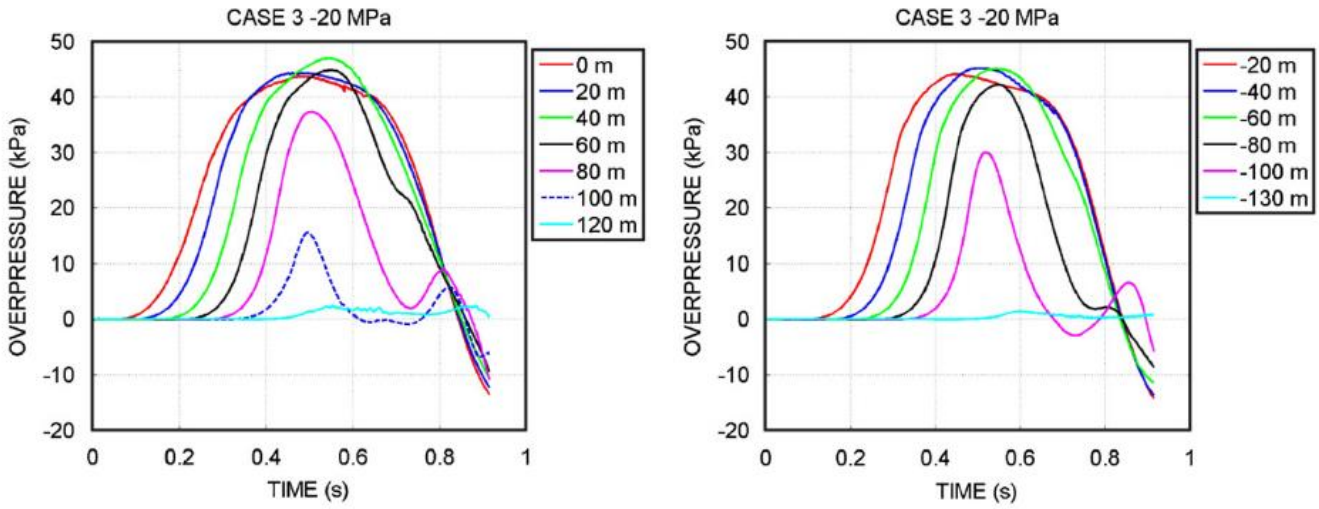

Figure 40: Overpressure values up and down tunnel of the bus for release Case 3 (from [126])

When reviewing these overpressure values, it is important to keep in mind what pressure values correlate to what level of property damage or human hazard. The tables listed in Section 1.2 help understand the damage and tenability thresholds. Case 3 scenario yields overpressure values capable of rupturing eardrums and creating harmful glass splinters up to a distance 80-100 m from the ignition point. Note that the range for the eardrum rupture threshold reported in Table 1 is 16.5-19.3 kPa. Venetsanos et al. [126] states that the blast wave maintains its strength for long distances inside of tunnels due to the high levels of confinement compared with urban environments where blast waves decay quicker. In addition to overpressure, Venetsanos et al. [126] reported the fireball length along the tunnel, the results for each scenario are displayed in Table 24.

Table 24: Combustion results within tunnel (from [126])

Scenario				Effect	
Case	Fuel	Pressure (MPa)	Energy (MJ)	Fireball Length along the tunnel (m)	Overpressure Peak overpressure (kPa)
1	H_2	20	346	62	2.3
		35	377	58	2.3
		70	448	47	2.3
	NG	20	19	S	S
3	H_2	20	3890	220[a]	42.5
		35	3900	285[a]	150
		70	NM	NM	NM
	NG	20	5380	198	45

Notes: S: Small flammable mass. Calculations were not performed, as the overpressures and fireball size were not expected to be significant. NM: Not modelled. Typical overpressure effects (based on various scientific sources): 2 kPa: Threshold of window breakage. 21 kPa: Threshold of eardrum rupture and moderate building damage. 35 kPa: Severe building damage, i.e. unusable.

[a]The flame extends beyond the limits of the tunnel (tunnel length = 212 m).

For Case 3, the NG combustion produced a flame length which traveled nearly the length of the tunnel, 198 of the total 212 m. The flame length for Case 1 NG combustion was reported to be negligible. It is worth noting that in this study, Case 3 represents an implausible scenario of rapid and complete fuel release, ignition when the peak flammable mass is present, and static air within the

tunnel. This study further identifies the importance ventilation plays on mitigating risk during an accidental release of fuel in a tunnel.

4.5.2.3. Natural Gas Vehicle Explosion Risk in Tunnels

Middha et al. [127] used CFD modeling to support the evaluation of explosion risks for NGV (both cars and buses) in tunnels. The objective of the modeling was to predict a quantitative explosion risk for CNG in tunnels. The solver utilized for simulations is commercial code FLACS.

Both NGV and H2 vehicles were studied in the simulations but this section will only make comment on results pertaining to CNG. As mentioned, both a CNG car and bus fuel release was modeled. The CNG car and bus parameters are described by Middha et al. as follows:

1. City bus with a storage pressure of 200 bar and a mass of 26 kg in each cylinder. It is assumed that the release occurs from a set of four cylinders with a total inventory of 104 kg.
2. Car with a storage pressure of 200 bar and a total gas mass of 26 kg.

The values described above represent configurations of standard CNG vehicles as described in Section 4.1.

As for the tunnels, two different cross sections were evaluated, rectangle and horseshoe shape, see Figure 41 for cross-sectional dimensions. Both tunnels were modeled with a length of 500 m.

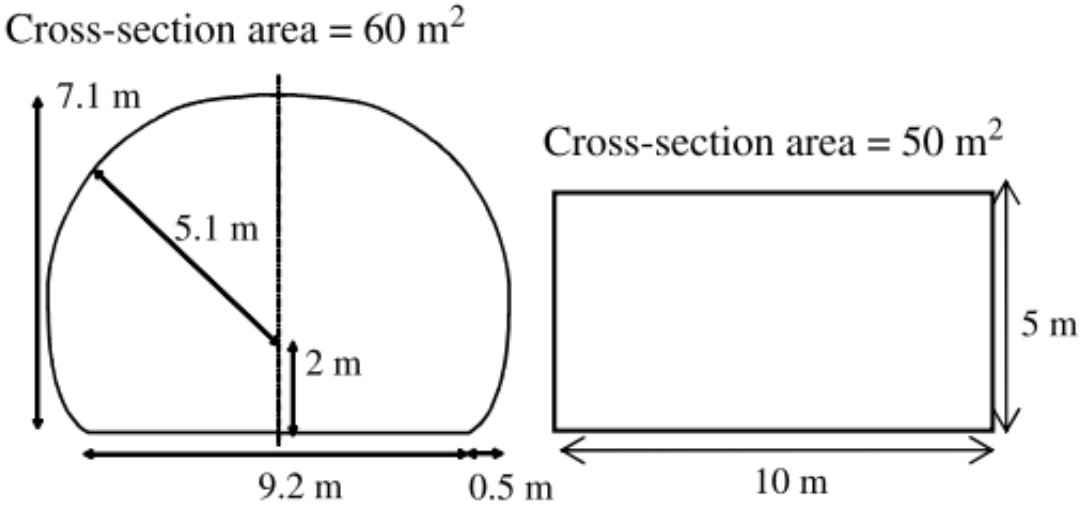

Figure 41: Tunnel cross-sectional dimensions (from [127])

In addition to the cross-sectional dimensions and length, the geometry of the modeled tunnel included vehicles. The tunnels were dual lane with traffic running a single direction. The tunnel was assumed to be full of cars and buses spaced out evenly with 1.5 m between each. The vehicle distribution was a repeated pattern of 6 cars follow by 1 bus. The vehicles were placed such that one bus and one car were at the exact center of the tunnel length in separate lanes. The same geometry was used for both the car and bus release. The releases were assumed to be choked flow. The mass flow rate of the CNG for choked flow at 200 bar is displayed in Figure 42. Note that this was computed assuming a discharge coefficient of 0.8 and a 6 mm opening.

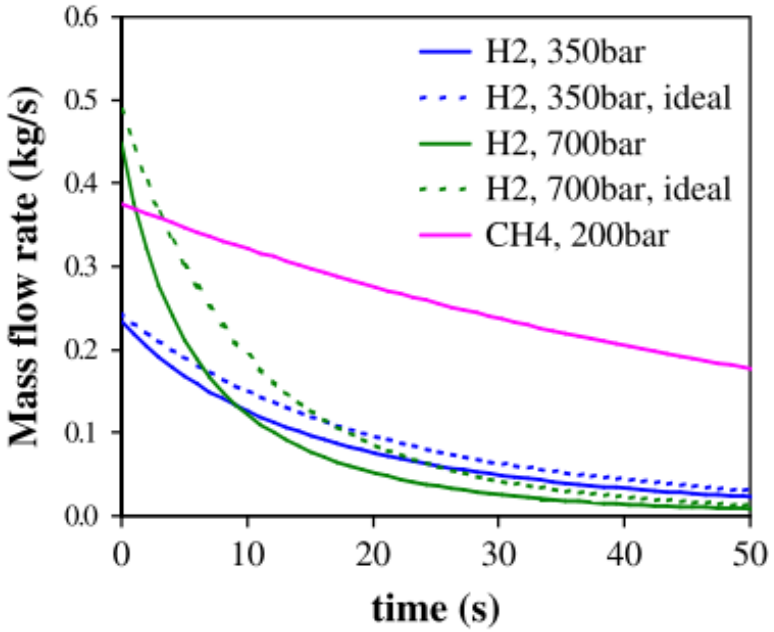

Figure 42: Mass flow of release for CNG and various H2 simulations (from [127])

Ignition points were varied from the center of the vapor cloud to the outer edges (length wise of the tunnel). Ventilation velocities were also varied between the models.

A dispersion model simulating the release of the fuel systems was carried out. Table 25 lists the maximum flammable gas cloud size for each configuration as well as the equivalent stoichiometric cloud or the Q9 quiescent cloud. This is a scaled smaller stoichiometric gas cloud that represents the same explosion load as the non-homogenous larger cloud. It is scaled based off the weighted volume expansion, flammable volume, and laminar burning velocity. The flammable cloud and its stoichiometric and Q9 equivalents along with the maximum pressures for the combustion of the flammable gas clouds are listed in Table 25 below:

Table 25: Summary of gas cloud & overpressure for various vehicles in both tunnels (from [127])

Vehicle/Release Characteristics	Inventory (kg)	Maximum flammable gas cloud size in m³ (kg)		Maximum equivalent stoichiometric flammable gas cloud size in m³ (kg)		Max. pressure for max. equiv. cloud Q9 Quiescent/Pre-ignition turb.	
		Horseshoe Tunnel	Rectangular Tunnel	Horseshoe Tunnel	Rectangular Tunnel	Maximum Q9 Equivalent Volume (m³)	Maximum overpressure (barg)
Bus CNG 200 bar	26	3.4 (0.15)	4.6 (0.19)	1.15 (0.08)	1.18 (0.08)	1.2	0.01/0.01
Bus CNG 200 bar	104	45 (2.01)	647 (26.0)	13.47 (0.90)	113.48 (7.60)	113.0	0.03/0.30
Car CNG 200 bar (vent up)	26	2.1 (0.10)	3.4 (0.15)	0.85 (0.06)	1.03 (0.07)	1.0	0.01/0.01
Car CNG 200 bar (vent down)	26	17 (0.78)	15 (0.65)	6.31 (0.42)	5.25 (0.35)	6.3	0.01/0.07

From the coupled dispersion combustion simulations, it is predicted that overpressure values can produce minor damage to people and property within the tunnel. Referring to Table 1, these overpressures fall between the threshold for injury from flying glass and in the pre-ignition

turbulence case up to potentially serious wounds from flying glass near 50% probability. The data presented in Table 25 were combined to create a frequency of exceedance curve for overpressures during combustion of CNG vapor clouds, shown in Figure 43. Overpressure values outside the hazardous range (less than 0.1 barg) are much more likely than higher overpressures that can be hazardous to tunnel occupants.

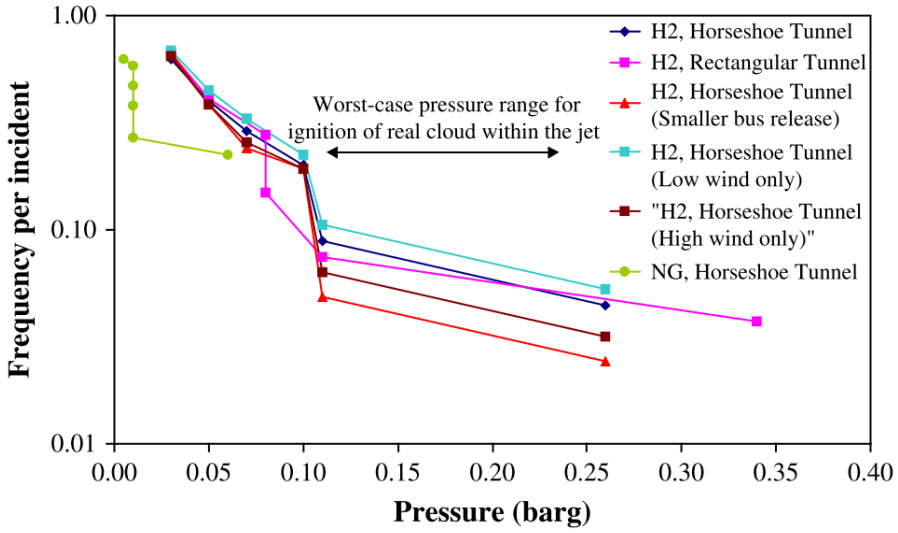

Figure 43: Exceedance curves for overpressure values per fuel type (from [127])

4.5.2.4. Harm effects of Cryo-compressed hydrogen versus natural gas

Zhiyong et al. [128] evaluated CNG, LNG, and cryo-compressed hydrogen in terms of harm, lethality, and separation distances. Both flammable and non-flammable effects were considered. The potential hazards to people included cold hazard effects from cryo-release, thermal effects from combustion with both immediate and delayed ignition, and overpressure or projectile effect due to explosion. The simulated comparison was completed by coupling methodologies from several prior works. Specifically, dispersion was modeled by Witlox et al. [129], jet fires by Cook et al. [130], and overpressure from explosion by Tang et al. [131].

Two quantifications metrics were applied: a harm criterion which corresponds to a 1% probability of fatality and a fatality criterion which corresponds to a 100% probability of fatality. The criteria for cold effects was taken in reference to a European Industrial Gases Association document [14] which states which states that a temperature of -40°C corresponds to harmful effects. The thermal effects on people within the flammable mass region during ignition or in direct contact with an ignited jet flame is considered fatal. In terms of heat radiant heat transfer, harm is quantified by thermal dose units, which is a combination of heat flux intensity and time of exposure. From the literature [132] values for a dangerous thermal dosage range from 420 $(kW/m^2)^{4/3}$ to 1655 $(kW/m^2)^{4/3}$. The lower value was utilized to remain on the conservative side of harm analysis. Additionally, for flash fires, no standard criterion is present but Marangon et al. [133] suggests that a flash fire occurring even at ½ LFL could have lethal effects.

The modeling assumption for each fuel type as well as other release conditions are summarized in Table 26. Conservative model choices were selected for release situations, such as the release direction was assumed to be horizontal and in the downwind direction with respect to a 5 m/s wind. Additionally, the release orifice was set to 10 mm diameter which corresponded to an expected leak

size in the connecting parts of the fuel systems where leaks are more likely to occur. The release height was also assumed to be 1 m from the ground which was assumed to be a good average effect height for a person.

Table 26: Assumed modeling parameters for simulation (from [128])

Item	Cryo-Comp. H_2	CNG	LNG
Release pressure (bar)	350	250	1
Release temperature (°C)	-210	15	-152
Release inventory (kg)	5.6	28.8	28.8
Release direction	Horizontal and downwind for continuous release		
Release hole size (mm)	10		
Atmospheric Pressure (atm)	1		
Wind velocity (m/s)	5		
Result output height (m)	1		

Also note the fuel capacities were selected based on equivalent mileage instead of energy density. The results are shown in Figure 44 where the two graphs display the harmful and fatal distances for each incident per fuel type based on an assumed instantaneous release of the inventory, which is implausible. The non-flammable effects are without ignition of the flammable cloud, whereas the flammable effects correspond to immediate or delayed ignition depending on which produced the larger hazard.

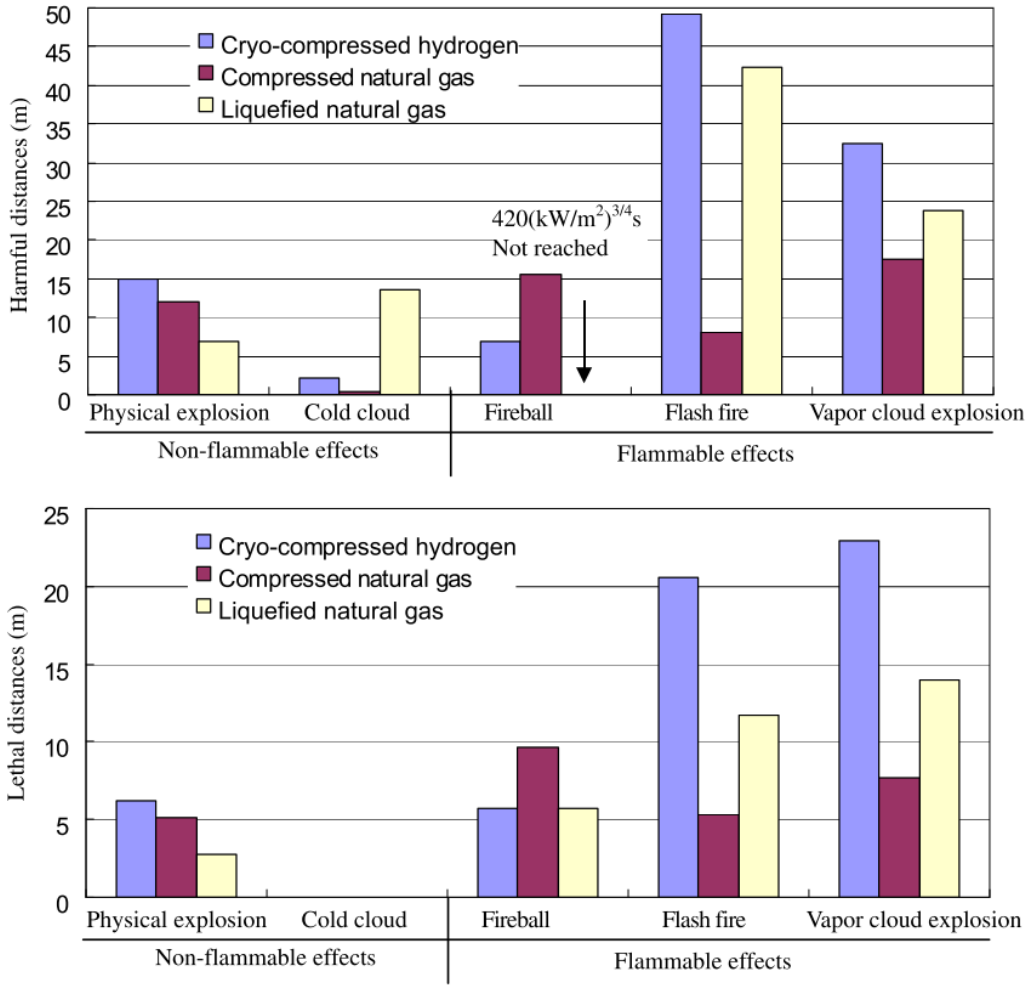

Figure 44: Harmful/fatal distances per incident for instantaneous release (from [128])

For non-flammable effects, LNG posed long distance hazards due to the potential for cryogenic injuries. For flammable effects, overpressure damage from flash fires or vapor cloud explosions were larger with LNG compared to CNG when ignition was delayed. The hazards associated with LNG are intuitive due to the low storage temperature (111 K) and the larger volume of stored fuel forming larger flammable masses. For CNG the risk of physical explosion and thermal hazards are higher due to the high storage pressure and high heat flux associated with a jet fire (see Figure 45 below). As mentioned in Section 4.3, it should be noted that BLEVE is a risk associated more closely with cryogenic fuels due to the higher chance of rapid expansion due to phase change during a release event.

Below Figure 45 shows the hazard distances for each fuel when the release occurs at a continuous rate rather than instantaneous:

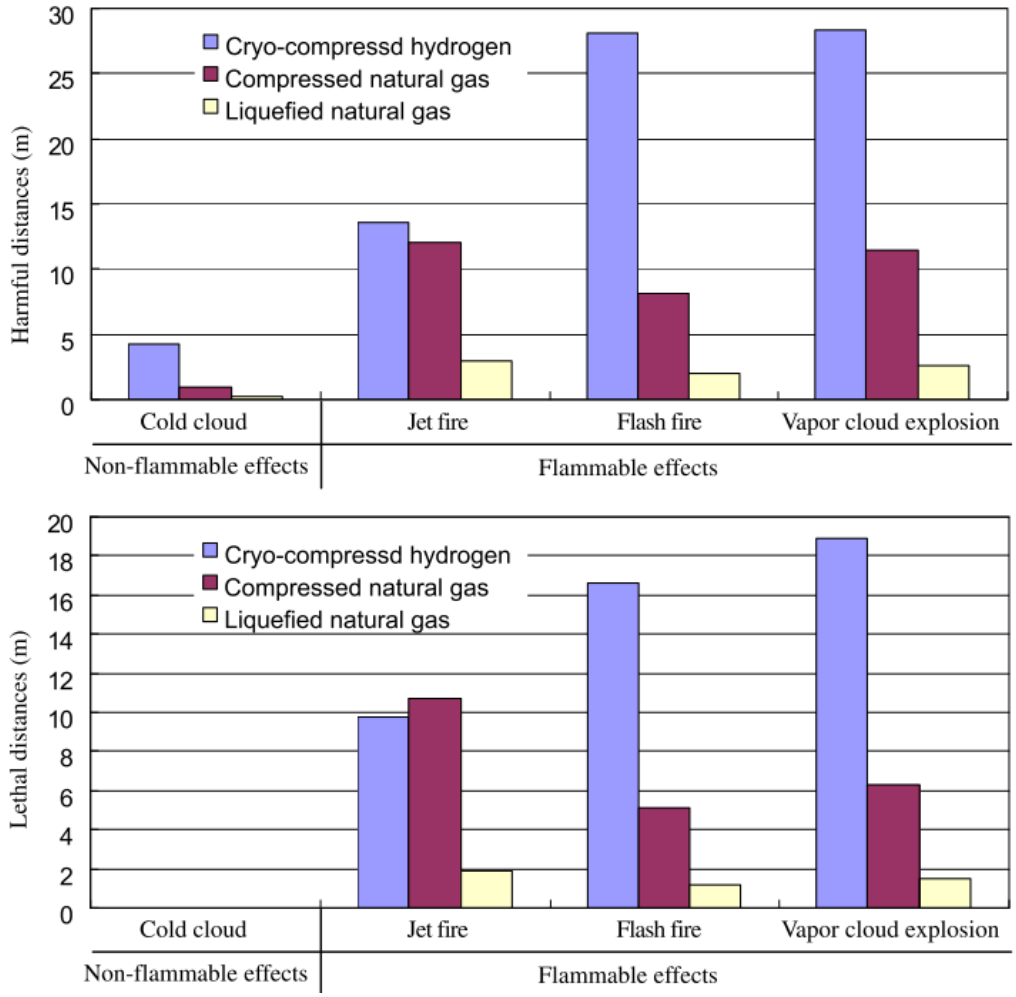

Figure 45: Harmful/fatal distances per incident per fuel type for continuous releases (from [128])

Due to the high storage pressure, CNG will release at a more rapid rate and thus produce higher hazard distances for continuous releases. Li [134] shows that LNG vehicles pose their own unique hazards which exceed CNG in risk in specific situations. It should be understood there is a low probability of a BLEVE, and instantaneous releases are implausible.

4.5.3. Analysis

Scenario identification as well as probabilistic risk assessments have been carried for CNG vehicles in the context of vehicular failure on the roadways. To our knowledge, there are no specific evaluations of NGV risks within tunnels including event sequence diagrams. However, a study comparing a CNG powered buses related hazards to that of current conventionally diesel-powered buses showed that CNG posed higher probabilistic risks.

4.5.3.1. Compressed Natural Gas Bus Safety: A Quantitative Risk Assessment

The analysis carried out by Chamberlain and Modarres [135] compared the fire safety risk associated with a CNG bus against that of a more conventional diesel-fueled bus. Since the data involving critical failures of heavy-duty CNG vehicles is limited, a probabilistic risk assessment (PRA) was performed with a two-step approach. The first step was to perform a qualitative risk analysis (QRA)

followed by quantitative PRA. The QRA was used to determine the possible fire scenarios that should be further studied in the PRA.

Chamberlain and Modarres identified the associated fire-safety hazards used to assess the risk of using CNG fuel:

- Fire potential from fuel leakage.
- Explosion potential from uncontrolled dispersion and mixing of CNG in the presence of an ignition source.
- Impacts and missile-generated hazards due to fuel being stored at high pressure.
- Chemical hazards (gas toxicity, asphyxiation potential, and higher hydrocarbons in CNG may be considered neurotoxins even though CNG is relatively nontoxic).
- Electrostatic discharge.

A failure mode and effect analysis (FMEA) was used to identify the most significant failure modes. These failure modes were determined based on the frequency of occurrence as well as the overall consequence. From there, a PRA with event trees and fault tree modeling to describe the events leading to various fire and explosion hazards was performed. Parameter uncertainty was also discussed and how it affected the PRA results. The entire bus fuel system as well as the supporting infrastructure (such as fueling stations) was included in the evaluation. Figure 46 represents a typical CNG bus fuel system.

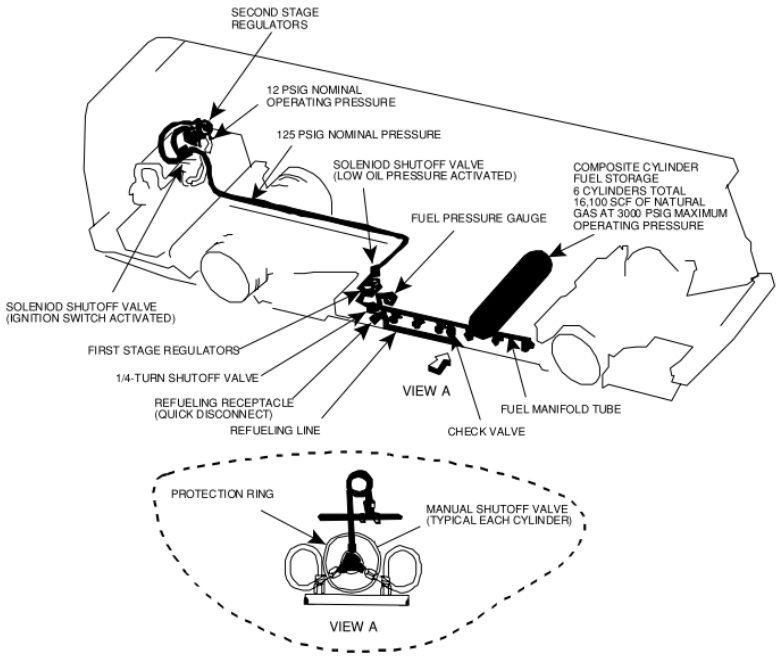

Figure 46. Fuel supply system of a CNG bus (from [135])

Through the FMEA performed, the severity of an accident scenario was categorized, and a ranking matrix was created for CNG systems. Based on a variety of inputs regarding the expected occurrence frequency, scenarios, ignition potential, etc. detailed in the literature, the results in terms of frequency per year, per distance traveled, and total risk are shown in Table 27.

Table 27. Quantitative Risk Assessment (from [135])

Results of Quantitative Risk Assessment			
Scenario Groups Leading to Fire and Fatality	Risk (Mean Fatalities/Bus/Year)	Risk (Mean Fatalities/100-M Miles)	Percent of Total Risk
Catastrophic failure of bus or station hardware components	2.4×10^{-6}	2.5×10^{-2}	10.84
Degraded failure of bus or station hardware components	8.7×10^{-6}	9.0×10^{-2}	38.77
Electrostatic discharge of CNG	2.7×10^{-6}	2.8×10^{-2}	12.21
Accidental impacts mainly due to collision	4.9×10^{-6}	5.1×10^{-2}	21.70
Non-CNG-related fires	3.4×10^{-6}	3.5×10^{-2}	14.94
Operator error	3.6×10^{-7}	3.7×10^{-3}	1.54
Total mean fire fatality risk	2.2×10^{-5}	2.3×10^{-1}	100

From this QRA Chamberlain and Modarres approximated the total mean fire risk to be 2.5 times larger for CNG buses compared to diesel-powered buses. The overall results identified CNG buses as higher risk in terms of fire and explosion hazards due to failure rates of relief valves, CNG cylinders, and piping. This conclusion differs compared to the study by Zalosh et al. [112] which compared CNG and gasoline vans. The CNG vans were shown to pose lower risks regarding flammable gas dispersion compared to the flammable vapor dispersion from a gasoline leak from an equivalent van. The difference is comparing CNG with gasoline and diesel. Zalosh concludes CNG is a lower risk than gasoline while Chamberlain and Modarres concludes it is a higher risk than diesel.

4.5.3.2. LANL Risk Analysis

A comparative risk analysis was performed by Los Alamos National Laboratories to put into perspective the relative hazards of alternative fuels, including LNG and CNG, compared to gasoline and diesel fuels [136]. As part of this analysis, data was collected about the physicochemical properties of natural gas and general petroleum and transportation information. Subsequently, the technical properties of the alternative fuels were ranked, safety data and vehicle accident statistics were reviewed, and specific accident scenarios were evaluated. One of the accident scenarios evaluated was a vehicle collision with fuel loss in a tunnel. An expert panel estimated the probabilities of different outcomes for the different alternative fuels compared to gasoline and diesel. Table 28 shows the results of the risk analysis. These probabilities are just expert judgement rather than data. As shown, the natural gas (both liquid and compressed) was estimated to be less likely to result in a fire with or without injury, or more likely to not ignite, and less likely to result in an explosion when compared to gasoline [136].

Table 28: Probabilistic Outcomes of a Tunnel Accident (from [136])

	Probability				
Consequence	CNG	LNG	LPG	Gasoline	Diesel
Fire without Injury	0.1	0.1	0.15	0.12	0.02
Fire with Injury	0.05	0.05	0.08	0.1	0.01
Explosion	0.05	0.05	0.12	0.2	0.01
No Ignition	0.8	0.8	0.65	0.58	0.93

4.6. NGV Research Gaps

Through this literature study, it was found that there are several existing studies that evaluate NGV vehicles in tunnels. There were several experiments conducted that evaluated the consequences of ignited NG vapor clouds and high-pressure jets and the relevant variables. Specifically, the likelihood of DDT, overpressure, and heat transfer of NGV accidents were evaluated. Also, there were a variety of literature studies that evaluate the risk and consequences of CNG and LNG releases. Specifically, modeling studies evaluated dispersion, failure modes, overpressure, and flame lengths. Analytical studies evaluated scenario identification through probabilistic risk assessments for CNG vehicles in the context of vehicular failure on roadways.

There are several conclusions about important variables and consequences from an NGV accident in a tunnel. One study showed that hazards associated with a CNG-powered bus posed higher probabilistic risks that that of a conventional diesel-powered bus. Also, it has been shown that the associated risks of harm to people and the structure of the tunnel itself is low in most cases of NGV vehicle failure. In implausible scenarios where full instantaneous fuel releases of commercial vehicles occur with no tunnel ventilation and perfect mixing, hazardous overpressures can develop. The occurrence of DDT was shown to be highly unlikely in multiple experiments, even in confined environments with obstructions. Also, a strong correlation for heat transfer to a ceiling based on the flame height to ceiling distance was shown for large scale flames impinging on a ceiling [120].

The following criteria were evaluated to determine where research gaps may exist regarding NGV's in tunnels.

1. Scenario Identification
2. Failure Modes
3. Consequences
4. Validation

The scenarios that lead to a failure mode have been identified as impacts to the vehicle or failure of the TPRD, hardware degradation or failure, and operator error which may lead to a release of fuel. Based on the vehicle and fuel composition state, a BLEVE scenario can be a risk. Failure modes include immediately ignited releases or delayed ignition of releases that might accumulate in tunnels. Component-level failure modes are beyond the scope of this document. Regulations on valves, pressure containers, and other overall fuel storage/delivery systems govern these risks. The failure modes are broken down for a CNG vehicle by Chamberlain and Modarres [135] as the following:

- Fire potential from fuel leakage.
- Explosion potential from uncontrolled dispersion and mixing of CNG in the presence of an ignition source.
- Electrostatic discharge.

Multiple experiments and simulations were reviewed pertaining to fuel releases from NGVs, the consequences, and the effects on tunnels. It was shown that the congestion at the roof of a tunnel can accelerate the flame speed during a vapor cloud combustion, but the chances of this yielding significant damage or DDT occurring are very low [121] [120] [122]. Furthermore, [137] showed that with proper ventilation, the risk from overpressure during a combustion are significantly mitigated. In terms of heat transfer, 60 kW/m^2 was shown to be around the maximum expected rate for a jet fire impinging on the ceiling. It was shown this applies to flames of a wide range of power [125]. Additional consequences of these failure modes include impacts/projectile-generated hazards due to

fuel being stored at high pressure, chemical hazards (gas toxicity, asphyxiation potential, and higher hydrocarbons in CNG may be considered neurotoxins even though CNG is relatively nontoxic), peak overpressure due to ignition ranging from 30 to 45 kPa based on the pressure of the release and release amount as shown in [126] and [127], and fireballs that can reach nearly 200 m down a tunnel based on the tunnel geometry and the release pressure [126].

Initial observations show that flammable cloud formation for CNG becomes negligible as ventilation increases [112]. The harmful and lethal effect distance of CNG for a continuous release event is significantly lower than an LNG release. A risk analysis for a CNG bus system shows the highest risk comes from degradation of the system and components [135].

Despite the large quantities of studies carried out pertaining to the risks and hazards associated with NG, research gaps were identified. As discussed thoroughly in Sections 4.5.1 and 4.5.3, the consequences of scenarios have been evaluated and validated in multiple experiments and simulations. Research gaps regarding consequences are the same as for scenario identification: limited evaluations of NGVs specifically in tunnels have been carried out. Several specific research needs include:

- The risk of spalling of tunnel surface from flame impingement or heat from a NG jet flame.
- Experimental studies of NG dispersion and overpressure in actual or scaled down tunnels (similar to HyTunnel evaluations).
- Partially pre-mixed (realistic extents of pre-mixing) ignition in tunnels to determine maximum overpressure.
- Large scale NG flames heat transfer analysis. So far only lab-scale or simulated data found in the literature.
- Validation of the experiments and modeling studies.

Additional attention should be given to the size or class of the vehicle. As vehicular class increases so does the amount of stored fuel. This can lead to an increased flame duration or formation of a larger flammable vapor cloud. Table 29 (below) shows the approximate equivalent ambient gas volumes of stored NG per vehicle class.

The vehicle class groups used were those defined by the Federal Highway Administration [138]. The storage volumes used for this approximation are representative of a typical tank size based on vehicle class. The actual storage volume varies from vehicle to vehicle within the same class based on design choices of the manufacturer. Since the vast majority of LNG vehicles are large scale commercial vehicles, the approximate LNG tank sizes are based off reported values from this vehicular class.

Table 29. Natural gas fuel amounts by vehicle class.

FHWA Class - CNG	Characteristic Mass	Characteristic Ambient Unmixed Volume
2	22.0 kg	34 m^3
3	132.0 kg	201 m^3
4	225.0 kg	343 m^3
5	125.0 kg	191 m^3
7	550.0 kg	838 m^3
FHWA Class - LNG	**Characteristic Mass**	**Characteristic Ambient Unmixed Volume**
5 or greater	200.0 kg	305 m^3
5 or greater	250.0 kg	381 m^3

Per the Federal Highway Administration, class 2 represents SUVs, pickups and utility vans, 3 delivery trucks and vans, 4 passenger buses, and 5-7 represent a wide range of multi axle commercial trucks. CNG classes 4 and 7 vehicles typically have multi-tank configurations. The listed LNG configurations consist of variously sized single tanks. There are many combinations of tank number and size variations and the values listed above are only representations of some typical configurations listed on select manufacturers websites [139] [140] [141].

This page left blank

5. PROPANE VEHICLES

5.1. Overview of Technology

What is commonly called propane is liquefied petroleum gas (LPG) that has constituents aside from the chemical propane. The terms propane and LPG will be used mostly interchangeably in the remainder of this report (depending in part on the source of information presented). Propane vehicles offer consumers an alternative transportation option to conventionally fueled vehicles. Propane vehicles are available as both dedicated and bi-fuel types. In dedicated propane vehicles, propane is the sole energy source. In bi-fuel propane vehicles, there are two separate fueling systems that allow the vehicle to use either propane or gasoline. Generally, propane vehicles are comparable to conventionally fueled vehicles in terms of power, acceleration, cruising speed, and driving range. There are several different types of propane vehicles currently in operation, including light, medium, and heavy-duty vehicle classes. Lower maintenance costs, good performance in cold-start conditions, and low carbon and low oil contamination characteristics make propane vehicles popular for trucks, taxis, street sweepers, and school buses [142].

5.2. Properties of Propane Storage

Generally, propane is stored under pressure in a two-phase state. When a storage tank is full, the propane is largely liquid with some gaseous vapor. The gaseous vapor in the storage tank is what is used as fuel.

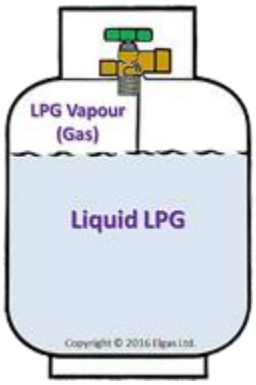

Figure 47: Example of Two-Phase Propane Storage (from [143])

The key properties that make propane an attractive auto fuel is its high-octane value and compatibility with spark-ignited internal combustion engines. Propane naturally occurs as a three-carbon alkane gas with the chemical formula C_3H_8. Propane can be liquefied through moderate pressurization at 1,220 kPa (177 psia) [144], which increases its energy density by a factor of 270 over the gaseous form [145]. In terms of vehicle usage, the propane fuel must consist of at least 90% propane, no more than 5% propylene, and no more than 2.5% other gases such as butane and butylene [146]. Table 30 shows some of the physical and chemical properties of propane [147].

Table 30: Physical and Chemical Properties of Propane (from [147])

Property	Value
Chemical Structure	C_3H_8
Energy Density	23,648 MJ/m^3
Stoichiometric Air/Fuel Ratio	15.5
Gas Density at 15 °C	1.85 kg/m^3
Liquid Density at 15 °C	505 kg/m^3
Auto-ignition Temperature	450 °C (724 K)
Specific Gravity at 15 °C	0.85

5.3. Associated Hazards

There are two main safety considerations related to propane vehicles. The first is tank over-pressurization due to either tank overfill or environmental changes. To address this issue, propane vehicles are equipped with overfill prevention devices (e.g., bleed valves) and pressure release devices to vent the tank if pressure rises beyond safe levels [146]. The second safety consideration is ignition of propane fuel that has either been released through the overfill prevention device/ pressure release device or released from a vehicle crash. Propane gas is heavier than air at standard temperature and pressure (STP) unlike natural gas or hydrogen. Therefore, vapors can collect in low areas such as service pits. Unlike hydrogen and natural gas, propane vapors will dissipate primarily based on air movement rather than buoyancy and will dissipate faster in windy conditions than in still conditions [146]. Table 31 shows relevant flammability properties of propane.

Table 31: Flammability Properties of Propane

Property		Propane
Flammability Concentration in Air (vol%) [27]	LFL	2.1%
	UFL	9.5%
Most Easily Ignited Mixture in Air (vol%)		4% [105]
Adiabatic Flame Temperature [107]		2250 K
Buoyancy (ratio to air)		1.52
MIE [108] [109]		0.25-0.26 mJ
Autoignition Temperature [110]		455 °C

5.4. Pertinent Regulations and Safety Standards

Propane vehicles have robust safety standards and regulations with regard to the energy storage system, the vehicle itself, and the roadway structures on which they operate.

5.4.1. National Fire Protection Association Standard 502

NFPA 502, *Standard for Road Tunnels, Bridges, and Other Limited Access Highways*, provides fire protection and life safety requirements as well as design criteria for authorities having jurisdiction (AHJs) to use in ensuring tunnel safety. Section 7.3.2 states that a tunnel shall be capable of withstanding the temperature exposure represented by the Rijkwaterstaat (RWS) time-temperature curve or other recognized standard time-temperature curve that is acceptable to the AHJ, as shown by an engineering analysis. The assumption is that every part of the tunnel should withstand these temperature exposures, irrespective of the fire location, ventilation rate or type [113].

5.4.2. ASHRAE HVAC Applications Ch. 16: Enclosed Vehicular Facilities (2019)

ASHRAE 2019 HVAC Applications Chapter 16: *Enclosed Vehicular Facilities* provides guidance on vehicular facilities that store and/or through which vehicles travel. These vehicles can be driven by an internal combustion engine or electric motors. Ventilation requirements including mechanical systems and natural ventilation, climate and temperature control, contaminant level control, and emergency smoke control. Additionally, ventilation concepts including normal operations and emergency operations are covered.

5.4.3. NCHRP Guidelines for Emergency Ventilation Smoke Control in Roadway Tunnels (2017)

NCHRP Guidelines for Emergency Ventilation Smoke Control in Roadway Tunnels Chapter 2: *Road Tunnel Fires* provides guidance on fire design parameters for tunnels. This includes consideration of the geometric parameters of the tunnel, fire protection features and response times that leads to decision making using NFPA 502. This is chapter provides a framework on how to understand and determine fire and hazardous materials management in tunnels [40].

5.4.4. National Fire Protection Association Standard 58

NFPA 58, *Liquefied Petroleum Gas Code*, provides storage, use, and handling requirements for liquid propane fuel in storage containers [148].

5.5. LPG Research Summary in Tunnels

This section documents the results of the evaluations regarding propane vehicle failure in a tunnel.

5.5.1. Experiments

This literature survey includes limited experiments that evaluate the hazard of propane vehicles in a tunnel. Because of this, other experiments are reviewed that have relevance to propane vehicles in tunnels and can help characterize the hazard.

5.5.1.1. Experimental investigation and CFD modelling of the internal car park environment in case of accidental LPG release

Brzezinska and Markowski [149] performed a series of full-scale experiments to help understand emissions and flammable cloud formation in order to help validate models using the CFD code Fire Dynamics Simulator (FDS) by NIST. While the focus of these experiments are releases into parking areas such as garages, it is still a confined space and characteristics and take-aways can be applied to help understand the hazard in a road tunnel. An event tree was used to help understand the initiating events and possible outcomes from an LPG vehicle. These outcomes are based on the leak type and location as well as the ignition sources and safety systems such as detection and ventilation. This can be seen below in Figure 48:

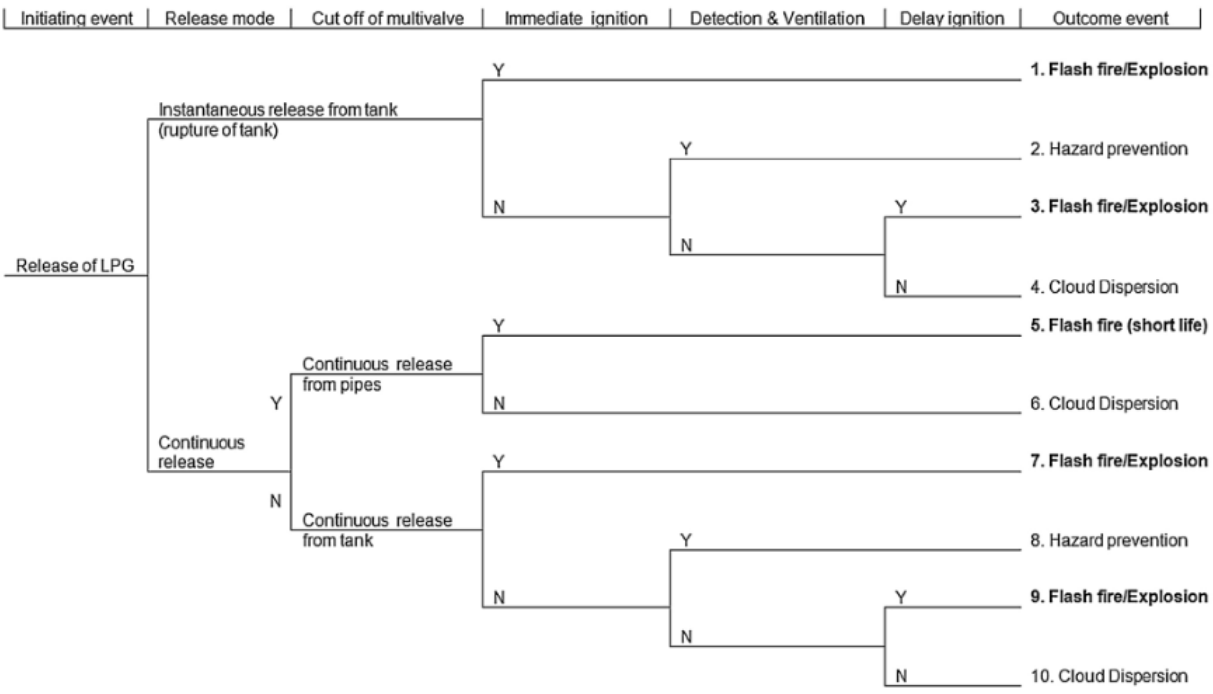

Figure 48: Event Tree for Propane Event Scenario (from [149])

Based on the event tree, release scenarios were determined which included three different release rates (from 1 mm, 3 mm, and 6 mm diameter holes) with and without the ventilation for a total of six different tests. The experimental setup featured concentration measurement points at both 10 and 30 cm off the ground and is shown in Figure 49 below:

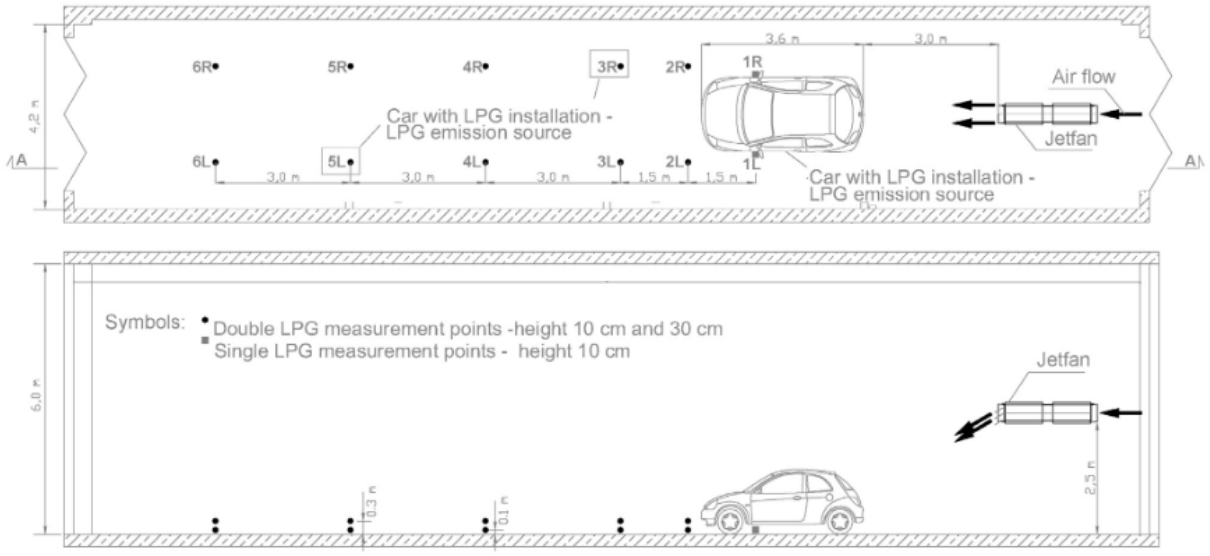

Figure 49: Experimental Setup (from [149])

The experiment was conducted in a test setup with dimensions of 23.7 m × 4.2 m and a height of 6 m. Semiconductor-type gas sensors are used to measure the concentration of LPG vapor. A total of 0.17 L of LPG was fitted in the car for each test. The ventilation system draws 0.61 m^3/s of air. Table 32 below gives more details for each individual test:

Table 32: Gas Flow Test Parameters (from [149])

Test Set #	Diameter of Release Hole (mm)	Release Duration (s)	Gas Outflow Rate (L/s)	Ventilation Switch on Time (s)
1	1	20.75	0.008	Not Active
2	3	5.30	0.032	Not Active
3	6	3.95	0.043	Not Active
4	1	20.75	0.008	150
5	3	5.30	0.032	25
6	6	3.95	0.043	27

Once the experiments were conducted, the data was used to compare with the various CFD simulations. These simulations are shown below in Figure 50 with emissions from the 6 mm hole. The color scale at 4 x 10^{-3} kg/m^3 (red) corresponds to 10% of LFL.

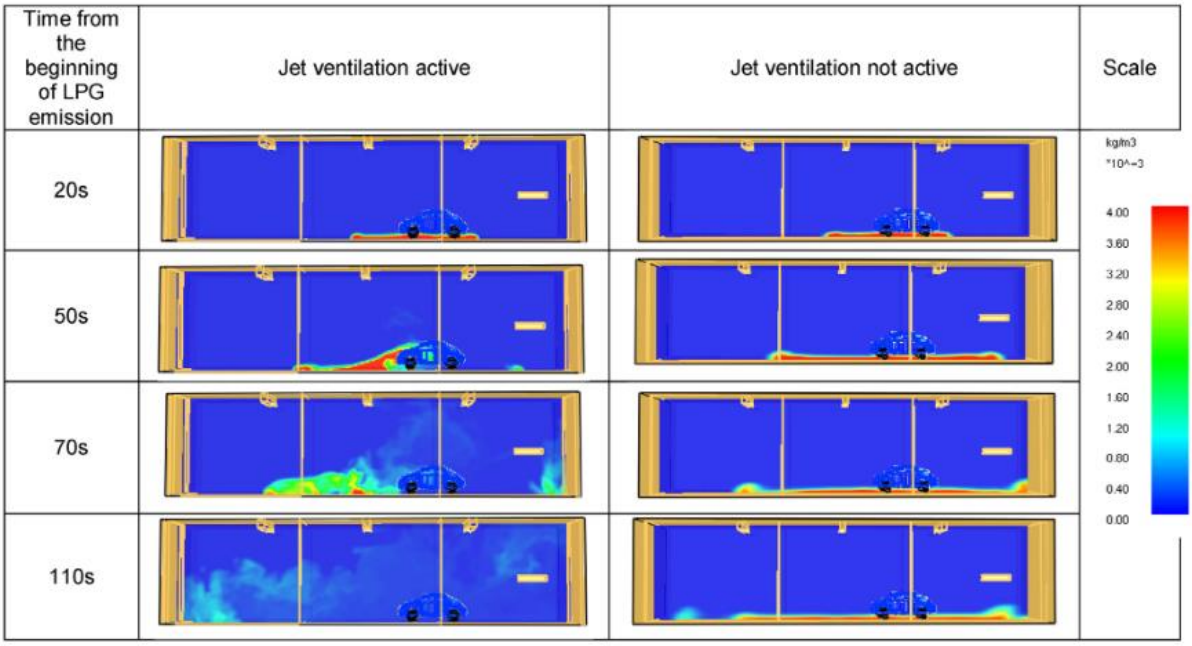

Figure 50: CFD Results based on Ventilation (from [149])

The results from the experiment show that the concentration varies considerably over time and space. The 6 mm experiment yielded the highest fuel concentration. The concentration was in the flammable range for approximately 10 seconds before dissipating. 10 cm above and 3 m away from the source, the concentration was 180% LFL, whereas 30 cm above it was only 33% of LFL. At a distance 9 m away, the concentration ranged between 10% to 20% LFL based on the height. These results can be compared with the equivalent CFD simulation in Figure 51 below (at 3 m from the source on the left, or 3L) with emissions from the 6 mm hole.

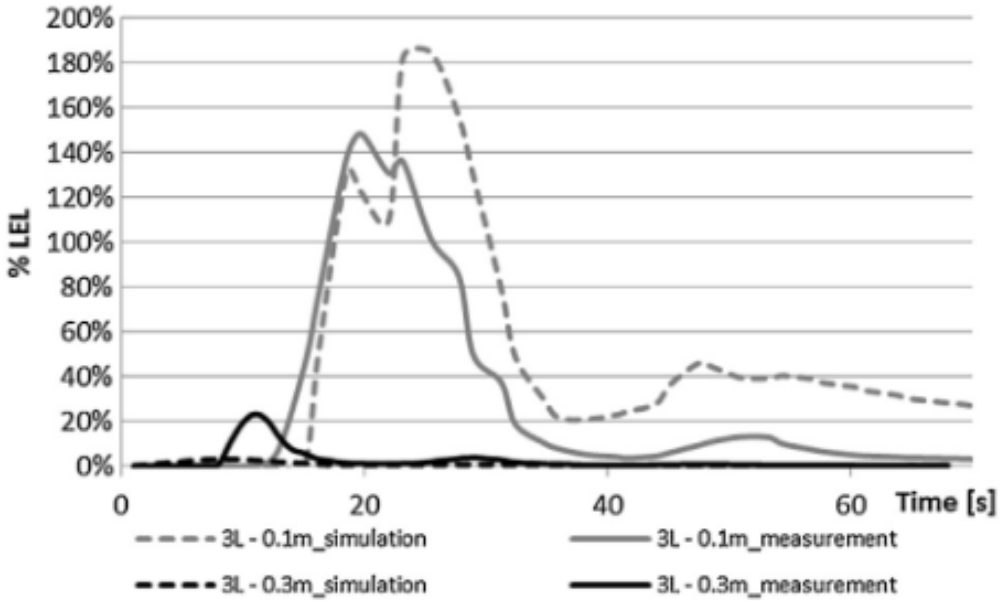

Figure 51: Concentration LPG Comparing Simulation vs. Experimental Results (from [149])

The results show very similar magnitudes and characteristics when comparing the model with the experimental data. Both the 10 cm and the 30 cm measurements off the ground have very similar characteristics to the model. This shows the value of using the CFD simulations to model the phenomenon of a LPG vehicle failure that causes gas dispersion.

5.5.1.2. Smoke Control in Sloping Tunnels

Atkinson and Wu [150] studied the effects of ventilation and smoke development due to a propane fire in a tunnel. Tunnel slopes from 0° to 10° were used to help develop a slope factor for smoke development and movement. A model tunnel with a height of 244 mm with an arch shape cross section which comprises a semicircular head on walls splayed out at 7 ° per Oka and Atkinson [151] shown in Figure 52.

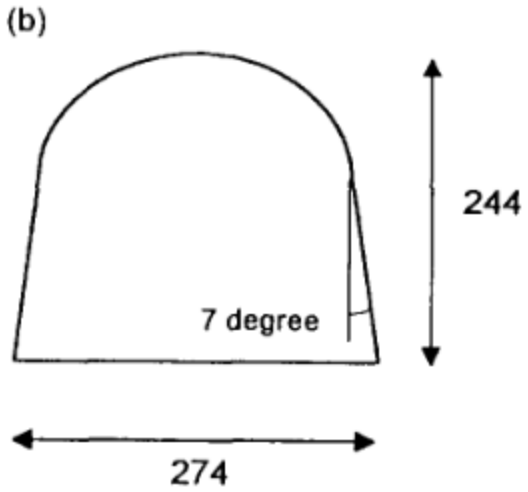

Figure 52: Tunnel Cross Section (from [151])

A 100 mm diameter porous bed propane burner was used with the top set flush with the tunnel floor. The flow rate ranged from 2 to 10 L/min. This corresponded to a 15 to 75 MW fire. The propane output velocity was about 0.4 to 2 cm/s. Understanding the gradient of a tunnel with a fire downhill is important in designing emergency smoke control to keep evacuation routes clear of smoke. The critical velocity is explored to help understand the minimum required ventilation velocity that does not allow the smoke to back flow past the fire. This can be shown in Figure 53 below:

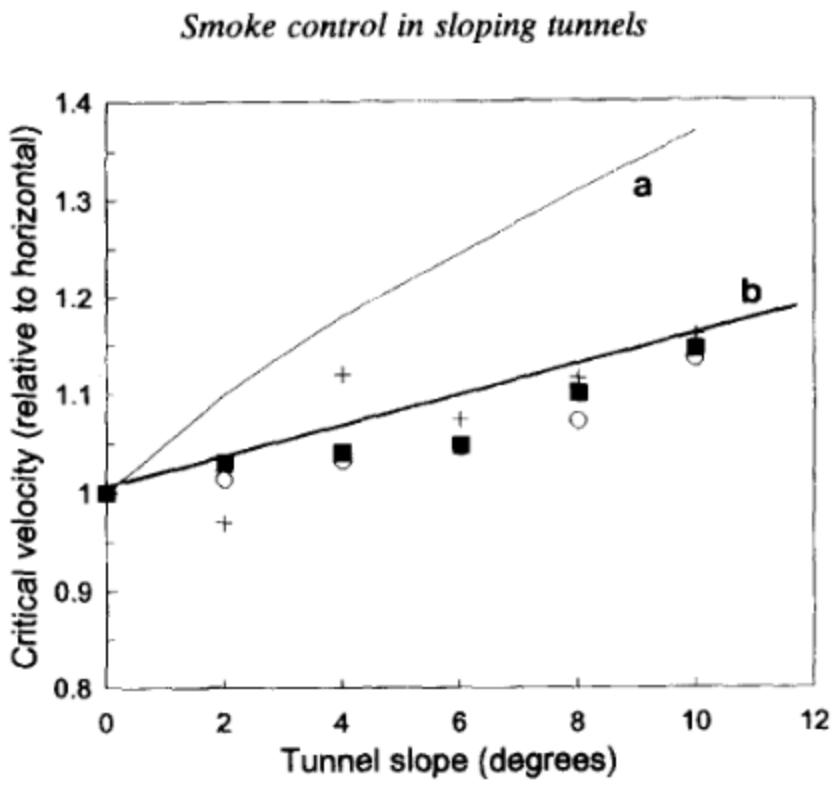

Figure 53: Critical Velocity vs. Tunnel Slope (from [150])

The critical velocity is a function of the slope of the tunnel θ, the volumetric flow of propane, and the dimensionless variables Q* and V*. These transitional values are determined via Froud scaling as shown by Oka and Atkinson [151]. In Figure 53 the black square indicate a flow of 10 L/min of propane & Q*=0.44, the circles indicate 5 L/min & Q*=0.22, the + indicates 2 L/min & Q*=0.088, and the line 'a' indicates SES (Subway Environment Simulations) computer program predications from a former methane experiment whereas the line 'b' indicate the predications based on this work. From there, the expressions for the critical velocity are given as the following:

$$V_{crit} = [gH]^{1/2} \cdot V^*_{max} \cdot [Q^*/1.2]^{1/3} \cdot [1 + 0.014 \cdot \theta] \quad \text{for} \quad Q^* < 0.12$$

$$V_{crit} = [gH]^{1/2} \cdot V^*_{max} \cdot [1 + 0.014 \cdot \theta] \quad \text{for} \quad Q^* > 0.12$$

Figure 54: Critical Velocity Correlations (from [150])

Figure 54 shows the critical velocity relationship in a tunnel as a function of the slope of the tunnel θ, the volumetric flow of propane V*, and the transitional value Q* as well as the tunnel height H and gravity constant g.

5.5.2. Modeling

An analysis of the release rates and dispersion from a propane vehicle showed that the maximum volume of the resulting flammable cloud is dependent on the ventilation type (see Section 5.5.2.1).

Also, the propane vehicle explosion in a tunnel was modeled and the explosion load and consequence were evaluated (see Section 5.5.2.2). Additionally, refer to Section 5.5.1.1 for CFD modeling information.

5.5.2.1. LPG Dispersion Analysis

A hazard analysis of LPG, LNG, and gasoline fueled vehicles, was performed for the Massachusetts Highway department by Zalosh et al. [137]. The study evaluated the release rates and subsequent dispersion from a LPG fueled vehicle in a tunnel with various types of ventilation systems. The primary accident scenario evaluated a fuel line break at the junction to the fuel tank of an LPG van. The liquefied gas was modeled to flow directly onto the tunnel road surface from the tank, which was assumed to be located under the van. The cross-section of the tunnel is rectangular with dimensions of 8.25 m wide by 4.27 m high. Both transverse and longitudinal ventilation was evaluated for release from tanks with and without excess flow valves, which limits the fuel release rate to 100 g/s [137].

The fuel release rates and fuel vaporization histories were calculated using a mathematical model similar to the work by Webber and Jones in 1987 [152] that evaluated the relevant phenomena (see Figure 55). The vaporization rate calculated from the mathematical model was input into a CFD simulation (Fluent) that calculated the vapor dispersion as a function of ventilation type [137].

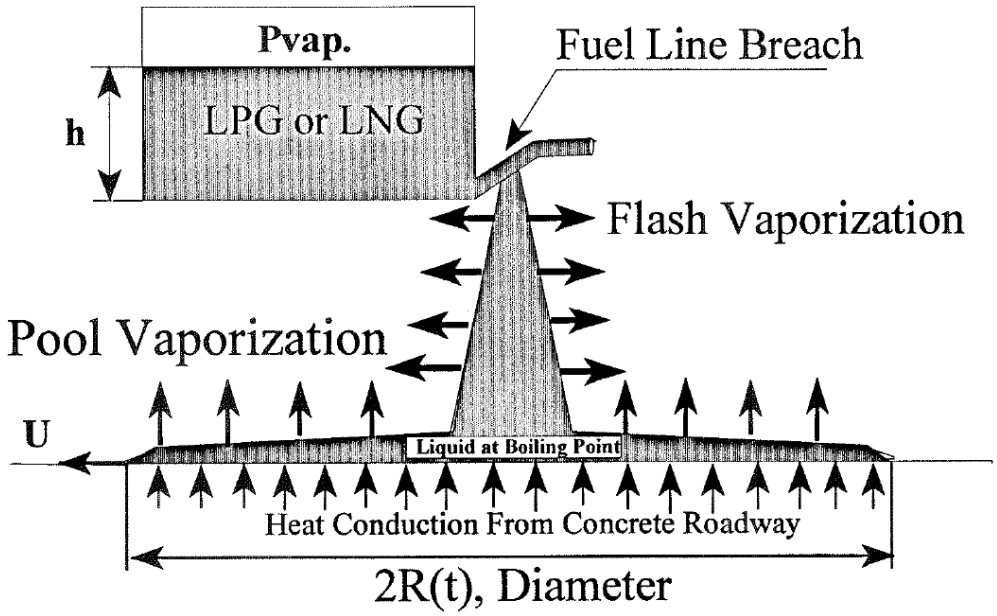

Figure 55: Relevant Phenomena in LPG Spill & Vaporization Mathematical Model (from [137])

For the cases without an excess flow valve, the maximum volume of the resulting flammable cloud is comparable to that of a gasoline spill for transverse ventilation. In the case of longitudinally ventilated tunnels, the vapor cloud is smaller than that of gasoline when the ventilation velocity is 1 m/s. For the case with an excess flow valve, in which the release rate is limited to 100 g/s, the LPG cloud would be no larger than that of gasoline. The growth and decay of the vapor cloud with 20 cfm per lane foot normal transverse ventilation showed that LPGs growth rate is like gasoline and slower than LNG. Each result is further summarized in below [137].

Table 33: Transient Dispersion for Transverse Ventilation (from [137])

Fuel	Vaporization Rate (kg/s)	Cloud Duration	Depth of Flammable Cloud	Max Half Length of Flammable Cloud	Max Volume of Flammable Cloud
LNG	Max: 0.477 Avg: 0.344	260 sec	0.77 m under the ceiling at 100 sec	43 m	840 m^3 at 100 sec
LPG	Max: 0.542 Avg: 0.435	900 sec	0.4 m under the van	60 m	722 m^3 at 492 sec
Gasoline A	Max: 0.621 Avg: 0.398	>500 sec	0.5 m	69 m at 353 sec	940 m^3 at 420 sec
Gasoline B	Max: 0.339 Avg: 0.139	980 sec	0.45 m	80 m at 589 sec	800 m^3 at 570 sec
CNG	Max: 0.78 Avg: 0.35	240 sec	0.55 to 0.82 m	50 m at 80 sec	530 m^3

5.5.2.2. Explosion Risks and Consequences for Tunnels

Weerheijm and van den Berg [153] developed engineering models to quantify the explosion load and consequence of an LPG explosion in a tunnel. The release rate of the gas, the duration of the flow, geometric parameters, and ventilation are inputs to a CFD code developed by TNO. The result is a model of gas dispersion and gas cloud size concentration as a function of time. The explosive loads for the gas explosion are then estimated by relating the cloud length and concentration to the overpressures of an equivalent stoichiometric cloud. The development of a flammable cloud is dependent on the ratio between the ventilation air speed and the leak rate of the LPG. The explosion strength is largely dependent on the length of the flammable cloud. Moreover, detonation could occur if the flammable cloud is sufficiently long [153].

The first case modeled a nearly full vessel in which a boiling liquid expanding vapor explosion (BLEVE) may occur. The tunnel cross-section rectangular with dimension of 5 m by 14.4 m (72 m^2). In the area around the bursting vessel (within 8 m), the explosion results in a high-pressure impact with the tunnel lining (600-800 kPa). The flow is then redirected in the axial direction of the tunnel and the magnitude of the pressure is reduced. The second case evaluated a blast load resulting from the rupture of a nearly empty LPG vessel. This case resulted in similar phenomena as the BLEVE; however, the magnitude of the pressure impact with the tunnel lining in the area around the bursting vessel (within 6 m) was much lower (200-500 kPa) [153].

5.5.3. Analysis

A risk analysis was performed which ranked the probabilistic outcomes of a tunnel accident for different fuel types (see Section 5.5.3.1). Additionally, refer to Section 5.5.1.1 which includes a risk informed failure tree.

5.5.3.1. LANL Risk Analysis

A comparative risk analysis was performed by Los Alamos National Laboratories to put into perspective the relative hazards of alternative fuels, including LPG, compared to gasoline and diesel fuels [136]. As part of this analysis, data was collected about the physicochemical properties of LPG and general petroleum and transportation information. Subsequently, the technical properties of the alternative fuels were ranked, safety data and vehicle accident statistics were reviewed, and specific accident scenarios were evaluated. One of the accident scenarios that was evaluated was a vehicle collision with fuel loss in a tunnel. An expert panel estimated the probabilities of different outcomes for the different alternative fuels compared to gasoline and diesel. Table 34 shows the results of the risk analysis. These probabilities are just expert judgement rather than data. As shown, the LPG was estimated to be more likely to result in a fire without injury or not ignite, and less likely to result in an explosion when compared to gasoline [136].

Table 34: Probabilistic Outcomes of a Tunnel Accident (from [136])

Consequence	Probability				
	CNG	LNG	LPG	Gasoline	Diesel
Fire without Injury	0.1	0.1	0.15	0.12	0.02
Fire with Injury	0.05	0.05	0.08	0.1	0.01
Explosion	0.05	0.05	0.12	0.2	0.01
No Ignition	0.8	0.8	0.65	0.58	0.93

5.6. LPG Research Gaps

Through this literature study, it was shown that studies of LPG vehicles in tunnels is limited. Experiments that explicitly evaluate the hazards of propane vehicles in tunnels were scarce. However, there were other experimental studies included that may have relevance to propane vehicles in tunnels and can help characterize the hazard. One such experiment evaluated emissions and flammable cloud formation in confined spaces such as parking areas and garages from an LPG vehicle [149]. Also, the effects of ventilation and smoke development due to a propane fire in a tunnel were evaluated [149]. Modeling studies have been conducted on the release rates and dispersion from a propane vehicle and the consequence of an explosion [137] [153]. Additionally, a risk analysis was performed which ranked the probabilistic outcomes of a tunnel accident for different fuel types, including propane [136].

The conclusions about important variables that can be derived from these studies is limited. As far as dispersion and cloud formation, the flammable propane cloud is dependent on the ventilation type and tunnel geometry. Initial findings show how much ventilation makes a difference on the overall concentration of a LPG spill. Figure 50 shows how after nearly two minutes the LPG concentration is negligible in compared to the case without ventilation. Analysis shows that the probabilistic outcome of a various consequences from LPG is very similar to that of gasoline [136]. Dispersion properties are very similar to that of gasoline as well [137].

The following criteria were evaluated to determine where research gaps may exist regarding LPG vehicles in tunnels.

1. Scenario Identification
2. Failure Modes
3. Consequences
4. Validation

In terms of scenario identification and failure modes, explicit studies on these topics were not found for propane vehicles. However, the failure modes can be determined from the event tree in Figure 48 by Brzezinska and Markowski [142]. These include release scenarios that lead to flash fires or explosions based on the amount of fuel released, ventilation and cloud dispersion, as well as when there is ignition. Also, a limited scenario identification study was conducted that documented the likelihood of different consequences of a tunnel accident. However, a more complete evaluation of failure modes would need to be completed.

For each of the initiating events, there are several variables that effect the magnitude of the consequence: LPG quantity released, ventilation, obstructions, ignition time, tunnel geometry, etc. The measurements of the consequences of the failure mode include overpressure, HRR, dispersion, and resulting structural damage. The study by Brzezinska and Markowski [142] completed validation by understanding the failure tree to inform the experimental setup. From there the experimental data was used and compared with a CFD model for validation and to use the model for other release events.

In contrast to the some of the other alternative fuels, there has not been significant research on LPG vehicles in tunnels. The following research gaps were identified:

- Fully evaluate the initiating events that are risk significant in terms of LPG vehicles in tunnels.

- Evaluate different classes of LPG vehicles, including buses, and multiple LPG vehicles.
- Evaluate the HRR, temperature, and structural damage resulting from different failure modes.
- Evaluate the effect that overpressure, deflagration, and DDT of released propane has on structural components of tunnels.
- Evaluate the effect that variables such as ventilation, obstructions, and tunnel geometry have on the consequence of an LPG vehicle failure.
- Investigate thermal consequences of failures, which have not been reported for many of the studies included in this literature survey.
- Perform additional validation of modeling efforts through direct comparison to experimental results.
- Additional attention should be given to the size or class of the vehicle. As vehicular class increases so does the amount of stored fuel.

This page left blank

6. HYDROGEN FUEL CELL ELECTRIC VEHICLES

6.1. Overview of Technology

Hydrogen fuel cell electric vehicles (FCEVs) are part of a comprehensive portfolio of technologies and can offer consumers an alternative transportation option to conventional options such as internal combustion engines (ICEs). Fuel cells are more efficient than combustion technologies and FCEVs qualify as zero emission vehicles, emitting no pollution – only water vapor and air through the tailpipe. Additionally, these vehicles offer fast fueling times, and comply with both manufacturer's requirements and consumer expectations for driving range [154]. There are several types of hydrogen FCEVs available to support the diversification of U.S. energy sources in the transportation sector. While there is growing interest in medium and heavy duty FCEVs, production of light-duty hydrogen FCEVs has been ongoing since the Hyundai ix35 fuel cell vehicle rolled off of the assembly line in February of 2013 [155]. An infrastructure of refueling stations has been developed both regionally in the U.S. and in several locations internationally [156]. As of late-2019, there were over 7,800 commercial (sold/leased) fuel cell passenger FCEVs on US roads, mostly in California, with that number projected by industry to exceed 23,000 in 2021 and 47,000 in 2024 [98]. Although these dates and number of deployments may be updated, global industry manufacturers have made a number of plans for commercial expansion, particularly for larger vehicles and trucks, to complement other vehicle platforms such as battery electric vehicles, plug in hybrids, and biofueled ICEs. In addition to FCEVs there are a number of other hydrogen fuel cell applications. For example, there are over ~30,000 fuel cell-powered forklifts operating in commercial warehouses and distribution centers by companies such as Amazon, Coca-Cola, FedEx, Kroger, Walmart, and more as of late-2019 and over 20 million hydrogen fuelings to date [157] [158] [159]. Buses and medium-/heavy-duty vehicles have utilized hydrogen fuel cell technology for public transportation and commodity distribution [160]. The implementation of hydrogen for these larger scale vehicles is expected to increase due to the difficulty in fully decarbonizing these modes of transport. Because of the growing market and diverse applications, a robust safety analysis of hydrogen FCEVs is necessary to ensure public safety.

6.2. Properties of Hydrogen

As an energy carrier, hydrogen fuel can either be a compressed gas or a low-pressure cryogenic liquid. Hydrogen is the lightest gas (~1/14 as dense as air) and at standard temperature and pressure exists in the form of a hydrogen molecule with two atoms: H_2. Liquid hydrogen has a boiling point of -252.88 °C and is much more dense than gaseous hydrogen [161]. Gaseous hydrogen can be stored in high pressure tanks to provide large amounts of energy; however, even more energy can be stored in low pressure cryogenic liquefied form. Hydrogen has an expansion ratio of 1:848, which means that gaseous hydrogen at atmospheric conditions occupies 848 times more volume than liquid hydrogen [162]. Table 35 shows physical and chemical properties of hydrogen [163].

Table 35: Physical and Chemical Properties of Hydrogen (from [163])

Property	Value
Molecular weight	2.0159
Gas Density	0.08988 g/L @ 0°C, 1 atm
Relative Vapor Density	0.07
Liquid Density	70.8 g/L @ -253°C
Melting Point	-259.35°C
Boiling Point	-252.88°C
Auto-ignition Temperature	500°C
Flammability Limits	4-75% (vol % in air)

6.3. Associated Hazards

The primary safety hazard associated with hydrogen is that it is flammable. Hydrogen properties require that the fuel delivery system be designed to mitigate all relevant safety hazards. Table 36 shows relevant flammability properties of hydrogen as compared to other common fuel sources.

Table 36: Flammability Properties of Hydrogen and Other Fuels

Property		Hydrogen	Methane	Propane	Gasoline Vapor
Flammability Concentration in Air (vol%) [27]	LFL	4.0%	5.0%	2.1%	1.2%
	UFL	75.0%	15.0%	9.5%	7.1%
Easily Ignited Mixture in Air (vol%)		29% [103]	8.5% [104]	4% [105]	2% [106]
Adiabatic Flame Temperature [107]		2483 K	2236 K	2250 K	2289 K
Buoyancy (ratio to air)		0.07	0.54	1.52	4
MIE [108] [109]		0.011-0.017 mJ	0.28-0.30 mJ	0.25-0.26 mJ	0.8 mJ
Autoignition Temperature [110]		500 °C	580 °C	455 °C	246 – 280 °C

Although hydrogen's lower flammability limit is comparable to the other fuels, it has a much higher upper flammability limit. Also, its minimum ignition energy is an order of magnitude lower than the other fuel types. This introduces the possibility of ignition even from weak electrostatic discharged. Sources such as NFPA 77 [164] give discharge ranges showing that even a corona type discharge at the end of a wire or other point could lead to enough energy to exceed the MIE for hydrogen. Figure 56 illustrates the MIE of different fuels as a function of concentration in air by volume. As shown in the figure, between approximately 10% and 60% volumetric concentration, hydrogen has a lower ignition energy than methane and gasoline over a much wider range of concentration. However, for hazard evaluation the MIE of lean mixtures is more relevant, and hydrogen does not differ from other fuels. At the LFL concentrations for each of the fuels, the ignition energies are much more similar between fuels.

However, it should be noted that these characteristics have led to robust system safety requirements to reduce the likelihood of hydrogen release after an accident.

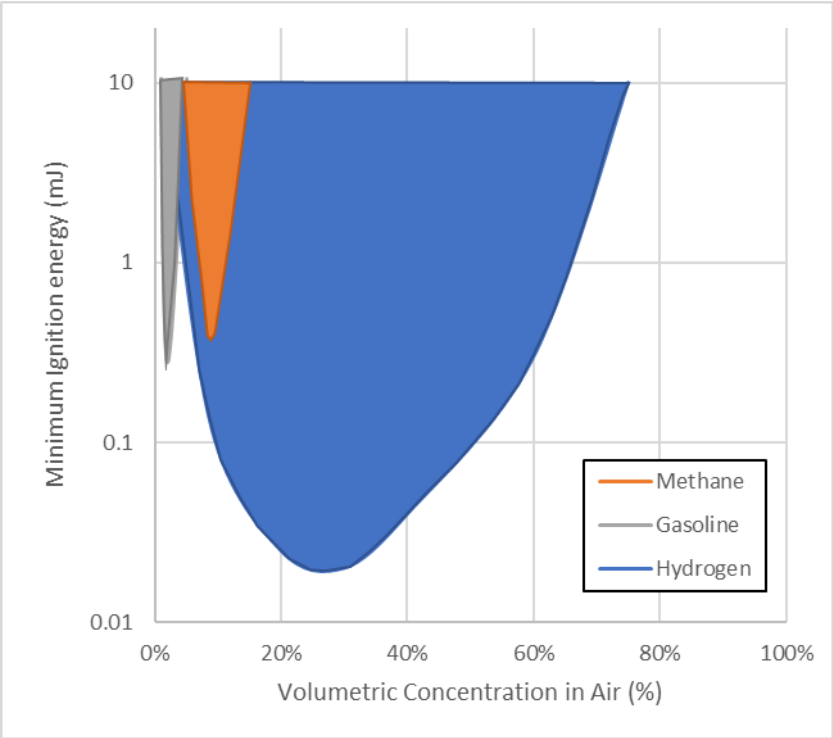

Figure 56: Minimum Ignition Energy for Different Fuels vs. Concentration (from [165])

To mitigate the ignition hazards of hydrogen, sensors are placed in indoor and enclosed locations where hydrogen has the potential to be trapped and accumulate flammable concentrations. These sensors can be programmed to alert when the hydrogen reaches some fraction of the LFL. Because hydrogen is lighter than air, sensors should be placed above potential release points but below ceiling height to avoid elevated temperatures. Consideration should be given to understand the effect of ventilation systems and how air flow might be altered [166]. Most of the hydrogen fuel system will be at a pressure that will result in momentum driven jets of hydrogen. In outdoor locations, hydrogen releases rise away from ignition sources because it is more buoyant than air. This means that hydrogen leaks can dissipate readily, potentially avoiding a concentrated, explosive atmosphere.

6.4. Pertinent Regulations and Safety Standards

Hydrogen FCEVs have robust safety standards and regulations regarding the fuel storage system, the vehicle itself, and the roadway structures on which they operate.

6.4.1. Global Technical Regulation No. 13

The Global Technical Regulation No. 13 (GTR #13) establishes vehicle requirements for hydrogen FCEVs that can attain equivalent levels of safety as those for conventional gasoline powered vehicles. GTR#13 is intended to be applied globally. However, it is up to specific regulatory bodies in each country to adopt the GTR. Because of the large number of countries implementing hydrogen vehicles and developing their jurisdiction-specific requirements, especially for tunnels, this report does not attempt to catalogue these requirements and regulations. However, during the IPHE RCSS Working group meeting in September 2018, many of those present shared the regulations regarding tunnels and enclosed spaces.

Hydrogen vehicle fuel is contained in a composite overwrapped pressure vessel and stored in the gaseous state. The pressure vessel includes a thermal pressure relief device which, in the event of a fire, releases the hydrogen to prevent the vessel from over-pressurizing. Current storage systems have pressures of up to 10 ksi (70MPa). GTR #13 provides requirements for the integrity of compressed and liquid hydrogen motor vehicle fuel systems, including pressure cycling tests, a burst test, a permeation test, and a bonfire test. The pressure cycling test evaluates a container's durability to withstand, without burst, 22,000 cycles of pressurization and depressurization. The burst test evaluates a container's initial strength and resistance to degradation over time. The bonfire test evaluates the ability of the container's thermal pressure relief device to open in a fire scenario (localized and engulfing) [167].

For Crash testing, GTR #13 specifies that participating countries will use existing national crash tests but develop and agree on maximum allowable levels of hydrogen leakage. In the U.S., these national crash tests are found in the Federal Motor Vehicle Safety Standards (FMVSS) which includes specified tests for barrier impacts, rear collisions, and side impact crashes. In a later phase of the requirement, the international crash test requirements are planned to be unified for FCEVs [113].

6.4.2. National Fire Protection Association Standard 502

NFPA 502, *Standard for Road Tunnels, Bridges, and Other Limited Access Highways*, provides fire protection and life safety requirements as well as design criteria for authorities having jurisdiction (AHJs) to use in ensuring tunnel safety. Section 7.3.2 states that a tunnel shall be capable of withstanding the temperature exposure represented by the Rijkwaterstaat (RWS) time-temperature curve or other recognized standard time-temperature curve that is acceptable to the AHJ, as shown by an engineering analysis. The assumption is that every part of the tunnel should withstand these temperature exposures, irrespective of the fire location, ventilation rate or type [113]. With regards to hydrogen vehicles in tunnels, appendix G recommends on-board detection and incident shutoff systems be provided in fuel-cell vehicles.

6.4.3. ASHRAE HVAC Applications Ch. 16: Enclosed Vehicular Facilities (2019)

ASHRAE 2019 HVAC Applications Chapter 16: *Enclosed Vehicular Facilities* provides guidance on vehicular facilities that store and/or through which vehicles travel. These vehicles can be driven by an internal combustion engine or electric motors. Ventilation requirements including mechanical

systems and natural ventilation, climate and temperature control, contaminant level control, and emergency smoke control. Additionally, ventilation concepts including normal operations and emergency operations are covered.

6.4.4. NCHRP Guidelines for Emergency Ventilation Smoke Control in Roadway Tunnels (2017)

National Cooperative Highway Research Program Guidelines for Emergency Ventilation Smoke Control in Roadway Tunnels Chapter 2: *Road Tunnel Fires* provides guidance on fire design parameters for tunnels. This includes consideration of the geometric parameters of the tunnel, fire protection features and response times that leads to decision making using NFPA 502. This is chapter provides a framework on how to understand and determine fire and hazardous materials management in tunnels [40].

6.4.5. National Fire Protection Association 55

NFPA 55, *Compressed Gases and Cryogenic Fluids Code*, provides storage, use, and handling requirements for both compressed and cryogenic liquid hydrogen in portable containers, cylinders, and tanks. Sections 10 and 11, specifically, deal with bulk hydrogen compressed gas systems and bulk liquefied hydrogen systems, respectively [115].

6.4.6. National Fire Protection Association 2

NFPA 2, *Hydrogen Technologies Code*, establishes the necessary requirements for hydrogen technologies. This includes requirements associated with general fire safety, explosion protection, fueling facilities, fuel cell power systems, hydrogen generation systems, combustion applications, laboratory operations, and enclosed spaces [168]. All hydrogen requirements from other NFPA documents, including NFPA 55, are included by reference in NFPA 2 to provide a single source of hydrogen requirements in in NFPA.

6.5. FCEV Research Summary in Tunnels

There has been substantial work in evaluating the effects of a failure of a hydrogen tank on an FCEV in a tunnel. This section documents the results of these evaluations.

6.5.1. Experiments

Several experiments have evaluated the consequences of a hydrogen FCEV failure in a tunnel. A series of experiments were performed to determine what would happen if hydrogen is released from the onboard pressure vessel. It was determined that spontaneous ignition is the most likely consequence (see Section 6.5.1.1). Qualitatively, this is the least severe and most likely consequence to a hydrogen release in a tunnel. However, there were also several experiments performed to evaluate more severe consequences. Multiple experiments were conducted to evaluate deflagration of hydrogen within a tunnel. These experiments investigated the consequences to delayed ignition of the released hydrogen, considered a worst-case scenario because if ignition does not occur immediately, a large volume of flammable gas could build up and impart more energy into the confined space of a tunnel once it does ignite. An immediate ignition scenario involves less accumulation of hydrogen involved in the ignition event. The concentration of hydrogen and presence of ventilation had a significant effect on the measured pressure pulses (see Section 6.5.1.2). A variety of quiescent and steady-state hydrogen ignition experiments were performed to evaluate the effect of congestion, hydrogen release rates, along with ventilation rates on overpressure. In general, congestion increased overpressure; however, low hydrogen leakage rates and increased ventilation air velocity resulted in lower overpressure (see Section 6.5.1.4). Also, deflagration was examined in stratified hydrogen layers to evaluate the potential of self-sustained detonation in flat layer hydrogen-air mixtures. The results indicated that a DDT was possible, however, a minimum layer thickness and sufficient congestion was required (see Section 6.5.1.5). A series of fire experiments and simulations of a car carrier in a tunnel loaded with hydrogen FCEVs simulated the HRR and showed similar results when compared to the experimental results (see Section 6.5.1.6). Also, experiments have been performed to validate the results of CFD models (see Section 6.5.1.3).

6.5.1.1. Spontaneous Ignition of Pressurized Releases of Hydrogen into Air

A series of experiments were performed to show that the spontaneous ignition of released hydrogen is caused by transient shock formation and mixing associated with rupture of a burst disk between compressed hydrogen and air [169]. Several different variables were evaluated through these experiments, including rupture pressure and internal geometry downstream of the burst disk. The rupture pressure of the burst disk was evaluated with both commercial and in-house manufactured disks with different rupture pressures. The majority of experimentation was performed outdoors, with ambient conditions (between 280K and 305K, with between 60-90% relative humidity). Figure 57 shows a schematic of the experimental configuration [169]

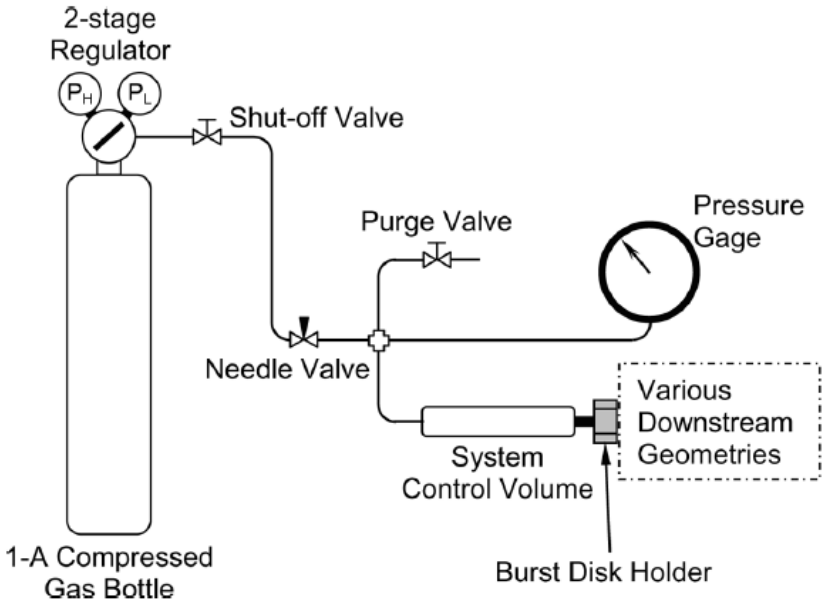

Figure 57: Schematic of Experimental Configuration (from [169])

Over 200 experiments were conducted with hydrogen failure pressures between 11.2 atm and 113.25 atm, with various upstream and downstream geometries. These experiments demonstrated that spontaneous ignition of compressed flammable hydrogen repeatedly occurs at the range of pressures seen in FCEV applications, given that sufficient mixing occurs as well. The short mixing time scales are provided by the pressure boundary failure geometry, multi-dimensional shock-boundary, the shock-shock interactions, and the molecular diffusion. Continued combustion can occur because the turbulent free jet hydrogen flames can be stabilized at sufficiently high jet velocities. The reflected shock and shock-shock interactions determine the minimum compressed hydrogen pressure at which spontaneous ignition occurs. Due to the repeatability of the ignition and the characteristic time scale, it was determined that alternative ignition sources, such as electrostatic discharge, did not contribute to these experimental results [169].

6.5.1.2. Large-scale Hydrogen Deflagrations and Detonations

A scaled down tunnel was used to perform spark-initiated deflagration tests using homogeneous hydrogen mixtures by Groethe et al. [170]. A 1/5-scale tunnel was used to perform multiple experiments with varying released quantities of hydrogen with and without ventilation. This was done to simulate the release from a fuel cell vehicle or storage cylinder on a hydrogen transport. Additionally, selected tunnel tests contained obstacles representing traffic to investigate turbulent enhancement. The cross-area blockage ratio was 0.03. Figure 58 and Figure 59 show the tunnel facility and model vehicles in the tunnel, respectively. Hydrogen was contained in a 37 m^3 volume at the center of the tunnel by HDPE plastic film barriers in homogeneous mixtures ranging from 9.5% (0.32 kg) to 30% (1 kg) hydrogen mixed with air in that volume. Prior to the spark ignition, the plastic barriers were cut. Additional experiments evaluated different release rates of hydrogen both with and without forced ventilation [170].

Figure 58: SRI Corral Hollow Experiment Site Tunnel Facility (from [170])

Figure 59: Model of Vehicles in Tunnel (from [170])

The results of the experiments showed that the 9.5% homogeneous hydrogen mixture produced pressure pulses that were too small for sensors to detect. When the hydrogen content in the mixture was increased to 20% and 30%, the pressure pulses measured 35 kPa and 150 kPa, respectively. It was shown that the presence of the vehicles had an insignificant effect on the deflagration as shown by the pressure pulse, but that ventilation during a release reduces the hazard dramatically. Also, release of hydrogen through a source like the vehicle fuel tank safety release valve produced very lean hydrogen concentrations which created very small pressure pulses [170]. Figure 60 below shows the pressure impulse and overpressure associated with the 30% hydrogen experiment:

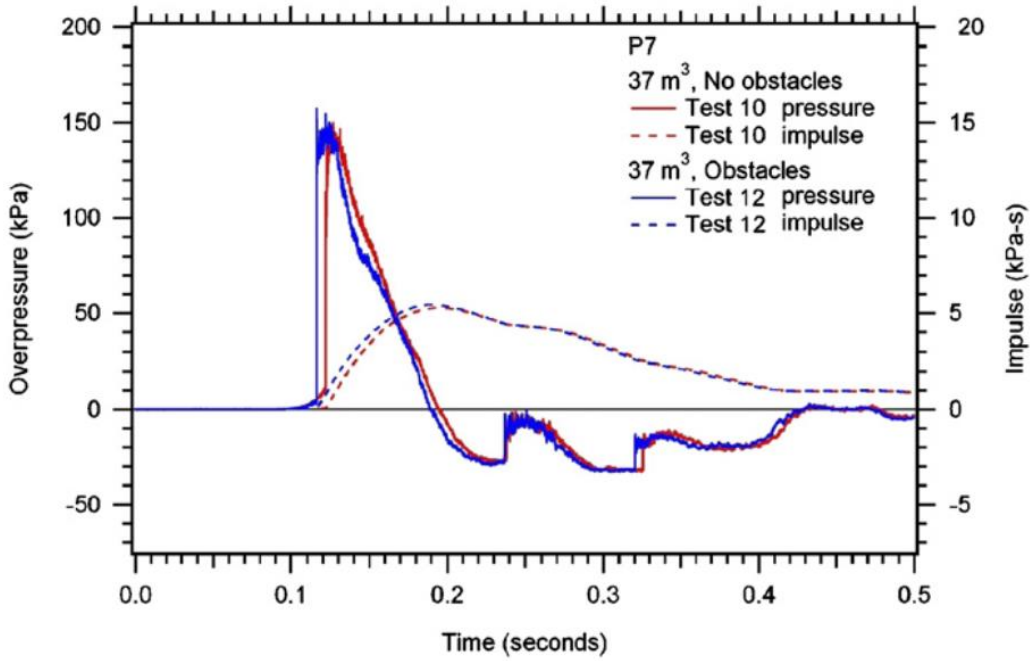

Figure 60: 1/5th Scaled Tunnel Impulse and Overpressure (from [170])

As the Groethe et al. points out, larger vehicles should be studied in this scaled experiment to understand the results. The scaling on how the overpressure changes with the size of tunnel and vehicle would need to be further investigated. As noted by Groethe, the tunnel has a larger aspect ratio than a normal tunnel, which might affect how these results scale up. This directly correlates to the L/D ratio or the length of the tunnel compared to the effective hydraulic diameter. Additionally, to compare with the other literature, the location of the overpressure measurements would need to be well known and using known scaling laws such as Hopkinson Blast Scaling and Sachs Blast Scaling could be used to help understand the total explosive energy. Sachs scaling law states that pressure, time, impulse, and other parameters can be expressed as functions of this scaled distance but assumes that air behaves as a perfect gas and assumes gravity and viscosity are negligible [171]. Additionally, how effects of confinement that could lead to turbulent flame speeds might not carry over at full scale. Further understanding these scaling laws would allow for better comparisons between experiments. Studies such as the one by Tamanini [172] provide additional insight on various scaling methods for sizing deflagration vents which helps understand important scaling factors.

6.5.1.3. Releases from Hydrogen Fuel-cell Vehicles in Tunnels

In order to validate the dispersion/deflagration modeling described later in Section 6.5.2.4 a set of experiments were performed at the SRI Corral Hollow Experiment Site (see Figure 58) by Houf et al. [173]. A set of scaled tunnel tests were performed to approximate the full-scale dimensions of the tunnel from the modeling effort. The hydrogen mass, release rate, initial tank pressure, and TPRD release diameter were scaled to approximate the modeling parameters. Figure 61 shows a comparison of the peak overpressures from the experiments with the results from the model

simulations. The peak overpressure from the experiments is in good agreement with the modeling results [173].

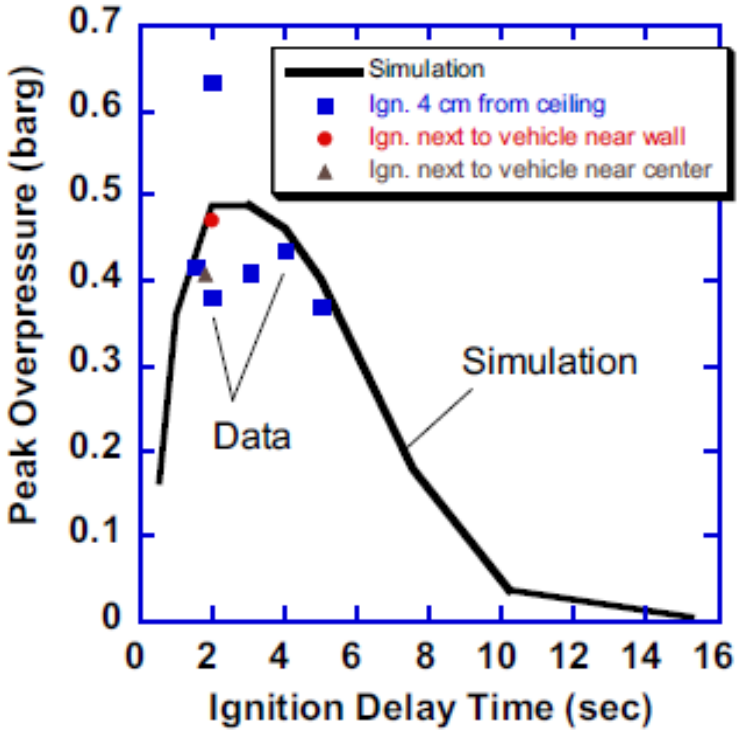

Figure 61: Comparison of Experimental and Modeling Results (from [173])

Figure 62 shows a comparison of the hydrogen concentration at discrete locations within the tunnel as a function of time. As shown, the predicted and measured values are generally in good agreement [173]. While the simulation does approximate the overpressure there are some points in the data that might be considered outliers.

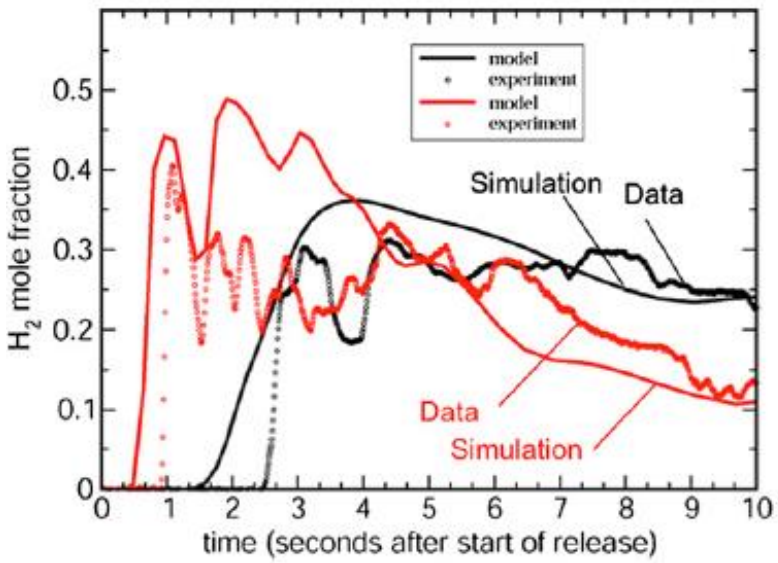

Figure 62: Comparison of Time-dependent Hydrogen Concentration Values (from [173])

6.5.1.4. HyTunnel Project to Investigate Hydrogen Vehicles in Road Tunnels

A set of experiments were performed by Kumar et al. [174] at the Health and Safety Laboratory to evaluate the influence of congestion and ventilation flow rates on the over-pressure produced from ignition of hydrogen stoichiometric clouds. Quiescent experiments were performed in a sealed enclosure with a stoichiometric hydrogen/air mixture and different congestion volumes/configurations. The congestion configurations consisted of different arrangement of pipes with variable spacing and orientation. Arrangement A is the tight configuration, consisting of four rows of pipes with a spacing of three diameters between pipes, with adjacent rows oriented at right angles and the pipes staggered between every other row. Arrangement B is the loose configuration, consisting of 3 rows of pipes with a spacing of five pipe diameters between pipes, and the same orientation of pipes as Arrangement A. Figure 63 shows the configuration of the ignition experiments. The enclosure (left) shows two modules; however, for the ignition experiments, a total of six modules were combined to give the enclosure a total length of 14.9 m and a volume of 93.1 m^3. The arrangement of the tight congestion setup is also shown (right) [174]. A single obstacle setup is used in each experiment which is shown in Figure 63.

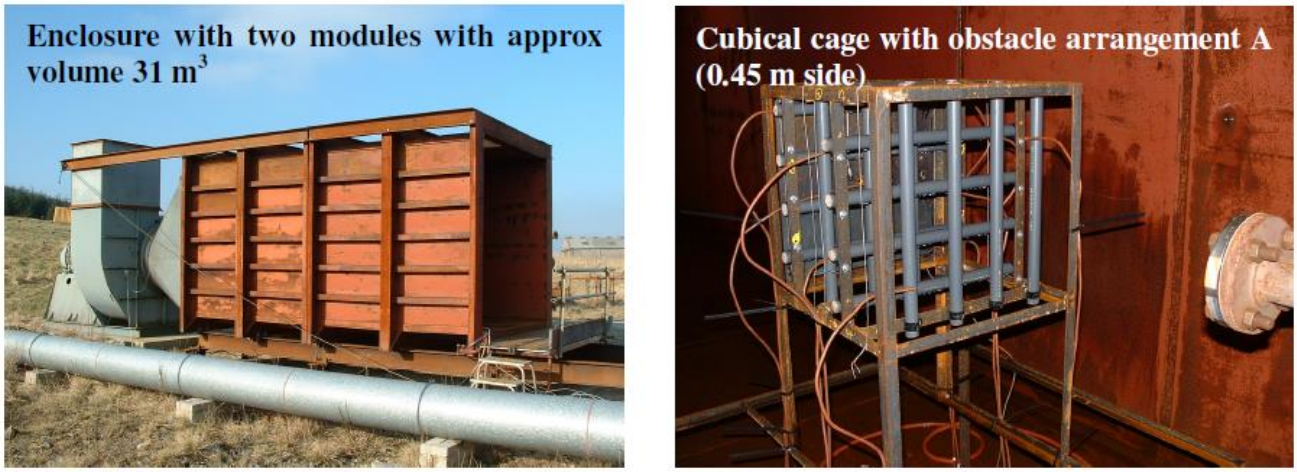

Figure 63: Configuration in Ignition Experiments (from [174])

Table 37 and Figure 38 show the results of the quiescent ignition experiments. A non-uniform pressure field resulted from these hydrogen ignition experiments. An increase in the volume of hydrogen/air mixture increased the maximum explosion overpressure. However, as shown in the table below, an initial increase in the congestion level increased the maximum explosion overpressures (from none to congestion configuration B). Further increase in congestion (from configuration B to configuration A) resulted in a reduction in overpressure [174].

Also, a set of steady-state experiments were performed with various hydrogen leak rates and ventilation flow rates (while also evaluating congestion arrangements A and B). Ventilation in the enclosure was produced through a variable speed fan producing suction through an end plate with 324 circular holes to create a homogeneous flow. Table 37 shows the results of the steady state ignition experiments. As shown, the maximum explosion overpressures increased with increasing hydrogen release rate and decreasing ventilation air velocity. At the lowest leakage rates, the highest explosion overpressures were seen for the more congested configurations. However, at the highest hydrogen leakage rates, the highest explosion overpressures were seen for the less congested configuration (except at the lowest ventilation rate) [174].

Table 37: Results of Steady State Ignition Experiments (from [174])

Hydrogen Release Rate	Air Velocity	Congestion Configuration	Overpressure from Transducer (mbar)		
			Enclosure Left-Hand Wall	Congested Volume Cage Wall Center	Enclosure Right-Hand Wall
1.5 g/s	1 m/s	A	28.2	124.2	63.5
		B	16.2	63.4	19.6
	2 m/s	A	13.6	66.6	12.6
		B	8.8	20.6	7.5
	4 m/s	A	12.1	39.5	10.5
		B	6	13.1	5
2.0 g/s	1 m/s	A	32.4	123.3	55.4
		B	27.5	106	46.6
	2 m/s	A	23.2	117.7	39.6
		B	25.7	66.3	46.6
	4 m/s	A	14.1	53.6	14.7
		B	39.4	25.4	28.9
4.0 g/s	1 m/s	A	48.9	255.8	71.2
		B	48.5	136.9	91.7
	2 m/s	A	37.3	222.5	66
		B	48.1	196.4	85.8
	4 m/s	A	26	160.4	39.2
		B	28.9	126.2	51.2

Table 38: Results of Quiescent Ignition Experiments (from [174])

Congested Volume	Congestion Configuration	Overpressure from Transducer (mbar)	
		Enclosure Left-Hand Wall	Enclosure Right-Hand Wall
0.098% of total enclosure volume	None	28.2	24.7
	B	37.2	42
	A	27.4	24.2
0.55% of total enclosure volume	None	Over-range	85
	B	Over-range	114.6

6.5.1.5. Deflagration and Detonation of Hydrogen Under a Tunnel Ceiling

A set of experiments were performed at Research Centre Karlsruhe in Germany by Friedrich et al. [175] that examined deflagration in stratified hydrogen layers to evaluate the potential of self-sustained detonation in flat mixture layers. Figure 64 shows the main experimental set up used in these evaluations. The chamber had dimensions of 5.7 m x 1.6 m x 0.6 m with layering heights of 0.15 m, 0.3 m, and 0.6 m. The hydrogen concentrations used in these experiments ranged between 15% and 25% (by volume in air). Also, variation in obstacles and hydrogen layer thickness were evaluated [175].

Figure 64: Experimental Setup for Deflagration Experiments (from [175])

In the set of experiments with no obstacles, slow flame propagation regimes were observed. The experiments with obstacles showed three distinct combustion regimes. The obstructions in the ceiling may have added turbulence to the flame propagation, which would make the explosions more severe. These results indicate that ceiling design and mitigation measures in tunnels are important which can be understood in the volume and layer height matrix shown in Figure 65 [175].

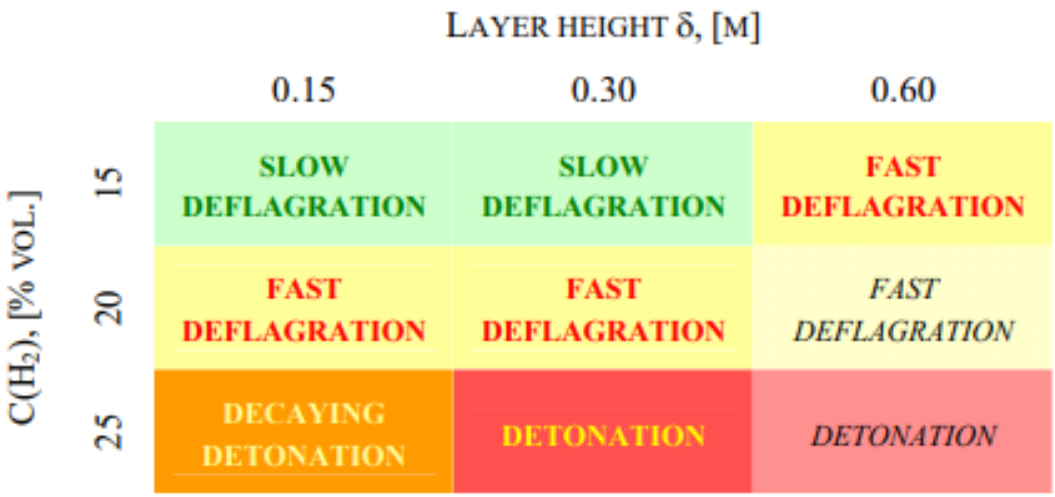

55

Figure 65: Concentration and Layer Height Effect on Combustion (from [175])

6.5.1.6. Fire experiments of carrier loaded FCEV in full-scale model tunnel

A series of fire experiments and numerical simulations of a carrier loaded with hydrogen FCEVs in a full-scale tunnel were conducted to calculate heat release and smoke generation rates by Seike et al. [176]. As shown in Figure 66, the experimental tunnel is 80 m long, 12.4 m wide, and 7.36 m wide with a horseshoe cross-section. The total HRR of the carrier loaded with hydrogen FCEVs was determined from the experimentally obtained temperature variation near the fire [176].

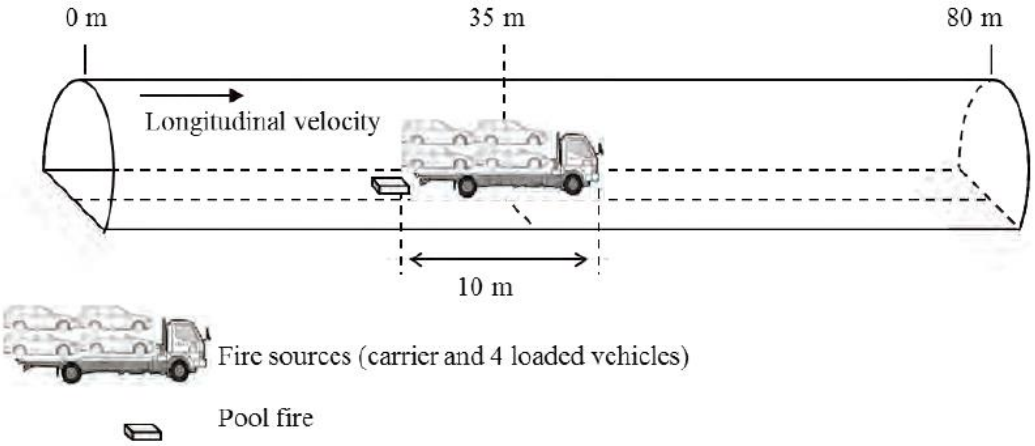

Figure 66: Experimental Tunnel Configuration and Carrier (from [176])

The total HRR was also estimated through numerical simulation. The individual HRR of each part of the car was calculated and summed to determine the total HRR. The different parts of concern were the carried vehicles without fuel, the hydrogen fuel which was approximately 17.6 m^3 of low-pressure hydrogen and another case of 43.6 m^3 of high-pressure hydrogen, the rear wheels, the driver's seat in the carrier vehicle, and a 1 m^2 gasoline pool fire. The methodology of estimating the HRR of each part and superimposing them to obtain the total HRR was then compared to the experimental results. As shown in Figure 67, for a vehicle containing 43.6 m^3 of compressed hydrogen, the numerical method and experimental results are in fairly good agreement [176].

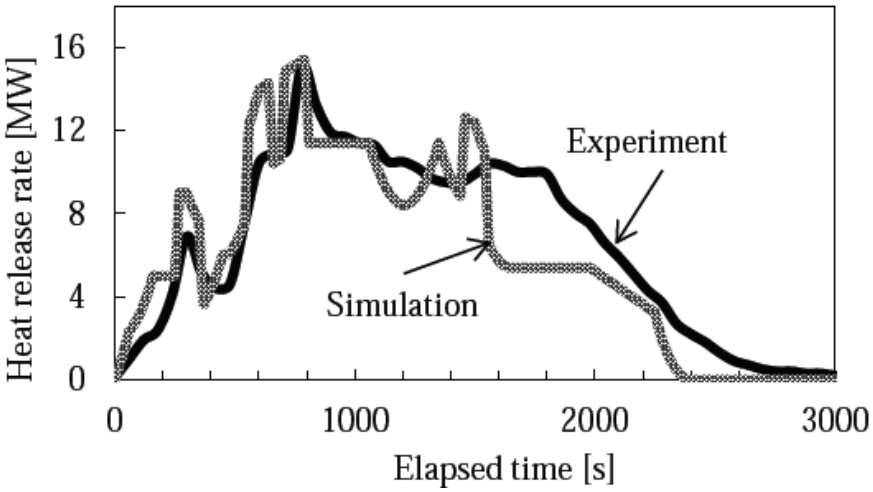

Figure 67: Comparison of Experimental & Simulated HRR for High Pressure Case (from [176])

This methodology was extended to predict the HRR of a carrier loaded with eight hydrogen FCEVs. It was determined that, when compared to a large bus fire, the HRR was larger after 10 minutes and the maximum HRR was 1.5 times greater [176].

6.5.1.7. Vapor Cloud Explosions from Ignition of Gaseous Mixtures in a Congested Region

A series of studies were carried out by Royle et al. [123] to measure the overpressure produced from methane and methane/hydrogen mixtures premixed with air when ignited within congested spaces. The experimental space was a 3 x 3 x 2 m region containing multiple layers of pipes. An image of the congested region is shown in Figure 68. A concrete wall sits adjacent to the one side of the congested region. The wall is positioned there to protect the control room and has been shown to not interfere with free field overpressure [123]. Additionally, the wall has embedded pressure sensors at different heights. For this series of experiments, the blockage ratio was reported as 4.40% the total volume. The outside of the grid was covered in a 23 μm thin plastic film which contained the gas prior to ignition. The plastic film was used only to contain the premixed gas mixtures prior to combustion and did not significantly restrict the outflow of gas or the pressure wave.

Figure 68: Congestion region or grid where gas was filled then ignited (from [123])

Hydrogen gas was mixed with air to form a stoichiometric ratio of 1.2 which reportedly produces the highest overpressures. Other gases evaluated in this study were mixtures of methane, air, and hydrogen which are all included in some of the figures and tables below. For this section, only results pertaining to hydrogen alone are discussed. Section 4.5.1.3 discusses the methane portion of this experiment.

The ignition source was located at a height of 0.5 m off the ground and positioned at the center of the grid. For ignition a 2.25 J capacitor was discharged through a spark gap of 6 mm. It was noted that the spark exhibited lower energy than what was discharged from the capacitor. For the instrumentation, overpressure values were measured by an array of low- and high-pressure pressure sensors. The location of the pressure sensors can be seen in Figure 69. All pressure sensors were positioned 500 mm above the ground except for the far field pressure sensors, which were mounted at higher locations due to the topology of the testing pad.

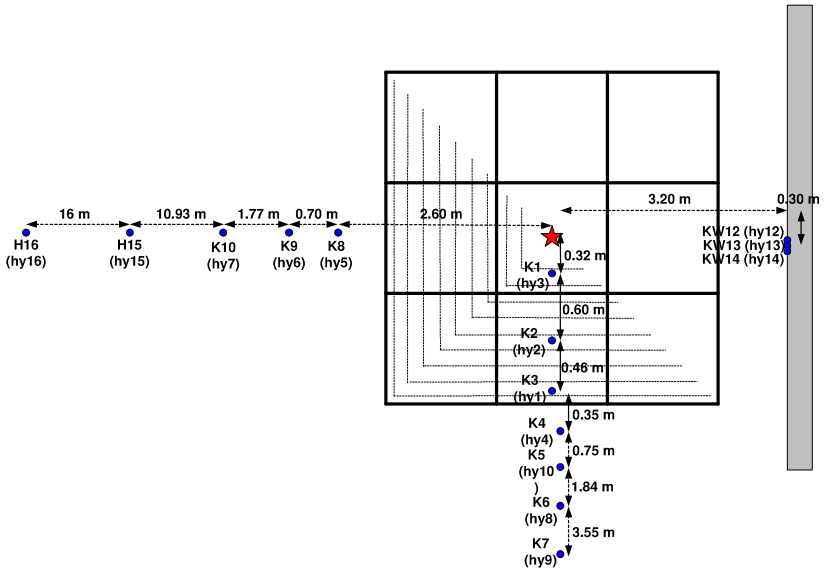

Figure 69: Pressure Sensors distributed in and around grid structure (from [123])

Pressures were measured across a wide span of locations including up the adjacent wall. Table 39 lists the initial conditions prior to ignition. The pure hydrogen is labeled as NatHy_01. For the results of hydrogen/methane mixture experiments, we refer the reader to the paper [123].

Table 39: Initial Conditions of Experiment (from [123])

Measurement	Test Conditions: NatHy_01
Hydrogen (vol. %)	100
Number of Layers	9
Free Volume	17.207
Gas mixture temperature (°C)	11.0
Relative Humidity (%)	30.7
Atmospheric Pressure (kPa)	97.72
Mean Oxygen Concentration (%)	13.59
Partial Oxygen Pressure (kPa)	0.1359
Partial Nitrogen Pressure (kPa)	0.5127
Partial Water Vapor Pressure (kPa)	0.0041
Partial Fuel Gas Pressure (kPa)	0.3474
Mass of Hydrogen (kg)	0.498

It was noted that during experiment the humidity was uncontrolled but was assumed to have a minor effect on the resultant explosion overpressure values. Figure 70 displays an image of the explosion immediately after ignition.

Figure 70: Image of pure methane combustion right after ignition (from [123])

Figure 71 and Figure 72 show the measured overpressure values at various locations for all mixtures. Recall that NatHy_01 corresponds to the hydrogen gas. Pressures were reported in the near-field (within and just outside of the grid) and far-field (further out from the grid) regions.

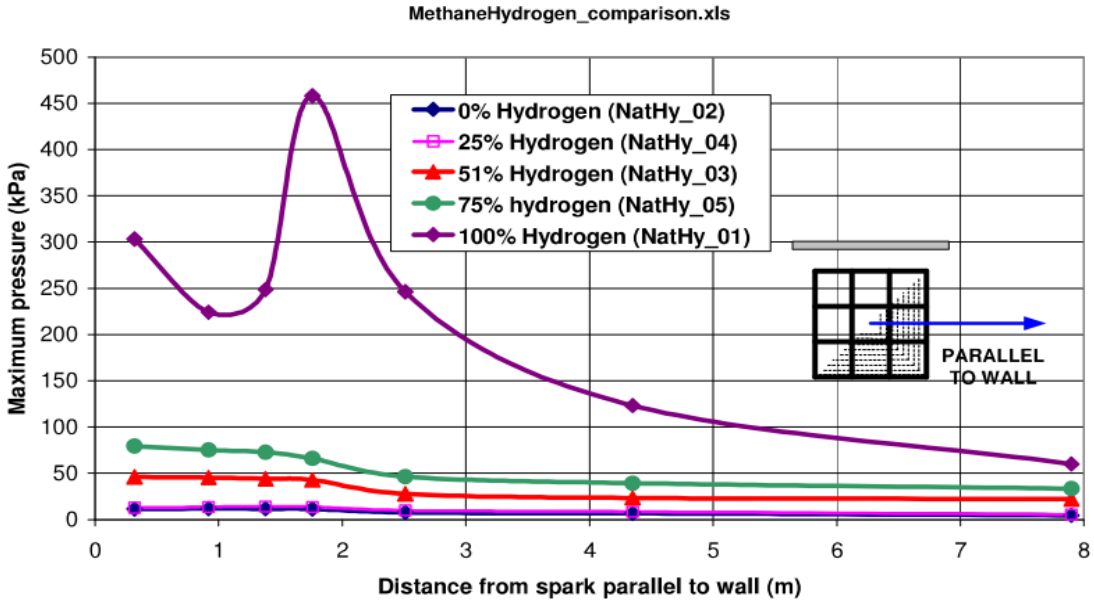

Figure 71: Overpressure vs. of distance parallel to the wall in the near field region (from [123])

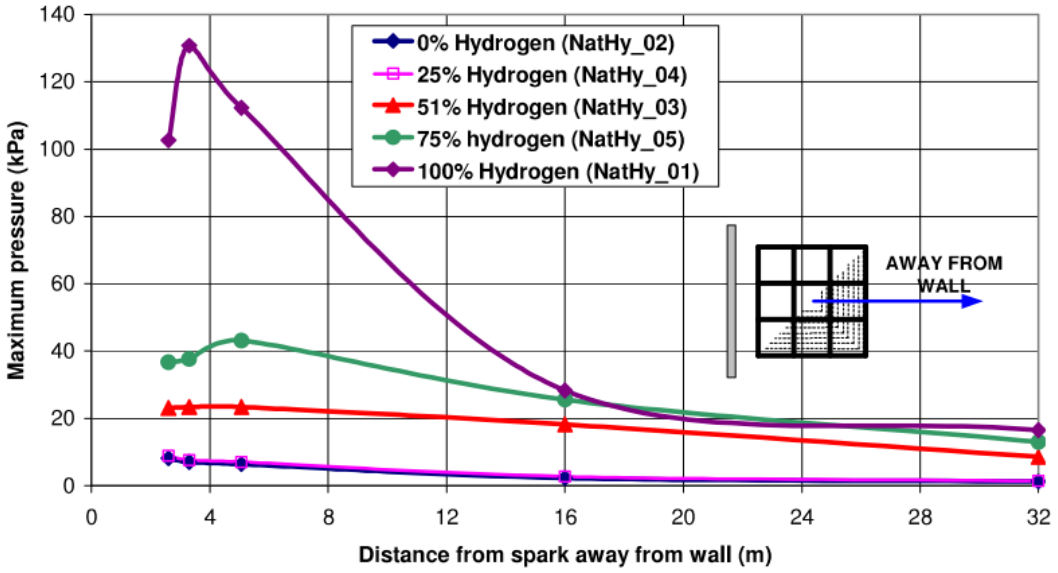

Figure 72: Overpressure vs. distance perpendicular to the wall in the far field region (from [123])

In the near field, values were well over 100 kPa and up to 450 kPa based on the distance parallel to the wall. At 32 m away, the overpressure drops to less than 20 kPa in the perpendicular direction and just above 50 kPa in the parallel direction. Referring to Table 1, 100 kPa is the fatality threshold for direct blast effects. Anything above 200 kPa has a 99% probability of fatality from direct blast effects. Note that this experiment represented the ignition of a pre-mixed 18 m^3 region with a high level of congestion— both the stoichiometric mixture size and level of congestion are probably unlikely to occur in a tunnel, especially simultaneously.

6.5.2. Modeling

A series of modeling efforts have been undertaken to understand hydrogen dispersion, deflagration, and hydrogen jet flame hazard in tunnels. Modeling was used to support a risk analysis of a hydrogen FCEV accident in a tunnel. The objective of the modeling was to predict the thermal expansion of the structural members and the temperature of the epoxy when a hydrogen jet flame impinges on the suspended tunnel ceiling (see Section 6.5.2.1). Furthermore, a CFD evaluation showed that the flame resulting from hydrogen release had the potential to damage tunnel equipment and structure (see Section 6.5.2.6). In another study, CFD modeling was performed in support of the evaluation of explosion risk of hydrogen vehicles (both cars and buses). A dispersion analysis determined realistic cloud sizes and hydrogen concentrations expected after a tunnel accident of various hydrogen vehicles (assuming delayed ignition). It was determined that the resulting overpressure is insignificant in terms of risk to human life (see Section 6.5.2.2). Another effort involved a turbulence modeling study evaluating hydrogen release and combustion, variable tunnel ventilation, and variable delayed ignition time. These results showed that larger ventilation rates decreased the growth rate of overpressure after ignition and the attenuation rate after reaching the peak while increased ignition time delay had the opposite effect (see Section 6.5.2.5). Also, a series of CFD simulations were performed to evaluate diffusion of leaked hydrogen in tunnels. These simulations showed that in tunnels without ventilation, the geometry effects the hydrogen diffusion (see Section 6.5.2.7). Finally, CFD models of hydrogen deflagration in a tunnel were compared with the results from experiments to validate the results of the CFD code (see Section 6.5.2.3 and 6.5.2.4).

6.5.2.1. Hydrogen FCEV Tunnel Safety Study

CFD, heat transfer, and solid mechanics modeling was performed by Sandia National Laboratories [113] in support of the risk analysis of a hydrogen FCEV accident in a tunnel. The scenario modeled in support of the risk analysis was a hydrogen vehicle in an accident exposed to a resulting fire (see Section 6.5.4 for additional details).

The objective of the modeling was to predict the thermal expansion of the structural members and the temperature of the epoxy when a hydrogen jet flame impinges on the tunnel ceiling. The analysis was divided into three parts: 1) a CFD simulation of the flame, 2) a heat transfer simulation of the structural members, and 3) a solid mechanics analysis of the structural members. A Sandia-developed code called Sierra was used to perform the simulations. Sierra is divided into different modules that can interact with each other. The Fuego module was used for the CFD simulation, the Aria module was used for the heat transfer model, and the Adagio module was used to calculate the deflection of the structural members. The CFD simulation provided the boundary conditions for the heat transfer simulation, specifically the radiative and convective heat flux on the tunnel ceiling. Note that due to computational limitations, the smallest reasonable tank orifice diameter that can be modeled is 5.25 cm. This is conservative because the velocity was kept constant for the larger diameter, so the mass flow and total heat release are larger than what is expected for the realistic 2.25 mm tank orifice diameter. While the velocity could be decreased in order to compensate for the larger release diameter, the flame impingement would be underestimated [113].

These boundary conditions served as input to Aria to calculate the temperature profiles across the structural members. Specifically, the reference temperature, heat transfer coefficient, and the irradiation from the CFD model were used as boundary conditions on the surface in direct contact with the heated gases. The temperature profiles on the structural members were input into Adagio to calculate the deflection due to thermal strain on each structural member. A simplified analysis was also performed to determine if the stainless-steel hangers can hold the concrete panels when the hydrogen jet is impinging the stainless-steel bar surface. Note that the different tunnel structures (Central Artery North Area or CANA tunnel and Ted Williams Tunnel) were each evaluated with and without ventilation [113].

Table 40 shows a summary of the maximum temperature and deflection for the CANA and Ted Williams (TW) structures. The worst-case scenarios were seen when the ventilation is not operating. Both the CANA and Ted Williams Tunnel results show that the thermal conditions may result in localized concrete spalling in the area where the hydrogen jet flame impinges the ceiling. If the ventilation is operating, the maximum temperature is significantly lower, and spalling is not expected to occur. The total stress on the steel structure was significantly lower than the yield stress of stainless steel and ASTM A36 at the maximum steel temperature even when the ventilation was not on. Therefore, the steel structure is not expected to be compromised. Also, the epoxy remains at ambient temperature and so should not degrade or fail due to this exposure. The maximum deflection of the steel hanger is 7 mm, which will not impact the structural integrity of the beam. Note that several conservative assumptions were made in this modeling, so the temperature observed should be lower than what which results in spalling [113]. Table 40 shows the results of the modeling. Each jet flame fire curve is created with ventilation (V) and without ventilation (NV). The hydrocarbon and ISO 834 curves are discussed in Section 2.5.1 in more detail.

Table 40: Results Summary of Hydrogen FCEV in Tunnels Risk Modeling (from [113])

Fire Curve		Maximum Temperature (°C)	Maximum Deflection (mm)	Yield Stress (MPa)
Hydrocarbon		~750	~5	-
ISO 834		~750	~10	-
H_2 Jet Flame CANA (NV)		592	19.4	-
H_2 Jet Flame CANA (V)		336	7.6	-
H_2 Jet Flame TW (NV)	Concrete	1,088	<200	-
	Stainless Steel	706	~7	147.79
	ASTM A36	-	-	399.9
H_2 Jet Flame TW (V)	Concrete	805	43.5	-
	Stainless Steel	436	1.3	214.76
	ASTM A36	-	-	172.37

6.5.2.2. Hydrogen Vehicle Explosion Risk in Tunnels

CFD modeling was performed by Middha and Hansen [127] in support of the evaluation of explosion risk of hydrogen vehicles (both cars and buses) in a tunnel (see Section 6.5.4.1 for additional details) [127]. The objective of the modeling was to predict a quantitative explosion risk for hydrogen vehicles in tunnels. All the scenarios described in Section 6.5.4.1 were evaluated using the CFD code FLACS. Both NGV and H2 vehicles were studied in the simulations but this section will only comment on results pertaining to H_2. The H_2 car and bus parameters are described by Middha and Hansen as follows:

1. Compressed hydrogen gas city bus with 40 kg H_2 stored in 8 cylinders (two sets of 4 each) – 5 kg per cylinder at a storage pressure of 350 bar. The vehicle was represented as a rectangular block (12.0 m x 2.55 m x 2.9 m) with the distance to the top of the tanks being 3.1 m.
2. Compressed hydrogen gas car with 5 kg H_2 stored in 1 cylinder at a storage pressure of 700 bar. The car was represented as a simple rectangular block (5.0 m x 1.9 m x 1.5 m) located 0.3 m above the ground.

As for the tunnels, two different cross sections were evaluated, rectangle and horseshoe shape, see Figure 73 for cross-sectional dimensions. Both tunnels were modeled with a length of 500 m.

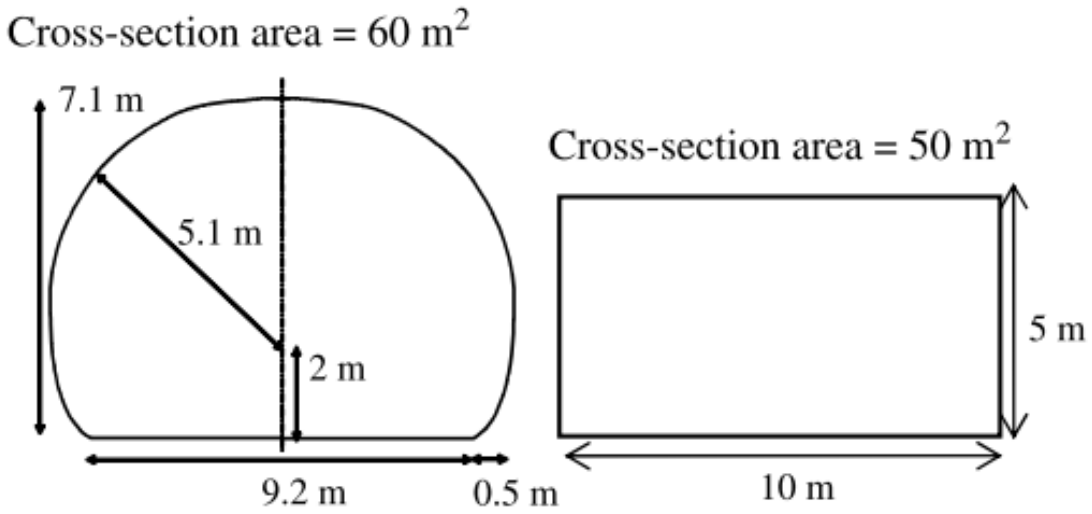

Figure 73: Tunnel cross-sectional dimensions (from [127])

In addition to the cross-sectional dimensions and length, the geometry of the modeled tunnel included vehicles. The tunnels were dual lane with traffic running a single direction. The tunnel was assumed to be full of cars and buses spaced out evenly by 1.5 m. The vehicle distribution was a repeated pattern of six cars follow by one bus. The vehicles were placed such that one bus and one car were at the exact center length wise of the tunnel in separate lanes. The same geometry was used for both the car and bus release. The releases were assumed to be choked flow. The mass flow rate of the H_2 for choked flow at 350 and 700 bar is displayed in Figure 74. Note that this was computed assuming a discharge coefficient of 0.8 and a 4 mm opening.

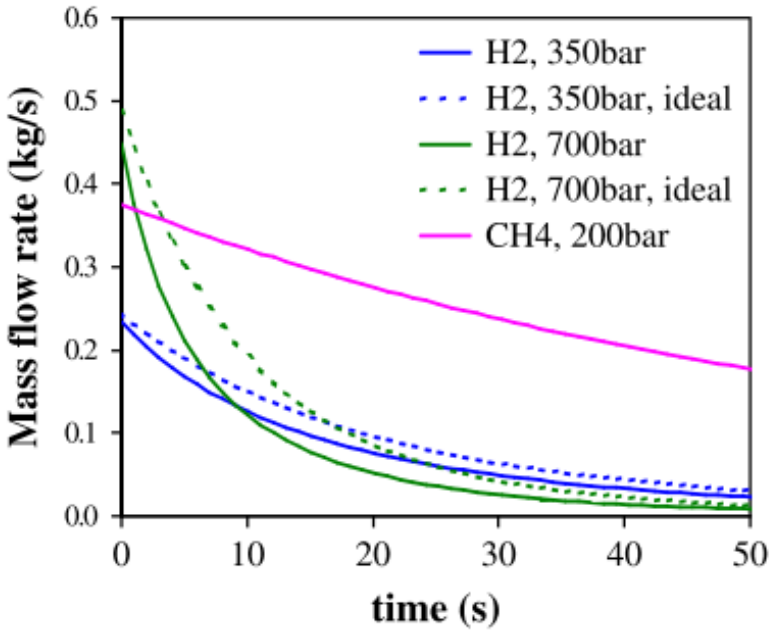

Figure 74: Mass flow of release for CNG and various H2 simulations (from [127])

Ignition points were varied from the center of the vapor cloud to the outer edges (length wise of the tunnel). Ventilation velocities were also varied between the models.

A dispersion model simulating the release of the fuel systems was carried out. Table 41 lists the maximum flammable gas cloud size for each configuration as well as the equivalent stoichiometric cloud or the Q9 quiescent cloud. This is a scaled smaller stoichiometric gas cloud that represents the same explosion load as the non-homogenous larger cloud. It is scaled based off the weighted volume expansion, flammable volume, and laminar burning velocity. The flammable cloud and its stoichiometric and Q9 equivalents along with the maximum pressures for the combustion of the flammable gas clouds are listed in Table 41 below:

Table 41: Summary of gas cloud & overpressure for various vehicles in both tunnels (from [127])

Vehicle/Release Characteristics	Inventory (kg)	Maximum flammable gas cloud size in m³ (kg)		Maximum equivalent stoichiometric flammable gas cloud size in m³ (kg)		Max. pressure for max. equiv. cloud Q9 Quiescent/Pre-ignition turb.	
		Horseshoe Tunnel	Rectangular Tunnel	Horseshoe Tunnel	Rectangular Tunnel	Maximum Q9 Equivalent Volume (m³)	Maximum overpressure (barg)
Car LH2	10	1.4 (0.007)	1.8 (0.009)	0.02 (0.003)	0.02 (0.004)	0.0	<0.05/0.1
Car H2 Gas 700 bar (vent up)	5	281 (1.14)	273 (1.21)	4.42 (0.07)	4.31 (0.09)	4.4	0.05/0.10
Car H2 Gas 700 bar (vent down)	5	268 (1.33)	308 (1.39)	17.75 (0.29)	8.77 (0.18)	17.8	0.11/0.34
Bus H2 Gas 350 bar	5	213 (0.89)	190 (0.81)	2.16 (0.04)	1.94 (0.04)	2.2	0.05/0.10
Bus H2 Gas 350 bar	20	1795 (7.46)	3037 (13.97)	27.46 (0.45)	24.67 (0.49)	27.5	0.11/0.34

From the coupled dispersion combustion simulations, it is predicted that overpressure values can produce minor damage to people and property within the tunnel. The data presented in Table 41 were combined to create a frequency of exceedance curve for overpressures during combustion of gaseous hydrogen clouds, shown in Figure 75. Overpressure values outside the hazardous range (less than 0.1 barg) are much more likely than higher overpressures that can be hazardous to tunnel occupants. This is important information to perform a risk analysis, but the method used to create the exceedance curves is not discussed in detail.

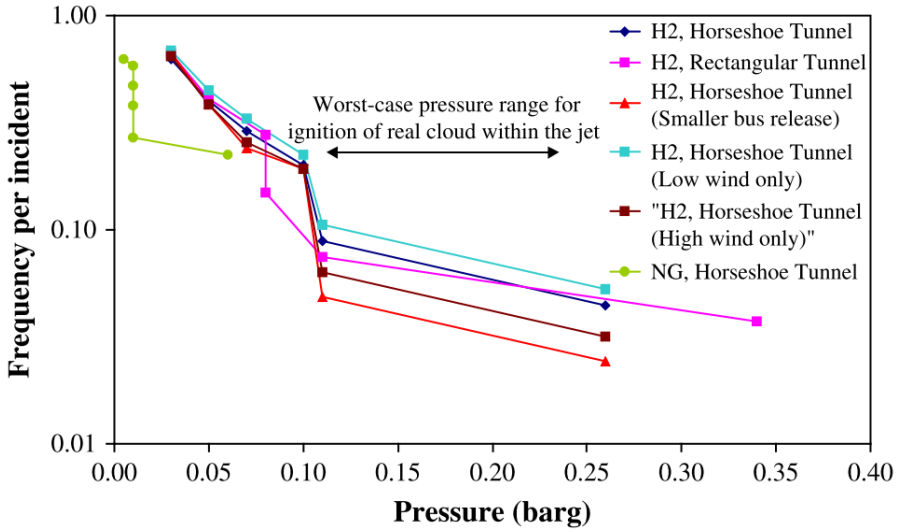

Figure 75: Exceedance curves for overpressure values per fuel type (from [127])

6.5.2.3. CFD Modeling of Hydrogen Deflagration in a Tunnel

Deflagration in homogenous, near stoichiometric hydrogen/air mixtures in a model of a tunnel were simulated through CFD modeling techniques by Tolias et al. [177]. The ADREA-HF CFD code was used for this modeling. The purpose of this modeling was to baseline the results from the ADREA-HF CFD code with that of the experiment discussed in Section 6.5.1.2. Specifically, the time-dependent overpressure data generated from the CFD modeling was compared directly with the experimental data. The two cases that were examined were the empty tunnel and tunnel with simulated traffic with a homogeneous hydrogen/air mixture with a 30% hydrogen concentration by volume. While this experiment used this concentration for each scenario, more plausible concentration would need to be used in future work. Figure 77 shows the experimental and computational overpressure results at different locations along the tunnel. As shown, the computational results are in general agreement with the results of the experiment. Therefore, the CFD code was able to simulate the combustion process and estimate the resulting overpressures.

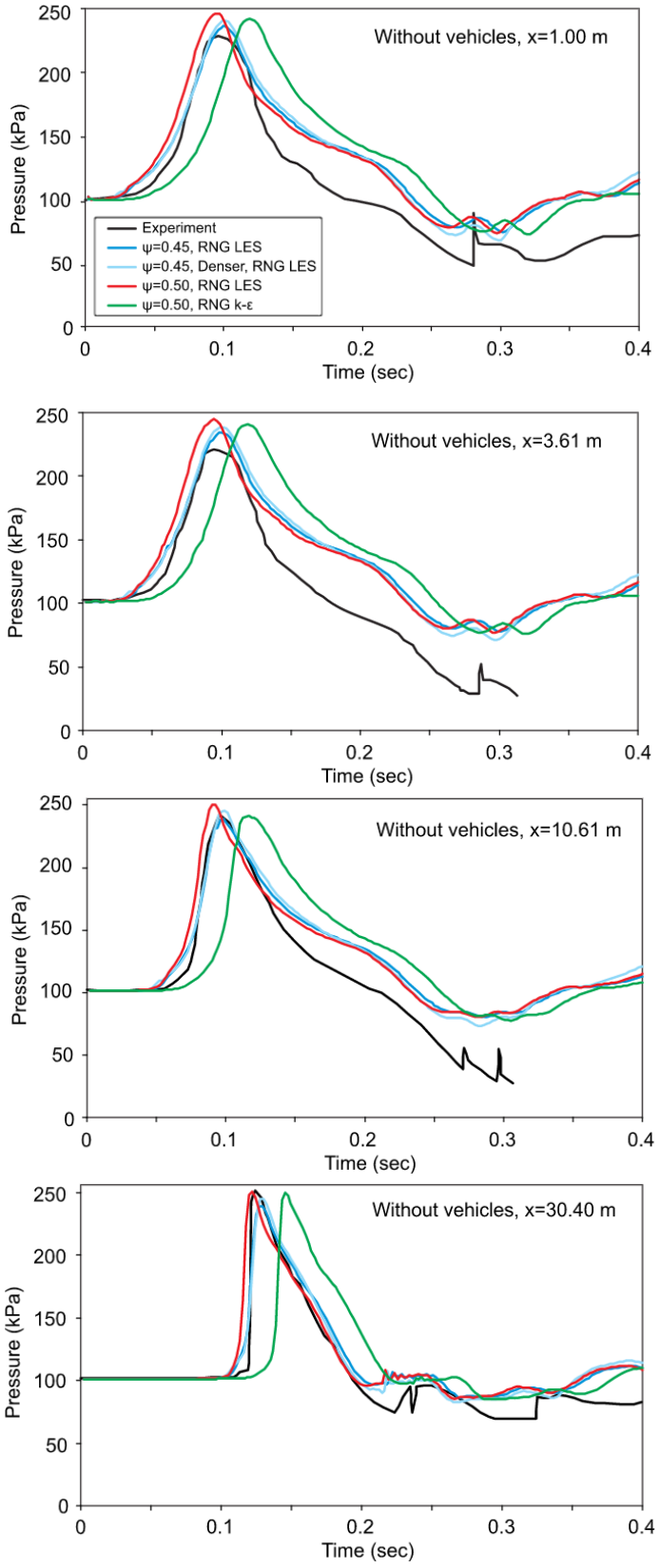

Figure 76: Overpressure Results without Vehicles (from [177])

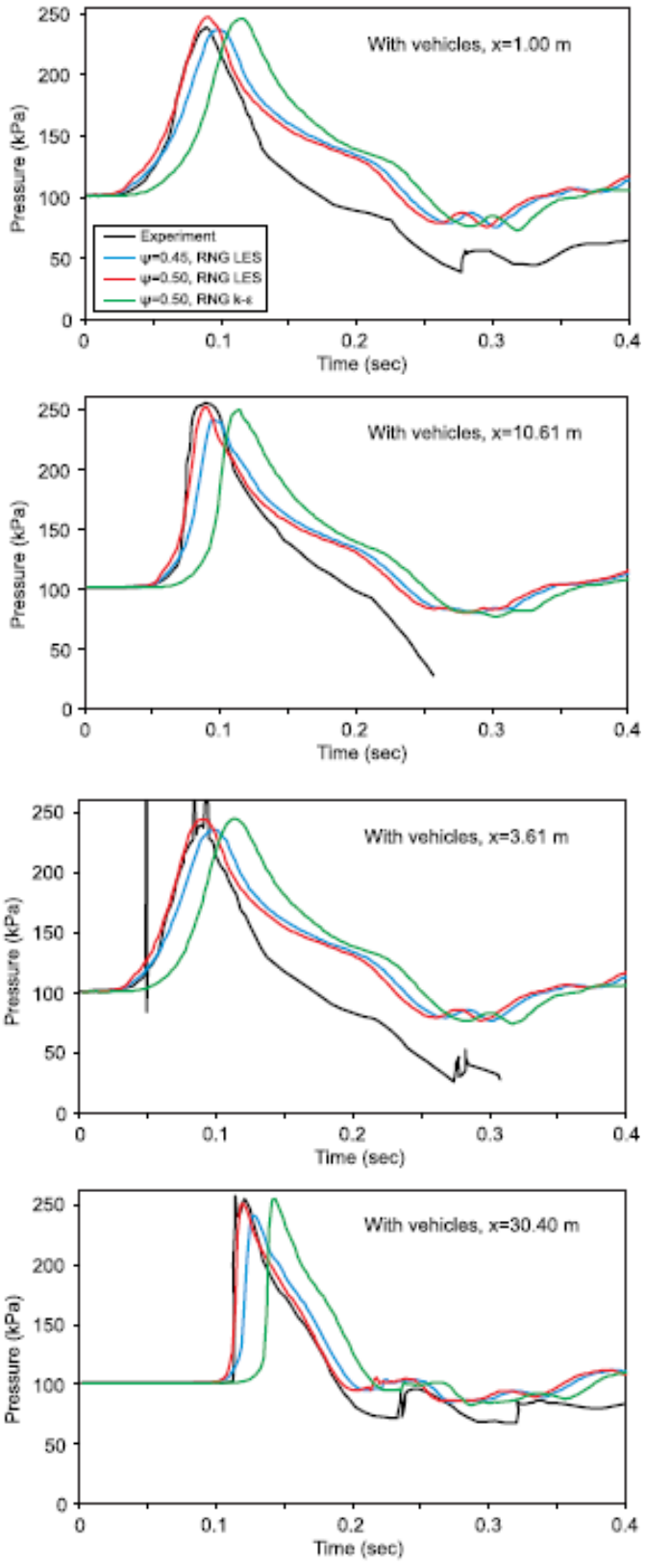

Figure 77: Overpressure Results with Vehicles (from [177])

6.5.2.4. Releases from Hydrogen Fuel-cell Vehicles in Tunnels

Houf et al. [173] modeled the consequence of hydrogen TPRDs being activated, the flammable gas venting to the environment and the time-delay to ignition within a tunnel. Multiple simulation tools were used to perform the evaluation. To model the TPRD releases inside ventilated tunnels, Sandia's computational fluid mechanics code, Fuego, was used. An FCEV was modeled with three separate tanks, each containing 1.67 kg of hydrogen at 70 MPa. For these simulations, high-pressure hydrogen gas was vented simultaneously from three separate onboard tanks through three separate TPRD vents located on the bottom of the FCEV. Figure 78 shows a diagram of the tunnel model layout with transverse ventilation. The evolution of the hydrogen/air mixture was modeled after blowdown from the TPRDs on the FCEV. A Sandia developed code, NETFLOW, was used to model the transient nature of the tank blowdown [173].

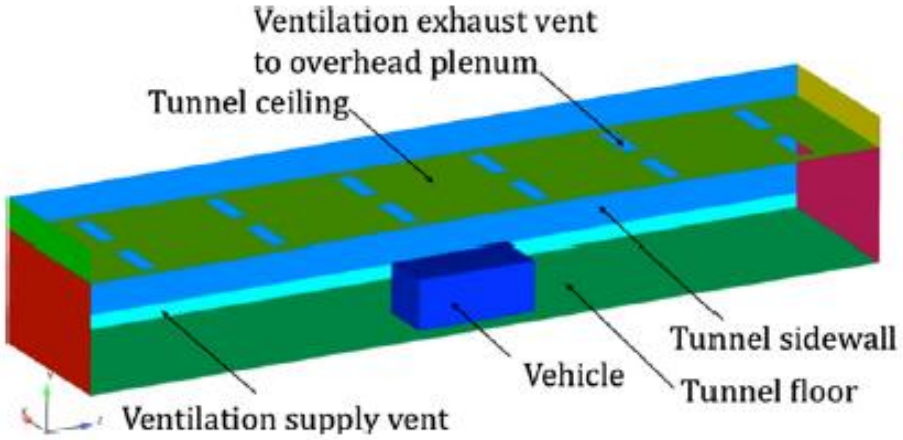

Figure 78: Tunnel Model with Transverse Ventilation (from [173])

Figure 79 shows the simulation results of the hydrogen release and mixing in the tunnel model. Note that the solid lines are the total flammable volume in both the tunnel and ventilation plenum, and the dashed lines represent the flammable volume in the ventilation plenum only. As shown, a range of ventilation rates were evaluated, and the flammable volume decreases with increasing ventilation rate. Also, the flammable volume disperses quicker with a higher ventilation rate [173].

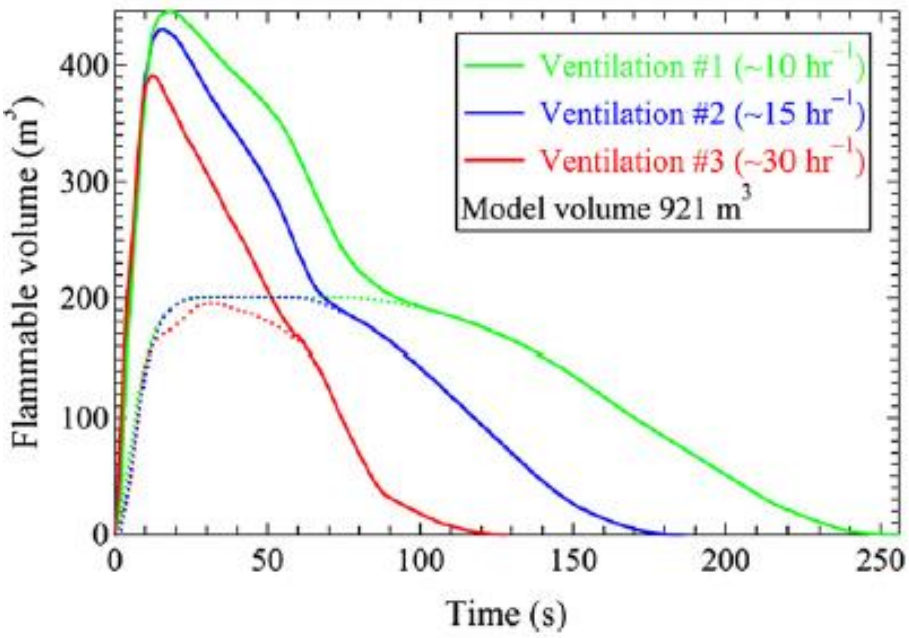

Figure 79: Simulation Results Showing Evolution of Flammable Hydrogen Volume (from [173])

A FLACS model was developed to perform ignition overpressure simulations for the simulations evaluated in Fuego. Figure 80 shows the results from the simulation modeling at different ignition times and locations of the ignition source after the beginning of the TPRD release. As shown, overpressure peaks at an ignition delay of around 5 seconds [173]. Referring to Table 1, ignition delays of about 4 to 8 seconds result in overpressures approaching or above the fatality threshold level. These results show the importance and sensitivity to various ignition locations and delays.

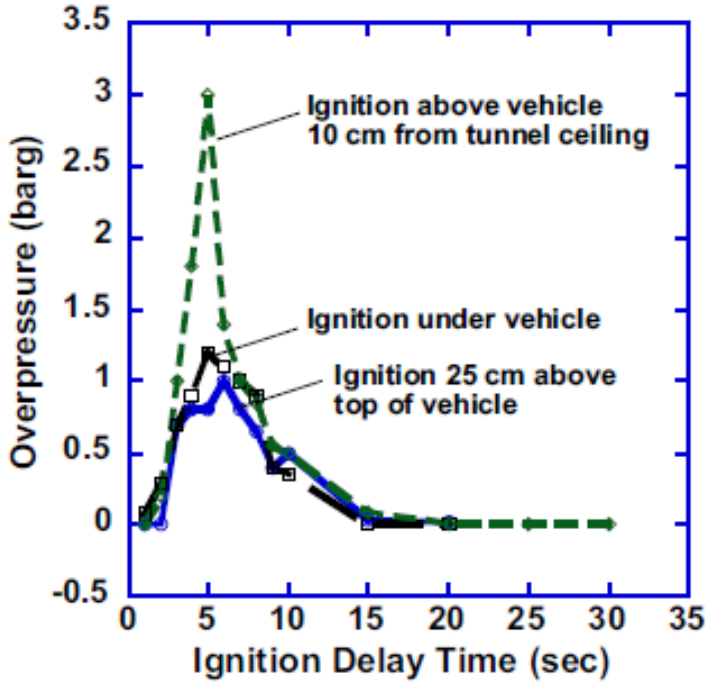

Figure 80: Simulation of Peak Ignition Overpressures vs. Ignition Delay (from [173])

6.5.2.5. Hydrogen Release and Combustion in Subsea Tunnels

Turbulence modeling was used to evaluate hydrogen release events from vehicles in subsea tunnels by Bie and Hao [178]. As part of this study, variable tunnel ventilation conditions and the resulting hydrogen cloud sizes, as well as delay in ignition time, were assessed to fully characterize this risk. The partially averaged Navier-Stokes turbulence model was used to research the hydrogen release and combustion phenomena as it related to the risk inside highway tunnels. The physical tunnel used as the basis of this modeling effort was the Bay subsea tunnel, a three-lane highway. The model of the tunnel was 13.5 meters wide, 5 meters high, and 500 meters long. A typical mid-sized hydrogen FCEV was modeled containing 4.955 kg H_2 at 70 MPa. Varying ventilation conditions of 0 m/s (no ventilation), 1 m/s, 3 m/s, and 6 m/s were evaluated with five monitoring points spaced at 5 meter horizontal intervals (see Figure 81) [178].

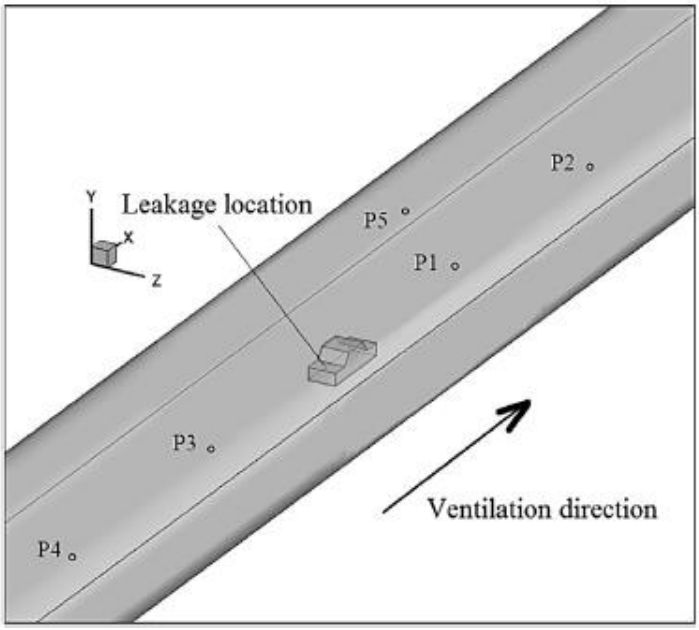

Figure 81: Subsea Tunnel Model with FCEV and Monitoring Points (from [178])

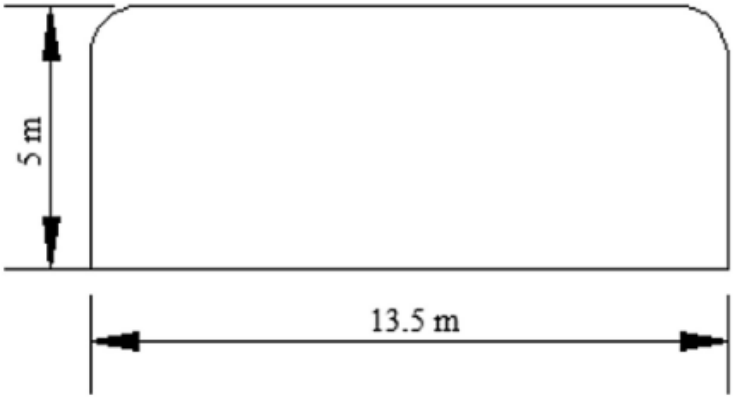

Figure 82: Subsea Tunnel Model Cross Section (from [178])

Figure 83 and Figure 84 show the longitudinal and traverse hydrogen concentration contours at three seconds after event initiation for different ventilation conditions. As shown, the ventilation

rate has a significant influence on the hydrogen distribution after the TPRD release event. The upstream monitoring points showed less hazardous concentrations of hydrogen than the downstream monitoring points [178].

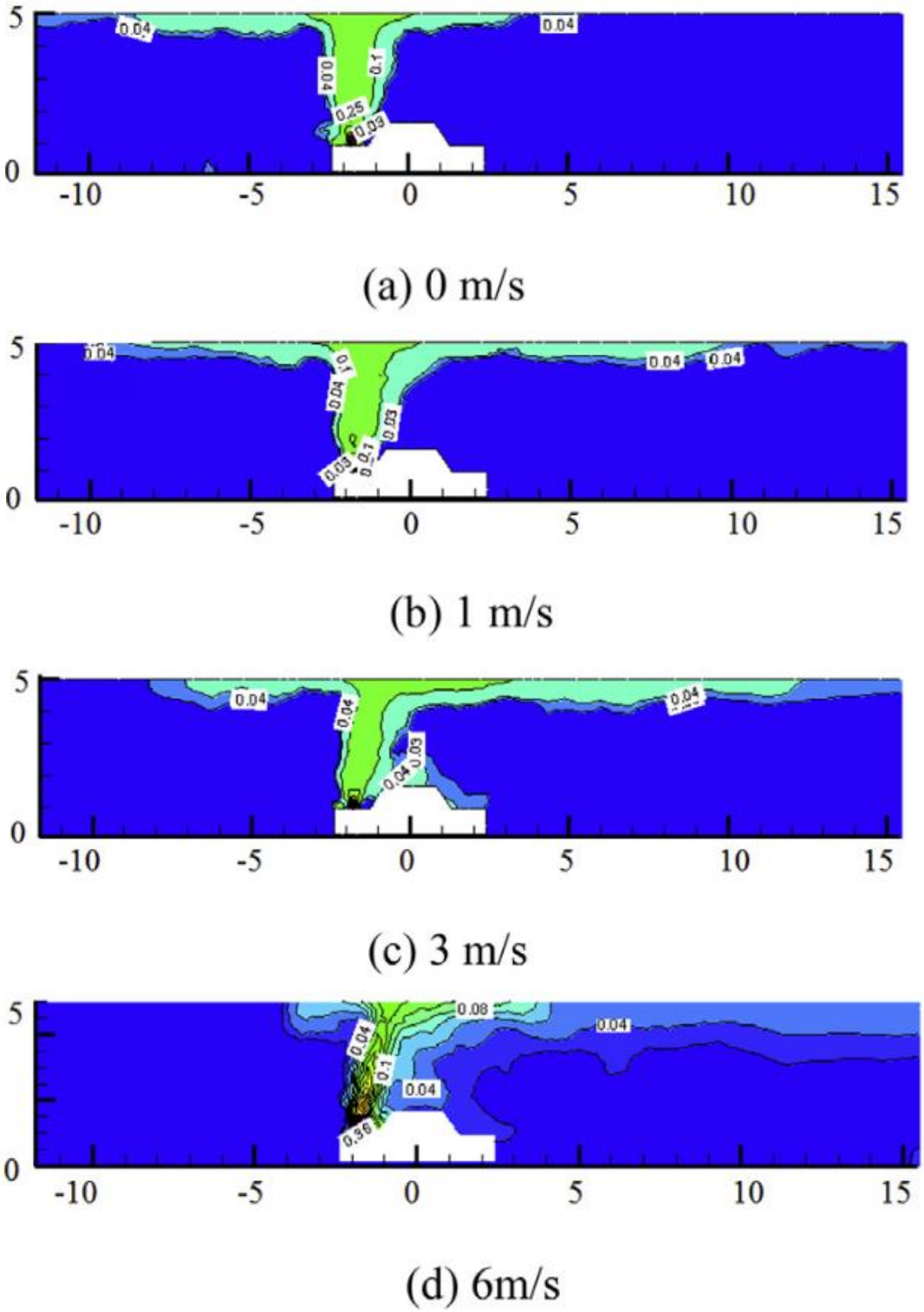

Figure 83: Longitudinal H2 Distribution Various Ventilation Conditions (from [178])

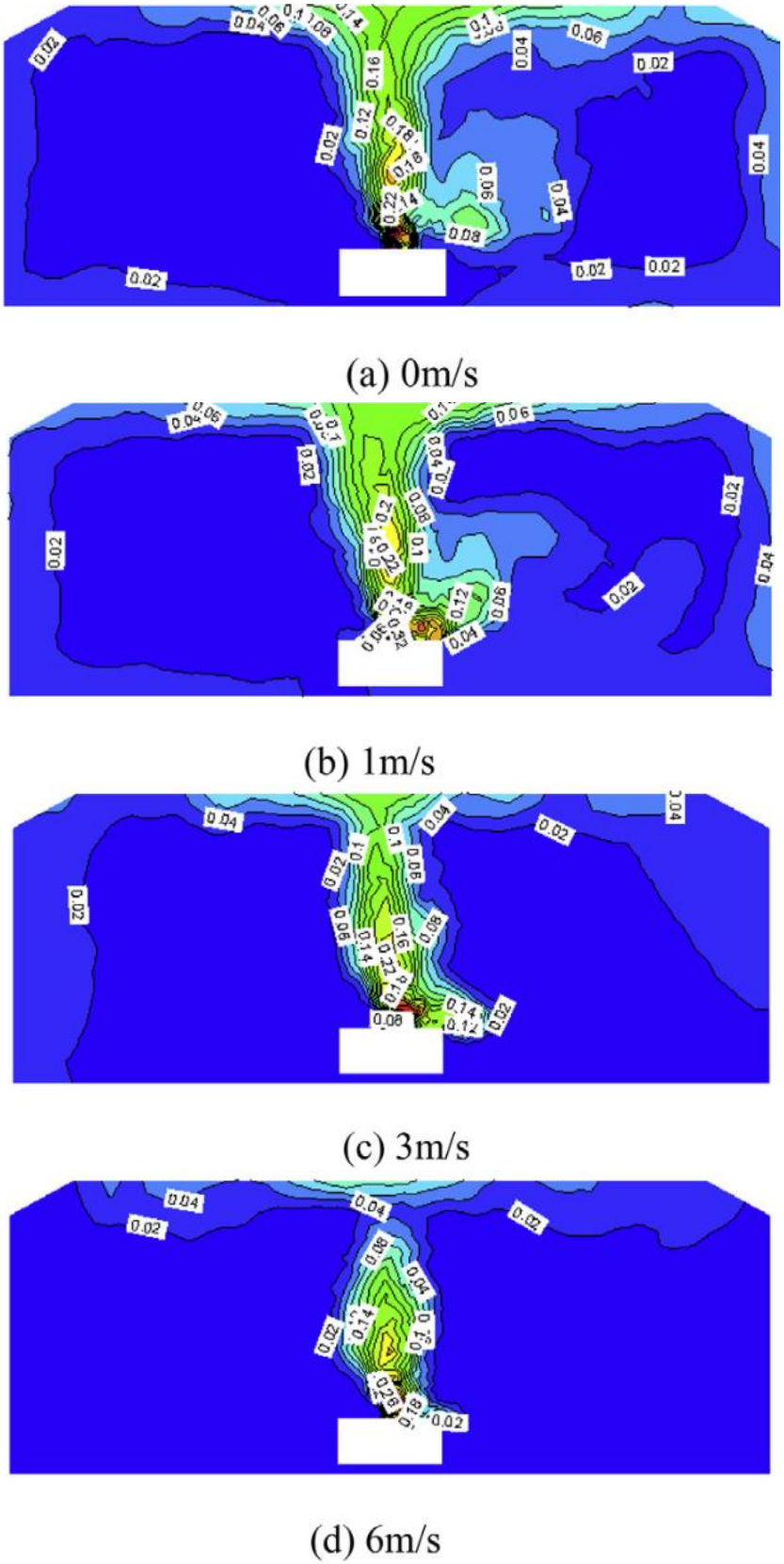

Figure 84: Traverse H2 Distribution Various Ventilation Conditions (from [178])

Figure 85 and Figure 86 show the overpressure history for different ventilation conditions at ignition times of 3.1 s and 6.1 s, respectively. There are four monitoring points (P1, P2, P3, and P4) that measure the overpressure. P1 was arranged 5 m away from the leakage location along the direction of traffic, P2 was arranged 10 m away from the leakage location along the direction of traffic, P3 was arranged 5 m away from the leakage location in the inverse direction of vehicle, and P4 was arranged 10 m away from the leakage location in the inverse direction of vehicle per Bie and Hao [178]. The literature specifies that P1 and P2 are downstream, while P3 and P4 are upstream [178].

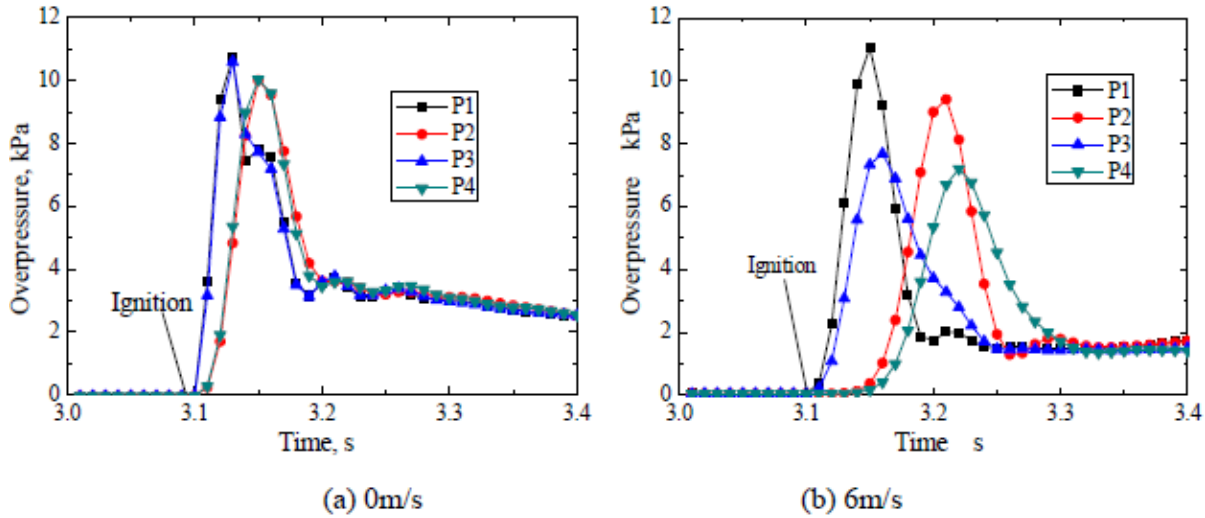

Figure 85: Overpressure History at Ignition Time of 3.1 Seconds (from [178])

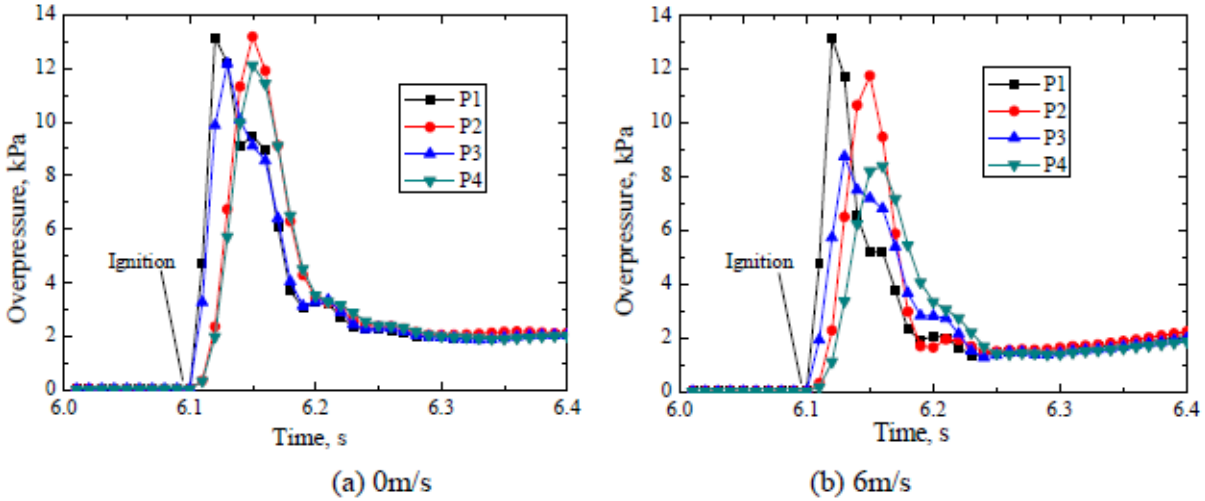

Figure 86: Overpressure History at Ignition Time of 6.1 Seconds (from [178])

The overpressure shown in Figure 85 and Figure 86 shows the peak overpressures for the upstream locations (P3 & P4) are appreciably reduced with ventilation from 10-12 kPa at 3.1 seconds down to 7.5-8 kPa and 12 kPa down to 9 kPa at 6.1 seconds. Only P2 downstream shows a small reduction in the overpressure measured comparing with and without ventilation.

6.5.2.6. Hydrogen Jet Flame Hazard in Tunnels

An evaluation of the possible fire scenarios of hydrogen cars in tunnels was conducted to assess the implications on a tunnel ventilation system. To accomplish this, CFD simulations were evaluated on a tunnel with a length of 102 m and a cross-section of 5 m by 5 m. Fluent was used to simulate the smoke flow in the tunnels after a fire. Figure 87 shows the tunnel geometry and boundary conditions of the CFD case. As shown, the hydrogen FCEV is located 40 m from the air inlet [179].

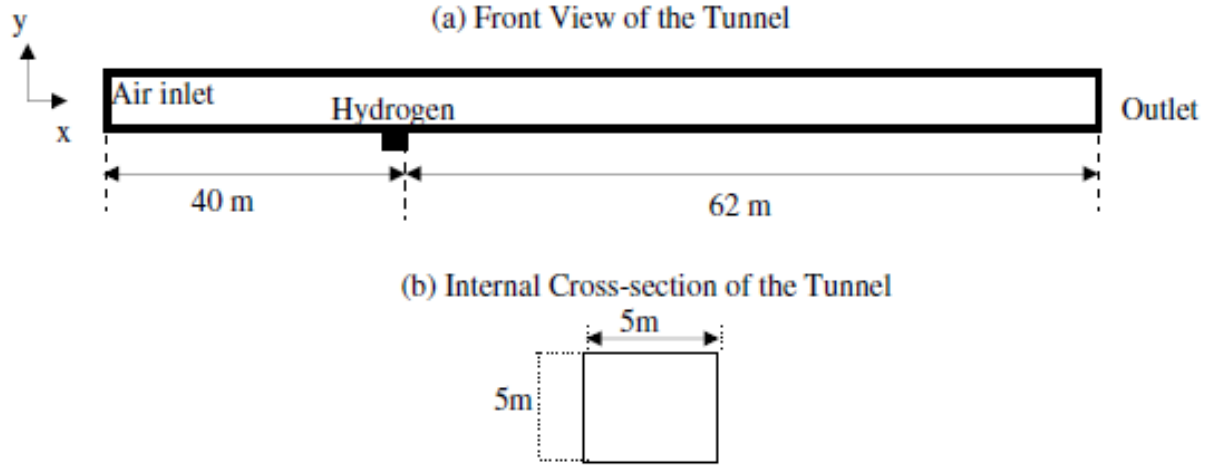

Figure 87: Tunnel geometry and Boundary Conditions of CFD Model (from [179])

Two scenarios were evaluated: a) 6 MW hydrogen fire with 2.5 m/s ventilation, and b) 30 MW hydrogen fire with 2.5 m/s ventilation. This study selected these two specific scenarios based on realistic hydrogen release conditions from a hydrogen car. Hydrogen was released at a rate of 0.05 kg/s and at a velocity of 10 m/s which resulted in a 6 MW hydrogen fire lasting about 1 minute in the first scenario. In the second scenario, hydrogen was released at a rate of 0.25 kg/s and a velocity of 50 m/s, which resulted in a 30 MW fire for a shorter duration. The results of the CFD evaluation show that the ventilation in the 6 MW fire can fully eliminate the backlayering of smoke. However, this is not true of the 30 MW fire. Moreover, the 30 MW fire resulted in the flame reaching the tunnel ceiling and spreading under the ceiling for large distances. This could result in serious damage to the tunnel equipment and structures along the ceiling [179].

6.5.2.7. Diffusion of Leaked Hydrogen in Tunnels

A series of CFD simulations were performed to evaluate diffusion of leaked hydrogen in tunnels [180]. Multiple tunnels with variations in slope, leak location, cross-section geometry, ventilation rate, and ventilation type were evaluated for a 60 m^3 (unmixed, approximately 5 kg) hydrogen leak. In the vehicle tunnel simulations (Case A), long model tunnel and an underwater model tunnel were evaluated. Figure 88 illustrates the differences between these tunnels. Each tunnel was evaluated with varying ventilation flow rates [180].

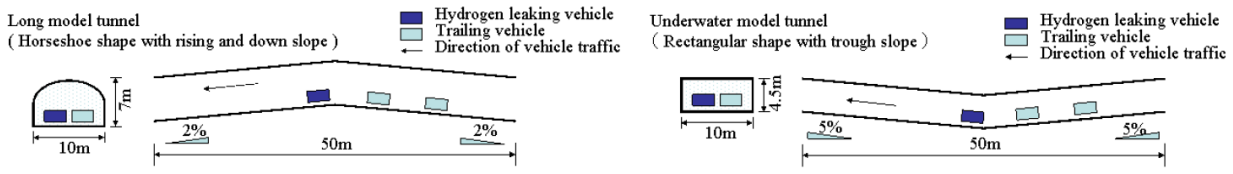

Figure 88: Case A Simulation Tunnel Geometries (from [180])

The general flow modeling software code STAR-CD was used in the calculation model. It was found that in tunnels without ventilation, the geometry effects hydrogen diffusion. The slope of the long tunnel model resulted in hydrogen collecting in the tunnel for several dozen minutes. In tunnels with the underwater model tunnel slope, hydrogen is rapidly cleared from the tunnel. For each Case A tunnel geometry with ventilation, the hydrogen is removed by the ventilation flow within several dozen seconds. In the Case B simulations, there is a brief time in which hydrogen with a concentration at about LFL flows into the power collector. For the Case C simulations, there is no concern about inflow of hydrogen at concentrations greater than LFL since that time is very short [180].

Figure 89 illustrates the tunnel evaluated in the Case B simulations. In these simulations, an electrostatic dust collector is in a branch off the main tunnel. The location of the leaked hydrogen is varied [180].

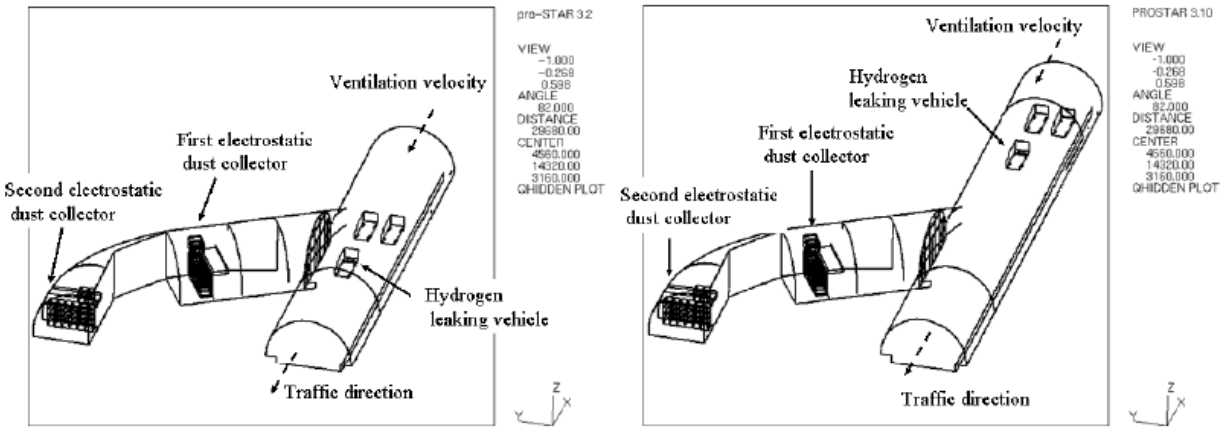

Figure 89: Case B Simulation Tunnel Geometry (from [180])

Figure 90 illustrates the tunnel evaluated in the Case C simulations. In these simulations, an underground ventilation facility is in a branch off the main tunnel and air is released through a vertical shaft opening to the outside. The location of the leaked hydrogen is varied [180].

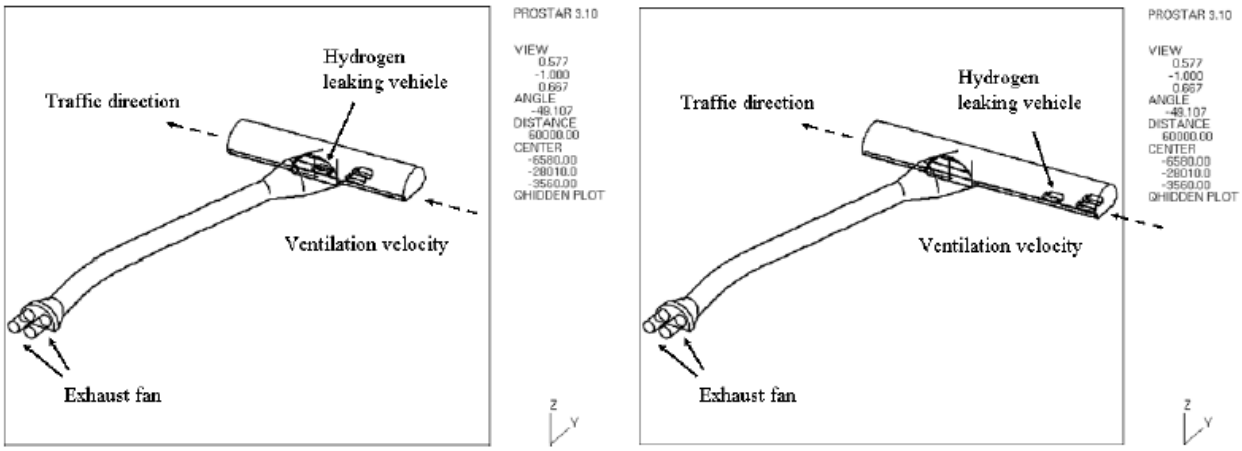

Figure 90: Case C Simulation Tunnel Geometry (from [180])

6.5.2.8. Gaseous release, dispersion, and combustion for automotive scenarios

Venetsanos et al. [126] CFD was used to study the effects of a compressed gas release from a commercial vehicle in urban areas. One urban area simulated was a tunnel with a single deck city bus located centrally along the length. Variable releases from both hydrogen and CNG fuel tanks were evaluated. The fuel storage systems modeled represented that of a typical European bus with fuel containers located along the roof, forward from the midpoint. The system consisted of 2 sets of 4 tanks connected as displayed in Figure 91. The specific CFD solvers utilized were ADREA-HF for dispersion and REACFLOW for combustion.

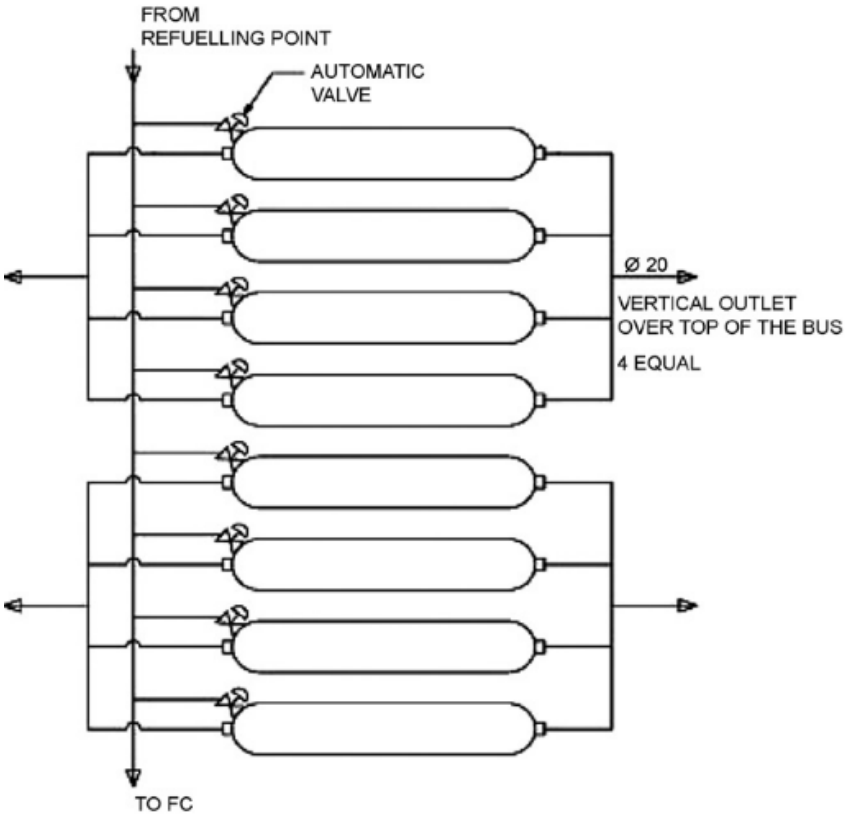

Figure 91: Fuel tanks configuration for both CNG and CH2 gas (from [126])

The tanks contained a total of 40 kg at 20, 35, and 70 MPa of H_2. This is representative of a standard CGH_2 bus and the 70 MPa case exceeds normal bus configurations. The main vent lines are controlled by thermally activated pressure relief devices (TPRD). As shown, each TPRD is attached to manifold connected to 4 tanks (2 TPRDs per set of 8 tanks). Multiple release scenarios were evaluated by varying TPRD orifice size and tank evacuations. A summation of storage parameters is shown in Table 42. Note this study and the figures below have results for hydrogen and methane.

Table 42: Storage Configurations Details (from [126])

Fuel	Pressure (MPa)	Fuel density at 15 °C (kg m^{-3})	Total storage volume (l)	Single cylinder volume (l)	Total fuel mass (in 8 cylinders) (kg)	Fuel mass in one cylinder (kg)
H_2	20	14.96	2672	334	40	5
H_2	35	24.02	1600	200	40	5
H_2	70	40.18	996	124.5	40	5
CH_4	20	168	1000	125	168	21

The computational domain was modeled as a tunnel of 212 m length with a cross-sectional area displayed in Figure 92. As mentioned, the bus was located along half the length of the tunnel in a centralized location. Besides the bus, the tunnel was assumed to be empty and the walls were modeled as smooth surfaces. Additionally, the air was assumed quiescent to represent a worst case scenario.

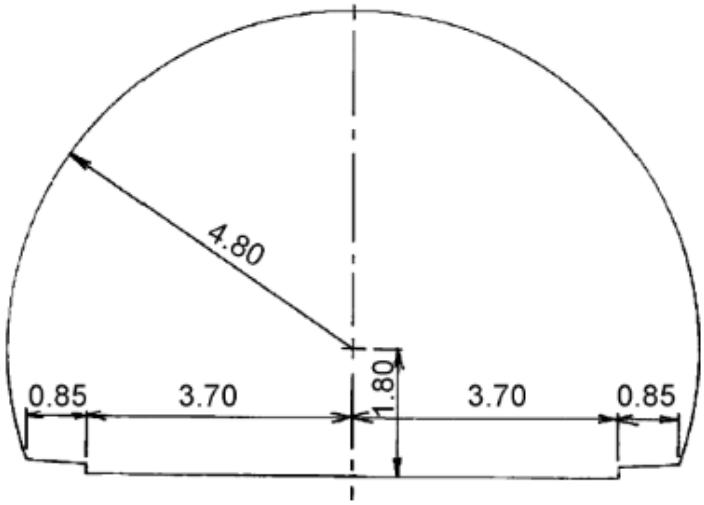

Figure 92: Tunnel Cross Section (from [126])

Two release cases were evaluated for CNG. Table 43 lists the descriptions of all cases, Case 1, and 3 were selected since Case 2 lies between them.

Table 43: Storage Configurations Details (from [126])

Case no.	Possible release	Description	Gas released (kg)
1	Vehicle out of service (automatic valves closed) and one random PRD fuse fails open OR Fire causes a single PRD to trigger[a]	Gas from one cylinder released through 1 PRD vent and 1 outlet	Hydrogen—5 Natural gas—21
2	Vehicle in service (automatic valves open) and one random PRD fuse fails open OR Fire causes a single PRD to trigger[a]	Gas from all cylinders released through 1 outlet	Hydrogen—40 Natural gas—168
3	Fire causes all PRDs to trigger simultaneously[a]	Gas from all cylinders released through all 4 outlets	Hydrogen—40 Natural gas—168

[a]It is assumed that the fire does not ignite the gas. Anecdotal reports by various research and testing organizations indicate that fires that cause temperature triggered PRD to open may not immediately ignite the vented gas. The fire that triggers the thermally activated PRD may not be in a position that causes the vented gas to ignite, since the exit from the vent may not be situated in the fire.

The results for Case 1, where only one cylinder was released through a single TPRD, are shown in Figure 93. The left frame shows the flammable mass and the right frame the total available energy.

The available energy was computed by multiplying the released mass of fuel by the lower heat of combustion. The flammable mass was calculated from the amount of fuel/air mixture released which was within the FL. Figure 94 displays the results for case 3, where all 8 cylinders released through all 4 TPRDs simultaneously.

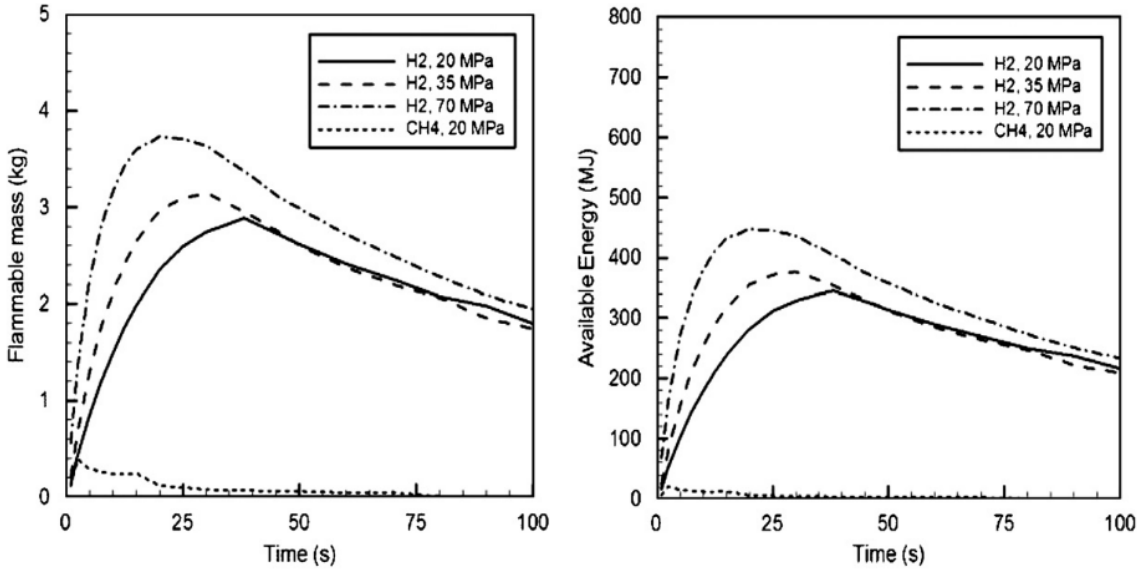

Figure 93: Flammable mass and available energy of released gas in Case 1 (from [126])

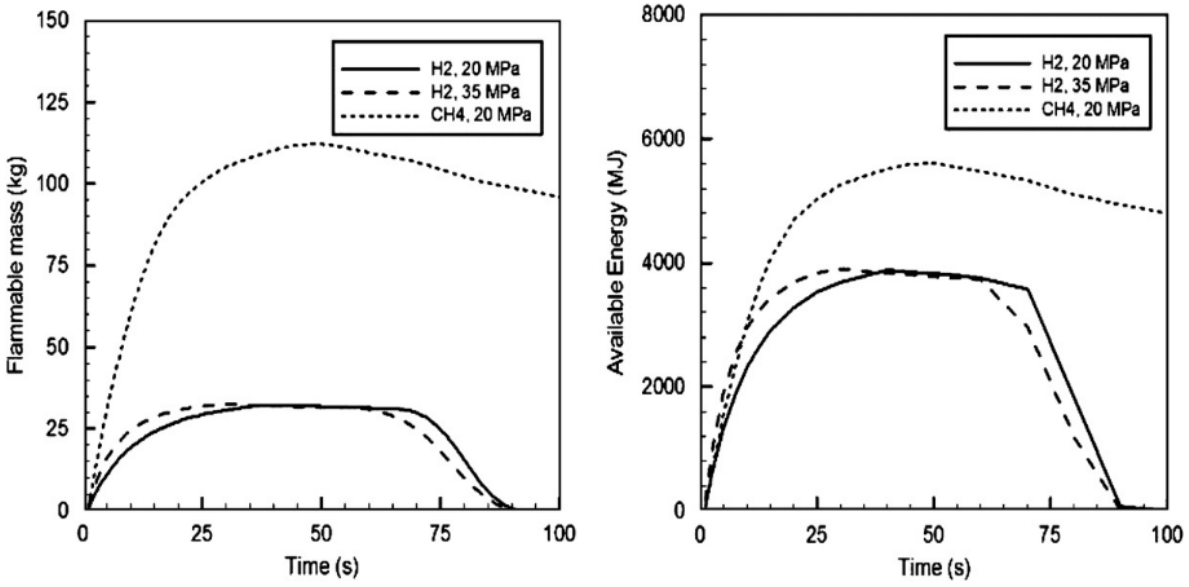

Figure 94: Flammable mass and available energy of released gases in Case 3 (from [126])

Note the change in scales between Figure 93 and Figure 94 For Case 1 both the flammable mass and available energy maintained lower values and dissipated rapidly in time. For Case 3 the flammable mass and available energy reached dangerous levels which persisted over the length of the simulation. It was assumed the Case 1 overpressures would be negligible because the total flammable mass was less than 0.5 kg. The overpressure values are displayed in Figure 96. The overpressure was

calculated assuming that the cloud was ignited after 40 seconds, corresponding to maximum flammable mass. The ignition point was assumed to be at the center of tunnel at the top of the bus.

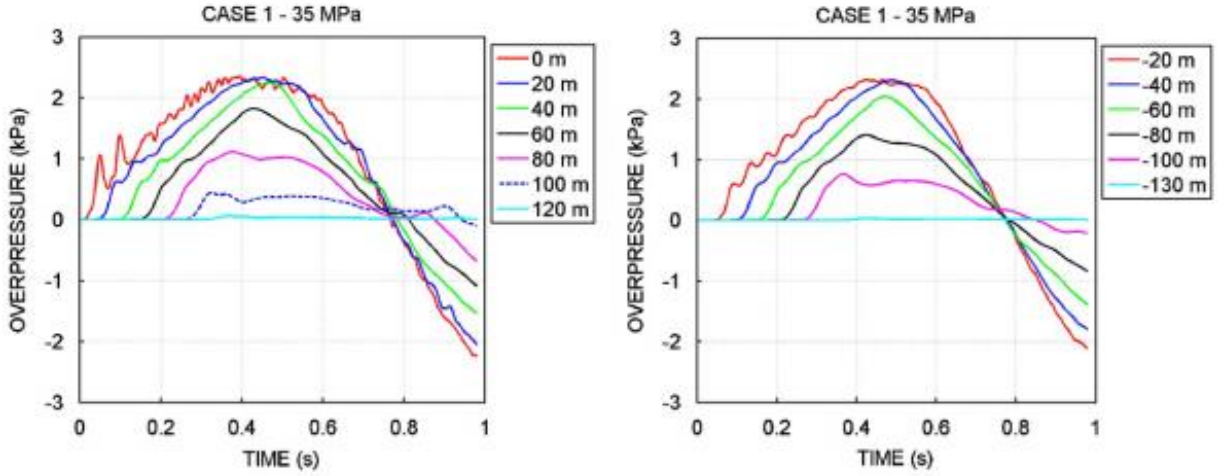

Figure 95: Overpressure values up and down tunnel of the bus for release Case 1 (from [126])

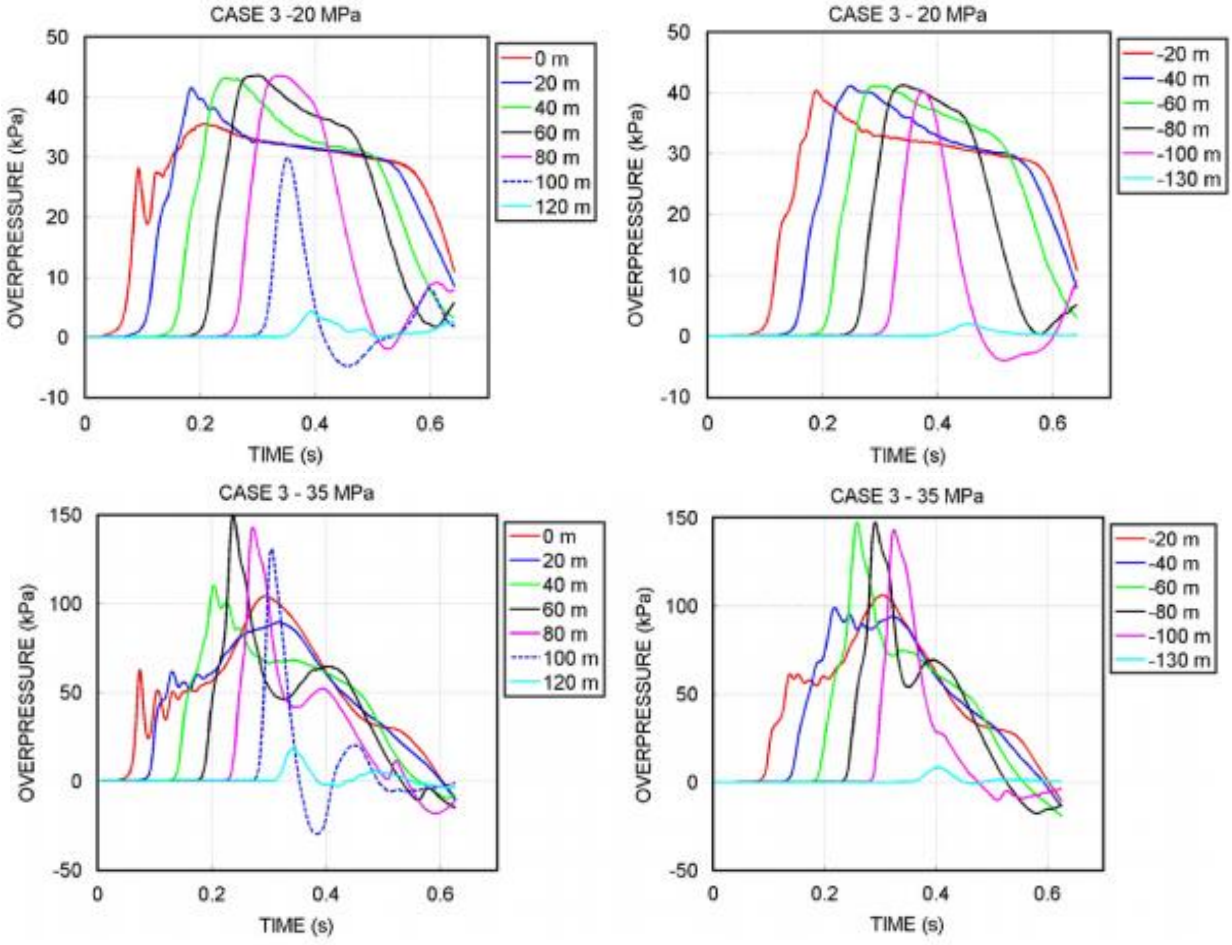

Figure 96: Overpressure values up and down tunnel of the bus for release Case 3 (from [126])

When reviewing these overpressure values, it is important to keep in mind what pressure values correlate to what level of property damage or human hazard. The tables listed in Section 1.2 help understand the damage and tenability thresholds. Case 3 scenario yields overpressure values capable of rupturing eardrums and creating harmful glass splinters up to a distance 80-100 m from the ignition point. Note that the range for the eardrum rupture threshold reported in Table 1 is 16.5-19.3 kPa. For the 35 MPa scenario, the overpressure goes into the threshold for fatality per Table 1. Venetsanos et al. [126] states that the blast wave maintains its strength for long distances inside of tunnels due to the high levels of confinement compared with urban environments where blast waves decay quicker. In addition to overpressure, Venetsanos et al. [126] reported the fireball length along the tunnel, the results for each scenario are displayed in Table 44.

Table 44: Combustion results within tunnel (from [126])

Scenario				Effect	
Case	Fuel	Pressure (MPa)	Energy (MJ)	Fireball Length along the tunnel (m)	Overpressure Peak overpressure (kPa)
1	H_2	20	346	62	2.3
		35	377	58	2.3
		70	448	47	2.3
	NG	20	19	S	S
3	H_2	20	3890	220[a]	42.5
		35	3900	285[a]	150
		70	NM	NM	NM
	NG	20	5380	198	45

Notes: S: Small flammable mass. Calculations were not performed, as the overpressures and fireball size were not expected to be significant. NM: Not modelled. Typical overpressure effects (based on various scientific sources): 2 kPa: Threshold of window breakage. 21 kPa: Threshold of eardrum rupture and moderate building damage. 35 kPa: Severe building damage, i.e. unusable.

[a]The flame extends beyond the limits of the tunnel (tunnel length = 212 m).

For the Case 3 model, the hydrogen combustion produced a flame length which traveled farther than the length of the tunnel, 220 m for the 20 MPa and 285 m for the 35 MPa case of the total 212 m. The flame length for Case 1 hydrogen combustion was reported as 58 m for the 20 MPa and 47 m for the 35 MPa. It is worth noting that in this study, Case 3 represents an implausible scenario of rapid and complete fuel release, ignition when the peak flammable mass is present, and static air within the tunnel. This study further identifies the importance ventilation plays on mitigating risk during an accidental release of fuel in a tunnel.

6.5.3. Analysis

Multiple analyses have been performed to evaluate the risk associated with hydrogen vehicles in tunnels. One analysis was performed to characterize the most likely consequence of an accident by developing an event sequence diagram and further characterizing severe consequence scenarios. It was shown that the most likely consequence is no additional hazard from the hydrogen (see Section 6.5.4). Another assessment was performed to evaluate the consequence of a delayed ignition of hydrogen released from several different types of vehicles (both cars and buses with compressed hydrogen, as well as a car with LH_2 fuel). It was shown that the maximum pressure loads resulting from ignition from a hydrogen cloud would be insignificant (see Section 6.5.4.1). Another analysis evaluated the possible incidents and consequences of hazardous events in a tunnel for several different alternative fuel vehicles. This analysis showed that although the HRR is higher for hydrogen when compared to other fuels, the overpressure is relatively low (see Section 6.5.4.1).

6.5.4. Hydrogen FCEV Tunnel Risk Analysis

A risk analysis was performed to estimate what scenarios were most likely to occur in the event of a hydrogen FCEV accident in a tunnel by Ehrhart et al. [113]. An event sequence diagram for a hydrogen vehicle accident was developed for a hydrogen FCEV accident in a tunnel, including all outcomes along with associated values and probabilities. Figure 97 shows the event sequence diagram developed in the risk analysis.

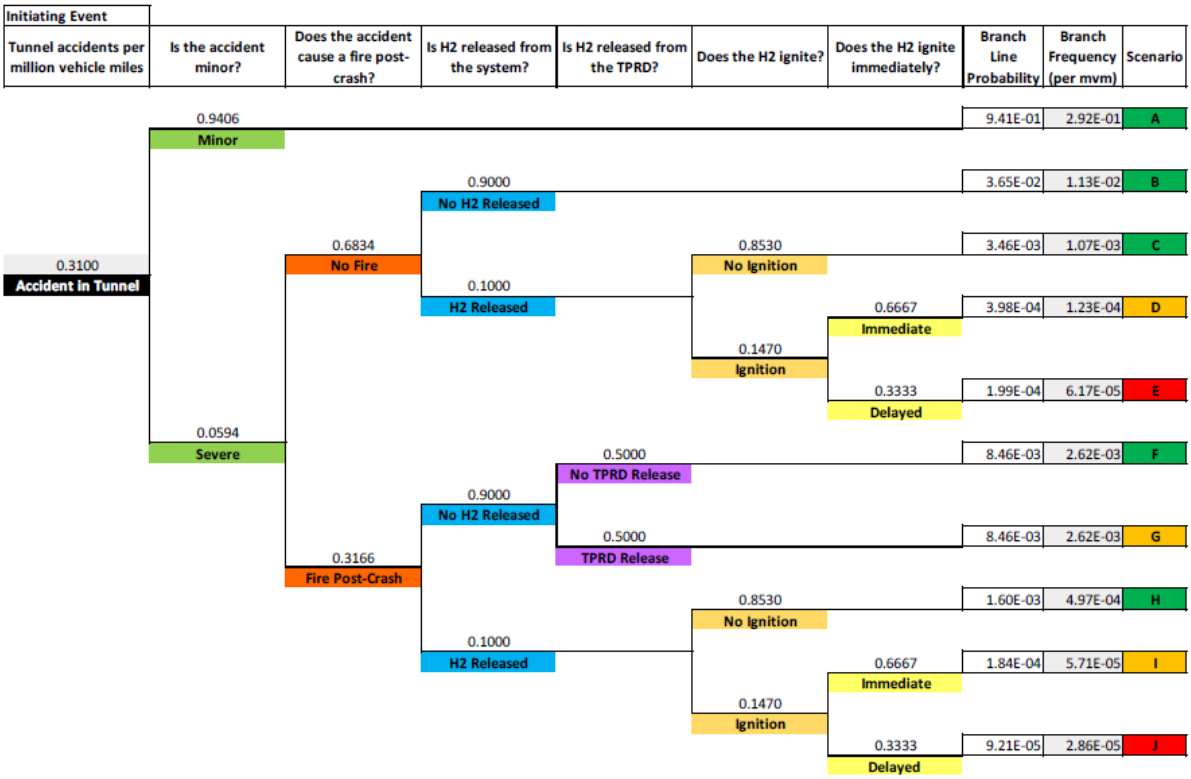

Figure 97: Event Sequence Diagram for a Hydrogen FCEV in a Tunnel (from [113])

Each event was evaluated to determine whether the respective scenario warranted further characterization with heat transfer and CFD models. Based on an evaluation of the risk of each scenario (both the likelihood and consequence), the scenario evaluated further with modeling was a hydrogen vehicle in an accident exposed to a resulting fire. A typical hydrogen FCEV was considered in this analysis, with a 125 L, 70 MPa tank of hydrogen with a typical TPRD orifice of 2.25 mm. Note that due to computational limitations, the smallest reasonable tank orifice diameter that can be modeled is 5.25 cm. This is conservative because the velocity was kept the same for the larger diameter, and so the mass flow and total heat release are larger than what is expected for the realistic 2.25 mm tank orifice diameter. Taking this into account, the worst-case scenario is based on a 5.25 cm release diameter with a constant velocity of 700 m/s. Conservative assumptions were made in terms of the hydrogen fuel released from the TPRD, including having the vehicle flipping over in the crash to orient the jet flame toward the ceiling of the tunnel. Three Boston tunnels with different structural configurations were investigated: the CANA Tunnel, the Ted Williams Tunnel, and the Sumner Tunnel [113]. See Section 6.5.2.1 for information on the CFD, heat transfer, and solid mechanics modeling used for this risk analysis.

The results show that the most likely consequence is no additional hazard from the hydrogen, although some factors need additional data and study to validate. This includes minor crashes and scenarios with no release or ignition. When the hydrogen does ignite, it is most likely a jet flame from the pressure relief device release due to a primary hydrocarbon fire. This scenario was considered in detailed modeling of specific tunnel configurations. Localized concrete spalling may result where the jet flame impinges the ceiling, but this is not expected to occur with ventilation. Structural epoxy remains well below the degradation temperature. The total stress on the steel structure will not be compromised. It is important to note that this study took a conservative approach in several factors, so observed temperatures should be lower than predicted by the models [113].

6.5.4.1. Hydrogen Vehicle Explosion Risk in Tunnels

An assessment was performed to evaluate the risk of explosion for hydrogen vehicles in tunnels. For all accident scenarios, the hydrogen release is attributed to the activation of the pressure relief device. Two different hydrogen vehicles were evaluated: 1) a city bus with 40 kg H_2 at a storage pressure of 350 bar, and 2) a car with 5 kg H_2 at a storage pressure of 700 bar. Additionally, two different tunnel layouts (horseshoe and rectangular) and several longitudinal ventilation conditions were considered. The following hydrogen release scenarios were evaluated [127]:

1. Hydrogen Passenger Vehicle (vent up) releasing 5 kg of H_2 for 84s
2. Hydrogen Passenger Vehicle (vent down) releasing 5 kg of H_2 for 84s
3. Hydrogen Bus releasing 5 kg of H_2 for 147s
4. Hydrogen Bus releasing 20 kg of H_2 for 147s
5. Hydrogen Passenger Vehicle releasing 10 kg of LH2 for 900s

The ignition probabilities and intensities were developed from information relevant to the oil and gas industry. Initially, stoichiometric gas clouds of different sizes are considered to explode to calculate the maximum overpressure near the tunnel ceiling [127]. As a refinement, dispersion modeling was performed to determine the gas cloud size and hydrogen concentration that can be realistically expected. CFD modeling was used to evaluate both the dispersion and explosion simulations for each of the scenarios described previously (see Section 6.5.2.2).

The worst-case deterministic evaluation of each of the scenarios involved the tunnel filling with stochiometric hydrogen gas clouds of varying size. This showed unacceptable results in terms of very high overpressures. However, a dispersion study was performed to determine a more realistic gas cloud from hydrogen release and their subsequent ignition. This more realistic evaluation showed that the worst-case overpressures were reduced by two orders of magnitude. Moreover, a probabilistic study was performed that reduced the expected risk of an explosion due to a hydrogen vehicle even more. The maximum pressure loads (between 0.1 barg [threshold for skin laceration from flying glass] and 0.3 barg [serious wounds from flying glass near 50% probability]) predicted by the simulations could be significant [127].

6.5.4.1. Fire and Explosion Hazards in Tunnels of Alternative Fuel Vehicles

An analysis of the possible incidents and consequences of hazardous events in a tunnel was evaluated for several different alternative fuel vehicles, including gaseous and liquid hydrogen

vehicles by Li [134]. The likelihood of the events was not evaluated, but event trees were defined for both liquefied fuel vehicles and compressed gas vehicles (see Figure 98 and Figure 99).

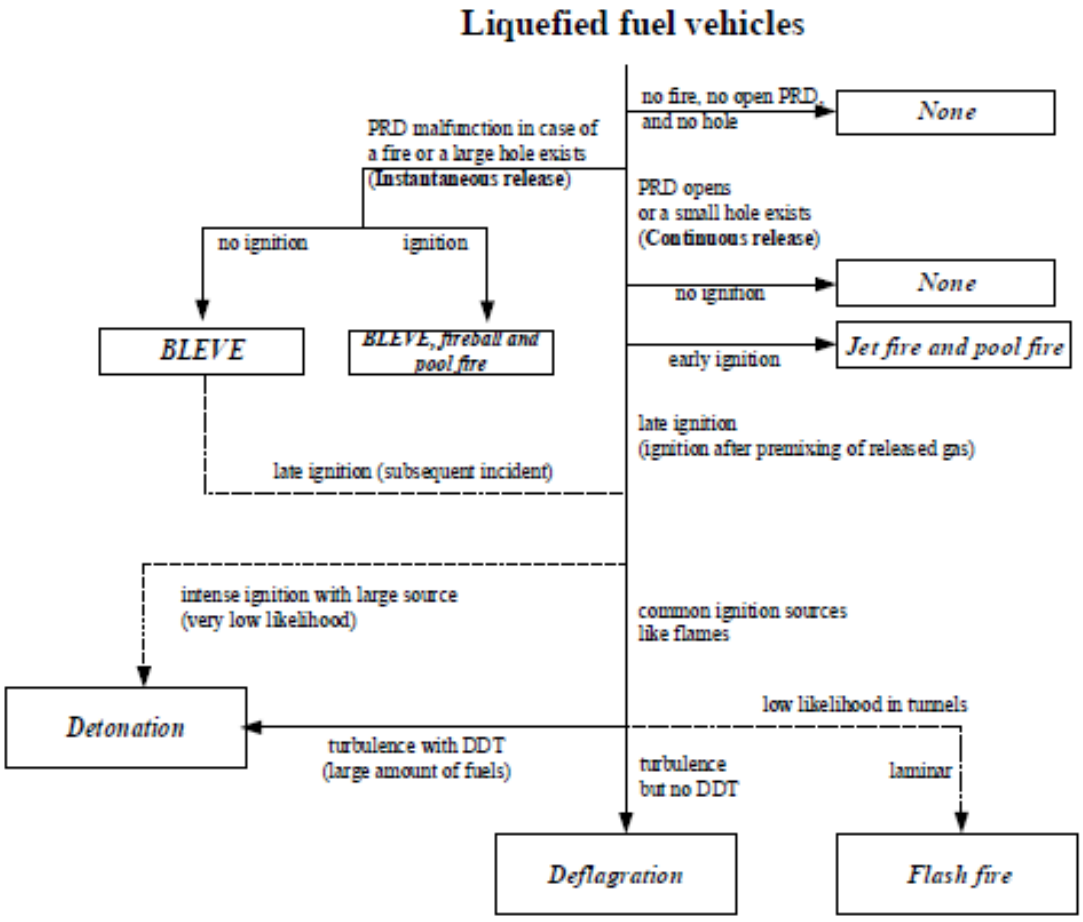

Figure 98: Liquefied Fuel Vehicle Event Tree for Incidents in Tunnels (from [134])

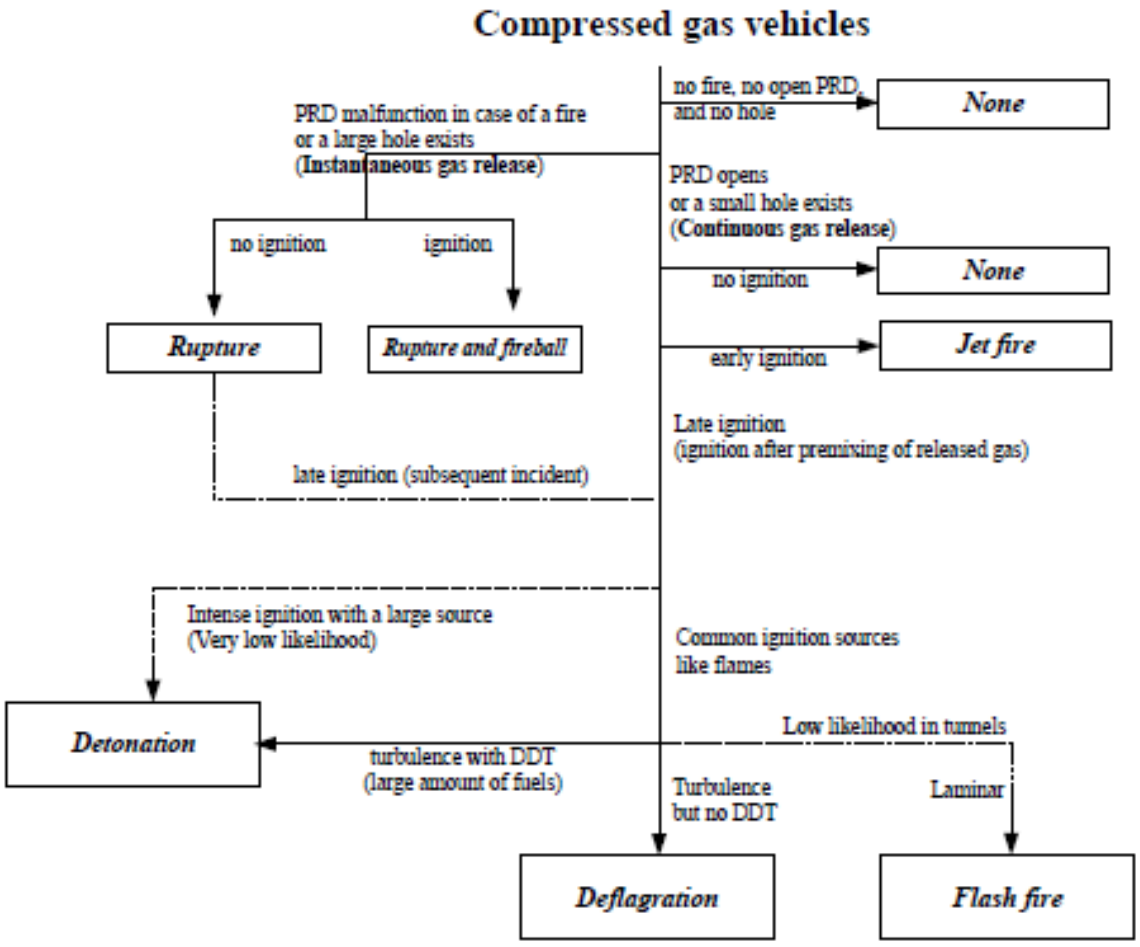

Figure 99: Compressed Gas Vehicle Event Tree for Incidents in Tunnels (from [134])

Each event was evaluated through simple modeling to determine the potential consequence. An analysis of spilled fuel fires for liquid hydrogen vehicles showed that the heat release rate per unit fuel area of liquid hydrogen is around 60 times higher than ethanol and methanol. For jet fires, the analysis showed that the heat release rates for hydrogen vehicles were significantly higher than those of compressed natural gas tanks, while the flame length was only slightly greater. Figure 101 shows the peak overpressure as a function of distance resulting from rupture of the pressure vessel. As shown, the overpressure decreases rapidly within the first 50 m [134].

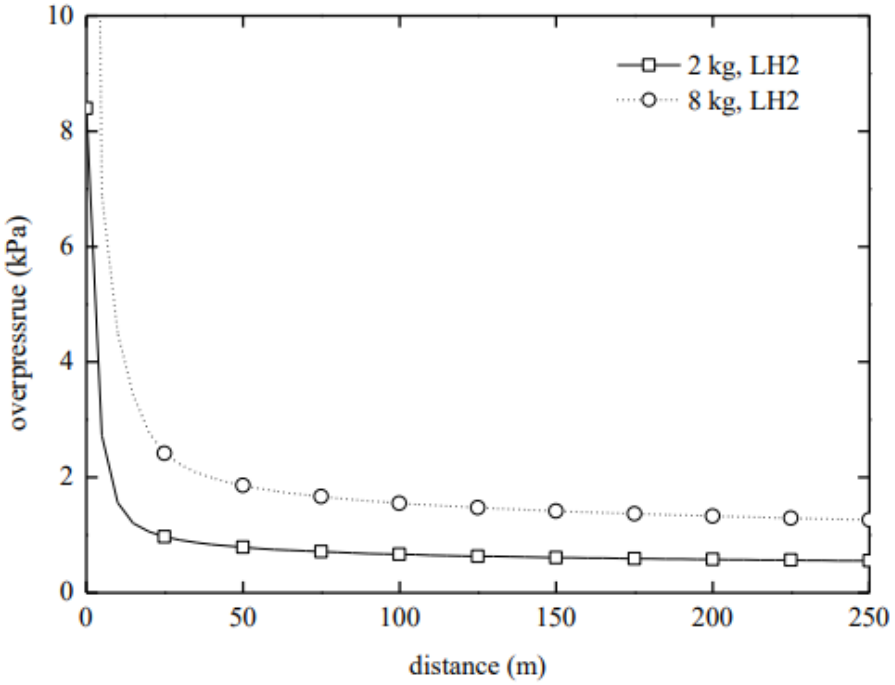

Figure 100: Overpressure vs. Distance for Liquid H_2 tank at 350 bar (from [127])

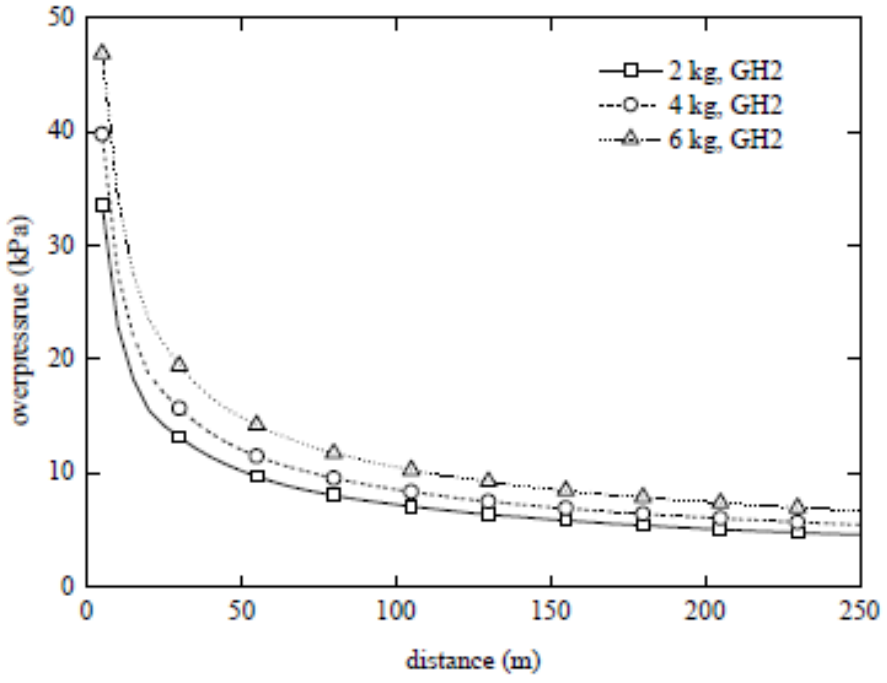

Figure 101: Overpressure vs. Distance for Gaseous H_2 tank at 350 bar (from [127])

Finally, the peak overpressure resulting from a gas cloud explosion was evaluated for both gaseous and liquefied hydrogen. The overpressures for each case were relatively low when compared to the other alternative fuels such as natural gas due to the small fuel mass for the hydrogen case which leads to lower explosion energy [134].

6.6. FCEV Research Gaps

Through this literature study, it was found that there are several existing studies that evaluate the failure modes and consequences associated with hydrogen fuel cell electric vehicles (FCEVs) in tunnels. There have been multiple experimental studies that have investigated overpressures resulting from delayed hydrogen ignition, HRR, hydrogen dispersion, and thermal effects of jet fires. Modeling studies have been conducted on the consequences of release, including hydrogen accumulation followed by ignition and the resulting overpressure. Also, risk analysis has been conducted on the thermal effects on tunnel components from a jet fire rather and identification of release events that could occur. Additionally, analysis has been performed to quantify probabilities and likelihoods for these various events.

Conclusions about important variables can be derived from comparison of the different literature. As ventilation increases, the overpressure decreases in a congested area [173] [174]. However, CFD results of a tunnel including vehicles as blockage show that the overpressure stays about the same. This could mean that ventilation is a stronger factor in varying the overpressure. The exceedance curve shown in Figure 75 shows the various hydrogen leak scenarios and the frequency of each one. In the event of a leak, the layer height and concentration were used to create a matrix to understand how different leak scenarios might lead to various deflagrations or even detonations [175].

Although significant work has been accomplished, there are still areas that should be evaluated further. The following criteria were evaluated to determine where research gaps may exist regarding hydrogen FCEVs in tunnels.

1. Scenario Identification
2. Failure Modes
3. Consequences
4. Validation

In terms of scenario identification included in this literature survey, the scenarios that lead to a failure mode have been identified as impacts to the vehicle or failure of the TPRD, hardware degradation or failure, and operator error which may lead to a release of fuel. Fault trees for both liquid and gaseous fuel release can be seen in Figure 98 and Figure 99. Failure modes were addressed through several studies evaluating the mechanism and consequences associated with hydrogen FCEVs in tunnels. The failure modes with potentially hazardous consequences identified in the scenario identification effort included a release with either immediate or delayed ignition.

The measurements of the consequences of the failure mode include overpressure, HRR, hydrogen dispersion, and resulting structural damage determine the extent of the hazard. There are several variables that effect the magnitude of the consequence: hydrogen quantity released, ventilation, obstructions, ignition time, tunnel geometry, etc. Results of the consequences include overpressures that range from 34 kPa [127] to over 100 kPa [126], HRR that can peak near 16 MW [176], and fireballs that can exceed 250 m long [126]. Also, validation of the results has been achieved through comparison studies between the modeling and experiments with regard to various consequences like HRR [176].

The research of hydrogen FCEVs in tunnels has evaluated, in some manner, a significant combination of failure modes, consequences, and influencing variables. Despite this, the following research gaps were identified:

- Temperature and thermal effects to structures. A diagnostic to the consequence of a failure mode is temperature or thermal effects. Although this has been addressed in a single modeling/analysis report, additional research should be conducted on this topic.
- Ventilation effects. The study of spontaneous ignition was conducted at ambient conditions outdoors. The effect that ventilation in a tunnel has on the results could be evaluated.
- Hydrogen-specific fires. The power associated with the fires in Section 6.5.2.6 should be related to specific hydrogen vehicle types (e.g., cars, buses, etc.).
- The effect of deflagration/detonation on structural components of a tunnel for each of the different hydrogen vehicle classes.
- The effect of overpressure effects on life safety to people within the tunnel.
- The extent to which hydrogen can accumulate due to partial confinement and restriction, rather than complete confinement.
- Additional attention should be given to the size or class of the vehicle. As vehicular class increases so does the amount of stored fuel. Several different classes of vehicles were evaluated in the studies, including hydrogen cars and buses, liquid hydrogen cars, and multiple hydrogen cars on a cargo truck.

The International Conference on Hydrogen Safety (ICHS) in 2019 showcased a variety of topics for hydrogen safety [181]. As the papers are published from this event, some of the identified research gaps may be addressed. Some of these gaps as well as others will be addressed in the output of the current HyTunnel-CS project [182]. The intent of this project is to perform research regarding hydrogen powered vehicle safety in tunnels and confined spaces. The goal is for hydrogen vehicles entering underground environments to maintain comparable risk as fossil fuels. Experiments in tunnels, modeling using tools such as CFD, and analysis using risk assessment methodologies will be covered in this project.

The HyTunnel-CS project has identified the following work packages (WP) to address research gaps:

WP1 – The state-of-the-art in safety provisions for underground transportation systems and accident scenarios prioritization

WP1 will review the state-of-the-art in safety provisions for underground transportation systems and the accident scenarios prioritization will aid at identifying the knowledge gaps in both safety science and regulations, codes, and standards to be addressed

WP2 – Effect of mitigation systems on hydrogen release and dispersion in confined spaces

An intensive experimental program empowered by theoretical and numerical studies will be performed under this work package. The work addresses the knowledge gaps highlighted in WP1 and the development of novel engineering solutions for the prevention and mitigation of accident involving hydrogen releases.

WP3 – Thermal and pressure effects of hydrogen jet fires and structure integrity

Under this work package jet fires will be investigated through a comprehensive set of experimental, theoretical, and numerical studies to improve the principal understanding of hydrogen jet fire on life safety provisions in underground transportation systems and their structural integrity.

WP4 – Explosion prevention and mitigation

WP4 investigates explosion prevention and mitigation through numerous experimental tests realized in tunnels and other confined spaces and theoretical and numerical studies on accident scenarios involving hydrogen tanks. The aim of the WP is to provide engineering tools to evaluate the associated hazards, as well as innovative preventive and mitigation solutions and to improve the principal understanding of hydrogen explosion hazards in tunnels and similar confined spaces using complementarities of theoretical, numerical and experimental studies.

WP5 – First responders' intervention strategies and tactics for hydrogen accidents in underground transportation systems and risk assessment

Under WP5, the research findings from WPs 2-4 will be translated into suitable information, guidelines, and recommendations for first responders intervening in an accident involving hydrogen-powered vehicles in tunnels or other confined spaces. This includes examining and supplementing available knowledge in such a way that it can be taught to all first responders and can also be practically applied by them.

WP6 through WP8 –Outreach/Dissemination, Management, and Ethics are not summarized since these are not technical research gaps.

This page left blank

7. CONCLUSIONS

In this report, as a result of requests from multiple stakeholders across government and industry, including code officials, Sandia National Laboratories has completed a preliminary assessment of safety research and incidents for the use of alt fueled vehicles in tunnels. While a lot of research for traditional fuels has been completed through studies, modeling, and experiments, alternative fuels have limited tunnel research that has been completed. Various experiments have been completed to understand release of hydrogen, natural gas, and propane in both the gaseous and liquid form into confined space which can be applicable to alternative fuels in tunnels. These studies and experiments can be used to understand the hazard characteristics of alternative fuels in tunnels.

7.1. Battery Electric Vehicles

Overall, BEVs have a variety of research gaps listed due to the complexity of scaling battery systems to power the various classes of vehicles. Additionally, the wide variety of cell chemistries, battery pack designs, and battery management systems makes it difficult to assess specific safety metrics for BEVs as a whole. One large-scale test [86] showed that BEVs have comparable HRR and THR to ICE vehicles, but with a higher hydrogen fluoride production during a fire. Specific modeling for BEVs in tunnels has not been conducted, and modeling for lithium-ion batteries is still at the cell and module level. A tunnel experiment conducted looked at various failure scenarios and the effect inside a tunnel downstream of the failed battery cells [86]. The release quantities were measured which included toxic aerosols such as cobalt, lithium, and manganese. There is some analysis conducted to further understand the consequences. Data from mechanically and thermally failed modules was analyzed to understand the fire effluents and required ventilation in the space [91]. A systems safety approach from the cell level, to modules, battery system, and complete BEV should be studied to further understand how the components and sub-components interact. Using a system safety V-diagram to define testing and safety requirements for each system level (cell, module, and battery system) would help further understand how to safely design these systems. This will directly tie into understanding consequence metrics for further evaluations in tunnels. Future work characterizing fire spread within a BEV and tactics to slow or stop thermal propagation would be beneficial.

7.2. Natural Gas Vehicles

Multiple studies for both CNG and LNG powered vehicles have been conducted, including experiments to understand flame speed and overpressure and the effects of congestion on these hazard metrics. Vapor cloud explosions and heat flux from flames have also been studied. Modeling to understand CNG dispersion has been conducted for various tunnels. An FMEA of CNG-powered buses has also been completed to understand the risk of these vehicles. However, the majority of these studies involve CNG only, showing the need to further understand LNG hazards and the differences for this liquefied fuel. Continuous release of LNG compared to CNG showed that the harmful and lethal distances for CNG exceed those for LNG due to the higher storage pressures. Further studies to understand and compare the hazard difference between LNG and CNG should be considered. A variety of tunnel studies have used CNG release quantities that are considered equivalent to the amount of CNG used in a city bus and passenger car. Other classes of vehicles should be further studied for release characteristics for both CNG and LNG.

7.3. Propane Vehicles

There are relatively few studies evaluating the failure modes and consequences associated with LPG vehicles in tunnels. A scenario identification study was conducted that estimated the likelihood of different consequences of a tunnel accident through expert elicitation, but a more rigorous evaluation of failure modes should be completed. One study focuses on creating and using a failure tree to inform release scenarios for an LPG vehicle. This then helped inform the experimental setup where six different tests using different ventilation and releases were used. The experimental data was then compared with a CFD model for validation. This model can be further used to understand the gaseous dispersion characteristics of propane from vehicles failing in tunnels and other confined spaces. Additionally, experiments have been conducted to determine the effect of ventilation and tunnel slope on smoke dispersion in a tunnel using a propane fire. Modeling helps understand the dispersion and evaporation phenomena of an LPG spill.

7.4. Hydrogen Fuel Cell Vehicles

A variety of studies and experiments have been completed for hydrogen fuel cell electric vehicles, specifically in tunnel applications. Just as for CNG, batteries, and other fuels, industry plans to use hydrogen fuel cells for larger class vehicles (e.g. class 8 trucks). Therefore, studies to understand how the increase of vehicle class affects the hazard should be considered. Consequence models for tunnel safety studies have been conducted using CFD models and should be further used to evaluate larger classes of vehicles. Future work and studies to improve characterization of the risks include the HyTunnel-CS project [182]. This project will use experiments in tunnels, modeling using tools such as CFD, and analysis using risk assessment methodologies. Through this work, over-conservatism will be reduced which will help increase effectiveness of safety systems along with cost savings of tunnel and confined space safety systems.

7.5. Closing Remarks and Future Work

In this report, Sandia National Laboratories has compiled the first comprehensive overview of key studies and experiments to date on the safety of alternative fuel vehicles specifically within tunnels. While there have been various studies at different levels of rigor and complexity, and several real-world incidents with alternative fuel vehicles in tunnels, it is clear that hazards can never be completely prevented regardless of the type of vehicle or fuel being used. Different classes of vehicles and the different hazards represented by each fuel need to be considered during development of regulations. The phase of the fuel (solid, liquid, or gas) plays a role in the hazards associated with each fuel type and should be considered when determining tunnel design specifications required.

These studies help to develop relevant information on how best to construct, site, and maintain tunnels and other enclosed spaces and determine key specifications such as ventilation requirements, etc. to enable the safe use of emerging technologies. Analysis of these studies will also enable research gaps to be identified and research prioritized to close the gaps. This overview will allow stakeholders, AHJs, and tunnel owners to actively participate in the discussions on further studies and tunnel regulations. As more studies and experiments are conducted, they will help to provide a complete analysis of the hazards and recommendations for the use of alternative fuel vehicles in tunnels and other confined spaces such as parking garages and locomotive tunnels.

8. REFERENCES

[1] A. M. Glover, A. R. Baird and C. B. LaFleur, "Hydrogen Fuel Cell Vehicles in Tunnels," Sandia National Laboratories (SAND2020-4507 R), Albuquerque, 2020.

[2] A. K. Coker, "9 - PROCESS SAFETY AND PRESSURE-RELIEVING DEVICES," in *Ludwig's Applied Process Design for Chemical and Petrochemical Plants (Fourth Edition)*, Burlington, Gulf Professional Publishing, 2007, pp. 575-770.

[3] Los alamos National Laboratory, "What's the difference between an explosion and a detonation?," [Online]. Available: https://www.lanl.gov/museum/news/newsletter/2018/08/detonation.php. [Accessed 19 05 2020].

[4] California Institute of Technology, "Flammability and Explosion Limits," [Online]. Available: https://shepherd.caltech.edu/EDL/PublicResources/flammability.html. [Accessed 05 12 2019].

[5] W. D. Manha, "Chapter 20 - Propellant Systems Safety," in *Safety Design for Space Systems*, Oxford, Butterworth-Heinemann , 2009, pp. 661-694.

[6] J. G. Quintiere, in *Fundamentals of Fire Phenomena*, John Wiley & Sons, 2006, pp. 77-115.

[7] M. Huth and A. Heilos, "14 - Fuel flexibility in gas turbine systems: impact on burner design and performance," in *Modern Gas Turbine Systems*, Cambridge, Woodhead Publishing Limited, 2013, pp. 635-684.

[8] G. Jomaas, "Fundamentals of Premixed Flames," in *SFPE Handbook 5th Edition*, New York City, Springer, 2016, pp. 373-395.

[9] NOAA Office of Response and Restoration, "Overpressure Levels of Concern," NOAA Office of Response and Restoration, [Online]. Available: https://response.restoration.noaa.gov/oil-and-chemical-spills/chemical-spills/resources/overpressure-levels-concern.html. [Accessed 20 09 2019].

[10] MIT Thermodynamics and Propulsion, "Thermodynamics and Propulsion," MIT Thermodynamics and Propulsion, [Online]. Available: https://web.mit.edu/16.unified/www/FALL/thermodynamics/notes/node111.html. [Accessed 20 09 2019].

[11] DOE Office of Energy Efficiency and Renewable Energy's Fuel Cell Technologies Office, "H2 Tools," DOE Office of Energy Efficiency and Renewable Energy's Fuel Cell Technologies Office, [Online]. Available: https://h2tools.org/hyarc/calculator-tools/lower-and-higher-heating-values-fuels. [Accessed 20 09 2019].

[12] National Institute of Standards and Technology, "Fire Dyanmics," NIST, 17 07 2018. [Online]. Available: https://www.nist.gov/el/fire-research-division-73300/firegov-fire-service/fire-dynamics. [Accessed 01 10 2019].

[13] National Fire Protection Association, NFPA 921: Guide for Fire and Explosion Investigations, Quincy, 2017.

[14] EUROPEAN INDUSTRIAL GASES ASSOCIATION AISBL , "DETERMINATION OF SAFETY DISTANCES IGC Doc 75/07/E," Brussels, 2007.

[15] DOE Energy Efficiency & Renewable Energy, "Maps and Data - Vehicle Weight Classes & Categories," DOE Energy Efficiency & Renewable Energy, [Online]. Available: https://afdc.energy.gov/data/10380. [Accessed 19 09 2019].

[16] DOE Energy Efficiency & Renewable Energy, "Alternative Fuels Data Center," [Online]. Available: https://afdc.energy.gov/data/. [Accessed 25 09 2019].

[17] DOE Energy Efficiency & Renewable Energy, "Alternative Fuels Data Center," DOE Energy Efficiency & Renewable Energy, [Online]. Available: https://afdc.energy.gov/fuels/ethanol_e85_specs.html. [Accessed 06 09 2019].

[18] Office of Energy Efficiency & Renewable Energy, "Ethanol," Office of Energy Efficiency & Renewable Energy, [Online]. Available: https://www.fueleconomy.gov/feg/ethanol.shtml. [Accessed 06 09 2019].

[19] US Energy Information Administration, "How much gasoline does the United States consume?," US Energy Information Administration, 04 09 2019. [Online]. Available: https://www.eia.gov/tools/faqs/faq.php?id=23&t=10. [Accessed 06 09 2019].

[20] Bureau of Transportation Statisitics, "Diesel-powered Passenger Cars and Light Trucks," Bureau of Transportation Statisitics, 10 2015. [Online]. Available: https://www.bts.gov/archive/publications/bts_fact_sheets/oct_2015/entire. [Accessed 06 09 2019].

[21] V. Honig, M. Pexa and Z. Linhart, "Biobutanol Standardizing Biodiesel from Waste Animal Fat," *Jounrla of Enviromental Studies,* vol. 24, no. 6, pp. 2433-2439, 2015.

[22] D. Gi and C. Lee, "Combustion and emissions behaviour for ethanol–gasoline-blended fuels in a multipoint electronic fuel injection engine," *International Journal of Sustainable Energy,* 2014.

[23] M. I. Khan, T. Yasmin and A. Shakoor, "Technical overview of compressed natural gas (CNG)," *Renewable and Sustainable Energy Reviews,* vol. 51, pp. 785-797, 2015.

[24] P. Martinez, E. Rus and J. Compana, "FLASH POINT DETERMINATION OF BINARY MIXTURES OF ALCOHOLS, KETONES AND WATER," Departamento de Ingeniería Química. Facultad de Ciencias. Universidad de Málaga, Málaga.

[25] IPCS INCHEM, "Diesel Fuel No. 2," IPCS INCHEM, 10 2004. [Online]. Available: http://www.inchem.org/documents/icsc/icsc/eics1561.htm. [Accessed 06 09 2019].

[26] D. Alviso, F. Krauch, R. Roman, M. Hernando, R. Goncalves dos Santos, J. C. Rolon and N. Darabiha, "Development of a diesel-biodiesel-ethanol combined chemical scheme and analysis of reactions pathways," *Fuel,* vol. 191, pp. 411-426, 2017.

[27] Matheson Tri Gas, "Lower and Upper Explosive Limits for Flammable Gases and Vapors (LEL/UEL)," Matheson Tri Gas, [Online]. Available: https://www.mathesongas.com/pdfs/products/Lower-(LEL)-&-Upper-(UEL)-Explosive-Limits-.pdf. [Accessed 04 12 2019].

[28] DOE Office of Energy Efficiency and Renwable Energy, "Many Factors Affect Fuel Economy," DOE Office of Energy Efficiency and Renwable Energy, [Online]. Available: https://www.fueleconomy.gov/feg/factors.shtml. [Accessed 20 09 2019].

[29] J. S. Bartlett, "Study Shows Top Tier Gasoline Worth the Extra Price," Consumer Reports, 03 04 2019. [Online]. Available: https://www.consumerreports.org/car-maintenance/study-shows-top-tier-gasoline-worth-extra-price/. [Accessed 20 09 2019].

[30] US Enviromental Protection Agency, "Gasoline Reid Vapor Pressure," US Enviromental Protection Agency, [Online]. Available: https://www.epa.gov/gasoline-standards/gasoline-reid-vapor-pressure. [Accessed 09 09 2019].

[31] J. Gehandler, P. Karlsson and L. Vylund, "Risks associated with alternative fuels in road tunnels and underground garages," 2017.

[32] J. Sjostrom, G. Appel, F. Amon and H. Persson, "Experimental results of large ethanol fuel pool fires," Science Partner, 2015.

[33] D. Schütz, "Fire protection in tunnels: Focus on road & train tunnels," SCOR Global P&C, 2014.

[34] National Academies of Sciences, Engineering, and Medicine, "Signiticant Fire Incidents in Road Tunnels- Literature Review," in *Design Fires in Road Tunnels*, Washington, The National Academies Press, 2011, pp. 21-26.

[35] P. Johnson and D. Barber, "The Brunley Tunnel Fire- Implications for Current Design Practice," in *Third International Symposium on tunnel Safety and Security*, Stockholm, 2008.

[36] BBC News, "Five killed in Austria tunnel fire," 07 08 2001. [Online]. Available: http://news.bbc.co.uk/2/hi/europe/1476385.stm. [Accessed 10 09 2019].

[37] A. Leitner, "The fire catastrophe in the Tauern Tunnel: experience and conclusions for the Austrian guidelines," *Tunnelling and Underground Space Technology,* vol. 16, pp. 217-223, 2001.

[38] National Fire Protection Association, NFPA 502: Standard for Road Tunnels, Bridges, and Other Limited Access Highways, Quincy, 2020.

[39] ASHRAE, Handbook- HVAC Applications, Atlanta, 2019.

[40] I. Maevski, "Road Tunnel Fires," in *Guidelines for Emergency Ventilation Smoke Control in Roadway Tunnels*, Washington, NATIONAL COOPERATIVE HIGHWAY RESEARCH PROGRAM, 2017, pp. 16-22.

[41] National Cooperative Highway Research Program, "Design Fires in Road Tunnels," 2011.

[42] E. Cafaro and V. Bertola, "Fires in Tunnels: Experiments and Modelling," *The Open Thermodynamics Journal,* vol. 4, pp. 156-166, 2010.

[43] Working Group No.6 Maintenance and Repair, "Structural Fire Protection For Road Tunnels," International Tunneling Association, 2017.

[44] A. Lönnermark and H. Ingason, "Gas temperatures in heavy goods vehicle fires in tunnels," *Fire Safety Journal,* vol. 40, no. 6, pp. 506-527, 2005.

[45] Promat Tunnels, "Fire curves," Promat , [Online]. Available: https://www.promat-tunnel.com/en/advices/fire-protection/fire%20curves. [Accessed 17 12 2019].

[46] ASTM International, West, "E119-18ce1, Standard Test Methods for Fire Tests of Building Construction and Materials," Conshohocken, 2018.

[47] Underwriters Laboratory, "1709: Standard for Rapid Rise Fire Tests of Protection Materials for Structural Steel," 2017.

[48] J. Brekelmans, R. ven den Bosch and K. Both, "Summary of large scale fire tests in the Runehamar tunnel in Norway," *UPTUN, TNO, PROMAT,* 2003.

[49] H. Ingason, A. Lonnermark and Y. Z. Li, "Runehamar tunnel fire tests," *fire Safety Journal,* vol. 71, pp. 134-149, 2015.

[50] V. Babrauskas and R. D. Peacock, "Heat release rate: the single most important variable in fire hazard," *Fire safety journal,* vol. 18, no. 3, pp. 255-272, 1992.

[51] T. Lemaire and Y. Kenyon, "Large Scale Fire Tests in the Second Benelux Tunnel," *fire Technology,* vol. 42, pp. 329-350, 2006.

[52] NIST, "CFAST, Fire Growth and Smoke Transport Modeling," [Online]. Available: https://www.nist.gov/el/fire-research-division-73300/product-services/consolidated-fire-and-smoke-transport-model-cfast. [Accessed 17 12 2019].

[53] W. Chow, "Simulation of Tunnel Fires Using a Zone Model," *Tunneling and Underground Space Technology ,* vol. 11, no. 2, pp. 221-236, 1996.

[54] A. Haghighat and L. Kray, "Determination of critical parameters in the analysis of road tunnel fires," *International Journal of Mining Science and Technology,* vol. 29, pp. 187-198, 2019.

[55] S. Shafee and A. Yozgatligil, "An analysis of tunnel fire characteristics under the effects of vehicular blockage and tunnel inclination," *Tunnelling and Underground Space Technology,* vol. 79, pp. 274-285, 2018.

[56] A. Andwari, A. Pesiridis, S. Rajoo, R. Martinez-Botas and V. Esfahanian, "A Review of Battery Electric Vehicle Technology and Readiness Levels," *Renewable and Sustainable Energy Reviews,* vol. 78, pp. 414-430, 2017.

[57] University of Washington Institue of Clean Energy, "What is a lithium-ion battery and how does it work?," [Online]. Available: https://www.cei.washington.edu/education/science-of-solar/battery-technology/. [Accessed 03 02 2020].

[58] M. Hannan, M. Hoque, A. Mohamed and A. Ayob, "Review of Energy Storage Systems for Electric Vehicle Applications: Issues and Challenges," *Renewable and Sustainable Energy Reviews,* vol. 69, pp. 771-789, 2017.

[59] X. Zhang, L. Ji, O. Toprakçı, Y. Liang and M. Alcoutlabi, "Electrospun Nanofiber-Based Anodes, Cathodes, and Separators for Advanced Lithium-Ion Batteries," *Polymer Reviews,* vol. 51, no. 3, pp. 139-264, 2011.

[60] Y. Wu, S. Saxena, Y. Xing, Y. Wang, C. Li, W. K. C. Yung and M. Pecht, "Analysis of Manufacturing-Induced Defects and Structural Deformations in Lithium-Ion Batteries Using Computed Tomography," *Energies,* vol. 11, no. 4, p. 925, 2018.

[61] V. Ruiz, A. Pfrang, A. Kriston, N. Omar, P. Van den Bossche and L. Boon-Brett, "A review of international abuse testing standards and regulations for lithium ion batteries in electric and hybrid electric vehicles," *Renewable and Sustainable Energy Reviews,* vol. 81, pp. 1427-1452, 2018.

[62] SAE International, J2464: Electric and Hybrid Electric Vehicle Rechargeable Energy Storage System (RESS) Safety and Abuse Testing, 2009.

[63] SAE International, "Electric and Hybrid Vehicle Propulsion Battery System Safety Standard - Lithium-based Rechargeable Cells," 18 02 2011. [Online]. Available: https://saemobilus.sae.org/content/J2929_201102/#scope. [Accessed 20 09 2019].

[64] Underwriters Laboratory, 2580: Batteries for Use In Electric Vehicles, 2013.

[65] D. Doughty and C. Crafts, "FreedomCAR Electrical Energy Storage System Abuse Test Manual for Electric and Hybrid Electric Vehicle Applications," Lithium Battery Research and Development Department Sandia National Laboratories (SAND2005-3123), Albuquerque, 2005.

[66] C. F. Lopez, J. A. Jeevarajan and P. P. Mulherjee, "Experimental Analysis of Thermal Runaway and Propagation in Lithium-Ion Battery Modules," *Journal of the Electrochemical Society,* vol. 162, no. 9, pp. 1905-1915, 2015.

[67] G. Berdichevsky, K. Kelty, J. Straubel and E. Toomre, "The Tesla Roadster Battery System," Tesla Motors, 2006.

[68] P. Balakrishnan, R. Ramesh and T. P. Kumar, "Safety mechanisms in lithium-ion batteries," *Journal of Power Sources,* vol. 155, pp. 401-414, 2006.

[69] A. R. Baird, E. J. Archibald, K. C. Marr and O. A. Ezekoye, "Explosion hazards from lithium-ion battery vent gas," *Journal of Power Sources,* vol. 446, pp. 227-257, 2020.

[70] V. Somandepalli, K. Marr and Q. Horn, "Quantification of Combustion Hazards of Thermal Runaway Failures in Lithium-Ion Batteries," *SAE International Journal of Alternative Powertrains ,* vol. 3, no. 1, pp. 98-104, 2014.

[71] D. Yoney, "Come count kilowatt-hours with us," INSIDEEVs, 02 06 2018. [Online]. Available: https://insideevs.com/features/336680/7-electric-cars-with-the-biggest-batteries/. [Accessed 19 09 2019].

[72] P. Vandell, "First report of Suprise APS battery explosion that hospitalized firefighters offers few answers," azcentral: Part of the USA Today Network, 09 08 2019. [Online]. Available: https://www.azcentral.com/story/news/local/surprise/2019/08/09/report-surprise-aps-battery-explosion-hosptialized-hazmat-offers-few-answers/1951399001/. [Accessed 16 09 2019].

[73] A. W. Golubkov, D. Fuchs, J. Wagner, H. Wiltsche, C. Stangl, G. Fauler, G. Voitic, A. Thaler and V. Hacker, "Thermal-runaway experiments on consumer Li-ion batteries with metal-oxide and olivin-type cathodes," *Royal Society of Chemistry,* vol. 4, pp. 3633-3642, 2014.

[74] P. Ribière, S. Grugeon, M. Morcrette, S. Boyanov, S. Laruelle and G. Marlair, "Investigation on the fire-induced hazards of Li-ion battery cells by fire calorimetry," *Energy & Enviromental Science,* vol. 5, pp. 5271-5280, 2012.

[75] V. Somandepalli and H. Biteau, "Cone Calorimetry as a Tool for Thermal Hazard Assessment of Li-Ion Cells," in *SAE 2014 World Congress & Exhibition*, 2014.

[76] W. Zhang, C. X, Q. Chen, C. Ding, J. Liu, M. Chen and J. Wang, "Combustion calorimetry of carbonate electrolytes used in lithium ion batteries," *Journal of Fire Sciences,* vol. 33, no. 1, pp. 22-36, 2015.

[77] E. G. Gebresilassie, S. Grugeon, S. Laruelle, S. Boyanov, A. Lecocq, J.-P. Bertranda and G. Marlair, "In-depth safety-focused analysis of solvents used in electrolytes for large scale lithium ion batteries," *Royal Society of Chemistry,* vol. 15, pp. 9145-9155, 2013.

[78] F. Larsson, P. Andersson, P. Blomqvist and B.-E. Mellander, "Toxic fluoride gas emissions from lithium-ion battery fires," *Scientific Reports,* vol. 7, 2017.

[79] Board of the National Research Council, Acute Exposure Guideline Levels for Selected Airborne Chemicals Volume 4, Washington: National Academy of Sciences, 2004.

[80] National Highway Traffic Safety Administration, "Chevrolet Volt Battery Incident Overview Report DOT HS 811 573," National Highway Traffic Safety Administration, 2012.

[81] D. Orf, "Tesla Model 3 Blows Up ... Twice ... on Busy Highway," Popular Mechanics, 13 August 2019. [Online]. Available: https://www.popularmechanics.com/cars/hybrid-electric/a28687473/tesla-model-3-explosion/. [Accessed 29 August 2019].

[82] National Highway Safety Board, "Battery Fire in Electric-powered Passenger Car HWY18FH014 Preliminary," National Highway Safety Board, 2018.

[83] V. Tangermann, Futurism, 23rd April 2019. [Online]. Available: https://futurism.com/the-byte/tesla-fire-shanghai-parking-garage.

[84] E. Shilling, "Jalopnik," Jalopnik, 26 03 2019. [Online]. Available: https://jalopnik.com/firefighters-drop-smoking-bmw-i8-into-a-giant-tub-of-wa-1833582453. [Accessed 05 09 2019].

[85] L. Mellert, U. Welte, M. Hermann, M. Kompatscher and P. X., "Electric Mobility and Road Tunnel Safety Hazards of Electric Vehicle Fires," in *9th International Conference 'Tunnel Safety and Ventilation'*, Graz, 2018.

[86] L. Mellert, U. Welte and M. Hermann, "Electric Mobility and Road Tunnel Safety Hazards of Electric Vehicle Fires," in *9th International Conference 'Tunnel Safety and Ventilation'*, Graz, 2018.

[87] A. S. Boe, "Full-scale fire test of electric car," *SP Fire Research AS,* 2017.

[88] A. Lecocq, M. Bertana, B. Truchot and G. Marlair, "Comparison of the fire consequences of an electric," *International Conference on Fires In Vehicles,* pp. 183-194, 2012.

[89] R. Xiong, H. He, H. Guo and Y. Ding, "Modeling for Lithium-Ion Battery used in Electric Vehicles," *Procedia Engineering,* vol. 15, pp. 1869-2874, 2011.

[90] D. P. Finegag, J. Darst, W. Walker, Q. Li, C. Yang, R. Jervis, T. M. Heenan, J. Hack, J. C. Thomas, A. Rack, D. J. Brett, P. R. Shearing, M. Keyser and E. Darcy, "Modelling and experiments to identify high-risk failure scenarios for testingthe safety of lithium-ion cells," *Journal of Power Sources,* vol. 417, no. 31, pp. 29-41, 2019.

[91] K. Davidsson, I. Karlsson, P. Leisner, M. Bobert and P. Blomqvist, "Safety test methods for EV batteries," *Wolrd electric Vehicle Journal,* vol. 4, pp. 414-420, 2010.

[92] "Train car carrying Lithium batteries explodes near downtown Houston," KHOU-11, 24 04 2017. [Online]. Available: https://www.khou.com/article/news/local/train-car-carrying-lithium-batteries-explodes-near-downtown-houston/433576556. [Accessed 23 04 2020].

[93] NGV Global, "Current Natural Gas Vehicle Statistics," NGV Global, 31 07 2019. [Online]. Available: http://www.iangv.org/current-ngv-stats/. [Accessed 04 09 2019].

[94] DOE Energy Efficiency & Renewable Energy, "Alternative Fuels Data Center," [Online]. Available: https://afdc.energy.gov/fuels/natural_gas_cng_stations.html. [Accessed 23 12 2019].

[95] DOE Energy Efficiency & Renewable Energy, "Alternative Fuels Data Center," [Online]. Available: https://afdc.energy.gov/. [Accessed 09 07 2019].

[96] NGV America, "Enviroment," [Online]. Available: https://www.ngvamerica.org/environment/. [Accessed 23 12 2019].

[97] NGV Global News, "U.S. EIA's 2017 Outlook Forecasts Strong Growth for Natural Gas," [Online]. Available: https://www.ngvglobal.com/blog/u-s-eias-2017-outlook-forecasts-strong-growth-natural-gas-0917. [Accessed 23 12 2019].

[98] California Air Resources Board, 2018 Annual Evaluation of Fuel Cell Electric Vehicle Deployment & Hydrogen Fuel Station Network Development, July 2018.

[99] World Nuclear Association, "Heat Values of Various Fuels," World Nuclear Association, 08 2018. [Online]. Available: https://www.world-nuclear.org/information-library/facts-and-figures/heat-values-of-various-fuels.aspx. [Accessed 05 09 2019].

[100] The Engineering ToolBox, "Engineering ToolBox," [Online]. Available: https://www.engineeringtoolbox.com/. [Accessed 23 12 2019].

[101] I. H. Bell, Wronski, Jorrit, Quoilin, Sylvain and V. Lemort, "Pure and Pseudo-pure Fluid Thermophysical Property Evaluation and the Open-Source Thermophysical Property Library CoolProp," *Industrial & Engineering Chemistry Research ,* vol. 53, no. 6, pp. 2498-2508, 2014.

[102] NGV Global, "Natural Gas Vehicle Database," [Online]. Available: https://www.iangv.org/. [Accessed 08 07 2019].

[103] R. Ono, N. Masaharu, S. Fujiwara, S. Horiguchi and T. Oda, "Minimum ignition energy of hydrogen–air mixture: Effects of humidity and spark duration," *Journal of Electrostatics,* vol. 65, no. 2, pp. 87-93, 2007.

[104] C. J. Coronado, J. A. Carvalho Jr., J. C. Andrade, E. V. Cortez, F. S. Carvalho, J. C. Santos and A. Z. Mendiburu, "Flammability limits: A review with emphasis on ethanol for aeronautical applications and description of the experimental procedure," *Journal of Hazardous Materials,* vol. 32, no. 54, pp. 241-242, 2012.

[105] R. Eckhoff, M. Ngo and W. Olsen, "On the minimum ignition energy (MIE) for propane/air," *Journal of Hazardous Materials,* vol. 175, no. 1-3, pp. 293-297, 2010.

[106] Air Products and Chemicals Inc., *Ignition Energy of H2, CH4, and gasoline with Air,* Air Products, 2001.

[107] The Engineering ToolBox, "Adiabatic Flame Temperatures," [Online]. Available: https://www.engineeringtoolbox.com/adiabatic-flame-temperature-d_996.html. [Accessed 04 12 2019].

[108] H. Haase, Electrostatic Hazards: their evaluation and control, Verlag Chemie, 1977.

[109] V. Babrauskas, Ignition Handbook, 2003.

[110] The Engineering ToolBox, "Fuels and Chemicals - Autoignition Temperatures," [Online]. Available: https://www.engineeringtoolbox.com/fuels-ignition-temperatures-d_171.html. [Accessed 04 12 2019].

[111] J. M. Kuchta, "Investigation of Fire and Explosion Accidents in the Chemical, Mining, and Fuel-Related Industries: A Manual," *US Bureau of Mines,* vol. Bulletin 680, 1985.

[112] R. G. Zalosh, J. Amy, C. E. Hofmeister and W. Wang, "Dispersion of CNG fuel releases in naturally ventilated tunnels," *Center for Firesafety Studies, Worcester Polytechnic Institue ,* vol. 1, 1994.

[113] B. D. Ehrhart, D. M. Brooks, A. B. Muna and C. B. LaFleur, "Risk Assessment of Hydrogen Fuel Cell Electric Vehicles in Tunnels," *Fire Technology,* pp. 1-22, 2019.

[114] National Fire Protection Association, NFPA 52: Vehicular Natural Gas Fuel Systems Code, Quincy, 2019.

[115] National Fire Protection Association, NFPA 55: Compressed Gases and Cryogenic Fluids Code, Quincy, 2013 Edition.

[116] National Fire Protection Association, NFPA 57: Liquefied Natural Gas (LNG) Vehicular Fuel Systems Code, Quincy, 2002.

[117] National Fire Protection Association, NFPA 59A: Standard for the Production, Storage, and Handling of Liquefied Natural Gas (LNG), Quincy, 2019.

[118] SAE International, J1616: Recommended Practice for Compressed Natural Gas Vehicle Fuel, 1994.

[119] SAE International, J2406: Recommended Practices for CNG Powered Medium and Heavy-Duty Trucks, 2002.

[120] B. Lowesmith, G. Hankinson and D. Johnson, "Vapour cloud explosions in a long congested region involving methane/hydrogen mixtures," *Process Safety and Environmental Protection,* vol. 89, no. 4, pp. 234-247, 2011.

[121] D. Bjerketvedt, J. R. Bakke and K. v. Wingerden, "Gas explosion handbook," *Journal of Hazardous Materials,* vol. 52, no. 1, pp. 1-150, 1997.

[122] R. Harris and M. Wickens, "Understanding vapour cloud explosions-an experimental study," *The Institution of Gas Engineers,* vol. 1408, 1989.

[123] M. Royle, L. Shirvill and T. Roberts, "Vapour cloud explosions from the ignition of methane/hydrogen/air mixtures in a congested region," in *International Conference on Hydrogen Safety*, 2007.

[124] R. K. Zipf, V. N. Gamezo, K. M. Mohamed, E. S. Oran and D. A. Kessler, "Deflagration-to-detonation transition in natural gas–air mixtures," *Combustion and Flame,* vol. 161, no. 8, pp. 2165-2176, 2014.

[125] M. Kokkala, "Experimental study of heat transfer to ceiling from an impinging diffusion flame," *Fire Safety Science,* vol. 3, pp. 261-270, 1991.

[126] A. Venetsanos, D. Baraldi, P. Adams, P. Heggem and H. Wilkening, "CFD modelling of hydrogen release, dispersion and combustion for automotive scenarios," *Journal of Loss Preventation in the Process Industries,* vol. 21, no. 2, pp. 162-184, 2008.

[127] P. Middha and O. Hansen, "CFD Simulation Study to Investigate the Risk from Hydrogen Vehicles in Tunnels," *Int J Hydrogen Energy,* vol. 34, pp. 5875-5876, 2009.

[128] L. Zhiyong, X. Pan, K. Sun and J. Ma, "Comparison of the harm effects of accidental releases: Cryo-compressed hydrogen versus natural gas," *Internation Journal of Hydrogen Energy,* vol. 38, no. 25, pp. 11174-11180, 2013.

[129] H. Witlox and A. Holt, "Unified Dispersion Model," DNV Software Product and Development, London, 2000.

[130] J. Cook, Z. Bahrami and R. Whitehouse, "A comprehensive program for calculation of flame radiation levels," *Journal of Loss Prevention in the Process Industries,* vol. 3, no. 1, pp. 150-155, 1990.

[131] M. Tang and Q. Baker, "A new set of blast curves from vapor cloud explosion," *American Institute of Chemical Engineers,* vol. 18, no. 4, pp. 235-240, 2004.

[132] J. LaChance, A. Tchouvelev and A. Engebo, "Development of uniform harm criteria for use in quantitative risk analysis of the hydrogen infrastructure," *International Journal of Hydrogen Energy,* vol. 36, no. 3, pp. 2381-2388, 2011.

[133] A. Marangon, M. Carcassi, A. Engebo and S. Nilsen, "Safety distances: Definition and values," *International Journal of Hydrogen Energy,* vol. 32, no. 13, pp. 2192-2197, 2007.

[134] Y. Z. Li, "Fire and Explosion Hazards of Alternative Fuel Vehicles in Tunnels," Brandforsk, Stockholm, 2018.

[135] S. Chamberlain and M. Modarres, "Compressed natural gas bus safety: a quantitative risk assessment.," *Risk Analysis,* vol. 25, no. 2, 2005.

[136] M. Krupka, A. Peaslee and H. Laquer, "Gaseous Fuel Safety Assessment for Light-Duty Automotive Vehicles," Los Alamos National Laboratory Report LA-9829-MS, November 1983.

[137] R. Zalosh, W. Wang and J. Amy, "Hazard Analysis of Alternative Fueled Vehicles in Tunnels Part 2: LPG and LNG Fueled Vehicles," Center for Firesafety Studies, Worcester Polytechnic Institute, November 1995.

[138] US Department of Transpotation Federal Highway Administration, "Verification, Refinement, and Applicability of Long-Term Pavement Performance Vehicle Classification Rules FHWA-HRT-13-091," Federal Highway Administration, 2014.

[139] Power Solutions International, "GM G2500/G3500 Express & Savana," Power Solutions International, [Online]. Available: https://psiengines.com/wp-content/uploads/2018/02/PSI_SVM_G2500-G3500_Van_CNG_Spec.pdf. [Accessed 05 09 2019].

[140] O. Topal and I. Nakir, "Total Cost of Ownership Based Economic Analysis of Diesel, CNG and Electric Bus Concepts for the Public Transport in Istanbul City," *Energies,* vol. 11, no. 9, p. 2369, 2018.

[141] Daimler Truck Cascadia Freightliner, "Natural Gas Fuel Your Future," Daimler, 13 06 2019. [Online]. Available: https://freightlinerads.azureedge.net/3642-new_cascadia_natural_gas_sell_-2019-06-13-1.pdf. [Accessed 05 09 2019].

[142] "Alternative Fuels Data Center," US Department of Energy: Energy Efficiency & Renewable Energy, [Online]. Available: https://afdc.energy.gov/vehicles/propane.html. [Accessed July 2019].

[143] E. Hahn, "Is Propane a Liquid or Gas? Liquid Propane vs Gas Propane," ELGAS - LPG Gas for Home & Business, 20 10 2019. [Online]. Available: https://www.elgas.com.au/blog/726-what-is-the-difference-between-liquid-and-vapour-lpg. [Accessed 12 3 2020].

[144] The Engineering ToolBox, "Propane - Vapor Pressure," [Online]. Available: https://www.engineeringtoolbox.com/propane-vapor-pressure-d_1020.html. [Accessed 24 12 2019].

[145] Argonne National Laboratory, "Propane Vehicles: Status, Challenges, and Opportunites ANL/ESD/10-2," May 2010.

[146] A. Brecher, A. Epstein and A. Breck, "Review and Analysis of Potential Safety Impacts of and Regulatory Barriers to Fuel Efficiency Technologies and Alternative Fuels in Medium- and Heavy-Duty Vehicles," U.S. Department of Transportation, June 2015.

[147] A. Pundkar, S. Lawankar and S. Deshmukh, "Performance and Emissions of LPG Fueled Internal Combustion Engine: A Review," *International Journal of Scientific and Engineering Research,* vol. 3, no. 3, March 2012.

[148] National Fire Protection Association, NFPA 58: Liquefied Petroleum Gas Code, Quincy, 2017.

[149] D. Brzezinska and A. S. Markowski, "Experimental investigation and CFD modelling of the internal car park environment in case of accidental LPG release," *ProcessSafetyandEnvironmentalProtection,* vol. 110, pp. 5-14, 2017.

[150] G. Atkison and Y. Wu, "Smoke Control in Sloping Tunnels," *Fire Safety Journal,* pp. 335-341, 1996.

[151] Y. Oka and G. T. Atkinson, "Control of Smoke Flow in Tunnel Fires," *Fire Safety Journal,* vol. 25, pp. 305-322, 1995.

[152] D. Webber and S. Jones, "A Model of Spreading Vaporising Pools," in *International Conference on Vapor Cloud Modeling*, 1987.

[153] J. Weerheijm and B. van den Berg, "Explosion Risks and Consequences for Tunnels," in *Sixth International Symposium on Tunnel Safety and Security*, Marseille, France, March 12-14, 2014.

[154] National Renewable Energy Laboratory, On-Road Fuel Cell Electric Vehicles Evaluation: Overview, March 2019.

[155] Hyundai Motor America, "Hyundai ix35 Fuel Cell," Hyundai Media Center, [Online]. Available: https://www.hyundainews.com/en-us/releases/1624. [Accessed 04 04 2020].

[156] J. Kurtz, S. Sprik, G. Saur and S. Onorato, "On-Road Fuel Cell Electric Vehicles Evaluation: Overview NREL/TP-5400-73009," National Renewable Energy Laboratory, March 2019.

[157] Plug Power, "WHO'S USING GENDRIVE?," [Online]. Available: https://www.plugpower.com/customer/whos-using-gendrive/. [Accessed 03 02 2020].

[158] Fuel Cell & Hydrogen Energy Association, "[Company] Celebrates National Hydrogen and Fuel Cell Da," [Online]. Available: http://www.fchea.org/sample-press-release-2019. [Accessed 03 02 2020].

[159] International Partnership for Hydrogen and Fuel Cells in the Economy, [Online]. Available: https://www.iphe.net/united-states. [Accessed 20 April 2020].

[160] N. LePan, "The Evolution of Hydrogen: From the Big Bang to Fuel Cells," Visual Capitalist, 23 4 2019. [Online]. Available: https://www.visualcapitalist.com/evolution-of-hydrogen-fuel-cells/. [Accessed 3 1 2020].

[161] K. Kunze and O. Kircher, "CRYO-COMPRESSED HYDROGEN STORAGE," BMW Group, Oxford, 2012.

[162] College of the Desert, Hydrogen Fuel Cell Engines and Related Technologies, Module 1: Hydrgoen Properties, December 2001.

[163] I. Abe, Energy Carriers and Conversion Systems - Vol. I - Physical and Chemical Properties of Hydrogen.

[164] National Fire Protection Association, NFPA 77: Recommended Practice on Static Electricity, Quincy, 2019.

[165] C. LaFleur, "Large Scale Hydrogen System Safety Issues," *Chemical Engineering Progress,* vol. 115, no. 8, pp. 42-46, 2019.

[166] National Fire Protection Association, NFPA 2: Hydrogen Technologies Code, Quincy, 2020 Edition.

[167] Global Registry, "Addendum 13: Global technical regulation No. 13 Global technical regulation on hydrogen and fuel cell vehicles," UNITED NATIONS, 2013.

[168] National Fire Protection Association, NFPA 2: Hydrogen Technologies Code, Quincy, 2016 Edition.

[169] F. Dryer, M. Chaos, Z. Zhao, J. Stein, J. Alpert and C. Homer, "Spontaneous Ignition of Pressurized Releases of Hydrogen and Natural Gas into Air," *Combust. Sci. and Tech. 2007,* 2007.

[170] M. Groethe, E. Merilo, J. Colton, S. Chiba, Y. Sato and H. Iwabuchi, "Large-scale Hydrogen Deflagrations and Detonations," *Int J Hydrogen Energy ,* vol. 32, no. 13, pp. 2153-2133, 2007.

[171] J. M. Chock, "Review of Methods for Calculating Pressure Profiles of Explosive Air Blast and its Sample Application," Virginia Polytechnic Institute and State University, Blacksburg, 1999.

[172] F. Tamanini, "Scaling parameters for vented gas and dust explosions," *Journal of Loss Prevention in the Process Industries,* vol. 14, pp. 455-461, 2001.

[173] G. Houf, G. Evans, E. Merilo, M. Groethe and S. James, "Releases from Hydrogen Fuel-cell Vehicles in Tunnels," *Int J Hydrogen Energy,* vol. 37, pp. 715-719, 2012.

[174] S. Kumar, S. Miles, P. Adams, A. Kotchourko, D. Heldey, P. Middha, V. Molkov, A. Teodorczyk and M. Zenner, "HyTunnel Project to Investigate the use of Hydrogen Vehicles in Road Tunnels," in *3rd International Conference on Hydrogen Safety (ICHS3)*, 2009.

[175] A. Friedrich, J. Grune, T. Jordan, A. Kotchourko, N. K. M. Kotchourko, K. Sempert and G. Stern, "EXPERIMENTAL STUDY OF HYDROGEN-AIR DEFLAGRATIONS IN FLAT LAYER," in *Proc. 2nd ICHS International conference on hydrogen safety*, San Sebastian, 2007.

[176] M. Seike, Y. Ejiri, N. Kawabata, M. Hasegawa and H. Tanaka, "Fire experiments of carrier loaded FCV in full-scale model tunnel - Estimation of heat release rate and smoke generation rate," in *Third International Converence on Fire in Vehicles*, Berlin, Germany, 2014.

[177] I. Tolias, A. Venetsanos, N. Markatos and C. Kiranoudis, "CFD Modeling of Hydrogen Deflagration in a Tunnel," *Int J Hydrogen Energy,* vol. 39, pp. 20538-20546, March 2014.

[178] H. Bie and Z. Hao, "Simulation Analysis on the Risk of Hydrogen Releases and Combustion in Subsea Tunnels," *Int J Hydrogen Energy,* 2016.

[179] Y. Wu, "Assessment of the impact of ject flame hazard from hydrogen cars in road tunnels," *Transportation Research Part C,* vol. 16, pp. 246-254, 2008.

[180] S. Mukai, J. M. H. Suzuki, K. Oyakawa and S. Watanabe, "CFD simulation on diffusion of leaked hydrogen caused by vehicle accident in tunnels," in *Proceedings of the International Conference on Hydrogen Safety (ICHS'05)*, 2005.

[181] ICHS, [Online]. Available: https://hysafe.info/ichs2019/. [Accessed 24 03 2020].

[182] HyTunnel-CS, "About HyTunnel-CS," HyTunnel-CS, 2019. [Online]. Available: https://hytunnel.net/?page_id=31. [Accessed 26 09 2019].

[183] I. Abe, Energy Carriers and Conversion Systems - Vol. I - Physical and Chemical Properties of Hydrogen.

[184] Global Registry, "Addendum 13: Global technical regulation No. 13 Global technical regulation on hydrogen and fuel cell vehicles," UNITED NATIONS, 2013.

[185] Sandia National Laboratories, Hydrogen Fuel Cell Electric Vehicle Tunnel Safety Study, October 2017.

[186] F. Dryer, M. Chaos, Z. Zhao, J. Stein, J. Alpert and C. Homer, "Spontaneous Ignition of Pressurized Releases of Hydrogen and Natural Gas into Air," *Combust. Sci. and Tech. 2007,* 2007.

DISTRIBUTION

Email—External

Name	Company Email Address	Company Name
Laura Hill	laura.hill@ee.doe.gov	DOE Office of Energy Efficiency & Renewable Energy
Mark Richards	mark.richards@ee.doe.gov	DOE Office of Energy Efficiency & Renewable Energy
Neha Rustagi	neha.rustagi@ee.doe.gov	DOE Office of Energy Efficiency & Renewable Energy
Stephen Bartha	stephen.bartha@dot.gov	DOT Federal Highway Administration
Cyrus J. Jordan	cjjordan@ncsu.edu	North Carolina State University (Former Sandia Intern)

Email—Internal

Name	Org.	Sandia Email Address
Alice B. Muna	05814	amuna@sandia.gov
Ethan S. Hecht	08367	ehecht@sandia.gov
Jonathan A. Zimmerman	08367	jzimmer@sandia.gov
Myra L. Blaylock	08751	mlblayl@sandia.gov
Austin R. Baird	08854	arbaird@sandia.gov
Brian D. Ehrhart	08854	bdehrha@sandia.gov
Austin M. Glover	08854	amglove@sandia.gov
Chris B. LaFleur	08854	aclafle@sandia.gov
Technical Library	01977	sanddocs@sandia.gov

This page left blank

Sandia National Laboratories

Sandia National Laboratories is a multimission laboratory managed and operated by National Technology & Engineering Solutions of Sandia LLC, a wholly owned subsidiary of Honeywell International Inc. for the U.S. Department of Energy's National Nuclear Security Administration under contract DE-NA0003525.